A seismic refraction study of crustal structure between the Faeroe Isles and Scotland

Smith, Peter Joseph

A Seismic Refraction Study of crustal structure between the Faeroe Isles and Scotland

A Thesis submitted for the Degree of Doctor of Philosophy in the University of Durham

by

Peter Joseph Smith

Graduate Society

September, 1974.

ABSTRACT

A seismic refraction project known as the North Atlantic Seismic Project (NASP) was carried out in the NE North Atlantic between Scotland and Iceland during July 1972. This thesis presents the results and interpretation of the data obtained between Scotland and the Faeroe Islands.

The first arrival travel time data was analysed by firstly fitting straight line segments by least squares, and secondly by time term analysis. The shot-station configuration of the project favoured time term analysis as this method combines the large quantity of data obtained, and the interpretation is not limited by apparent velocities. Amplitude measurements were made on some of the data in order to positively identify the large amplitude secondary arrivals observed as the reflected phase from the Moho, PmP. This phase was used to supplement the crustal structure information obtained from the first arrivals, and theoretical travel times have been calculated for these reflections. Little use has been made of S wave arrivals.

Two main crustal layers were established beneath the Scottish shelf with a Moho depth of 25-26 km. The upper basement layer is at a depth of about 2-3 km beneath mainly Palaeozoic sediments (5.0 km s^{-1}) and has a P wave velocity of 6.1 km s^{-1}. It is interpreted as Lewisian schists and gneisses. The lower layer at a depth of about 9 km has a P wave velocity of 6.48 km s^{-1} and is interpreted in terms of granulite facies Lewisian material. A normal Moho Pn velocity of 7.99 km s^{-1} was found.

A continental crustal thickness of about 30 km was determined beneath the Faeroe Plateau. There is quite an abrupt transition in the basement material between the north-west and south-east regions of the Plateau. The material in the north-west has a velocity of about 6.1 km s^{-1} and is interpreted as normal continental metamorphic rocks such as gneisses. In the south-east the velocity of about 5.5-5.6 km s^{-1} is interpreted in terms of slates, and the transition between the two as a change in metamorphic grade.

The crustal structure was not well determined beneath the Faeroe/Shetland Channel but the region appears to be underlain by anomalous oceanic material with a Moho depth of 11-18 km. Two main crustal layers were identified with velocities of about 4.65 km s^{-1} and 6.16 km s^{-1}, and at depths of about 2.2 km and 7.9 km respectively.

ACKNOWLEDGEMENTS

I wish to thank Professors M.H.P. Bott and G.M. Brown for providing Departmental facilities for this research, and Professor M.H.P. Bott for his supervision and help. I am most grateful to Dr. R.E. Long for his advice and direction in particular in the use of the Departmental recording equipment and processing laboratory. In addition I wish to thank Dr. J. Sunderland for his supervision of the shot-firing programme and his encouragement in the data interpretation and Mr. J.H. Peacock for his supervision of the receiving ship MV Miranda. I am also indebted to Drs. Ashcroft, Khan, King, Jacob and Thirlaway, and Professors Blundell and Murphy for providing receiving stations during the project and making available their results and processing facilities. Similarly I wish to express my thanks to Professor Saxov of Aarhus University and Dr. Zverev of the Soviet Institute of Physics of the Earth, and their colleagues for making available the results they obtained during the project.

I also wish to thank the officers and crews of MV Hawthorn, MV Miranda and the Soviet vessel Mikail Lomonosov, and many members of the Department of Geological Sciences, University of Durham for their help during the data collection.

The work has been financed by a Natural Environment Research Council Studentship for three years, for which I am grateful.

C O N T E N T S

List of Figures

List of Tables

CHAPTER I

INTRODUCTION

A large scale seismic refraction experiment was undertaken in the NE Atlantic ocean between the north of Scotland and Iceland during July 1972. The experiment, known as the North Atlantic Seismic Project (NASP), was organized by members of the Department of Geological Sciences, University of Durham and carried out with the assistance of many other scientific establishments. The general aim of the project was to determine the crustal and upper mantle structures of the area studied and therefore help to elucidate some of the problems concerned with the evolution of the North Atlantic.

This thesis describes the project and the reduction and interpretation of the data collected from all the lines over and to the south of the Faeroe Plateau, with the exception of line F shot in the North Minch.

1.1 The Region of Study

This region of the NE Atlantic can be subdivided, on the basis of bathymetry, into three distinct areas (Fig. 1.1).

1. The North Scottish Continental Shelf including the Moray Firth.
2. The Faeroe/Shetland Channel and Channel slopes.
3. The Faeroe Plateau.

The known structures of these three areas, determined both from nearby land geology and previous geophysical work, indicate that as well as the bathymetry differences, the three areas are geologically dissimilar. Therefore, the NASP results have been interpreted for the separate areas.

Figure 1.1 : Physiographic map of the NE North Atlantic (from Birch, 1973), and showing the location of the seismic refraction profiles A, B, L, K, M of Browitt (1971), and the profile E12 of Ewing and Ewing (1959). Bathymetric contours are in fathoms.

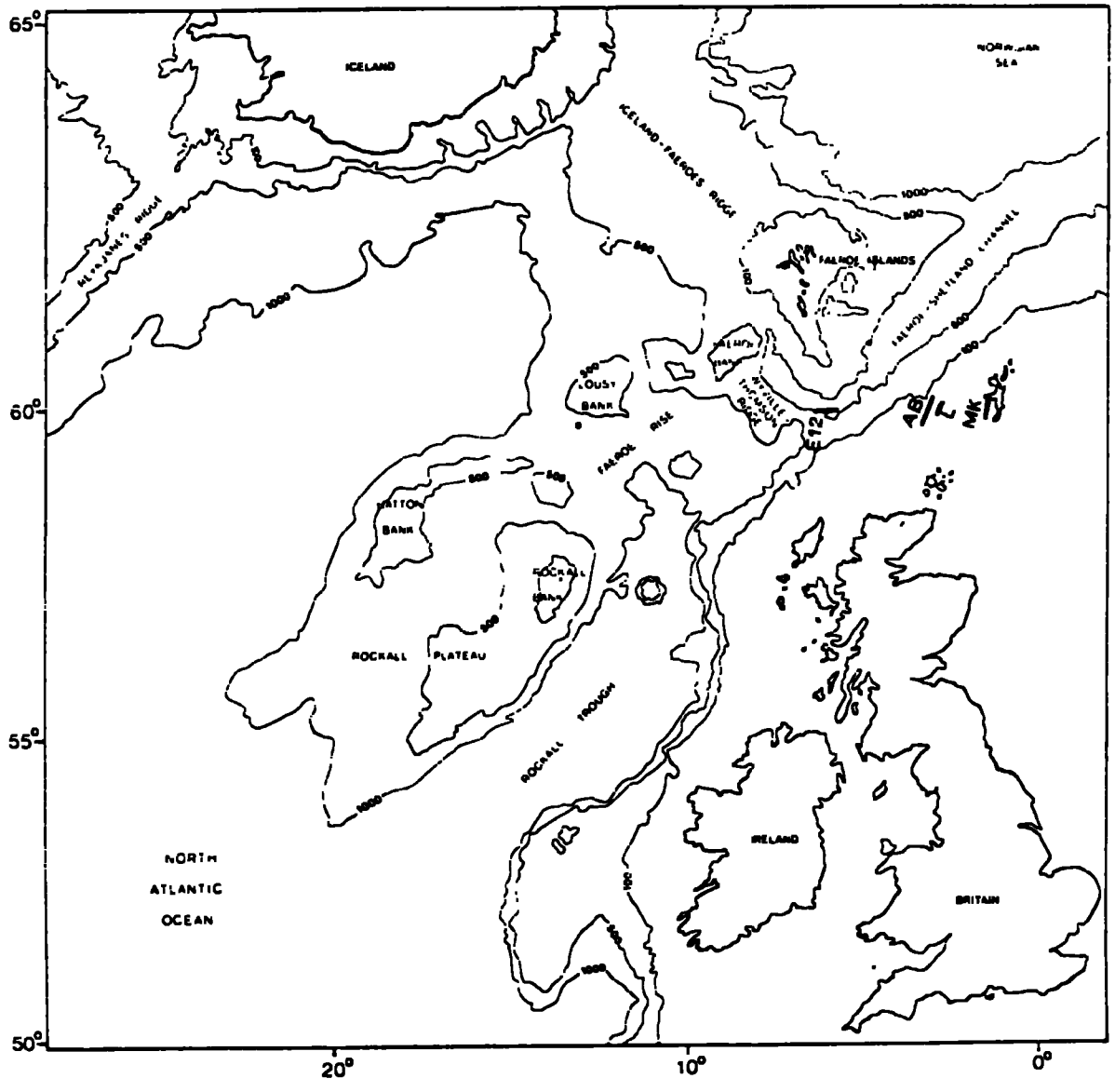
65°
60°
55°
50°
20°
10°
0°
ICELAND
ICELAND - FAEROES RIDGE
FAEROE ISLANDS
FAEROE - SHETLAND CHANNEL
WYVILLE THOMSON RIDGE
GEIKIE SEAMOUNT
LOUSY BANK
FAEROE RISE
HATTON BANK
ROCKALL PLATEAU
ROCKALL TROUGH
ROCKALL BANK
IRELAND
BRITAIN
NORTH ATLANTIC OCEAN
1000
500
100
E12

1.2 The North Scottish Continental Shelf Area - Geological Description

1.2.1 The Land masses

The Scottish mainland can be divided into two structural units separated by the Caledonian front which is marked by the Moine and related thrusts (Fig.1.2). These units are the Caledonian Foreland lying to the WNW, and the Caledonian Orogenic Belt lying to the ESE. The exposed rocks of these two areas also differ.

On the Foreland Lewisian rocks outcrop in West Sutherland, the Outer Hebrides, North Rona and the Skerries. Scourian granulites occupy the central area of the Lewisian outcrop both on the mainland (Watson, 1965) and on the Outer Hebrides (Dearnley, 1962). To the north and south WNW-ESE trending belts of banded biotite gneisses of Laxfordian age outcrop (Watson, 1965). The Scourian granulites are a meta-igneous assemblage formed by folding and metamorphism during the Scourian orogeny (2,700-2,450 m yr ago). The Laxfordian assemblages have been described as remobilised Scourian material metamorphosed during the Laxfordian orogeny (1,600-1,300 m yr ago) (Watson, 1965), and alternatively, as sediments derived from the Scourian and metamorphosed only by burial at a depth of about 20 km. (Holland, private communication). Gneisses in NW-SE trending belts in the central region of the Lewisian outcrop on the Foreland have been identified as the remnants of the Inverian orogeny (2,200-1,950 m yr ago). These are the only dated Inverian assemblages and so the details of this orogeny are obscure.

The Lewisian basement of the Foreland is overlain with strong unconformity by Torridonian sandstone deposited during

Figure 1.2 : The geology of northern Scotland and the continental shelf extending to the Shetland Islands.

NASP SHOT POSITIONS ON THE SCOTTISH CONTINENTAL SHELF

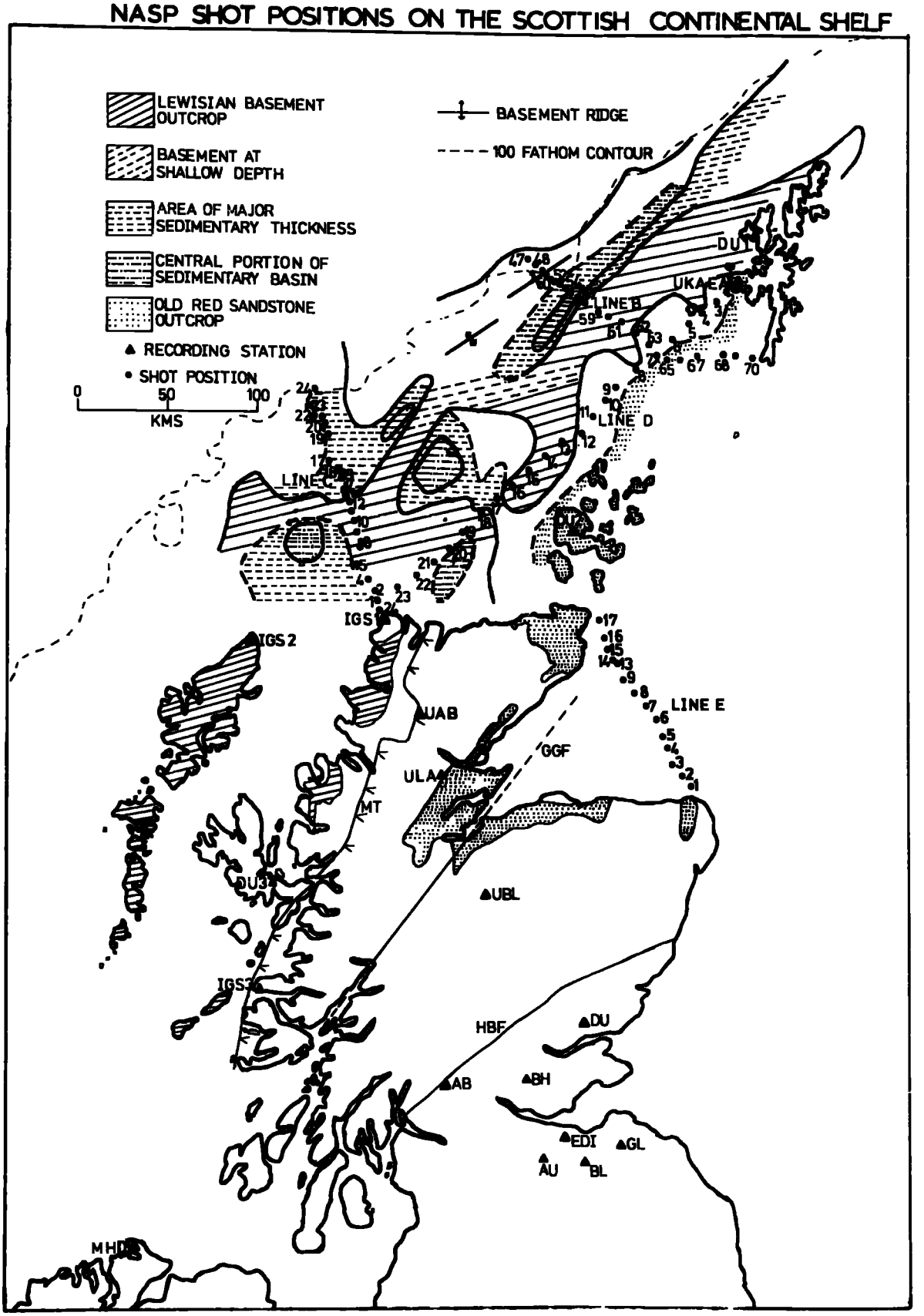

the late Pre-Cambrian (Johnson, 1965). The Torridonian is relatively undeformed and unmetamorphosed. A lower Palaeozoic sequence of quartzites and dolomites of Cambrian and Ordovician age unconformably overlies the Torridonian sandstone (Walton, 1965), and is preserved along a narrow belt just to the west of the Moine thrust.

The Caledonian orogenic belt to the east is covered in large part by outcropping Moine schists. These schists are the result of the late Silurian - early Devonian metamorphism and folding of sands and shales which were probably deposited contemporaneously with the Torridonian sandstone widespread on the Foreland (Johnson, 1965). The Moine thrust forms the boundary between the Moinian and Torridonian rocks, but the Moinian rocks may have been transported to the fault from the east. (Watson, 1963).

There is no evidence of Dalradian rocks to the north of the Great Glen Fault but south of it schists and gneisses of Dalradian age overlie the Moinian in central Scotland. Similar rocks also compose the metamorphic basement east of the Walls Boundary Fault on the Shetland Islands. Mineralogical differences have led to these Shetland metamorphic rocks being divided into three series (Miller and Flinn, 1966). The East Mainland Succession outcrops on the central mainland, the Quarff Succession to the south of the Whalsay-Clift Dislocation, and in the north and on the western sides of Yell, Fetlar and Unst, the Lunnasting Succession outcrops. These three successions also give rise to notably different gravity and magnetic fields (McQuillin and Brooks, 1967). The Quarff Succession is probably a part of the East Mainland Succession (Miller and Flinn, 1966) and these consist of

metasediments and metamorphosed igneous rocks similar to the Dalradian of central Scotland.

Devonian igneous activity involved the syn-orogenic injection and post-tectonic intrusion of granite in the Moinian and Dalradian rocks of Sutherland, Caithness and the Shetland Islands, with extrusions of lava in the Shetland and Orkney Islands (Flinn et al, 1968; Wilson et al, 1935).

Thick deposits of post-orogenic Old Red Sandstone covered the eastern part of the orogenic belt in Devonian times. These deposits are of intramontane type (Miller and Flinn, 1966) and were probably deposited in deep troughs adjacent to the orogenic belt, and extending from the borders of the Moray Firth through Caithness, the Orkney Islands, Fair Isle and Foula to the Shetland Islands (Waterston, 1965). Middle and Upper Old Red Sandstone deposits are preserved around the Moray Firth. The Orkney Islands, with the exception near Stromness where granitic and schistose rocks occur, and a few lavas and dykes, consist entirely of Middle and Upper (?) Old Red Sandstone. Recently it has been demonstrated that the Hoy Sandstone is not of Upper Old Red Sandstone age (Fannin, private communication). The Hoy Sandstone unconformably overlies a basalt lava flow on top of Middle Old Red Sandstone deposits. This lava flow has been dated by the K-Ar method as Westphalian in age, which indicates a post-Westphalian (Permian?) age for the Hoy Sandstone.

Middle Old Red Sandstone deposits unconformably overlie the Quarff Succession along the east coast of the Shetland mainland south of Lerwick. Middle Old Red Sandstone and contemporaneous volcanics outcrop throughout the area to the west of the Walls Boundary Fault apart from a small area of

metamorphic rocks adjacent to the fault (Miller and Flinn, 1966). The Walls Peninsular is covered by sandstone deposits except along the northern coastline where metamorphic rocks outcrop. The sandstone deposits have been interpreted as of Middle Old Red Sandstone age (Finlay, 1930), but Flinn et al (1968) suggests that the deposits are not of the Old Red Sandstone type and may be of post Old Red Sandstone age. However the Sandsting granite intrudes these deposits and has been given a K-Ar age of 330 m yr, so the sandstone deposits must be older than Lower Carboniferous.

Although Caledonian orogenic belt rocks have been identified on Shetland the tectonic relationship of the Island with the Scottish mainland is unresolved. The Great Glen Fault on the basis of aeromagnetic and bathymetry evidence (Flinn, 1969; Flinn, 1970) has been suggested to curve northwards from the Moray Firth and become the Walls Boundary Fault. However, this has been challenged by Bott and Watts, (1970) on the grounds that linearity is a main feature of transcurrent faults, and the failure of the fault to displace the metamorphic basement traced by gravity profiles to the north of Shetland.

Mesozoic sediments outcrop in both structural regimes on the Scottish mainland but are limited to the coastal areas. Sandy Rhaetic beds have been found on Mull and dark shales on Arran. Jurassic rocks outcrop on the east coast in Sutherland and on the west at Gruinard Bay and on the Hebrides. Along the north-west margin of the Moray Firth there is a discontinuous sequence of Trias to Kimmeridge. Mesozoic rocks younger than Kimmeridgian are not found east of the Caledonian front although Cretaceous rocks are present

in the glacial drift (Hallam, 1965). Many scattered minor outcrops of Cretaceous sediments occur in western Scotland. The thickest deposits are found at Morven where they are preserved by Tertiary lavas. The general lack of Mesozoic sediments over the Scottish mainland suggests that the area was approximately one large island during most of the Mesozoic (Hallam, 1965).

Tertiary sediments are also virtually absent apart from local terrestrial accumulations within lava sequences, indicating that the land was also above sea level during this period. Igneous activity was well developed along the west coast of Scotland, the Foreland, during the Tertiary. The area formed part of the Thulean igneous province extending from Northern Ireland to Greenland (Richey, 1961). This activity involved the outpouring of extensive lava flows, mainly basic, of which only the remnants are now preserved. Major intrusive centres, basic, ultrabasic and acidic, were developed in Skye, Rhum, Ardnamurchan, Mull Arran and St. Kilda. Extensive basaltic dyke swarms are associated with these centres.

1.2.2 The Continental Shelf

The geology of the continental shelf is similar to that of the adjacent land areas. Continuity of the Old Red Sandstone outcrops along the eastern part of the shelf is expected from the outcrop patterns seen on land. Watts (1971) has shown that the gravity and magnetic 'low' seen on land over the outcropping Old Red Sandstone also extends between the Orkney and Shetland Islands indicating that these deposits are continuous over the continental shelf.

Lewisian metamorphic basement outcrops to the west of the Old Red Sandstone deposits along most of the shelf. The outcrop forms a ridge trending NNE-SSW which has been detailed by gravity, magnetic and seismic reflection profiles (Bott and Watts, 1970; Watts, 1971). These geophysical surveys also found a series of fault bounded Mesozoic basins on the shelf. They have been interpreted as between 2-5 km deep and probably containing Palaeozoic and/or Torridonian sediments as well as the Mesozoic deposits. Basement ridges adjoining these basins have been traced over the shelf (Watts, 1971; Flinn, 1969). Boreholes sunk by I.G.S. (Chesher, private communication) in the North Minch, north-east of Cape Wrath, and adjacent to North Rona and the Skerries found Mesozoic sediments in all cores. Jurassic shales and Triassic New Red Sandstone deposits were identified.

The only Tertiary sediments found are on and near the shelf slope where a prograding sequence covers the earlier formations. Early Tertiary igneous activity affected the Hebridean region of the continental shelf. Intrusive centres were developed similar to those on the west coast of Scotland. Such centres as Blackstone Bank have been proved by geophysical methods (McQuillin et al, 1973).

Several short refraction lines have previously been shot on the continental shelf (Fig. 1.1) and the results of these were interpreted by Browitt (1971, 1972) in terms of the following P wave velocities, rock types and thicknesses:

PROFILE	P VELOCITY ($km\ s^{-1}$)	LAYER THICKNESS (km)	ROCK TYPE
LINE L (over gravity 'high A')	5.89	-	Lewisian metamorphic basement
REVERSED LINES A AND B (over gravity 'low E')	2.0	0.7	Mesozoic sediments
	2.69/3.59	2.4	Permo-Triassic sediments
	4.7	3.8	Palaeozoic sediments
	5.95	-	Lewisian metamorphic basement
REVERSED LINES K AND M (over gravity 'low F')	2.65	0.10	Permo-Triassic sediments
	5.25	1.18	Walls Old Red Sandstone

1.2.3 The Moray Firth

The Moray Firth is situated on the Caledonian Orogenic Belt in the region of post-orogenic intramontane Old Red Sandstone deposition. The north-west coastal margin of the Firth is formed by outcropping Upper and Middle Old Red Sandstone deposits and some Mesozoic sediments. Similar rocks outcrop along the southern coastal margin together with Dalradian metamorphics on the eastern part of this coastline (Fig. 1.3).

The Middle Old Red Sandstone deposits form a broad syncline centred on the Black Isle and extending in a NE-SW direction. The basal group of sandstones occur in fans which fringe the surrounding metamorphic Moinian and Dalradian rocks. This pattern, and the rapid lateral variation seen in these lower beds is taken to indicate that during the period of early deposition of Old Red Sandstone the Moray Firth formed a topographic basin (Waterston, 1965).

Figure 1.3 : The land geology surrounding the Moray Firth

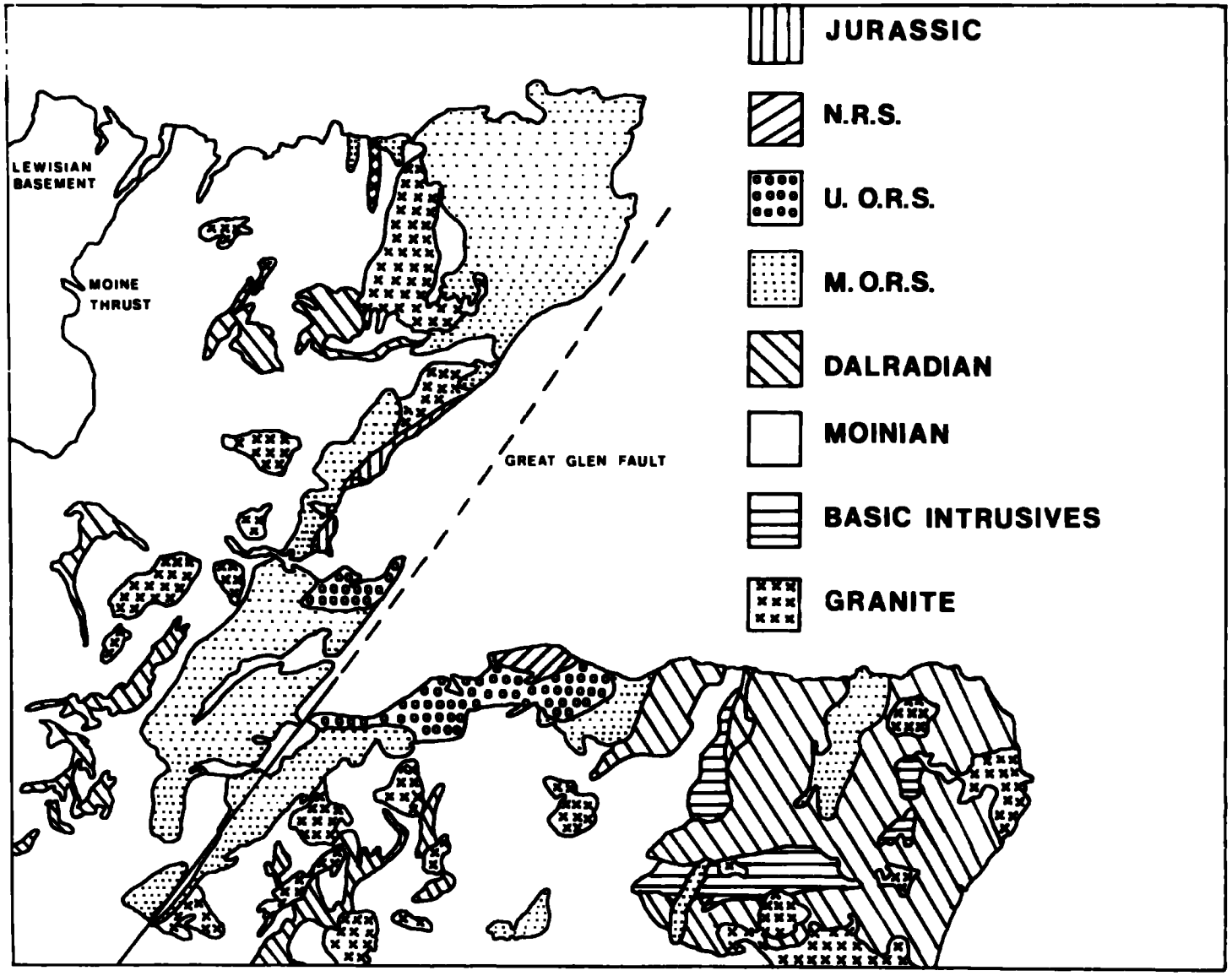
JURASSIC
N.R.S.
U. O.R.S.
M. O.R.S.
DALRADIAN
MOINIAN
BASIC INTRUSIVES
GRANITE
LEWISIAN BASEMENT
MOINE THRUST
GREAT GLEN FAULT

A Bouguer anomaly gravity map of the Moray Firth compiled by IGS (Sunderland, 1972) shows a large gravity low extending to the northwest into the North Sea. This gravity low was also seen on an earlier map produced by Collette (1960) and interpreted by him as caused by a granitic body. However, the Mesozoic sediments on the east coast of Scotland dip in general towards the Moray Firth (Hallam, 1965), suggesting that the Firth was also a basin during Mesozoic times. The gravity low has been interpreted as caused by a Mesozoic basin (Sunderland, 1972) and the result indicated a sediment thickness of less than 4 km. The presence of Permo-Triassic, Jurassic and Cretaceous rocks has since been proved by drilling and sampling by IGS (Chesher et al, 1972). Sediment horizons within the Moray Firth basin have been identified by seismic reflection profiling (Bacon, private communication). The horizons seen were:-

1. Inter-lower Cretaceous
2. Base of the lower Cretaceous
3. Mid Jurassic
4. Base of the Jurassic
5. Permo-Triassic?

The base of the Jurassic was the lowest horizon to be confidently identified and is interpreted as at a depth of about 3 km below the sea bed.

The seaward extension of the Great Glen Fault passes parallel to and just off the north-west coastal boundary of the Moray Firth. Normal faulting associated with the Great Glen Fault and affecting the Mesozoic sediments can be seen on the seismic reflection records. A recent interpretation of the Great Glen Fault (Winchester, 1973), based on the regional metamorphic pattern of Moinian assemblage rocks displaced by the fault, indicates a sinistral tear displacement

of 160 km. The fault is also seen to postdate the emplacement of Caledonian intrusives.

1.3 The Faeroe/Shetland Channel and Channel Slopes

1.3.1 The Faeroe/Shetland Channel

The Faeroe/Shetland Channel is the area of relatively deep water located between the Faeroe Plateau to the north-west, and the Scottish Continental Shelf to the south-east. (Fig. 1.1).

The channel extends in a NNE direction from the Wyville-Thomson Rise in the south to where it merges with the Norwegian Sea north-east of the Shetland Islands. At the southern boundary the channel turns to the north-west where it becomes the Faeroe Bank Channel separating the Wyville-Thomson Rise from Faeroe Bank. On merging with the Norwegian Channel in the north the channel identity is lost in the large area of deep water off the Norwegian shelf edge.

The position of the Faeroe/Shetland Channel is apparent on the Free Air Anomaly map of the Scotland to Faeroes region. The anomaly values decrease away from the Faeroe Plateau to the south-east, and also away from the Scottish Shelf to the north-west. Minimum values occur over the channel. A Bouguer anomaly map has been calculated for the area (Watts, 1970). This indicates a Bouguer anomaly high, which increases towards the north-east, is associated with the channel. Watts (1970) interpreted a gravity profile crossing the channel from the Scottish Shelf to the Faeroe Plateau. Assuming the Continental Shelf crust to be 27 km thick and 1 km of sediments in the channel, a crustal thinning of 6 km beneath the channel was found to explain the Bouguer anomaly high. This

interpretation was limited by lack of exact knowledge of the sediments in the channel.

A more satisfactory continental reconstruction of the North Atlantic is obtained if the Faeroe Plateau is considered to be continental as well as the Rockall Plateau. (Bott and Watts, 1971). This suggests that the Faeroe/ Shetland Channel is similar to the Rockall Trough as both are then deep water areas separating microcontinental fragments from the Scottish Shelf. The two areas are separated by the Wyville-Thomson Rise which has been interpreted (Himsworth, 1973) as formed by Tertiary basaltic lava extruded through similar vents to those observed on the Faeroe Islands. A seismic refraction experiment in Rockall Trough failed to detect Moho arrivals (Scrutton, 1972). Upper sediment velocities of 2.17 km s^{-1}, 3.5 km s^{-1} and 3.89 km s^{-1} were recorded and a basement velocity of 4.72 km s^{-1}. The interpreted depth to this basement was almost 8 km. Two other seismic refraction profiles have been shot in Rockall Trough (Ewing and Ewing, 1959). These profiles found unreversed velocities of 2.65 km s^{-1}, 3.22 km s^{-1} and 6.96 km s^{-1} (profile E10), and 2.08 km s^{-1} and 4.97 km s^{-1} (profile E 11) with sediment thicknesses above the basement of 2.6 km and 5.4 km respectively. Scrutton (1972), combined this data in a model with 5 km of sediment above the 4.7 km s^{-1} basement. This model was used in the interpretation of a gravity profile from the Hebridean Shelf out across the Rockall Trough and beyond the Rockall Plateau. To maintain isostatic equilibrium a Moho depth of 12 km was necessary beneath the Trough indicating an oceanic crustal structure.

1.3.2 Previous Work in the Faeroe/Shetland Channel

The Aeromagnetic map of the region shows that the channel is a relatively quiet zone. Magnetic highs and lows trending NNE-SSW are present and have been interpreted by Bidston (1970) as partly caused by basement relief and partly by lateral changes in the magnetic properties. A magnetic profile obtained on a line along the central part of the northern channel has been interpreted by power spectrum analysis (Himsworth, 1973). A sediment cover of 2.3 km was determined at approximately 61° 20'N, 4° 0'W.

A gravity profile across the channel has also been interpreted by Himsworth (1973). A sediment thickness of 3 km was assumed and the Moho depth calculated to be 18 km.

A seismic refraction line has been shot in the south of the channel (Ewing and Ewing, 1959). The two ship technique was used with one ship positioned where the Faeroe/Shetland Channel turns to become the Faeroe Bank Channel (59° 56'N, 06° 29'W), and the other ship positioned on the Wyville-Thomson Rise (59° 48'N, 07° 09'W). Sediment velocities were only recorded at the station in the channel with apparent velocities of 1.72 km s^{-1} and 2.24 km s^{-1}. Both ships recorded good basement arrivals giving a reversed velocity of 4.91 km s^{-1} and the refractor was interpreted to be at a depth of 1.81 km below the sea floor.

1.3.3 The Faeroe/Shetland Channel Slopes

If the Faeroe/Shetland Channel is similar to the Rockall Trough then the slope from the Scottish Shelf into the channel could represent a continental crust-oceanic crust transition zone. Similarly if the Faeroe Islands are continental in nature, then the slope from the channel to

the Faeroe Plateau would also be such a transition zone.

The Bouguer anomaly chart of the Scottish Shelf and Slope compiled by Watts (1970) shows that a number of circular gravity lows of about 20-30 mgal amplitude are associated with the slope. As thick accumulations of sediments are known to occur on the continental slopes west of Britain (Stride et al, 1969) these gravity lows are probably caused by such accumulations. A Bouguer anomaly profile across a gravity low has been interpreted by Watts (1970) and, depending on the sediment density contrast used, sediment thicknesses of 3.2 km and 2.5 km were determined. Magnetic anomaly lows occur with the gravity lows and terminate sharply at the shelf break in slope.

The thin Quaternary sediments on the shelf can be traced by seismic reflection profiles over the slope where they are seen to thicken. The thickness of sediment estimated over the slope is greater than the usual thickness of Tertiary/Quaternary sediments over the slopes around Britain suggesting, that unless local subsidence has occured, pre-Tertiary sediments are present.

Seismic reflection profiles on the Faeroe Shelf to the south/south-east of the islands, show that the basaltic basement outcrops to a distance of approximately 45 km from Torshavn, and is then unconformably overlain by sediments thickening towards the Faeroe/Shetland Channel (Watts, 1970). These sediments appear to be younger than the Tertiary lava. The Free Air Anomaly map of the Scotland to Iceland region compiled by Watts (1970) indicates a local gravity low of about 20 mgal amplitude on the south-east Faeroe Shelf. However, more recent gravity measurements (Lewis, private

communication) show that a local low probably does not exist, but instead the region of low gravity values extends to the south-east into the Faeroe/Shetland Channel. The low values on the Faeroe Shelf have been interpreted in terms of about 1.5-3 km of sediments overlying the lavas (Watts, 1970).

The Faeroe Shelf is associated with magnetic highs and lows which increase in wavelength towards the channel, and have a N-S trend. These are probably related to an extension of the fissure system of the Faeroe Islands or the later dyke instrusion (Avery et al, 1968; Watts, 1970).

Gravity, magnetic and seismic reflection data was collected over the channel and its slopes during July and August 1973 on a Durham University geophysical cruise, but as yet no results are available.

1.4 The Faeroe Plateau

1.4.1 Position and relation to Rockall Plateau and the Iceland-Faeroe Ridge

The Faeroe Plateau lies at the north-east end of a region of shallow banks in the North Atlantic known as the Rockall-Faeroe Plateau. The Plateau extends from Rockall and Hatton Banks in the south-west through the smaller banks (George Bligh, Lousy, Bill Bailey, Faeroe) to the Faeroe Plateau in the north-east (Fig. 1.1).

There is very good evidence that Rockall Plateau is underlain by continental crust. Seismic refraction profiles have been interpreted on Rockall Bank and on the Hatton-Rockall Basin (Scrutton, 1972). Two main crustal layers were identified on the Bank with P wave velocities of 6.36 km s^{-1} and 7.02 km s^{-1} at depths of about 5 km and 15 km respectively. These velocities are typical of continental block areas such

as the Seychelles (Davies and Francis, 1964). The Moho was interpreted to be at a depth of 31 km with a Pn velocity of 8.2 km s^{-1}. These values are within the ranges to be expected for continental crust around the British Isles (Holder and Bott, 1971; Blundell and Parks, 1969; Agger and Carpenter, 1965). The results from the Hatton-Rockall Basin indicated a crustal thickness of 22 km and a true Pn velocity of 8.07 km s^{-1}. A main crustal layer of P wave velocity 6.55 km s^{-1} was identified at about 5 km depth, and there was some evidence of a 7.15 km s^{-1} refractor which correlates well with the 7.02 km s^{-1} refractor observed beneath Rockall Bank. The upper crustal velocities observed were taken to indicate true sediment velocities of 2.8 km s^{-1}, and 4.54 km s^{-1}. By comparing this crustal structure with that of other areas of subsided continental crust, such as the Gulf of Mexico, Scrutton (1972) interprets the crust beneath the basin as representing a subsided continental structure. These crustal cross sections were used to compute a Free Air gravity anomaly model over Rockall Bank and the Hatton-Rockall Basin (Scrutton, 1972). A good agreement was found with the observed anomaly lending strength to the interpretation.

In addition to the geophysical evidence direct sampling of the Rockall Plateau indicates that it is underlain by continental material. The islet of Rockall consists of lower Eocene aegirine granite and is probably part of a Tertiary intrusive centre similar to those on the Scottish Continental Shelf (Roberts, 1969). An isotopic study of this granite (Moorbath and Welks, 1969) indicated that it had probably been contaminated by passage through a continental crust during intrusion. The lead isotope contents are similar to

those of Skye lavas which are considered to have risen through Lewisian crust.

Granulite cobbles with a similar mineral assemblage to that of the Lewisian found in the Outer Hebrides have been dredged from the south of Rockall Bank (Roberts et al, 1972). Photographic and palaeontological evidence is taken to indicate a local provenance.

Solid rock outcrops on the plateau have been drilled at two sites (Roberts et al, 1973). The cores investigated contained granulite facies metamorphic rocks showing some secondary alteration to hornblende. Radiometric age determinations gave a date for the hornblende of 1,566$\pm$ 33 m yr, and for the whole rock of 1,670$\pm$ 24 m yr. These drill samples were very similar to the cobbles dredged nearby and so confirm their in situ origin.

This evidence of Precambrian Lewisian type metamorphic rocks forming at least part of the plateau, together with the geophysical results, is taken to prove the continental nature of the underlying material. Therefore, Rockall Plateau should be included in any continental reconstruction of the North Atlantic. Bullard et al (1965) used the 500 fathom bathymetric contour as the continental boundary for their fit of the continents around the North Atlantic. The fit was poor in that there was some overlap to the north and north-west of Scotland, but to the west of Scotland a gap was left which was filled by retaining Rockall Plateau as continental. This fit was improved on by Bott and Watts (1971) by matching the edge of the Greenland Continental Shelf to the western edge of the combined Rockall-Faeroe Plateau. This is indirect evidence for a continental crust

beneath the Faeroe Islands.

Estimates of crustal thickness beneath some of the smaller banks have been obtained by gravity interpretations (Himsworth, 1973). A gravity profile crossing from the Hebridean Shelf onto George Bligh Bank has been interpreted to indicate a crustal thickness beneath the Bank of up to 25 km. Another profile extending from George Bligh Bank onto Bill Bailey Bank indicates a similar crustal thickness, 25-28 km, beneath Bill Bailey Bank. The Free Air Anomaly observed over Faeroe Bank (55 mgal) is the same as that measured over the previous two Banks and so Faeroe Bank probably has a similar crustal thickness. These crustal thicknesses are too large to explain the Banks in terms of seamounts and indicate a continental crust beneath them. A gravity interpretation along a line running E-W between George Bligh and Bill Bailey Banks (Lewis, private communication) also indicates a crustal thickness of 25 km suggesting that the areas between the Banks may also be underlain by continental crust.

The Faeroe Islands also lie at the south-east end of the Iceland-Faeroe Ridge, which has been interpreted (Bott et al, 1971; Bott, 1973) as underlain by anomalous Icelandic type oceanic crust. Gravity profiles show that the Bouguer anomaly drops steeply across the bathymetric scarp separating the Faeroe Islands from the Ridge. The limiting depth criterion of Bancroft (1960) has been applied to the gravity results (Bott et al, 1971) and indicates that the depth to the top of the anomalous body cannot be greater than 4-1¼ km. Refraction results from the Ridge (Bott et al, 1971) show that the Moho is deeper than 1¼ km and so much of the anomaly must be

caused by a lateral density variation within the crust. The lower density crust necessary beneath the Islands suggests that they could be underlain by continental material.

1.4.2 The Faeroe Islands

The Faeroe Islands form the emergent part of the Faeroe Plateau and consist almost entirely of flat lying early Tertiary plateau basaltic lavas with volcanic shales and agglomerates. Three series are recognised (Rasmussen and Noe-Nygaard, 1970), the lower, middle and upper series. The lower series is separated from the middle series by a coal bearing shale sequence up to 15 m thick. Another break in vulcanism separates the middle from the upper series. All three series have been radiometrically dated (Tarling and Gale, 1968) as probably between 50-60 m yr old. The basalts were probably extruded from NW-SE trending sub-aerial fissures and shield volcanoes, and were followed by the intrusion of sills and dykes (Noe-Nygaard, 1962). Finally the lavas were warped into a gentle NE-SW trending anticline.

The results of a refraction survey on the Islands (Palmason, 1965) indicated upper layer P wave velocities of 3.9 km s^{-1} and 4.9 km s^{-1}. These velocities were correlated with the upper series and middle and lower series respectively. At greater ranges the arrivals were interpreted as indicating a reversed basement velocity of 6.4 km s^{-1} beneath a variable lava cover (2.5-4.5 km). This suggested that the crustal structure was similar to that found beneath Iceland (Palmason, 1970). However, a more recent refraction experiment on the Islands (Casten, 1973) found an unreversed basement velocity of 5.9 km s^{-1}. This is in agreement with normal continental crust velocities.

1.5 The Aims of NASP

The experiment was designed to determine the variations in crustal and upper mantle structures from the Scottish Continental Shelf out to Iceland. This thesis is concerned with the south-east part of the experiment, and the results along the Iceland-Faeroe Ridge are not dealt with.

There have been several refraction investigations of crustal structure around the British Isles (Agger and Carpenter, 1965; Bamford and Blundell, 1970; Blundell and Parks, 1969; Holder and Bott, 1971) but none on the northern continental margin. The nature of the crust in this region and any differences between the Caledonian Foreland and Orogenic Belt were unknown. Large scale gravity features have been established on the shelf (Bott and Watts, 1971; Watts, 1970) and interpreted in terms of metamorphic basement outcrops and sedimentary basins. However, there was no information on the lower crustal structure and any Moho variation beneath these features. Similarly the Moray Firth region has been interpreted as a Mesozoic sedimentary basin (Sunderland, 1972) and the nature of the Moho beneath this basin was also unknown. The Moho topography beneath these features should help determine their origin.

The crustal structure beneath both the Faeroe Plateau and the Faeroe/Shetland Channel is of considerable importance to the history of the evolution of the NE North Atlantic. It has been postulated by Talwani and Eldholm (1972) that an escarpment, the Faeroe/Shetland escarpment, runs approximately down the western side of the Faeroe/Shetland Channel, and marks the position of the Tertiary opening of the southern Norwegian Sea. This escarpment was identified mainly by

bathymetric and seismic reflection data and correlated with the Voring Plateau escarpment identified further to the north (Talwani and Eldholm, 1972). The Voring Plateau escarpment was determined as marking the transition from thin sediments to the west of the escarpment to a region of thicker sediments, interpreted as those of a marginal basin, to the east. A transition from high amplitude magnetic anomalies to the west to a magnetic quiet zone in the east is also marked by the escarpment. The large amplitude anomalies were interpreted as typical of oceanic crust (Talwani and Eldholm, 1972) and the quiet zone as caused by subsided continental crust beneath a substantial thickness of sediments. However, lack of data in the Faeroe/Shetland Channel prevented any determination of sediment thickness to the east of the Faeroe/Shetland escarpment, and the magnetic anomaly variation over the escarpment was not very clear. This was attributed to a greater depth of burial, but Talwani and Eldholm, (1972) admitted that the evidence for the Faeroe/Shetland escarpment (interpreted as the position of the Tertiary continental split) was less strong than for the Voring Plateau escarpment.

Bott and Watts (1971) obtained a better fit of the continents around the North Atlantic by matching the coastline of Greenland to the western margin of the Rockall-Faeroe Plateau, suggesting, in contrast to the previous hypothesis, that the Faeroe Plateau is underlain by continental material. Similarly, an interpretation of a gravity profile extending from the Iceland-Faeroe Ridge onto the Faeroe Plateau (Bott et al, 1971) indicates a difference in the crustal structure beneath the two regions and suggests that the crust beneath

the Faeroes may be continental. However, a seismic refraction experiment on the Faeroe Islands (Palmason, 1965) found evidence of an upper crustal structure similar to that beneath Iceland. The problem of the nature of the crust beneath the Faeroe Plateau remained unresolved and refraction data on the crustal velocity structure and thickness was required.

Gravity interpretations across the Faeroe/Shetland Channel have found crustal thicknesses of 21 km (Watts, 1970) and 18 km (Himsworth, 1973). These interpretations, although limited by lack of exact knowledge of the sediment structure, suggest that the channel is not underlain by subsided continental crust as was interpreted by Talwani and Eldholm, 1972). Seismic refraction results were required to determine which, if either, of the two differing interpretations was correct.

The western boundary of the Faeroe/Shetland Channel may represent a continental crust - oceanic crust transition zone (Talwani and Eldholm, 1972) or alternatively if the channel is underlain by oceanic crust, the two channel slopes could both lie over such a transition zone. Two of the shot lines of NASP (lines B and C) were designed to cross these slope boundaries and therefore perhaps provide an interpretation of the Moho variation over a continental crust-oceanic crust transition zone.

CHAPTER 2

The North Atlantic Seismic Project - description and data collection and reduction

2.1 Introduction

The North Atlantic Seismic Project (NASP) took place between July 7th and August 4th, 1972 and involved firing explosive charges at sea from the shooting ship MV Hawthorn. The shots were fired along lines between Scotland and Iceland. Receiving stations were situated on the Scottish mainland and nearby islands, and also on the Faeroe Islands and Iceland. Two receiving ship stations, operated from MV Miranda and the Soviet research vessel Mikail Lomonosov, recorded on some of the shot lines. The shot-receiving station configuration is shown in Figure 2.1.

The majority of the shots on line A which extended from Iceland to the Faeroe Islands are not dealt with in this thesis. Only shots A1-A6 which were considered to lie over the Faeroe Plateau have been included. Similarly line F across the North Minch is not discussed. Lines B and C were shot from the Faeroe Islands across the Faeroe/Shetland Channel to the Scottish continental shelf, with line B terminating at the southern extremity of the Shetland Islands and line C at Cape Wrath. Line CB was a reversed line shot along the length of the Faeroe/Shetland Channel, firstly to the north-east (line CB) and then to the south-west (line BC). The line along the Scottish continental shelf, line D, was shot from the Walls peninsular on Shetland to Cape Wrath. Line E also over the continental shelf, was shot across the Moray Firth.

Figure 2.1 : The North Atlantic Seismic Project (NASP) shot-receiving station configuration for the part of the project considered in this thesis.

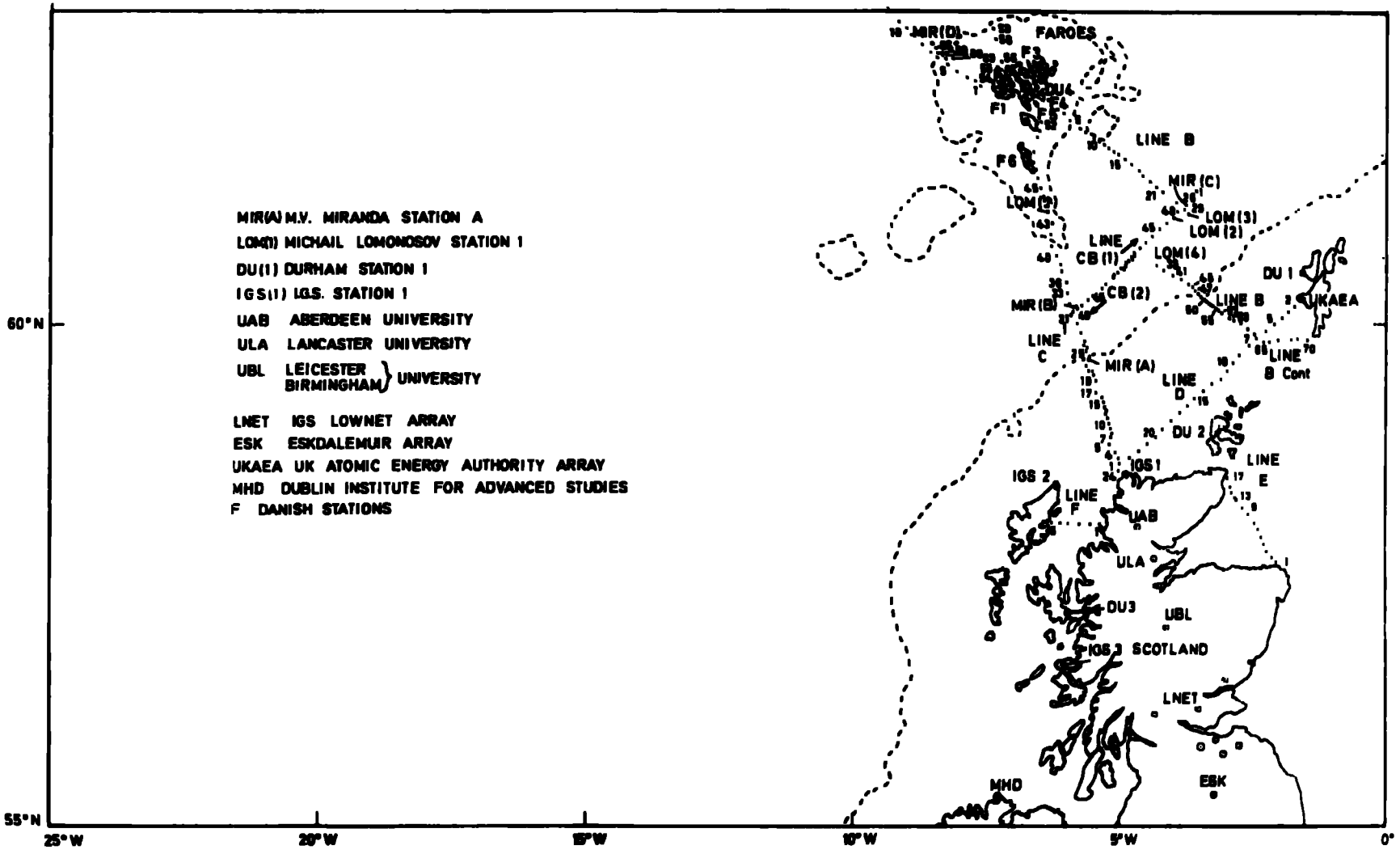
MIR(A) M.V. MIRANDA STATION A
LOM(1) MICHAIL LOMONOSOV STATION 1
DU(1) DURHAM STATION 1
IGS(1) I.G.S. STATION 1
UAB ABERDEEN UNIVERSITY
ULA LANCASTER UNIVERSITY
UBL LEICESTER, BIRMINGHAM } UNIVERSITY
LNET IGS LOWNET ARRAY
ESK ESKDALEMUIR ARRAY
UKAEA UK ATOMIC ENERGY AUTHORITY ARRAY
MHD DUBLIN INSTITUTE FOR ADVANCED STUDIES
F DANISH STATIONS
MIR(D)
FAROES
F1
F3
F6
DU4
LINE B
MIR(C)
LOM(3)
LOM(2)
LOM(4)
LOM(2)
LINE CB(1)
CB(2)
MIR(B)
DU 1
UKAEA
LINE B
LINE B Cont
LINE C
MIR(A)
LINE D
DU 2
IGS 1
LINE E
IGS 2
LINE F
UAB
ULA
DU3
UBL
IGS 3 SCOTLAND
LNET
MHD
ESK
60°N
55°N
25°W
20°W
15°W
10°W
5°W
0°

2.2 Experimental Procedure

All shots were fired from the shooting ship MV Hawthorn, which was operated by Durham University personnel under the supervision of the senior scientist, Dr. J. Sunderland. The charges consisted of geophex explosive varying in size from 25-1,200 lbs. 50lb. boxes of geophex were banded together with steel or plastic banding tape to make up the larger charges. Slow burning fuses were used to detonate the charges, 4-6 foot lengths being used for the 300 lb. charges, and 6-9 foot lengths for the 600 lb. charges. In the shallow water areas around the Scottish shelf and the Faeroe Plateau the shots were fired on the sea bed and in deeper water at close to the optimum depth. Marker floats were attached to all charges dropped within 12 nautical miles of the coast. A total of 274 shots were fired on these lines of which only 16 misfired.

The shot firing procedure on MV Hawthorn commenced with a five minute warning then a two minute warning followed by the announcement of shot drop transmitted by radio to the receiving stations. At the time of shot drop position fixes were taken and a stop-watch started to record the travel time of the water wave from shot to ship. The onset of the water wave was received at Hawthorn by a hull mounted geophone and recorded both on magnetic tape and an ultra violet paper recorder. In addition to the output of the geophone the outputs of a time encoder and a radio receiver tuned to MSF Rugby were also recorded. An announcement of the shot detonation was broadcast to the receiving stations and, finally, the expected time of the next shot. The transmissions then ended and both recorders on Hawthorn were switched off. The magnetic tape recorder was restarted just before the first warning announcement

and all broadcasts were recorded on a voice channel on the tape. The ultra violet recorder was only used for the short period of shot arrivals at the ship. At regular intervals throughout the shooting programme the time encoder output was recorded with MSF Rugby on magnetic tape in order to determine any drift of the encoder so that absolute time could still be obtained when MSF was not available. The output of the time encoder was also periodically transmitted so that any receiving stations unable to obtain MSF could calibrate their timing system against that of the shooting ship.

2.3 The Receiving Stations

All the receiving stations apart from the Soviet vessel Lomonosov employed frequency modulated magnetic tape recording. Absolute radio time, either MSF or WWV, was received at all stations and in addition most had a time encoder which was regularly calibrated against radio time. Most of the land receiving stations recorded continuously throughout the project and the ship receiving stations recorded continuously throughout each day's shooting.

Five land receiving stations were provided and operated by Durham University under the supervision of Dr. R.E. Long. Each station consisted of a three component set of Willmore MK I (1Hz) seismometers and a small portable recording system (Long, 1974). The recording system comprises a three channel amplifier and frequency modulator unit, a digital clock, and a tape recorder unit. Eight track $\frac{1}{4}$" magnetic tape was used to record the output of the three instruments, encoded time from the digital clock, radio time from MSF Rugby or WWV, and a standard frequency used for flutter compensation. A recording speed of 0.1"/sec was used which allowed up to 3 days

continuous recording on a single 7" tape reel. The amplitude response function of the system is flat up to about 20 Hz, apart from at high gains when a filter is introduced to limit the bandwidth to a range expected for distant events, and therefore, increase the effective dynamic range. One of the five stations was situated on Iceland but is not discussed here as it received no arrivals from the shots in the Scotland-Faeroe region. The other stations were:-

1. DU1 situated at Esha Ness on the Shetland Islands (60° 29.74'N, 1° 34.14'W). The seismometers were placed in a shallow peat pit on a concrete base laid on the extrusive rhyolite lava basement of Old Red Sandstone age.
2. DU2 situated at Chair of Lyde on the Orkney mainland (59° 03.02'N, 3° 06.67'W). The seismometers were placed on Rousay flags of the Middle Old Red Sandstone.
3. DU3 situated at Torrin on the Isle of Skye (57° 12.67'N, 6° 00.49'W). The seismometers were placed on the granite intrusion forming part of the Skye intrusive complex.
4. DU4 situated near the southern tip of Streymoy in the Faeroe Islands (61° 59.89'N, 6° 47.96'W). The seismometers were placed on the upper series Tertiary basalt lava.

At each of these stations there was one vertical and two horizontal seismometers, one aligned north-south and the other aligned east-west.

The IGS Global Seismology Unit provided and operated three land receiving stations under the supervision of Dr. B. Jacob. Each station employed Willmore MK II (1Hz) seismometers and all recording was on 24 track magnetic tape. The output of a time encoder, radio time, and a standard frequency used for flutter compensation were also recorded.

The stations occupied were:-

1. IGS1 situated at Cape Wrath (58° 37.45'N, 4° 59.77'W). A three component set of one vertical and two horizontal instruments with one horizontal seismometer aligned north-south and the other east-west, together with two outlying vertical seismometers approximately 1 km each away from the centre point. These were all placed on outcropping Lewisian gneiss.

2. IGS2 situated on the Butt of Lewis (58° 27.32'N, 6° 13.24'W). This station had only one vertical seismometer again positioned on the Lewisian metamorphic basement. The instrument was in line of sight and radio linked to station IGS1, the output of the seismometer being transmitted to the recording system at Cape Wrath.

3. IGS3 situated on the southern tip of Ardnamurchan (56° 41.18'N, 6° 8.21'W). A three component set aligned similarly to that at station IGS1 was placed on Jurassic sandstones and limestones adjacent to the Tertiary basaltic lava associated with the Ardnamurchan intrusive complex.

In addition to these temporary IGS stations, all the magnetic tapes recorded during NASP at the Lownet array station (Crampin, 1970) were made available for processing.

The UKAEA Seismology Unit under the direction of Dr. H. Thirlaway provided a seismometer array station which was operated by Durham University personnel. The station was situated near Walls on the Shetland Islands (60° 15.03'N, 1° 34.79'W). Eleven Willmore MK II (1Hz) seismometers were placed in pits in a cross pattern, the arms of the cross being aligned approximately north-south (345° true) and east-west (77° true) respectively. (Fig. 2.2). The pits were prepared several months before the project and were dug down

Figure 2.2 : The UKAEA array station located on the Shetland mainland.

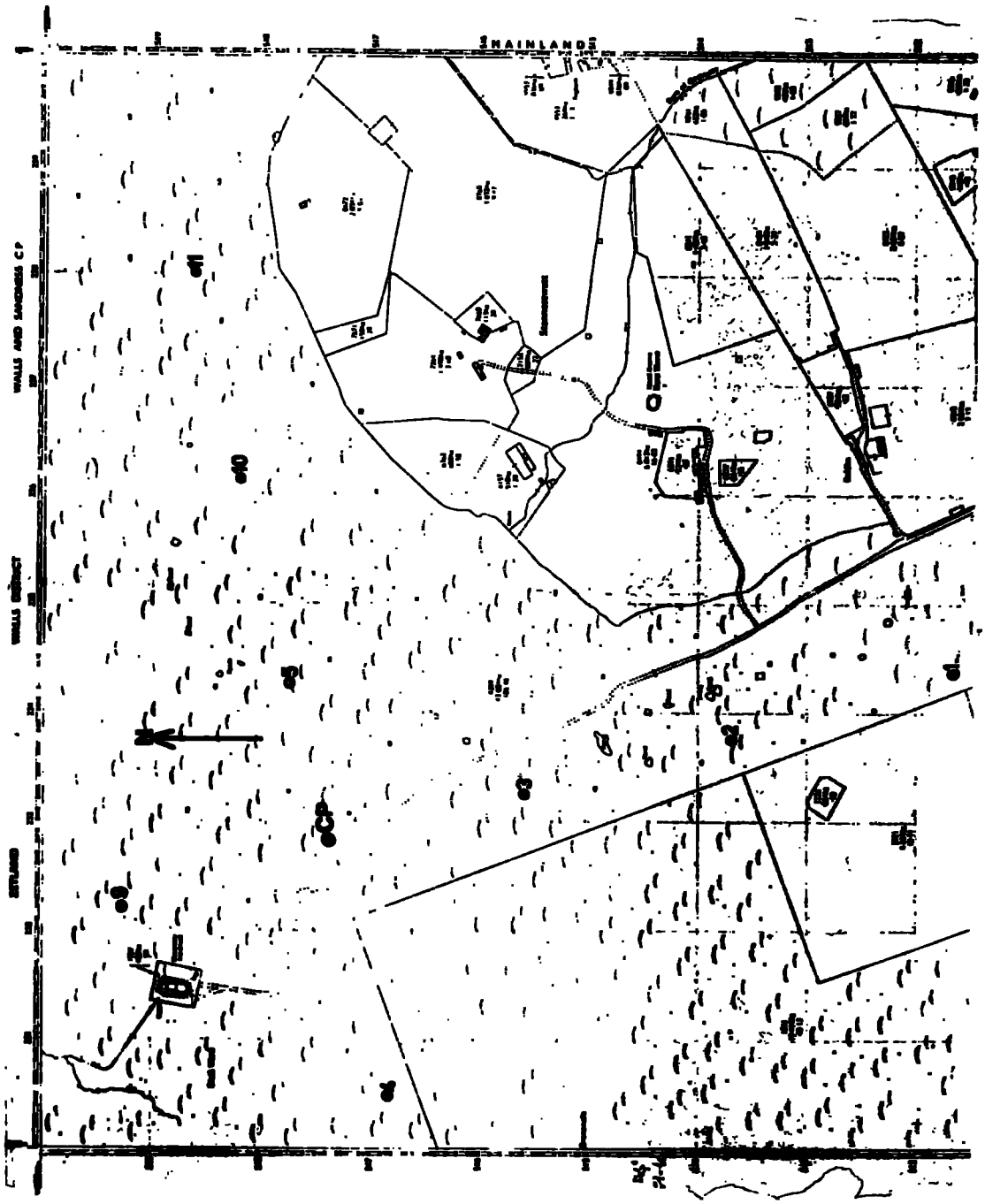
MAINLAND
WALLS AND SANDNESS CP
WALLS DISTRICT
STUARD

through a few feet of peat cover to the Walls Old Red Sandstone basement. Each pit had a concrete base and, apart from the large centre point pit, contained a plastic cylindrical tube covered at the surface in an attempt to keep the pit water-tight. All the seismometers were linked by cable to a central recording caravan located at the foot of the north-south arm of the array. The available cable limited the size of the array and it was just possible to obtain an aperture of 1 km. The centre point pit contained three seismometers, one vertical and two horizontal, with one horizontal aligned north-south and the other east-west. All the other pits contained only one vertical seismometer. Each arm of the array consisted of five pits with an approximate pit spacing of 200m.

An amplifier for each instrument was located in every pit adjacent to the seismometer. The output of the amplifier was then fed, via the cables, to the recording caravan and into a second or main amplifier with finer gain control. The outputs of these amplifiers were frequency modulated and recorded on 24 track magnetic tape. In addition to the output of the eleven seismometers, radio time, the output of a time encoder and two standard frequencies used for flutter and wow compensation were also recorded. This left nine tracks available on the magnetic tape which were used to record the outputs of nine of the seismometers after first being passed through a frequency filter. Unfortunately, these filters had fixed pass bands and none was suitable for recording the seismic arrivals. A lower pass band of 2-4 Hz was available or a higher pass band of 4-16 Hz but the frequency of the onset was estimated to be approximately 4 Hz. The 4-16 Hz pass

band was used. A 16 channel jet pen recorder was used to monitor the arrival wavetrain for each shot. No replay head was available on the tape recorder and so no monitoring of the recorded signal could be performed. The signal output of the amplifier was sent to the tape recorder, a frequency filter and the jet pen monitor, by means of a switching matrix pinboard system in the recording caravan.

Recording stations were also provided and operated on the Scottish Mainland by the Universities of Aberdeen, Lancaster and Birmingham/Leicester, and on the northern coast of Ireland by the Dublin Institute of Advanced Studies. The individual stations occupied were:-

1. UAB provided by Aberdeen University under the supervision of Dr. Ashcroft, and situated near Lairg (58° 4.33'N, 4° 42.0'W). Five vertical component (2 Hz) seismometers arranged in a cluster were positioned on outcropping siliceous Moine granulites. The outputs of the instruments were amplified, frequency modulated and recorded on eight track magnetic tape together with radio time (MSF Rugby) and a standard reference frequency used for flutter compensation. A recording speed of 15/16" per second was used. The radio broadcasts from the shooting ship, MV Hawthorn, were received from as far out as Iceland, and the tape recorder was only switched on at the time of each shot drop.

2. ULA provided by Lancaster University under the supervision of Dr. Blundell, and situated near Bonar Bridge (57° 45.27'N, 4° 22.45'W). A three component set of Geospace HS 10 (2 Hz) seismometers were situated on siliceous schists and granulites of the Moinian. One of the seismometers was aligned vertically and the other two horizontally, one north-south and the second

east-west. After amplifying and frequency modulating the seismometer outputs they were recorded on four track magnetic tape together with radio time (MSF Rugby). This station recorded continuously.

3. UBL provided by Birmingham and Leicester Universities under the supervision of Drs. King and Khan and situated near Kingussie (57° 4.59'N, 4° 8.54'W). A three component set of Geospace HS 10 (2 Hz) seismometers aligned similarly to those of station ULA, were situated on undifferentiated psammitic Moine schist. In addition to the seismic channels, radio time (MSF Rugby), encoded time from a crystal clock and a standard reference frequency for flutter compensation were also recorded.

4. MHD provided by the Dublin Institute for Advanced Studies under the supervision of Professor T. Murphy and situated at Malin Head (55° 18.63'N, 7° 18.66'W), on Dalradian quartzites. This station was only operated for shots C1-C33, B60-B70, and lines D, E and F, as it was thought that no arrivals would be received from the more distant shots. A three component set of Willmore MK II (1 Hz) seismometers was used from July 10th-12th (shots C1-C33). One of the instruments was aligned vertically and the other two horizontally, one north-south and the second east-west. During the remainder of the recording (July 28th-31st) two Willmore seismometers aligned vertically and located 200 m apart were employed. A three channel Akai tape recorder was used so only two seismometer outputs plus radio time (MSF Rugby) could be recorded. The station recorded continuously during the dates given above.

Six stations were provided on the Faeroe Islands by Aarhus University. However, as yet, very little information

about these stations or the results they obtained has been sent to Durham. Some of their results from the Faeroe Plateau have been included in this thesis.

MV Miranda provided a ship recording station at five positions during the project. Two of these positions were on line A and one of these recorded no arrivals from the shots dealt with in this thesis and so is not described here. The remaining four stations had the following mean positions determined by loran C position fixes:-

1. 59° 41.0'N, 05° 35.5'W MIR(A)

This position was approximately at the break in slope of the Scottish continental shelf and was maintained during July 11th and 12th for shots C1-C24.

2. 60° 08.0'N, 05° 54.0'W MIR(B)

This station was over the middle of the southern end of the Faeroe/Shetland Channel. It was maintained during July 14th and 15th for shots C25-C59 and shots CB1-CB48.

3. 61° 01.21'N, 03° 54.64'W MIR(C)

This station over the northern end of the Faeroe/ Shetland Channel was maintained during July 16th for shots BC1-BC49.

4. 62° 29.0'N, 08° 35.0'W MIR(D)

This station was situated over the north-west edge of the Faeroe Plateau. Only the arrivals at it from shots A1-A6 have been included in this thesis.

At these four stations Miranda operated two neutrally buoyant hydrophones floating approximately 30-40 m below the sea surface. The ship either hove-to or steamed gently against the tide in an effort to maintain her position and the hydrophones were trailed about 60 m astern. At each position

a buoy was launched and anchored and visual fixes were taken on it, so the relative accuracy of the ship position for each shot was very good. The absolute accuracy in Miranda's positions is estimated to be about 1-2 km. The outputs of the two hydrophones were led by cable to an amplifier and frequency modulator unit on board the ship, and then to a six channel magnetic tape recorder. Encoded time from a digital clock and absolute radio time, WWV or MSF, were also recorded. The digital clock was calibrated against radio time up to ten times each day.

The Soviet research vessel Mikail Lomonosov provided a ship recording station at five positions during the project and four of these were located on lines south of the Faeroes. The mean positions of these four stations determined by the loran C navigation system were:-

1. 61° 02.7'N, 06° 25.1'W LOM FS(A)

This station was at the extreme southern edge of the Faeroe Plateau and occupied during July 11th, 12th and 14th for shots C1-C52.

2. 60° 58.0'N, 04° 01.35'W LOM FS(B), LOM FS(C), LOM BS(A)

This station was over the middle of the northern end of the Faeroe/Shetland Channel. It was occupied during July 15th and 16th for all the shots on lines CB and BC. The position of the hydrophone station varied slightly for lines CB(LOM FS (B)) and BC(LOM FS(C)).

3. 60° 59.7'N, 03° 45.2'W LOM FS(D) LOM BS(B)

This station was in a position very similar to position 2. It was occupied during July 24th for all the shots on line B part 1 i.e. B1-B30.

4. 60° 41.3'N, 04° 40.3'W LOM FS(E) LOM BS(C)

This station was again over the middle of the northern end of the channel but south-east of the two previous positions. It was occupied during July 25th for all the shots on line B part 2 i.e. B31-B70.

At all four of these positions Lomonosov operated a single neutrally buoyant hydrophone station, FS, and at all but the first position an ocean bottom seismic station, BS, was also operated. The bottom station consisted of a three component set of seismometers, one vertical and the other two horizontal, with the two horizontal aligned perpendicular to each other. A crystal clock and time encoder, three seismic amplifiers, an AM unit and a four channel magnetic tape recorder were also part of the bottom station. The amplifier outputs were amplitude modulated and recorded with the encoded version of the crystal clock time output on the magnetic tape. All the bottom station equipment was mounted in a metal cylindrical casing and lowered to the sea bed where it was moored by cable to an overhead buoy.

The output of the hydrophone was also amplified, then amplitude modulated and recorded with absolute radio time, MSF Rugby, and the encoded version of a crystal clock output on magnetic tape on board Lomonosov. The crystal clock of the bottom station was regularly calibrated against absolute radio time during the periods between shooting different lines when the station was hauled on board ship.

2.4 Data Preparation and Reduction

2.4.1 Shot Point Data

2.4.1.1 Shot Positions

The shot positions were calculated from Decca and radar

fixes and plotted on the appropriate Admiralty charts. MV Hawthorn attempted to maintain a constant speed through the water along each shot line, and this was used as a check on the shot positions. For any three shots, A, B and C in line, if the ship's velocity determined between shots A and B was high and that between shots B and C was low, then most probably the position of shot B was incorrect. Strong tidal currents with velocities of a few knots occur on the Scottish Shelf near Cape Wrath and the Orkney and Shetland Islands. These had to be allowed for as they could cause the constant velocity of the ship through the water to be a variable velocity with respect to the land surface. However, tidal stream data was only available to the nearest hour and for widely separated positions. It was, therefore, only used to indicate what approximate variations in the velocity of the ship relative to the land surface would be expected along the line of shots. Almost all the shot positions plotted correctly, but, by using the ship's velocity as a check, a few were found to have obvious errors, such as an incorrect Decca lane reading, or a position fix taken at shot detonation used for the position of shot drop. The shot positions are listed in Appendix A. The estimated error in positions varied between 1-2 km.

2.4.1.2 Shot Depths

The depth of any individual shot could be determined if it were possible to identify on the arrival wavetrain record of MV Hawthorn the reflected arrival from the sea bed. The time difference between the onset of this arrival and that of the direct water wave was used with the shot to ship distance and the total water depth to determine the shot depth.

As the reflected arrival could only be identified for about 40-50% of the shots these shot depths had to be used to establish sink rates for each charge size. The remainder of the shot depths were then determined as the product of the appropriate sink rate with the burning time of the fuse. This method gave inaccurate results for some of the shots as the explosive charge did not sink immediately but floated on the surface. However, no note was made of the few charges which did float, and so, as an attempt to correct for these, any charge which had an abnormally large burn time, suggesting some time floating on the surface, was given a mean depth estimate. The accuracy of most of the shot depths is estimated to be about 20 m. The shot depths are given in Appendix A.

2.4.1.3. Water Depths

The water depth at the time of shot drop was read off the PDR record in the laboratory at Durham to remove any errors in the listing of these depths whilst at sea. The PDR on MV Hawthorn had been set up for a velocity of sound in sea water of 1.5 km s^{-1}, and so the water depths determined had to be corrected for the appropriate value of this velocity found in Matthew's Tables (1939).

2.4.1.4 Shot Instants

The shot instants were well recorded on MV Hawthorn and the onsets read to the nearest 0.01 seconds. A problem was encountered with the timing on lines CB and BC. No time marks were recorded for ten shots and so these shots were effectively lost.

A correction for the travel time of the water wave from

the shot to the shooting ship had to be applied to the shot instant time. The time between shot drop and shot detonation was recorded on MV Hawthorn by stop-watch for each charge, and this time was used with the ship's velocity to determine the distance astern of the shot. This distance divided by the appropriate value of the velocity of sound in sea water was the drop-bang correction that was applied to each shot instant. The corrected shot instants are listed in Appendix A.

2.4.2 Recording Station Data

All the data recorded by Durham University stations was replayed in the processing laboratory of the Department of Geological Sciences, Durham University. The tapes recorded at IGS stations were made available together with their processing facilities at the Global Seismology Unit in Edinburgh. Some of these tapes were also replayed in the Durham Laboratory. The Universities of Aberdeen, Lancaster and Birmingham/Leicester, and the Dublin Institute of Advanced Studies each replayed the tapes that they recorded during NASP and sent their paper playouts to Durham. However on many of the Lancaster University and Birmingham/Leicester University records, there was doubt as to the actual onset time, and so most of their tapes were also replayed again at Durham. The Soviet Institute of Physics of the Earth provided a comprehensive list of the travel times observed at the stations operated by their research vessel Lomonosov, and Aarhus University provided a list of some of the travel times recorded at their stations on the Faeroe Islands.

2.4.2.1 Magnetic Tape Replay and Filtering employed

The Durham University magnetic tape replay system allows

the output from each tape track to be displayed on either a sixteen channel oscilloscope or a sixteen channel jet pen recorder. It is also possible to audio monitor any of the tape tracks. The output from any tape track is firstly demodulated and then may be passed through up to three Krohn-hite frequency filters or, alternatively, digitised and fed into the Modular One computer for digital processing. The output from the frequency filters or computer is displayed on the oscilloscope or paper recorder. A maximum of 24 tape channels can be transcribed at any one time. The system has been designed to allow flutter to be automatically removed from each of the seismometer outputs if it is taken off the tape on either channel 7 or channel 11.

All the Durham University stations recorded in the field at a tape speed of 0.1 i.p.s., and were replayed onto paper in the laboratory at ten times real time. Initially it was attempted to read the first arrival onsets from the unfiltered records, but in the majority of cases this proved to be difficult. Optimum frequency filtering was then applied, by means of the Krohn-hite filters, and in general a pass band of 2-8 Hz was found to give the best improvement. The onsets were read off to the nearest 0.01 seconds although the accuracy with which this reading could be made varied considerably.

The onsets of some records were masked by noise of a similar frequency to the arrival, even though the signal to noise ratio was high. A polarisation filter was used to improve the picking of these onsets. This filter was programmed for the Departmental Modular One computer by Boynton (private communication), and discriminates in favour

of the rectilinearly polarised signal relative to the elliptically polarised noise (Shimshoni and Smith, 1964). The outputs of the vertical, and one horizontal seismometer were fed into the computer and their time averaged cross-product taken and multiplied by the original output of the vertical seismometer. This final product was output to the paper recorder and represents a function of ground motion in which rectilinearly polarised motion is enhanced. The filter was found to improve emergent arrivals but could not 'pull out' onsets that were almost completely immersed in noise.

The data obtained on the UKAEA array station tapes was recorded at a speed of 0.3 i.p.s. These tapes were replayed at three times real time in the same way as the Durham University tapes. However in addition to frequency filtering the arrivals at this station were also velocity filtered (Birthill and Whiteway, 1965), to discriminate between signal and noise on the basis of their velocity distributions. An attempt was first made to use the array to search for the correct phase velocity. However, for Moho arrivals it was found that using phase velocities of 7.9, 8.0 and 8.1 km s^{-1} produced no change in the amplitude of the processed output. This was probably due to the aperture of the array being too small (1 km) to allow such discrimination. A program was written for the Modular One computer in which the approximate velocity across the array (8 km s^{-1} for Moho arrivals) was used to delay the arrivals at each seismometer pit to the centre point pit. These delayed arrivals were then summed for each arm of the array, the two sums cross multiplied, and the product of this multiplication integrated over a time window of 0.2 seconds. To carry out this analysis the

demodulated tape outputs were digitised at a rate of 80 samples per second, and then fed directly into the Modular One computer. The velocity filtering was found to greatly clarify the identification of emergent onsets. (Fig. 2.3). However, as large a signal to noise ratio was obtained for the summed output of the two array arms as for the cross multiplied and integrated outputs.

The IGS, ULA and UBL tapes were replayed at Durham in a similar manner as for the Durham University tapes, but at speeds of eight times real time, 0.5 times real time, and eight times real time respectively. The tapes recorded in the field at the IGS stations and station ULA could be replayed in the Durham laboratory, but the tapes recorded at station UBL had to be transcribed onto other tapes in a format suitable for replay at Durham. This was kindly performed by Drs. Khan and Maguire at Leicester University. It was necessary to use the Modular One computer to remove flutter from the seismic channels of the UBL station tapes. This was due to flutter coming off the tape on either channel 9 or 10, neither of which can be automatically subtracted on the Durham replay system.

2.4.3 Shot-Station Ranges

Shot-station ranges were calculated on the NUMAC IBM 360/67 digital computer using the method of Rudoe (Bomford, 1962). The method treats the earth as an ellipsoid of revolution and uses a series formula to compute the distance between any two points, defined by their latitude and longitude, on this surface. An accuracy is claimed of 1 in 10^7 at any range. A check on the method was performed

Figure 2.3 : A velocity filtered record of the UKAEA array station.

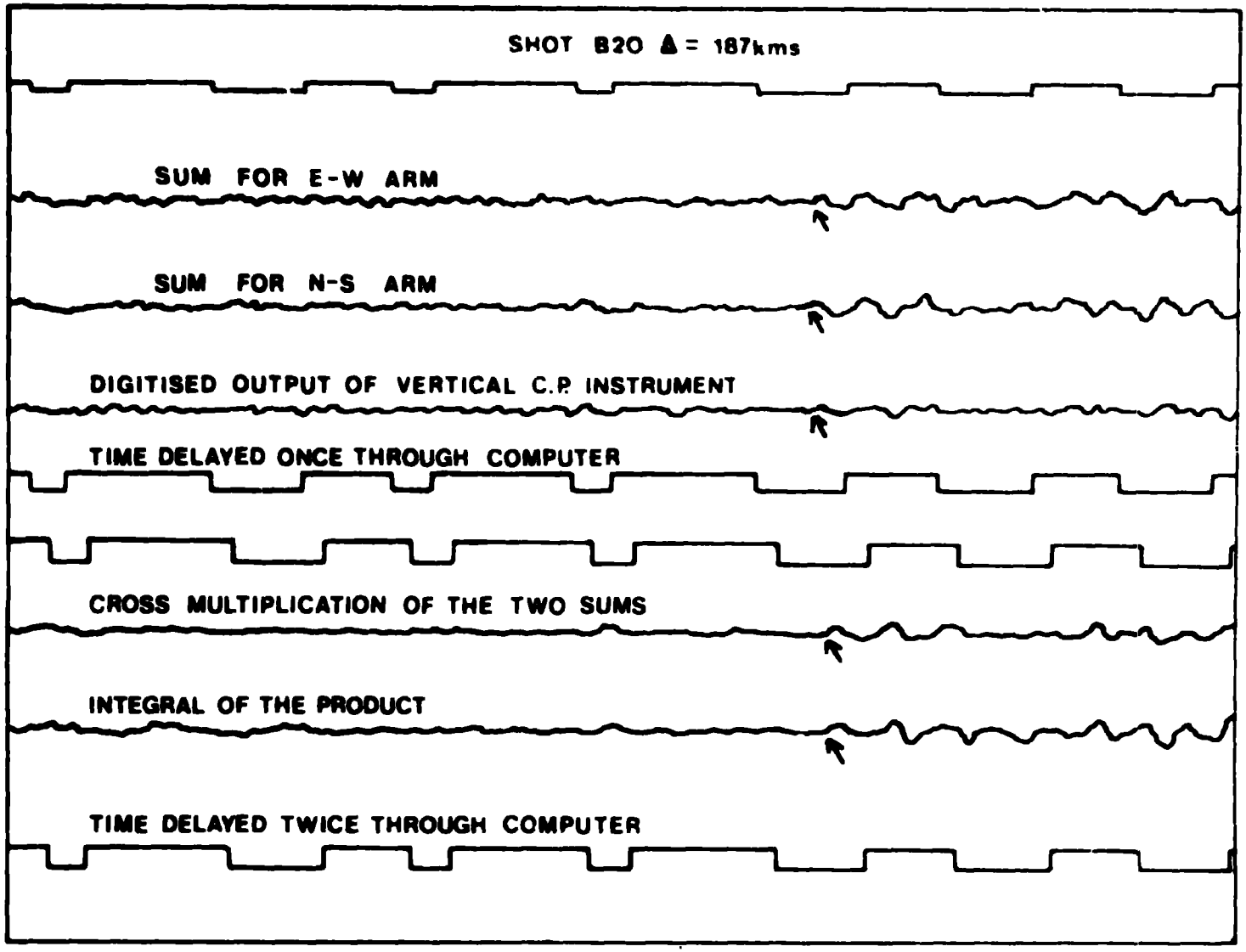
SHOT B20 Δ = 187kms
SUM FOR E-W ARM
SUM FOR N-S ARM
DIGITISED OUTPUT OF VERTICAL C.P. INSTRUMENT
TIME DELAYED ONCE THROUGH COMPUTER
CROSS MULTIPLICATION OF THE TWO SUMS
INTEGRAL OF THE PRODUCT
TIME DELAYED TWICE THROUGH COMPUTER

by calculating ranges along great circle paths both with this formula and by the normal arc length method, and also by calculating ranges between set coordinates previously determined by Holder (1969). The two sets of results were found to agree.

A complete list of all the shot-station ranges together with the first arrival travel times is given in Appendix B.

CHAPTER 3

Interpretation Methods

3.1 Introduction

The North Atlantic Seismic Project was designed to allow data interpretion by the classical method of reversed straight line travel time graphs, and by the more detailed method of time term analysis.

The first stage in any refraction interpretation is to fit straight line segments to the first arrival travel time-distance graphs for each station and line. This gives an indication of the number of refractors, and their P wave velocities, that are present in the area. If reverse coverage is available then true refractor velocities are obtained from the apparent velocities measured in opposite directions.

In some instances it can be difficult to decide if the velocities observed at different stations from the same shots represent one or more refractors. The minus time method of Hagedoorn (1959) can be used to solve this problem if the shot-station configuration sufficiently approximates a line of shots symmetrically located between two receiving stations.

Once it is decided which refractors are present and the arrivals that are from them time term analyses can then be carried out for the individual refractors. This will produce an estimate of the variation in structure from shot to shot.

After such a first arrival interpretation has been obtained later arrivals may then be considered. Stacked record sections provide an aid in the identification of useful later arrivals. These stacked record sections consist of all the arrivals from a particular line of shots at one recording station. The arrival wavetrain is traced for each shot and

mounted at the correct shot distance, and time since shot detonation on a reduced travel time, distance framework. The reduced travel time is given by:

$$T_{red} = T_{obs} - \Delta/6$$

where T_{red} is the reduced travel time in secs

T_{obs} is the observed travel time in secs

Δ is the shot-station range

6.0 is the reducing velocity chosen as an estimate of the crustal basement velocity

The stacked record section is very useful for identifying the reflected phase from the Moho (P_mP). This phase can be used to provide an estimate of the critical distance and from this, the average crustal velocity and mean thickness without having to assume a crust of constant velocity layers.

After a crustal structure model has been estimated by the previous interpretation methods it can be tested by calculating the arrival times for various phases travelling through the model. A good agreement between these calculated travel times and those actually observed demonstrates that although the crustal model is not unambiguous it can at least explain the observed travel times.

3.2 The classical method

This method involves the construction of travel time - distance graphs (Dobrin, 1960). Straight line segments are fitted to these graphs by the method of least squares which has been programmed for use on the IBM 360/67 computer. The layering in the earth beneath the line of shots and recording station determines the form of the travel time - distance graph. In the ideal case the number of segments on the graph

is equal to one plus the number of layers overlying a half-space. The first segment represents direct arrivals along the surface, and the final segment refracted arrivals from the top of the half-space. The intermediate segments represent refracted arrivals from the tops of all the intermediate layers. The apparent velocity of each layer is equal to the reciprocal gradient of the corresponding segment of the travel time graph, and the thickness of any layer is given by the formula:

$$Z_n = \frac{V_n V_{n+1}}{2\sqrt{V_{n+1}^2 - V_n^2}} \left(Ti_{n+1} - \frac{2Z_1\sqrt{V_{n+1}^2 - V_1^2}}{V_{n+1}V_1} - \frac{2Z_2\sqrt{V_{n+1}^2 - V_2^2}}{V_{n+1}V_2} - \ldots \right.$$

$$\left. \ldots - \frac{2Z_{n-1}\sqrt{V_{n+1}^2 - V_{n-1}^2}}{V_{n+1}V_{n-1}} \right) \ldots\ldots\ldots \quad (1)$$

where Z_n = thickness of nth layer

V_n = velocity of nth layer

Ti_{n+1} = time intercept for V_{n+1} segment

The method assumes homogeneous plane layering beneath the shot points and recording station, and also that the layers exhibit a discontinuous or step-like velocity increase with depth. Lateral structural and velocity changes are quite common in the upper crust and so the first assumption is not always valid. The second assumption may not always hold, particularly for deeper structures where occasionally a velocity increase with depth has been shown to occur (Holder and Bott, 1971).

Horizontal layering need not be assumed if reversed coverage of each layer is available. A true velocity and dip can be determined for the layer from the formulae:

$$\alpha = \tfrac{1}{2}(\sin^{-1}\mathrm{Vom}d - \sin^{-1}\mathrm{Vom}u)$$

$$i_c = \tfrac{1}{2}(\sin^{-1}Vomd + \sin^{-1}Vomu)$$

$$V_t = Vo/\sin i_c$$

where V_o = velocity of overlying layer

md = gradient of travel time-distance segment in downdip direction

mu = gradient of travel time-distance segment in updip direction

α = angle of dip of the refractor

i_c = critical angle

V_t = true refractor velocity

The updip and downdip thicknesses of the layer above the dipping refractor are determined from equation (1) with Ti_u (updip refractor intercept time) or Ti_d (downdip refractor intercept time) substituted for Ti_{n+1}, and the result divided by $\cos\alpha$.

Any unreversed velocity is unreliable and so the accuracy of the result of any calculation using such a velocity is decreased.

As well as errors in shot-station positions and picked onset times the classical method may also suffer from non-planar interfaces and hidden velocity layers at depth. A layer is considered to be 'hidden' if it does not give rise to any first arrivals at a recording station. This will occur if a deeper layer has a lower velocity than the overlying layer as no head waves will result for the layer. However a layer of higher velocity than the overlying layer may also be hidden if it is sufficiently thin to give rise to first arrivals only over a limited range of distance not covered by the shot-station spacing. Such hidden layers will normally cause the calculation of depths to horizons below the layers to be

underestimates of the true depths.

3.3 The Plus-Minus Method

The Plus-Minus method (Hagedoorn, 1959) is an approximation version of Thornbourgh's wavefront method (Thornbourgh, 1930). It is applicable for a system of shots lying between two receiving stations or, conversely, a system of receiving stations between two shots.

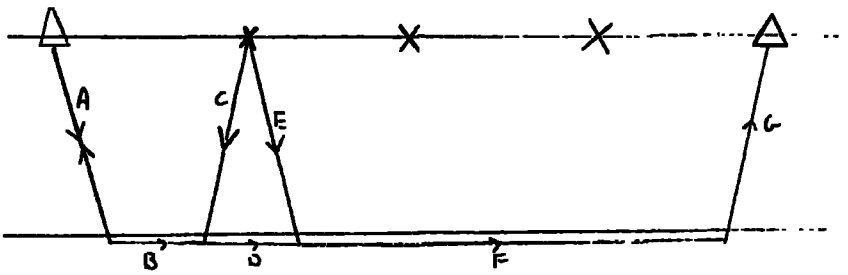

$$P.T. = A+B+C+E+G-(A+B+D+F+G) = C+E-D$$

$$M.T. = A+B+C-(E+F+G)$$

Plus times are determined as the sum of the two travel times from each shot point to the two symmetrically placed recording stations, minus the total travel time from one recording station to the other. In order to determine this total travel time it is necessary to have a shot point coincident with one of the recording stations. The Plus time values represent the time taken in travelling through the overlying layer to the refractor in two opposite directions. They are interpreted in terms of depths to the refractor by multiplying by the term:

$$V_2V_1/2\sqrt{V_2^2-V_1^2}$$

where V_1 is the velocity of the overlying material

V_2 is the refractor velocity

The data obtained by NASP was decided to be more suitable for

interpretation by time term analysis than by Plus times. Plus times are one particular case of time term analysis where the value for a shot point is found by averaging observations from two opposite directions. However, a shot point time term is obtained using observations in every direction for which a travel time is available, and is therefore better determined.

Minus times are the values obtained by subtracting the pair of travel times for each shot point to the two recording stations. As the same shot gives rise to arrivals from the same refractor at both stations the time delay caused by the overlying material beneath the shot point can be removed. This is accomplished by assuming the delay in opposite directions beneath the shot point to be constant, and by equating the differences in travel times to the differences in range.

$$t_{ij}-t_{ik} = (\Delta_{ij}-\Delta_{ik})/V + a_i - a_i+b_j-b_k$$

where t_{ij} is the travel time between shot i and station j

Δ_{ij} is the distance between shot i and station j

a_i is the delay time of shot i

b_j is the delay time of station j

A graph of minus times $(t_{ij}-t_{ik})$ against the distance differences $(\Delta_{ij}-\Delta_{ik})$ gives a measure of the refractor velocity beneath the shots unaffected by variations in shot point structure.

3.4 Time Term Analysis

The time term analysis method (Willmore and Bancroft, 1960) represents the travel time data for a system of shots and stations and a single refractor of velocity V as:

$$t_{ij} = \Delta_{ij}/V + a_i+b_j$$

where t_{ij} is the travel time between shot i and station j

Δ_{ij} is the distance between shot i and station j

a_i is the delay time or time term of shot i

b_j is the delay time or time term of station j

The method also assumes that the refractor has negligible dip and that the time terms are independent of azimuth. The independence of azimuth is inherent in the assumptions that the cone of rays between the refractor and the station or shot passes through overburden in which the velocity structure is a function only of depth normal to the refractor, and that all the points of refraction for the shot or station lie within a common plane.

Regression analysis is performed to minimise the sum of the squares of the residuals between the observed and theoretical travel times where:

$$R_{ij} = (T_{ij} - t_{ij})$$

R_{ij} is the residual for the travel time from shot i to station j

T_{ij} is the observed travel time between shot i and station j

To obtain a solution for the unknowns, the time terms and refractor velocity, the number of observed travel times and therefore the number of observational equations must be equal to or greater than the number of unknowns. If the solution obtained is to be unique one time term must be assigned a value or two time terms equated by one shot point and station having the same location.

The computational technique described by Berry and West (1966) and programmed by Bamford (1970) has been adapted for the IBM 360/67 computer available at Durham. Regression analysis is performed to minimise R where:

$$R = \sum_{i=1}^{K} \sum_{j=1}^{K} P_{ij}(T_{ij}-t_{ij})^2 \quad \ldots\ldots \quad (A)$$

for K sites

where $P_{ij} = 1$ if T_{ij} exists as data

$= 0$ if T_{ij} does not exist as data

The minimisation is achieved by differentiating equation (A) with respect to each of the k time terms and setting each resulting expression equal to zero. In the ith case:

$$\frac{\partial R}{\partial a_i} = 0$$

which is equivalent to:

$$\sum_{i=1}^{K}\sum_{j=1}^{K} a_j P_{ij} + \sum_{i=1}^{K} a_i \sum_{j=1}^{K} P_{ij} = \sum_{i=1}^{K}\sum_{j=1}^{K} P_{ij}(T_{ij}-X_{ij}/V)$$

A set of k of these normal equations is obtained which may be represented in matrix form by:

$$\left[A_{ij}\right]\left[a_j\right] = \left[\sum_{j=1}^{K} P_{ij}(T_{ij}-X_{ij}/V) + P_{ji}(T_{ji} - X_{ij}/V)\right]$$

where $A_{ij} = P_{ij}+P_{ji}$, $i \neq j$ $\qquad A_{ii} = \sum_{j=1}^{K}(P_{ij}+P_{ji})$

The matrix equation is solved for the time terms a_j by multiplying both sides of the equation by the inverse matrix $\left[A_{ij}\right]^{-1}$

thus: $$\left[a_j\right] = \left[A_{ij}\right]^{-1}\left[\sum_{j=1}^{K}(T_{ij}P_{ij}+T_{ji}P_{ji}) - (X_{ij}/V)(P_{ij}+P_{ji})\right]$$

After inverting the coefficient matrix $\left[A_{ij}\right]$ the following matrices are calculated:

$$\left[e_j\right] = \left[A_{ij}\right]^{-1}\left[\sum_{j=1}^{K} T_{ij}P_{ij}+T_{ji}P_{ji}\right]$$

$$\left[f_j\right] = \left[A_{ij}\right]^{-1}\left[\sum_{j=1}^{K} X_{ij}(P_{ij}+P_{ji})\right]$$

so that the time term matrix is then defined as:

$$\left[a_j\right] = \left[e_j\right] - \left[f_j\right]/V$$

The refractor velocity may be assigned a value or obtained by regression analysis. It is determined by differentiating equation (A) with respect to the reciprocal velocity and setting the resulting expression equal to zero. The final expression obtained for the velocity is:

$$V = \frac{\sum_{i=1}^{K}\sum_{j=1}^{K} P_{ij}(X_{ij}-f_i-f_j)^2}{\sum_{i=1}^{K}\sum_{j=1}^{K} P_{ij}(X_{ij}-f_i-f_j)(T_{ij}-e_i-e_j)}$$

The time terms are converted to depths using a constant velocity layer structure above each site. The thickness of the nth layer is given by:

$$Z_n = \left[a_n - \frac{Z_1\sqrt{V_n^2-V_1^2}}{V_nV_1} - \frac{Z_2\sqrt{V_n^2-V_2^2}}{V_nV_2} - \cdots \right.$$

$$\left. \cdots - \frac{Z_{n-1}\sqrt{V_n^2-V_{n-1}^2}}{V_nV_{n-1}} \right] \frac{V_{n+1}V_n}{\sqrt{V_{n+1}^2-V_n^2}}$$

where Z_n is the thickness of the nth layer

V_n is the velocity of the nth layer

a_n is the time term of the nth layer

A measure of the fit of the time term solution to the input observational data is given by the standard deviation of the solution , where:

$$\sigma = \left(\frac{\text{sum of squared residuals}}{\text{no. of degrees of freedom in the system}} \right)^{\frac{1}{2}}$$

i.e. (the experimental error variance)$^{\frac{1}{2}}$

This is given by: $\sigma = \left[\frac{\sum_{i=1}^{K} \sum_{j=1}^{K} P_{ij} R_{ij}^2}{\left(\sum_{i=1}^{K} \sum_{j=1}^{K} P_{ij} \right) - (k+1)} \right]^{\frac{1}{2}}$

The standard errors on the time terms have been determined assuming uniform variance of the data at each site. This gives a measure of the unreliability of the time term dependent only on the inconsistency of the data at the particular time term site and not at the rest of the sites. The standard error on the kth time term is given by:

$$SE(a_k) = \sigma_k / \left[\sum_{i=1}^{K} (P_{ik}+P_{ki}) \right]^{\frac{1}{2}}$$

where $\sigma_k = \left[\frac{\sum_{i=1}^{K} (P_{ik}R_{ik}^2 + P_{ki}R_{ki}^2)}{\sum_{i=1}^{K} (P_{ik}+P_{ki}) - 1} \right]^{\frac{1}{2}}$

the standard error on the velocity is given by:

$$SE(V) = \frac{1}{V} \frac{\sigma}{\sum_{i=1}^{K} \sum_{j=1}^{K} P_{ij} R_{ij}}$$

The standard error on a time term provides an estimate of the unreliability of the time term based only on the lack of fit of the observed data at the site to the time term found. Experimental measurement errors are not included in this estimate and neither are any errors introduced by violation of the assumptions of the time term method. The travel time residuals reflect all the errors in the analysis and can be used both to remove unreliable data and as a check that the assumptions of the analysis are valid. A very large residual indicates that a particular travel time is unreliable and, as a rigorous check, if the residual is greater than three standard deviations (of the residual population about the median) away from the residual population median for that site, the travel time can be removed. Any significant trend in the residuals such as correlation with distance or azimuth will probably be related to some violation of the assumptions of the method, such as refractor dip or lateral variation in refractor velocity.

The shot-station configuration affects the reliability of the time terms. A configuration which provides wide azimuthal coverage at each site with velocity reversals and several interchange positions is desirable.

3.5 Later Arrivals

Any later arrivals identified as normal P or S head waves have been interpreted by the classical method. The phase reflected from the Moho, PmP, has been treated in a separate manner.

3.5.1. The PmP Phase

An estimate of the critical distance can be obtained from the position of the maximum amplitude of this reflected phase. Holder and Bott (1971) demonstrated that the critical distance can be used with the Moho intercept time to determine a mean crustal thickness without assuming a crust consisting of constant velocity layers.

The velocity V at a depth Z within the crust can be represented by:

$$V = \overline{V}(1+\delta)$$

where $\overline{V}$ is the mean crustal velocity

δ is a function of depth Z only

If V_n is the velocity of the underlying layer, then the intercept time ti is given by:

$$ti = 2\int_0^T (V_n^2 - V^2)^{\frac{1}{2}} V^{-1} V_n^{-1} dz$$

$$= 2V_n^{-1} \int_0^T \left[V_n^2 - \overline{V}^2(1+\delta)^2\right]^{\frac{1}{2}} \overline{V}^{-1}(1+\delta)^{-1}\, dz$$

$$= 2F^{-\frac{1}{2}} V_n^{-1} \int_0^T \left[(1-F(2\delta+\delta^2)\right]^{\frac{1}{2}} (1+\delta)^{-1}\, dz$$

where $F = \overline{V}^2/(V_n^2 - \overline{V}^2)$

Assuming that terms in δ^3 and higher powers of δ are small enough to neglect them:

$$ti = 2F^{-\frac{1}{2}} T\, V_n^{-1}(1+\varepsilon_1) \quad \ldots\ldots\ldots \quad (A)$$

where $\varepsilon_1 = (1+\frac{1}{2}F-\frac{1}{2}F^2)T^{-1} \int_0^T \delta^2 dz$ and T = crustal thickness

as $\int_0^T \delta\, dz = 0$

Similarly the critical distance X_c is given by:

$$X_c = 2F^{\frac{1}{2}} T(1+\varepsilon_2)$$

where $\varepsilon_2 = \frac{3F}{2T}(1+F) \int_0^T \delta^2 dz \quad \ldots\ldots\ldots \quad (B)$

Solving (A) and (B) gives:

$$T = \tfrac{1}{2}\left(\frac{X_c\, ti\, V_n}{(1+\varepsilon_1)(1+\varepsilon_2)}\right)^{\frac{1}{2}}$$

and $$\overline{V} = V_n \left(\frac{V_n ti(1+\varepsilon_2)}{X_c(1+\varepsilon_1)} + 1\right)^{-\frac{1}{2}}$$

which provide estimates of mean crustal thickness (T) and average velocity ($\bar{V}$).

3.6 Theoretical Travel Times

A program was written (AppendixD) to determine the theoretical travel times of crustal and mantle head waves, and the Moho reflection (PmP) phase, for models assuming:

1. Horizontal layering with constant velocity layers
2. Horizontal layers of constant velocity apart from the lower crustal layer immediately above the Moho where the velocity is assumed to increase linearly with depth.

MODEL 1

The travel times of the refracted arrivals are determined from the delay time formula (Dobrin, 1960).

$$T = \frac{X}{V_{n+1}} + \frac{2Z_1\sqrt{V_{n+1}^2-V_1^2}}{V_{n+1}V_1} + \frac{2Z_2\sqrt{V_{n+1}^2-V_2^2}}{V_{n+1}V_2} + \ldots + \frac{2Z_n\sqrt{V_{n+1}^2-V_n^2}}{V_{n+1}V_n}$$

where T is travel time for the head wave of the n+1 th layer

Z_n is the thickness of the nth layer

V_n is the velocity of the nth layer

X is the shot-station range

The travel times of the reflected PmP phase are determined by a ray tracing technique, as there are no exact solutions of the geometrical expression relating the path length of the phase, in terms of the angle of incidence of the ray at the first boundary, to the total shot-station range. The expression would have to be solved for this angle by a linear interpolation method, and so it is more convenient to use a ray tracing technique. The initial angle of incidence is set at 0.1 radians and the range at which the Moho reflection will arrive at the surface is calculated. If this range is

within the limit of tolerance (set at 0.1 km) of the actual shot-station range then the travel time is calculated for the ray path. However, if the calculated range is not within this tolerance limit the incidence angle is incremented by 0.1 radians and the horizontal range calculated again. This is repeated until the desired tolerance is achieved. If the shot-station range is overshot then the previous value of the incidence angle is again used, and the increment angle reduced by a factor of two. Similarly, if, before the actual shot-station range is achieved a critical angle is reached for any of the intermediate boundaries, then again the previous value of the angle of incidence is used with half the increment angle. Once the correct path length is determined the travel time is obtained by dividing each segment by the appropriate layer velocity.

MODEL 2

The travel times of the refracted arrivals are again calculated by formaulae. An expression for the ray path length in each layer is determined from the layer thickness and angle of incidence of the ray at the lower boundary of the layer. The path length in the nth layer is given by:

$$PL(n) = Z(n)/\cos(i_n)$$

where $PL(n)$ = path length

$Z(n)$ = layer thickness

i_n = incident angle

$\sin i_n = V_n/V5$ for the case shown below

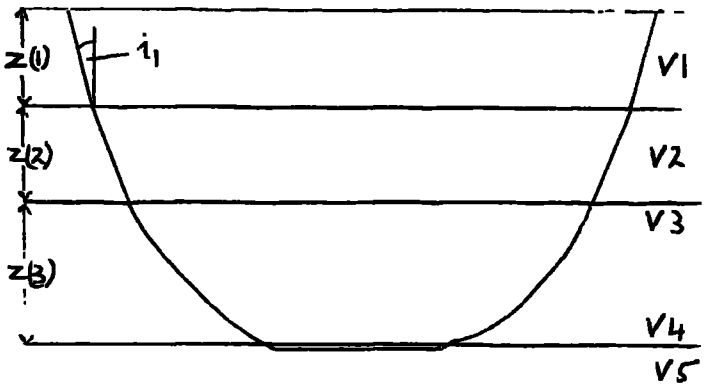

Twice the path length in each layer divided by the layer velocity gives the travel time for the ray path excluding the lower layer. The horizontal distance travelled in each layer is also calculated so that the total horizontal distance to be travelled in the lower layer is known.

Assuming the linear increase of velocity with depth in the lower layer can be represented by $V = V_3 + kd$

where k = the constant of velocity increase with depth

d = the depth within the lower layer

then the curved ray path in the lower layer is a segment of a circle, the centre of which lies on a plane of height V_3/k above the top of the lower layer (Heiland, 1968).

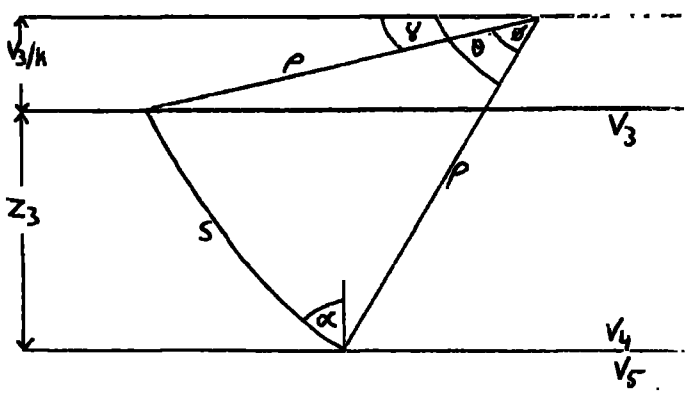

The path length in the lower layer, s, is given by $s = \rho\phi$

where ρ is the radius of the circle

ϕ is the angle defined by the limiting radii between the beginning and end of the curved ray path

or an increment of path length, ds, is given by:

$$ds = \rho d\phi$$

Now $\phi = \theta - \gamma$

and as γ is constant

$$d\phi = d\theta$$

$$\therefore ds = \rho d\theta$$

Geometrically θ is defined by:

$$\sin\theta = \frac{Z_3 + V_3/k}{\rho}$$

$$= \frac{kZ_3 + V_3}{k\rho}$$

$$= \frac{V}{k\rho} \text{ as } V = V_3 + kd$$

$$\therefore \theta = \sin^{-1} V/k\rho$$

$$\frac{d\theta}{dv} = \frac{1}{k\rho\sqrt{1-V^2/k^2\rho^2}}$$

$$d\theta = \frac{dv}{\sqrt{k^2\rho^2 - V^2}}$$

$$\therefore ds = \rho dv/\sqrt{k^2\rho^2 - V^2}$$

$$s = \int_{V_3}^{V_4} \frac{\rho\, dv}{\sqrt{k^2\rho^2 - V^2}}$$

$$t = S/V = \int_{V_3}^{V_4} \frac{\rho\, dv}{V\sqrt{k^2\rho^2 - V^2}}$$

$$t = \left[-\frac{1}{k}\cosh^{-1}\frac{\rho k}{V}\right]_{V3}^{V4}$$

$$t = \frac{1}{k}\left[\cosh^{-1}\frac{V_5}{V_3} - \cosh^{-1}\frac{V_5}{V_4}\right]$$

as for refraction $p = \frac{V_5}{k \sin\alpha} = \frac{V_5}{k \frac{V_5}{V_1} \sin i_1} = \frac{V_5}{k}$

$$\therefore kp = V_5$$

Therefore the total travel time down to, and up from the refractor in the lower layer is:

$$t = \frac{2}{k}\left[\cosh^{-1}\frac{V_5}{V_3} - \cosh^{-1}\frac{V_5}{V_4}\right]$$

and the travel time along the refractor is:

$$\frac{HD}{V_5} - \frac{2}{k}\left[\sqrt{1-(V_3/V_5)^2} - \sqrt{1-(V_4/V_5)^2}\right]$$

where HD is the horizontal distance between the ray entering and leaving the lowest layer.

Therefore, the total travel time from shot to receiver is:

$$T = \frac{PL(1)}{V(1)} + \frac{PL(2)}{V(2)} + \ldots + \frac{PL(n-1)}{V(n-1)} + \frac{2}{k}\left[\cosh^{-1}\frac{V_{n+2}}{V_n} - \cosh^{-1}\frac{V_{n+2}}{V_{n+1}}\right]$$

$$+ \frac{HD}{V_{n+2}} - \frac{2}{k}\left[\sqrt{1-(V_n/V_{n+2})^2} - \sqrt{1-(V_{n+1}/V_{n+2})^2}\right]$$

The travel times of the reflected PmP phase are determined by a similar ray tracing technique to that used in Model 1.

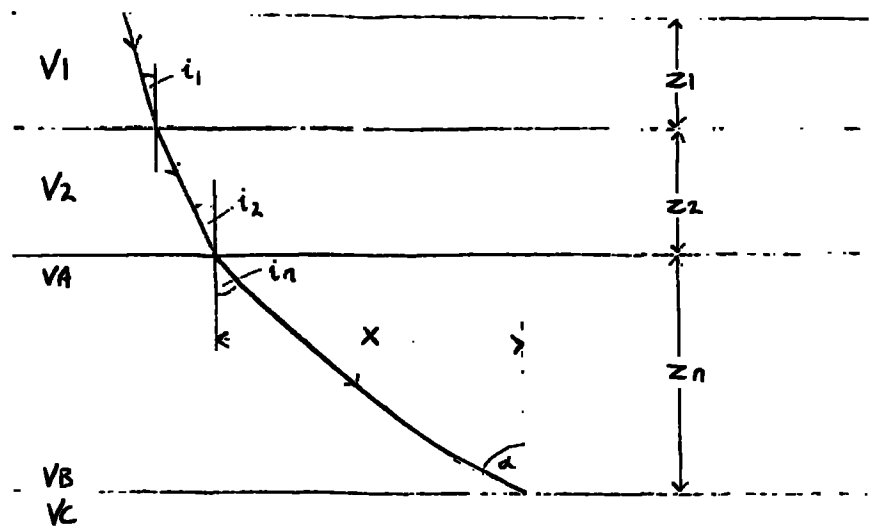

Starting with an initial value of incidence angle the horizontal distance travelled by the ray is calculated and checked to see if it is within the tolerance limit of the shot-station range.

The horizontal distance is given by:

$$2(Z_1 \tan i_1 + Z_2 \tan i_2 + \ldots + Z_{n-1} \tan i_{n-1} + X)$$

$$= 2hd + 2X$$

where $\sin i_r = \frac{V_r}{V_1} \sin i_1$ for $r = 1,n$

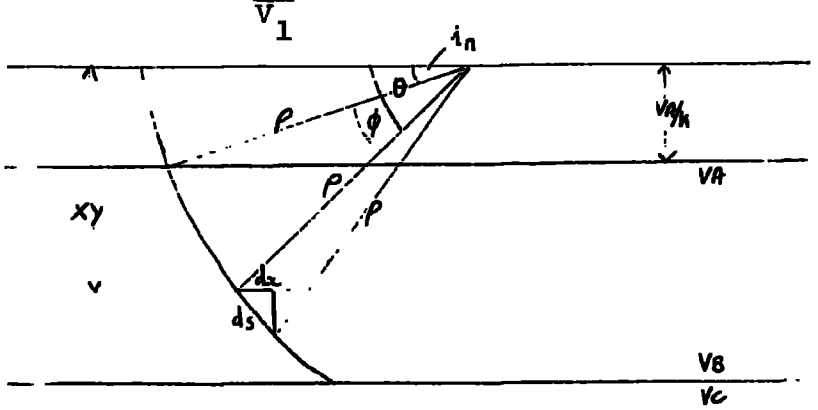

$$\phi = \theta - i_n$$

$$d\phi = d\theta$$

$$ds = \rho d\phi = \rho d\theta$$

horizontal distance $dx = ds \sin\theta$

$$= \rho d\theta \sin\theta$$

$$= \rho \sin\theta d\theta$$

Now $\sin\theta = XY/\rho = \frac{h+VA/k}{\rho} = \frac{VA + kh}{k\rho} = \frac{V}{k\rho}$

$$\theta = \sin^{-1}\frac{V}{k\rho}$$

$$\frac{d\theta}{dv} = \frac{1}{\sqrt{1-V^2/k^2\rho^2}} \frac{1}{k\rho}$$

$$\frac{d\theta}{dv} = \frac{1}{\sqrt{k^2\rho^2 - V^2}}$$

$$\therefore\ dx = \rho \frac{V}{k\rho} \frac{dv}{\sqrt{k^2\rho^2 - V^2}}$$

$$dx = \frac{V}{k\sqrt{k^2\rho^2 - V^2}}\, dv$$

$$\therefore\ x = \int_{VA}^{VB} \frac{v\,dv}{k\sqrt{k^2\rho^2 - V^2}}$$

$$= \left[-\frac{1}{k}(k^2\rho^2 - V^2)^{\frac{1}{2}} \right]_{VA}^{VB}$$

$$= \frac{1}{k}\left[\sqrt{k^2\rho^2 - VA^2} - \sqrt{k^2\rho^2 - VB^2} \right]$$

where $\rho = \frac{VA}{k \sin i_1} = \frac{VA V_1}{k\, V_1 \sin i_1} = \frac{V_1}{k \sin i_1}$

$$\therefore k^2\rho^2 = \frac{k^2 V_1^2}{k^2 \sin^2 i_1} = V_1^2 \operatorname{cosec}^2 i_1$$

$$\therefore\ X = \frac{1}{k}\left[\sqrt{V_1^2 \operatorname{cosec}^2 i_1 - VA^2} - \sqrt{V_1^2 \operatorname{cosec}^2 i_1 - VB^2} \right]$$

$\therefore$ Total horizontal distance = hd + 2X

When this horizontal distance is found equal to the shot-station range the travel time is then calculated. The travel time in the upper layers is easily determined in the same manner as for the refraction case. In the lower layer of velocity increasing with depth we have, as for refraction,

$$T = \frac{1}{k}\left(\cosh^{-1} \frac{\rho k}{VA} - \cosh^{-1} \frac{\rho k}{VB} \right)$$

but in this case $\rho = \frac{VB}{k \sin\alpha}$, where $\sin\alpha = \frac{VB}{V1} \sin i_1$

$$\therefore\ T = \frac{1}{k}\left(\cosh^{-1} \frac{VB}{VA \sin\alpha} - \cosh^{-1} \frac{1}{\sin\alpha} \right)$$

However, as the velocity is increasing with depth in this lower layer there comes a time when the continuous refraction causes the ray to be refracted back to the top of the layer without ever reaching the lower boundary. This

occurs when $\theta = 90^{\circ}$ i.e. $\sin\theta = 1$

$$\therefore \frac{V}{k\rho} = 1 \quad \text{or} \quad V = k\rho$$

The value of V at the base of the lower layer is VB

$$\therefore VB = k\rho = V1 \operatorname{cosec} i_1$$

$$\operatorname{cosec} i_1 = \frac{VB}{V1}$$

$$\therefore \sin i_1 = \frac{V1}{VB} \; ; \; i_1 = \sin^{-1}\left(\frac{V1}{VB}\right) = i \text{ max} = i_m$$

Therefore the maximum horizontal distance at which the lower boundary is reached is given by:

$$2(Z_1 \tan i_m + Z_2 \tan i_2 + \ldots + Z_{n-1} \tan i_{n-1} + \frac{1}{k}\sqrt{V_1^2 \operatorname{cosec}^2 i_m - VA^2})$$

No PmP arrivals can be identified beyond this range.

CHAPTER 4

The North Scottish Continental Shelf

4.1 Introduction

The area considered in this thesis as the North Scottish Continental Shelf extends from north of Scotland to the Shetland Islands. The western boundary of the area is marked approximately by the 100 fathom bathymetric contour and to the east the shelf extends across to the Norwegian coast (Fig. 1.1.).

The shots considered to be over the shelf are:

All line D i.e. D2-D24
All line E i.e. E1-E17
C1-C24
B47-B70

The North Scottish mainland was considered in terms of two separate structural units in section 1.2.1., the Caledonian Foreland to the WNW and the Caledonian Orogenic Belt to the ESE. As the thrusts separating the foreland from the orogenic belt dip towards the east the foreland structure probably extends at depth for several tens of kilometres eastwards beyond the surface boundary. Most of the shots on the shelf were fired over the Caledonian foreland but the few shots to the east of the Caledonian front were probably also over foreland crust at depth. (Fig.1.2). However recording stations were situated both on the foreland and on the orogenic belt. Some of these stations were located to the east of the Great Glen Fault, and some to the south of the Highland Boundary Fault. (Fig.2.1.).

The large scale gravity features outlined on the shelf (Bott and Watts, 1970) were traversed by shots on lines B and C. In particular the shots on line B crossed from the outcropping basement ridge, 'high A', to the deep sedimentary

basin, 'low E', interpreted from gravity observations (Bott and Watts, 1970) and further detailed by shallow seismic refraction (Browitt, 1972). Line E was fired over the Moray Firth basin and line D, parallel to the strike of the gravity contours, along the length of the North Scottish Shelf.

4.2 The first arrivals

The observed travel times were all reduced to a sea level datum to correct for the bathymetry variation and changes in shot depths and receiving station elevations. The correction term added to each travel time was:

$$\frac{\text{Water depth (km)}}{5.95} - \left(\frac{\text{Water depth (km)} - \text{Shot depth (km)}}{1.5}\right) - \frac{\text{Station elevation (km)}}{5.95}$$

A velocity of 1.5 km s^{-1} was assumed for sound in sea water, and 5.95 km s^{-1} as the basement velocity to be expected beneath much of the region. Such a basement velocity had been previously observed (Browitt, 1971).

The method of least squares was used to fit straight line segments to the first arrival time-distance graphs for each station and line. The velocities and intercepts obtained are given in Table 4.1. Reduced 'time minus distance/6.0' graphs were also plotted and those are shown in Figures 4.1-4.12.

The arrivals from lines C and D shots provide evidence of three distinct phases. Beyond distances of about 120 km the arrivals lie on segments with reciprocal gradients of about 8 km s^{-1} and are interpreted as the Moho head wave Pn. At distances between 40-80 km and 120 km some first arrivals lie on segments with reciprocal gradients of about 6.5 km s^{-1} and intercepts of about 1-1.4 s. These arrivals are interpreted

TABLE 4.1.

APPARENT VELOCITIES AND INTERCEPTS FROM LEAST SQUARES

Station	Shots	Phase	Velocity(km s^{-1})	Intercept(s)	S.E.
DU1	D47-B51		3.16±0.11	-16.24±1.19	0.07
	B52-B56		4.19±0.20	- 6.34±1.12	0.07
	B57-B61	Pg	5.90±0.10	- 0.30±	0.02
	B65-B70	+P*	9.03±0.75	4.99±0.70	0.12
	D2-D10	P*	6.31±0.04	0.96±0.08	0.08
	D11-D24	Pn	7.89±0.04	4.82±0.14	0.12
	E3-E17	+Pn	7.66±0.20	3.54±0.92	0.22
DU2	B44-B50	Pn	7.20±0.29	3.80±0.81	0.09
	B51-B56	Pn	7.83±0.80	5.49±1.68	0.12
	B57-B61	Pn	7.93±1.40	4.82±2.57	0.13
	C1-C11	P*	7.03±0.63	2.72±1.53	0.09
	C13-C24	Pn	8.24±0.30	5.90±0.61	0.16
	D2-D5	Pn	7.86±0.37	4.92±0.81	0.12
	D6-D15	Pg	5.95±0.04	0.15±0.08	0.08
	D16-D20	Pg	5.99±0.05	0.33±0.08	0.03
	D21-D24	P*	6.49±0.13	1.41±0.31	0.09
	E1-E17	+P*	6.32±0.11	1.63±0.33	0.34
DU3	D2-D24	Pn	8.12±0.04	5.95±0.18	0.20
IGS1	B65-B70	+Pn	7.48±0.13	3.54±0.51	0.08
	C1-C13	Pg	5.94±0.10	0.18±0.11	0.15
	C14-C24	P*	6.25±0.10	0.86±0.26	0.15
	D2-D13	Pn	7.93±0.07	4.80±0.22	0.15
	D14-D21	P*	6.40±0.09	1.06±0.18	0.16
	D22-D24	Pg	5.91±0.16	0.16±0.09	0.08
	E6-E9	+Pn	6.54±0.50	0.50±0.98	0.12
IGS2	C1-C11	Pg	6.25±0.17	0.46±0.35	0.09
	C13-C24	P*	6.63±0.10	1.80±0.26	0.10
	D2-D19	Pn	8.13±0.07	5.31±0.24	0.23
	D20-D24	Pg	5.96±0.09	-0.26±0.26	0.10
	E6-E16	+Pn	7.78±0.47	5.12±1.62	0.28
IGS3	C5-C24	Pn?	7.43±0.15	2.81±0.77	0.24
	D7-D24	Pn	8.00±0.08	6.10±0.40	0.29

TABLE 4.1. contd.

Station	Shots	Phase	Velocity(km s^{-1})	Intercept(s)	S.E.
UKAEA	B51-B56	P*	6.64±0.19	1.96±0.40	0.04
	B57-B61	P*	6.52±0.13	0.72±0.24	0.04
	B65-B70	+Pg	6.61±0.09	1.56±0.11	0.04
	C2-C21	Pn	7.83±0.15	3.60±0.60	0.06
	D2-D6	Pg	5.89±0.04	0.47±0.04	0.04
	D7-D13	P*	6.51±0.04	1.46±0.09	0.05
	D14-D24	Pn	7.92±0.05	4.85±0.18	0.11
	E2-E16	+Pn	7.93±0.15	5.21±0.59	0.16
UAB	B65-B70	+Pn	7.58±0.14	3.92±0.62	0.08
	C1-C14	P*	6.31±0.13	0.41±0.37	0.18
	C15-C24	Pn?	7.50±0.12	4.27±0.34	0.09
	D2-D17	Pn	7.95±0.04	5.30±0.15	0.12
	D19-D24	Pg	5.81±0.09	-0.41±0.23	0.09
	E1-E17	+P*	6.95±0.16	3.08±0.43	0.19
ULA	D10-D19	Pn	8.04±0.18	5.56±0.54	0.24
	D23, D24	Pg	5.92	0.10	
	E2-E8	+P*	6.90±0.40	3.29±1.05	0.12
UBL	C4-C24	Pn	8.03±0.10	6.15±0.40	0.18
	D2-D12, D15, D16		8.25±0.07	6.30±0.30	0.09
	D13-D24	Pn	7.96±0.09	5.60±0.32	0.14
	E1-E14	+Pn	7.74±0.45	5.42±1.12	0.15
MHD	D14-D24	Pn	7.98±0.14	6.14±0.98	0.28
LN1	C2-C15	Pn	8.30±0.39	6.28±2.05	0.26
LN5	C1-C24	Pn	8.20±0.12	7.09±0.61	0.24
	D3-D24	Pn	8.21±0.06	7.08±0.29	0.18
	E1-E17	+Pn	7.69±0.14	5.23±0.53	0.20
LN4	E1-E17	+Pn	7.38±0.18	3.56±0.88	0.30
LN6	C4-C24	Pn	8.07±0.08	5.78±0.50	0.13
	D3-D23	Pn	7.99±0.04	5.86±0.25	0.08
	E1-E16	+Pn	7.50±0.10	4.26±0.43	0.15
LN8	D3-D23	Pn	8.02±0.09	6.40±0.57	0.21
LN9	C4-C24	Pn	8.03±0.11	5.56±0.56	0.18
MIR(A)	C8-C13	Pg?	4.98±0.84	0.06±2.46	0.80
	C15-C23	P*	6.53±0.14	1.56±0.08	0.11

+ These values of velocity and intercept are defined by the observed travel times corrected only for variations in shot depth and station elevation. However the travel times were then corrected for sediment variation.

as the head wave, P*, from a lower crustal layer. All the first arrivals at ranges of up to 40 km, and some up to 120 km, define segments with reciprocal gradients of about 6 km s^{-1} and have small positive intercepts. These are interpreted as, Pg, travelling in the metamorphic basement beneath a thin sediment cover. Both the lower two refractors, P* and Pn, are observed from the line E shots over the Moray Firth. The Pg basement refractor was not identified, probably because the ranges of these shots were too great to produce first arrivals from this basement. The first arrivals from the line B shots also show the same three phases as for lines C and D, but the strongly variable near surface structure makes the situation less well defined.

4.3 Interpretation of the time-distance graphs

4.3.1 Line D

All fourteen of the time-distance graphs for line D (Figs.4.1-4.5.) have Pn segments with apparent velocities ranging from 7.86 to 8.21 km s^{-1}. Four of the graphs have a P* segment (6.31-6.51 km s^{-1}), and six have a Pg segment (5.81-5.99 km s^{-1}). The graphs for stations IGS1, UKAEA and DU2 have both Pg and P* segments indicating the presence of two distinct refractors. The mean velocities of the three refractors were 5.92 ± 0.04 km s^{-1}, 6.43 ± 0.04 km s^{-1} and 8.01 ± 0.03 km s^{-1}.

The stacked arrivals for all the line D shots at stations IGS1, DU1 and DU2 are shown in Figures 4.13-4.15.

There was no reversed measurement of the Pg velocity along line D but, as similar velocities were observed from different directions and different parts of the line, the mean velocity is probably close to the true refractor velocity.

Figure 4.1 : The reduced time-distance graphs for line D at (a) station IGS2, (b) station IGS3, (c) station IGS1.

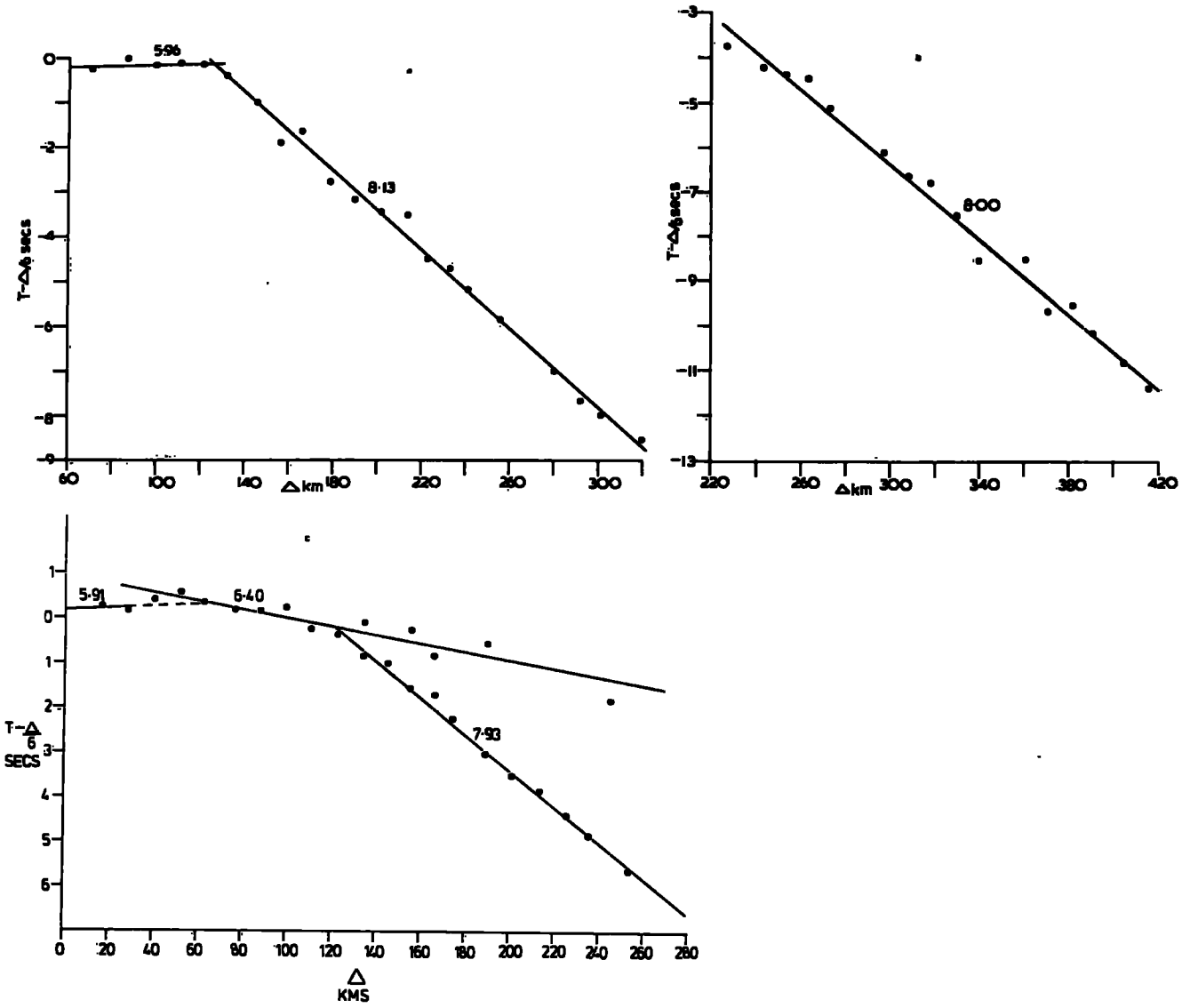
5·96
8·13
T-Δ/6 secs
Δ km
8·00
T-Δ/6 secs
Δ km
5·91
6·40
7·93
T-Δ/6 SECS
Δ KMS

Figure 4.2 : The reduced time-distance graphs for line D at (a) station DU3, (b) station DU1, (c) station DU2.

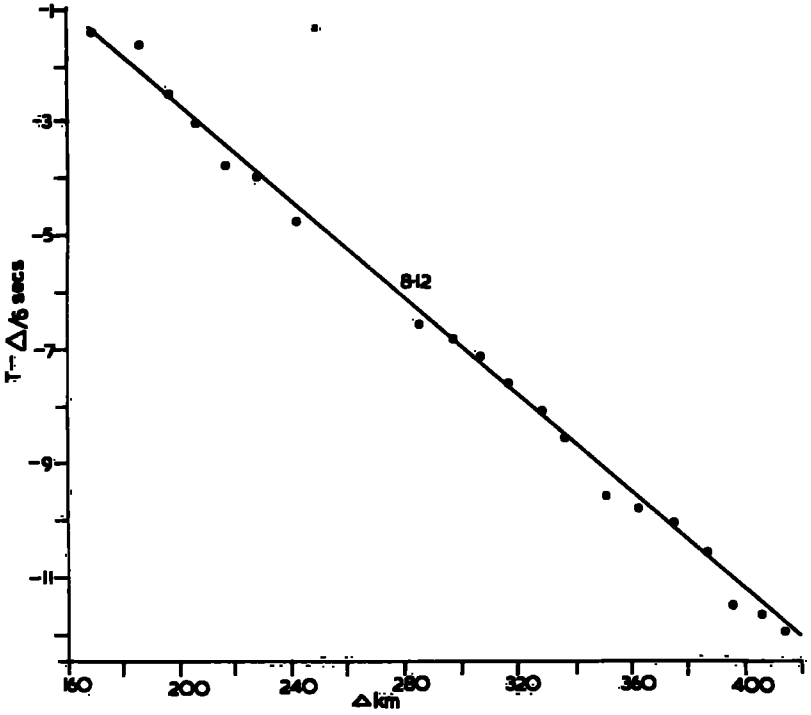
T−Δ/6 secs
8·12
160
200
240
280
320
360
400
Δ km

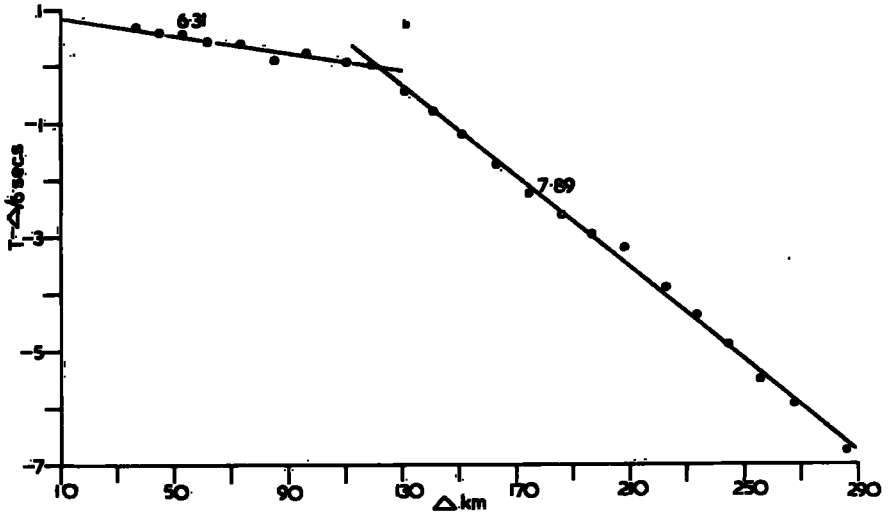
6·31
7·89
T−Δ/6 secs
10
50
90
130
170
210
250
290
Δ km

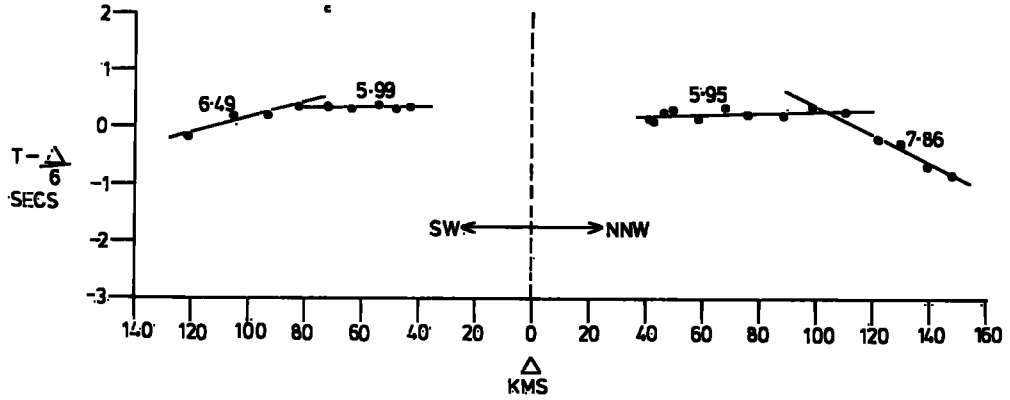
6·49
5·99
5·95
7·86
T−Δ/6 SECS
SW
NNW
140
120
100
80
60
40
20
0
20
40
60
80
100
120
140
160
Δ KMS

Figure 4.3 : The reduced time-distance graphs for line D at (a) Station ULA, (b) station UAB, (c) Station UBL.

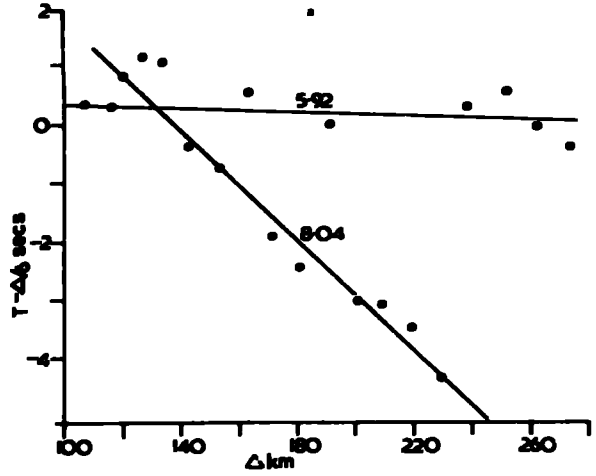
a
5·92
8·04
T-Δ/6 secs
100
140
180
220
260
Δ km

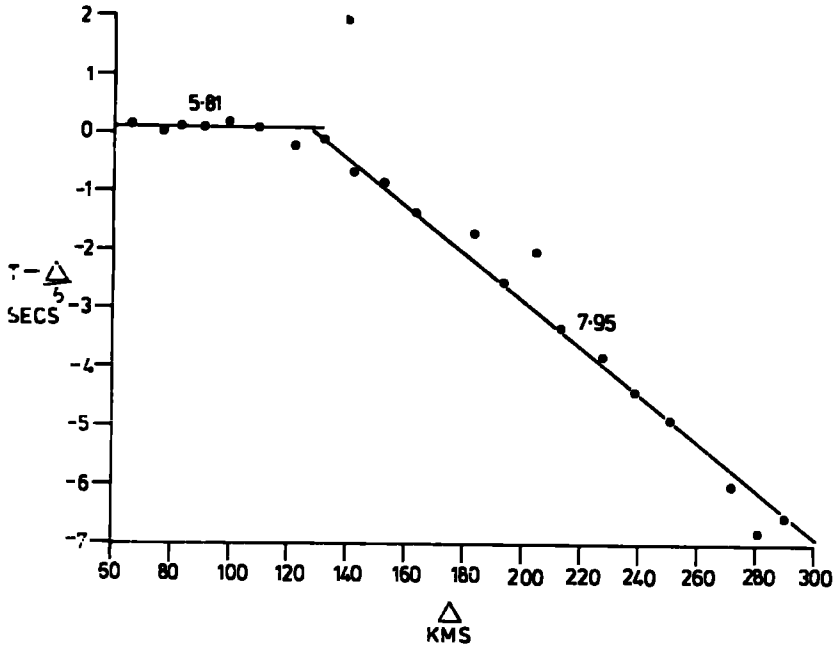
b
5·81
7·95
T-Δ/5 SECS
50
80
100
120
140
160
180
200
220
240
260
280
300
Δ KMS

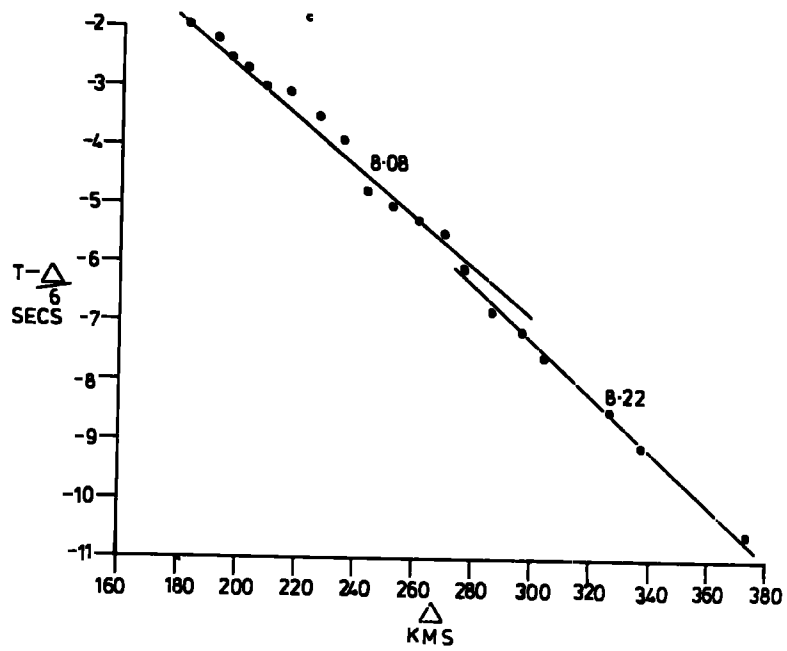
c
8·08
8·22
T-Δ/6 SECS
160
180
200
220
240
260
280
300
320
340
360
380
Δ KMS

Figure 4.4 : The reduced time-distance graphs for line D at (a) station MHD, (b) station UKAEA.

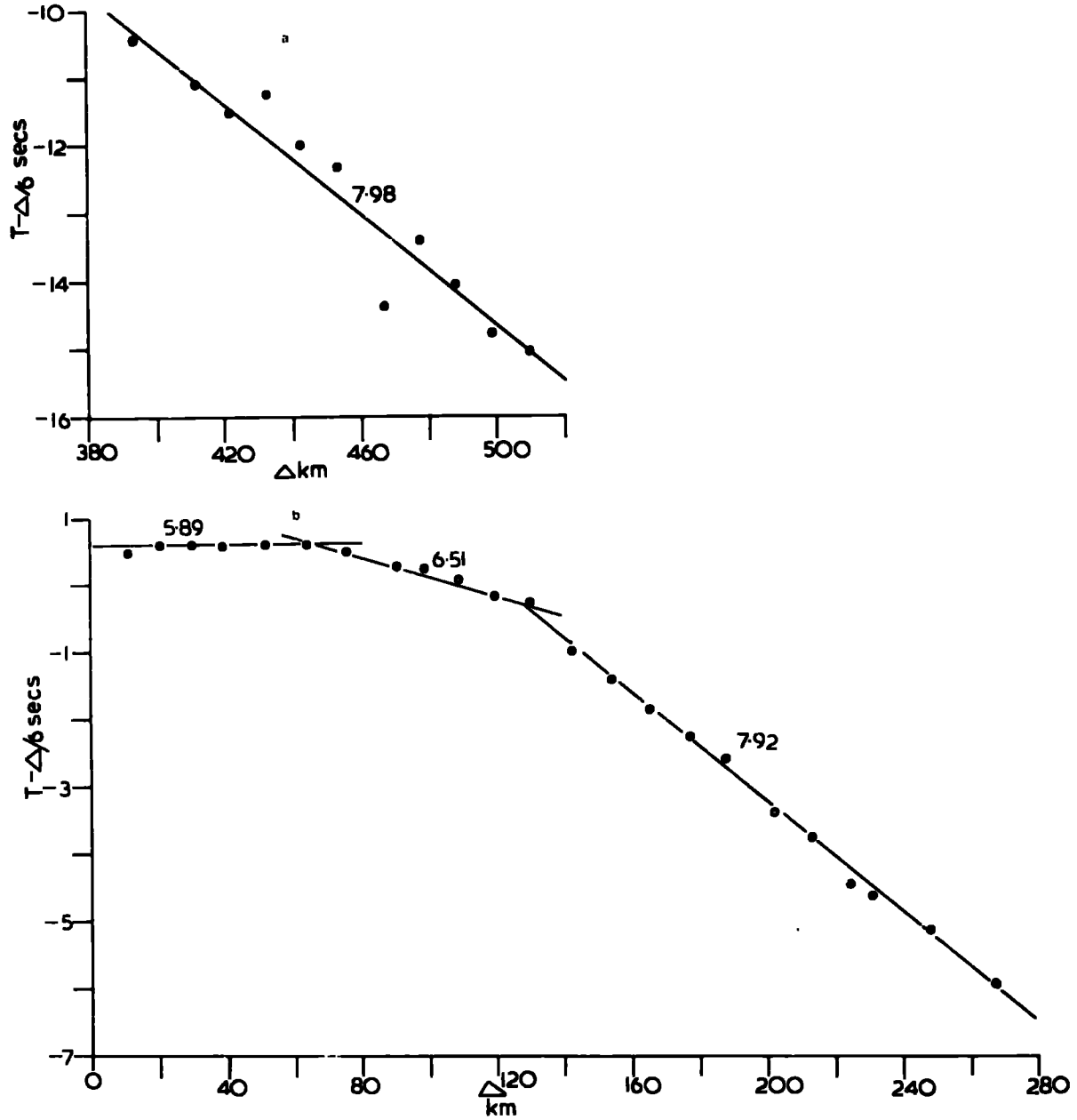
a
-10
-12
-14
-16
T-Δ/6 secs
7·98
380
420
460
500
Δkm
b
1
-1
-3
-5
-7
T-Δ/6 secs
5·89
6·51
7·92
0
40
80
120
160
200
240
280
Δ km

Figure 4.5 : The reduced time-distance graphs for line D at (a) station LN6, (b) station LN5, (c) station LN8.

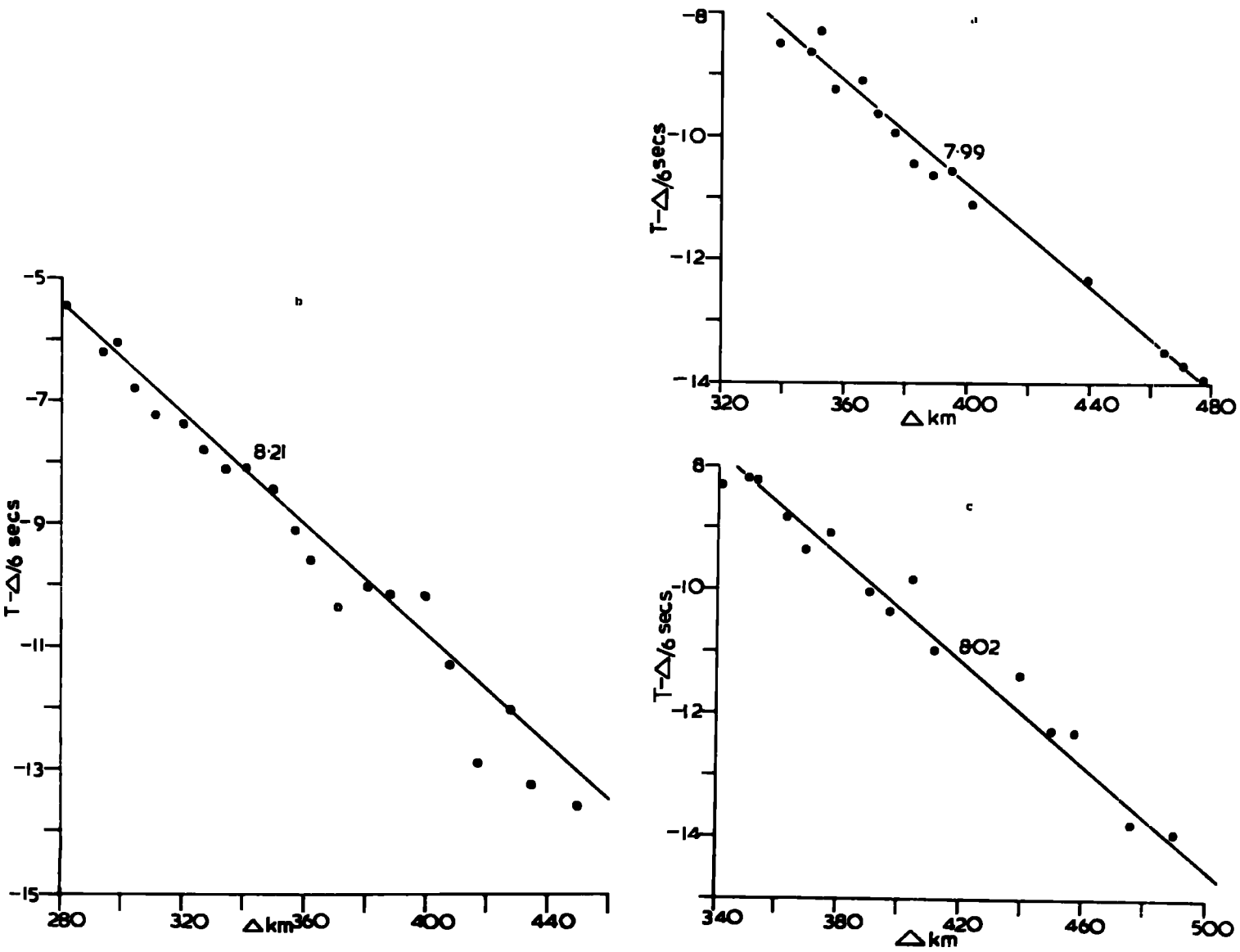
a
-8
-10
-12
-14
T-Δ/6secs
7·99
320
360
400
440
480
Δ km
b
-5
-7
-9
-11
-13
-15
T-Δ/6 secs
8·21
280
320
360
400
440
Δ km
c
8
10
12
14
T-Δ/6 secs
8·02
340
380
420
460
500
Δ km

Little variation was found in the Pg velocity values, and the mean of 5.92 ± 0.04 km s^{-1} is similar to the reversed basement velocity (5.95 km s^{-1}) measured by Browitt (1971).

The Pg intercept times observed were quite small and range from -0.41s to 0.47s. They are interpreted in terms of a thin sediment cover, variable in both thickness and velocity, above the basement. The standard error on the negative intercept observed at station IGS2 reduces this value to zero, and twice the standard error on the negative intercept observed at station UAB also reduces this intercept value to zero. The individual values of intercept time and Pg velocity for each station, together with an assumed mean sediment velocity of 5 km s^{-1} were interpreted in terms of sediment thickness by means of the layer thickness formula. The basement depths determined are given in Table 4.2.

First arrivals defining a P* velocity were observed from every shot on line D, except D13, indicating that this refractor is continuous along the length of the shelf. However there was no approximately constant Pg/P* crossover distance, as at some stations P* arrivals were observed from very short ranges (35-40 km at station DU1) and at othersPg arrivals were observed at up to Moho arrival ranges (stations IGS2, UAB, ULA). This suggests a variable depth Pg/P* interface. Good second arrivals at station IGS1 from shots D3, 8, 9, 10, 11 and 13 also defined a P* velocity. These arrivals were used with those of shots D7-D13 observed at station UKAEA to reverse the P* velocity and indicated a refractor dipping towards the north-east at 0.5^{o} with a true velocity of 6.46 km s^{-1}. However allowing for the ray offset in travelling down to the P* refractor true reversal is only provided by shot D13 at station UKAEA and shot D7 at station IGS1.

The individual values of P* velocities and intercepts observed at each station were interpreted in terms of refractor depths assuming overlying sediment and basement material of 5 km s^{-1} and 5.92 km s^{-1} respectively. The depths determined are given in Table 4.2.

A reversed estimate of Pn velocity along line D was provided by the observations at stations IGS1 and IGS2 looking to the north-east, and the observations at stations UKAEA and DU1 looking to the south-west. The apparent velocity in both directions for the same part of the Moho refractor was only observed over a small length of the line due to the ray offset in travelling down to the Moho. This portion of the line lies between the limit of Pn energy travelling towards the south-west and the limit travelling towards the north-east, and so true reversal of the Pn velocity was only provided by the following results:

Station DU1	D11-D19	7.79 ± 0.06 km s^{-1}
Station UKAEA	D14-D19	7.89 ± 0.09 "
Station IGS1	D6-D13	7.98 ± 0.13 "
Station IGS2	D6-D14	8.23 ± 0.19 "

The mean apparent velocities looking to the north-east and south-west are 8.1 ± 0.11 km s^{-1} and 7.84 ± 0.05 km s^{-1} respectively. These velocities are significantly different and were interpreted in terms of a Moho of true velocity 7.97 km s^{-1} dipping to the south-west at 1.3^{o}.

The observations at station UBL define, statistically, two separate phases at Pn ranges. Although the crossover distance of these two phases is approximately 210 km the arrivals identified out to about 270 km defined the first segment. This phase has a velocity of 7.96 km s^{-1} and is interpreted as the Moho head wave Pn. The arrivals at ranges of greater than 270 km define a segment of reciprocal gradient

8.25 km s^{-1}, which is significantly different to the Pn velocity. The higher velocity phase may represent waves travelling at a slightly greater depth in the mantle.

Moho depths were determined from the observed Pn velocities and intercept times of the individual stations. Mean sediment, Pg and P* velocities of 5.0, 5.92 and 6.43 km s^{-1} were assumed, together with 0.68 km of sediment cover and a P* refractor depth of 8.2 km. The Moho depths found are given in Table 4.2.

4.3.2 Line C

Nine of the twelve time-distance graphs of line C (Figs. 4.6-4.8) have Pn segments defining apparent velocities ranging from 7.43 to 8.30 km s^{-1}. Five of the graphs have a P* segment (6.25-7.03 km s^{-1}) and three have a Pg segment (4.98-6.25 km s^{-1}). The three velocity groups are the same as were observed for line D but each group shows a wider range of values. This may be explained by line C crossing the dominant structural trend of the region whereas line D runs approximately parallel to the strike direction. However it is possible that the scatter on the P* and Pn velocity groups is concealing the presence of an intermediate refractor with a velocity of approximately 7.3 km s^{-1}. A lower crustal refractor of this velocity has been observed beneath Cardigan Bay (Blundell and Parks, 1969).

The Pg velocity along this line should have been reversed by the observations at stations IGS1 and MIR(A). However the records obtained at station MIR(A) were poor and the velocity determined unreliable. A mean of these two velocities was

TABLE 4.2. LAYER THICKNESSES LINE D

Station	Sediment thickness(km)	Basement thickness(km)	L. crustal layer thickness(km)	Moho depth
IGS1	0.75	5.8	15.1	21.65
IGS2	0.0		19.0	26.3
IGS3			21.8	30.4
UKAEA	2.2	8.0	15.7	25.9
DU1			15.5	24.1
DU2 to SW	1.5	8.2		
DU2 to NE	0.7		16.2	25.5
DU3			20.2	28.8
UAB	0.0		20.2	28.8
UBL			20.6	29.2
MHD			22.2	30.8
LN5			25.6	34.2
LN6			20.5	29.1
LN8			23.3	31.9
ULA				

TABLE 4.3. LAYER THICKNESSES LINE C

Station	Sediment thickness	Basement thickness	L. Crustal layer thickness	Moho depth
IGS1	0.83	5.1		
IGS2	1.92	9.5		
IGS3			6.5	14.9
UKAEA			9.6	18.0
DU2		12.8	20.5	34.3
UAB		1.3	16.0	18.3
UBL			23.3	31.7
LN1			22.2	30.6
LN5			27.7	36.1
LN6			20.8	29.2
LN9			19.9	28.3
MIR	0.29	8.5		

Figure 4.6 : The reduced time-distance graphs for line C at (a) station IGS3, (b) station DU2, (c) station IGS1, (d) station IGS2.

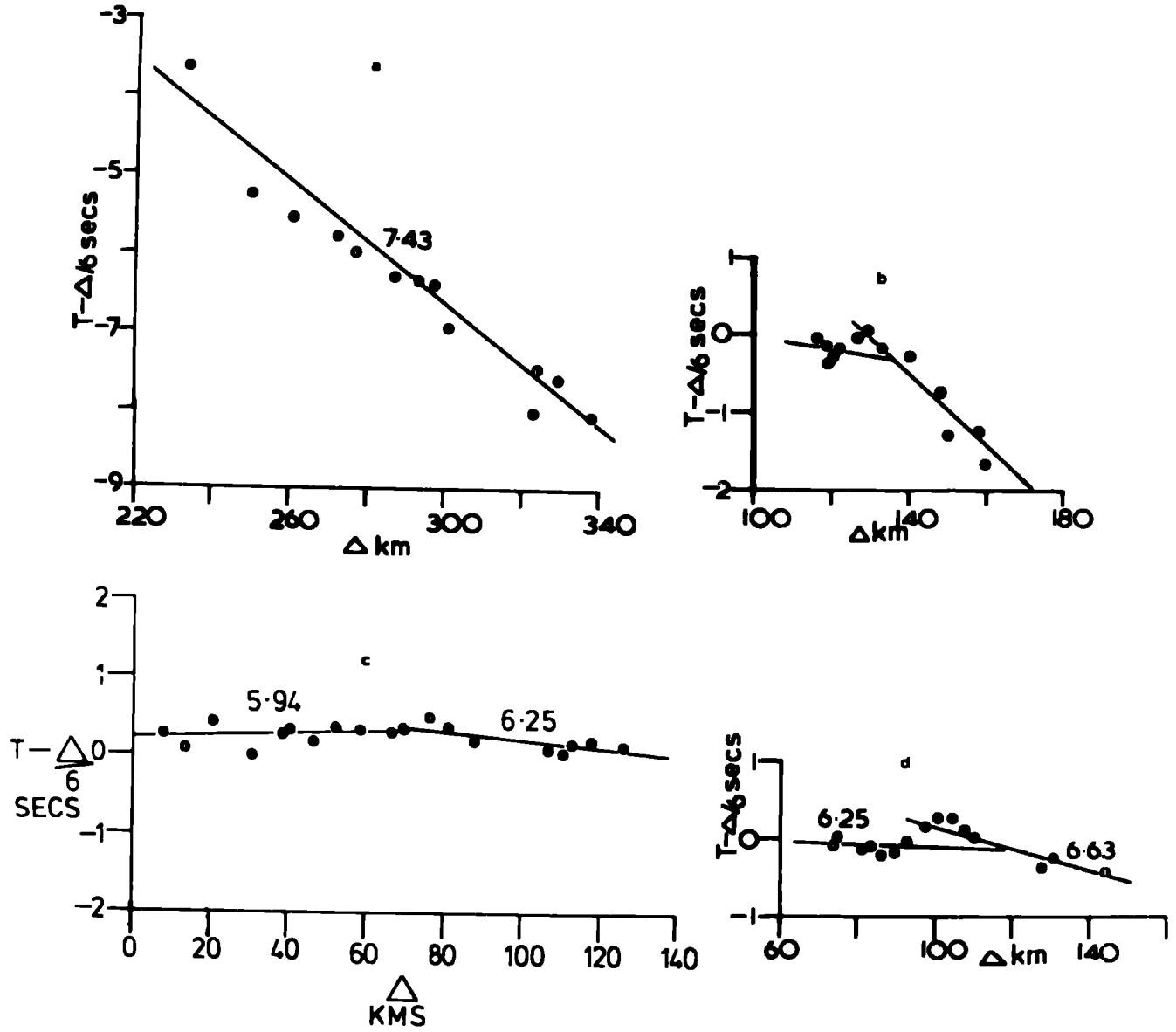
a
T−Δ/6 secs
−3
−5
−7
−9
7·43
220
260
300
340
Δ km
b
T−Δ/6 secs
0
−1
−2
100
140
180
Δkm
c
T − Δ/6 SECS
2
1
0
−1
−2
5·94
6·25
0
20
40
60
80
100
120
140
Δ KMS
d
T−Δ/6 secs
1
0
−1
6·25
6·63
60
100
140
Δ km

Figure 4.7 : The reduced time-distance graphs for line C at (a) station UAB, (b) station UKAEA, (c) station UBL, (d) station MIR(A).

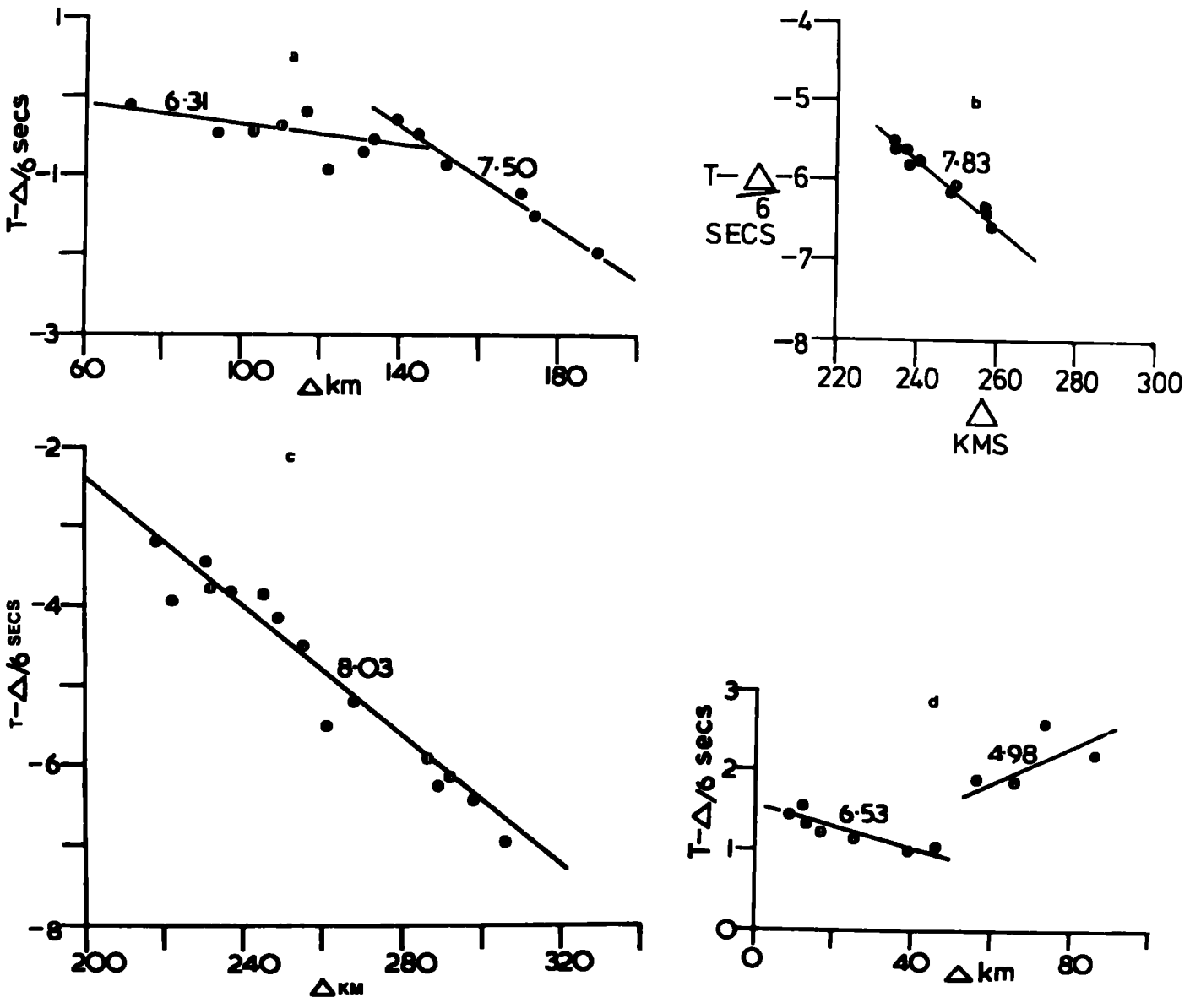
a
6·31
7·50
T−Δ/6 secs
Δ km
b
7·83
T−Δ/6 SECS
Δ KMS
c
8·03
T−Δ/6 SECS
Δ KM
d
6·53
4·98
T−Δ/6 secs
Δ km

Figure 4.8 : The reduced time-distance graphs for line C at (a) station LN6, (b) station LN1, (c) station LN5, (d) station LN9.

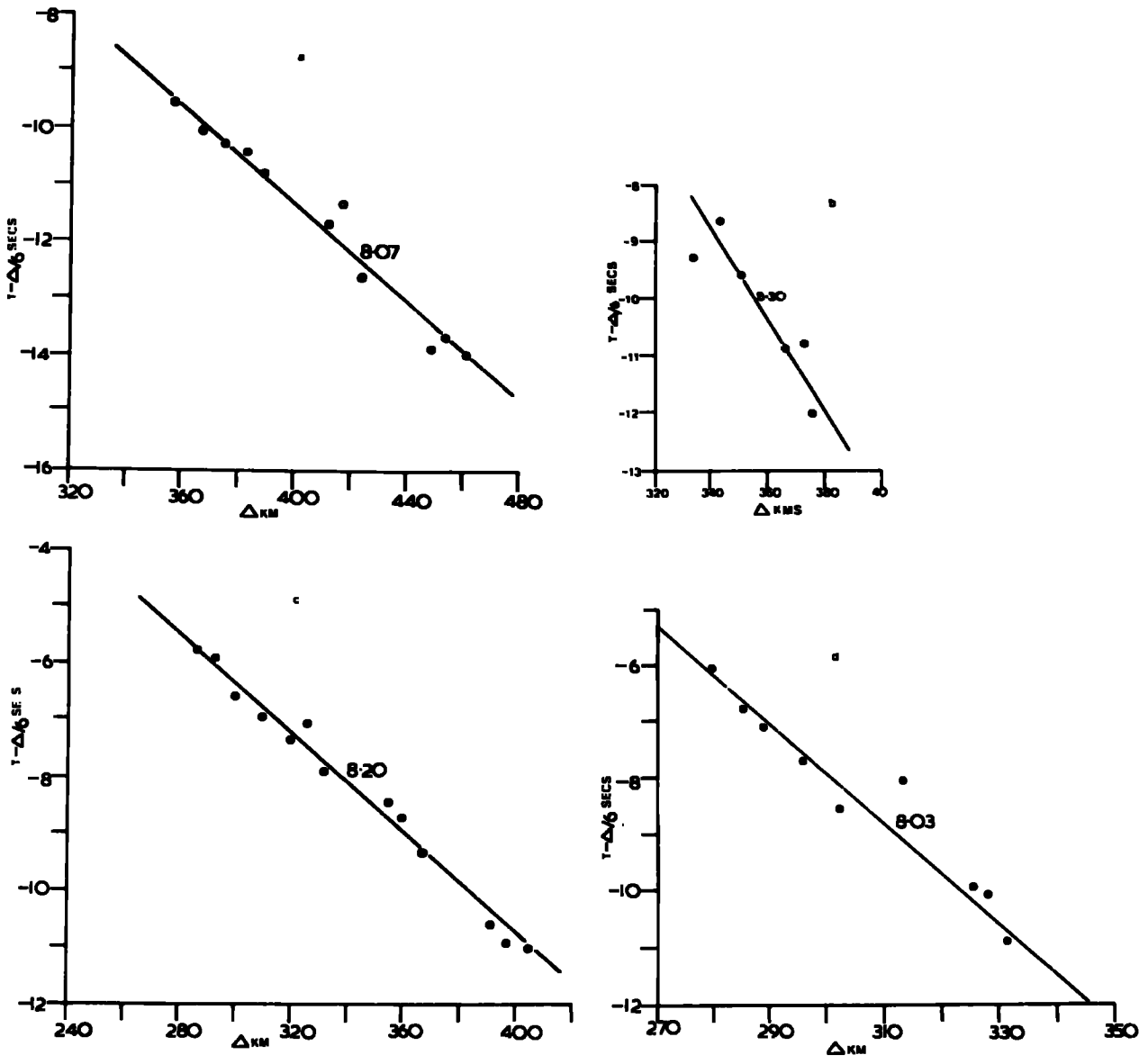
a
8·07
T−Δ/6 SECS
Δ KM
b
8·30
T−Δ/6 SECS
Δ KMS
c
8·20
T−Δ/6 SECS
Δ KM
d
8·03
T−Δ/6 SECS
Δ KM

obtained, weighting each velocity proportional to the inverse of the standard error on the velocity to decrease the effect of the observation at station MIR(A). The weighted mean velocity found was 5.84 ± 0.42 km s^{-1}.

Sediment thicknesses were determined for the individual Pg intercept times of each station using the mean Pg velocity of 5.84 km s^{-1} and an assumed sediment velocity of 5.0 km s^{-1}. The thicknesses found are given in Table 4.3.

The mean sediment thickness found was 1.01 km compared to 0.86 km for line D. However the values determined at station IGS1 for lines D and C were 0.75 and 0.83 km respectively, and the intercept times for the two lines 0.16s and 0.18s respectively. This similarity increases confidence in the interpretation.

The observed P* velocities have a large scatter (6.25-7.03 km s^{-1}) and, in addition, the P* velocity observed at station IGS1 is the same as the Pg velocity seen at station IGS2. The P* velocity observed at station IGS2 is considerably larger (6.63 ± 0.10 km s^{-1}). Estimates of the true refractor velocity causing these arrivals at the two stations were obtained by minus - time analysis (Hagedoorn, 1959) for the pairs of stations IGS1/MIR(A) and IGS2/MIR(A). The velocities determined were 6.45 and 6.59 km s^{-1} respectively, which are consistent with the P* velocities observed on line D and with the time term analysis value which will be presented in a later section. An anomalously high apparent P* velocity of 7.03 ± 0.63 km s^{-1} was observed at station DU2. This value may result from variations in local structure as the station is well offset from the shot line and the shot to station azimuth varies considerably for each shot, whereas the range only varies by 10 km. The apparent P* velocities observed at

stations IGS1 and MIR(A) can be taken to reverse the P* velocity and indicate a refractor of true velocity 6.38 km s^{-1} dipping towards the north-west at 1.6°. However assuming a refractor depth of 9 km the ray offset in travelling to and from the refractor is sufficiently large to prevent true reversal over any length of the line.

The mean P* velocity (6.55 ± 0.13 km s^{-1}) was used with the individual values of station intercept time to determine refractor depths. Mean sedimentary and basement velocities of 5 km s^{-1} and 5.84 km s^{-1} respectively were assumed, and the depths found given in Table 4.3.

The pattern of the Pg and P* first arrivals indicates that a significant change occurs in the basement at approximately shot C13. Previous geophysical surveys (Bott and Watts, 1971; Watts, 1970) have also shown that at about this same position there is a rapid transition from outcropping or shallowly buried metamorphic basement to the edge of a Mesozoic sedimentary basin (gravity low D). No Pg arrivals were observed from shots beyond C13. Such arrivals would be expected from these shots at station MIR(A) (due to the small range), and also at station IGS2 as the observed P* arrivals appear to be secondary arrivals. This indicates that there is either termination or substantial thinning and deepening of the Pg basement beneath the sediments of basin D.

Pn arrivals were observed at one or more stations from all the shots on line C, with a range in the observed apparent velocities of 7.43-8.30 km s^{-1} and mean value of 7.96 ± 0.06 km s^{-1}. The low velocity values of 7.43 km s^{-1} and 7.5 km s^{-1} at stations IGS3 and UAB may represent a high velocity lower crustal layer as was identified beneath Cardigan Bay (Blundell

and Parks, 1969). The Pn segments of the graphs of stations IGS3, UKAEA, UBL, LN1, LN5, LN6 and LN9 include travel times for shots from both sides of the transition in structure at approximately shot C13. No offsets are seen on these segments, but any variation in upper structure could be compensated for by variation in the lower crust.

There was no true reversal of the Pn velocity along line C. However estimates of the Pn velocity in the direction shot to station were obtained by plotting the travel times from one shot to several stations on the Scottish mainland. However Pn arrivals were only received at stations UAB and UBL and at some of the instruments of the Lownet array station on the mainland. As the Lownet stations were not directly in line with the shot line and as there could only be a few observations for each shot, the velocity estimates obtained are not very reliable and have large standard errors. The range in velocity obtained was 8.04-8.43 km s^{-1} with a mean value of 8.26 km s^{-1}, which is an estimate of the Pn velocity beneath the Scottish mainland. The mean Pn velocity in the direction station to shot was 7.96 km s^{-1} which, when reversed by the value determined for the opposite direction, gave a true Pn velocity of 8.1 km s^{-1} and a Moho dip of 1.4^{o} towards the north west.

Moho depths were determined for each station, using the intercept time and Pn velocity measured at the station. Sediment, Pg and P* velocities of 5.0, 5.84 and 6.55 km s^{-1} respectively were assumed, with a 1 km sediment cover and the P* refractor at a depth of 8.4 km. The depths found are given in Table 4.3.

4.3.3 Line B

Five time-distance graphs were constructed for this line, although arrivals from these shots at some of the other stations proved useful in time term analyses. On each graph presented (Fig. 4.9.) any arrivals from shots B68-B70 have been corrected for the underlying Mesozoic sediments which will be mentioned later. The difficulty in obtaining time-distance graphs for this line was probably at least partly due to the limited range variation between the shots and the receiving stations on the Scottish mainland. Line B crossed a series of large local gravity anomalies which indicate a highly variable upper crustal structure. The effect of this variation was seen in the offset segments of the graphs, and in the large departures of some of the observed velocities from the Pg, P* and Pn values established beneath the previous two lines. Three of the graphs have Pn segments with an apparent velocity range of 7.20-7.93 km s^{-1} (mean 7.60± km s^{-1}), two have P* segments (6.52-9.03 km s^{-1}, mean 7.40± km s^{-1}) and two have Pg segments (5.90-6.61 km s^{-1}, mean 6.25± km s^{-1}). These ranges and mean values were determined using the travel times corrected to a sea level datum only. After correcting for the Mesozoic sediments beneath shots B68-B70, the ranges and mean values were altered to:

1.	Pn	7.20-8.36 km s^{-1}	7.88±	km s^{-1}
2.	P*	6.52-7.45 "	6.87±	"
3.	Pg	5.90-5.91 "	5.90±	"

The structure of the Mesozoic sedimentary basin beneath shots B68-B70 had been previously determined by shallow seismic refraction, reflection and gravity investigations (Browitt, 1971; Bott and Browitt, in preparation), and using this information sediment thicknesses of 0.8 km, 1.3 km and 1.3 km

Figure 4.9 : The reduced time-distance graphs for line B at (a) station DU1, (b) station DU2, (c) station UAB, (d) station IGS1, (e) station UKAEA.

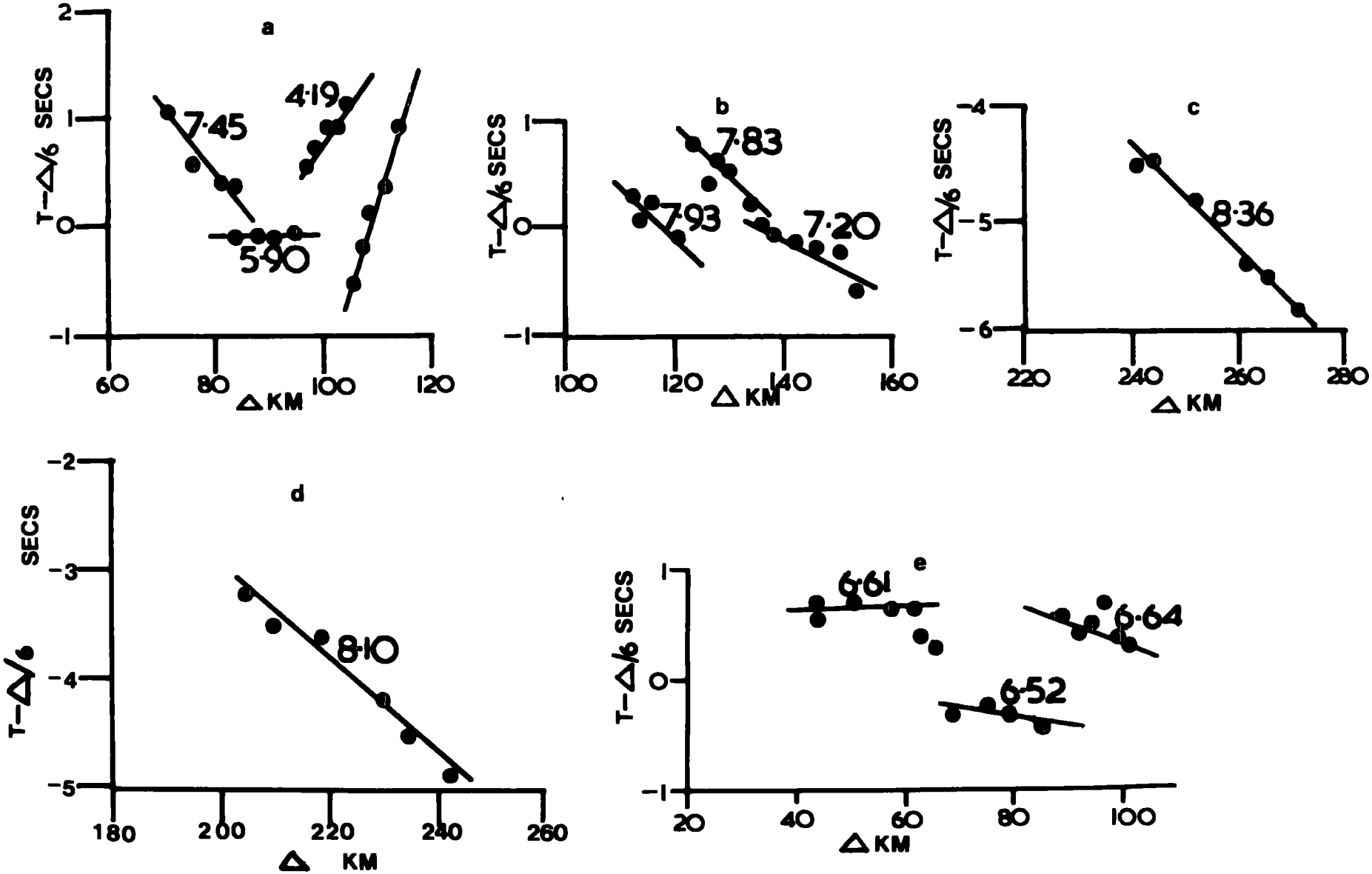
a
b
c
d
e
T−Δ/6 SECS
Δ KM
7·45
4·19
5·90
7·83
7·93
7·20
8·36
8·10
6·61
6·64
6·52

were assumed beneath shots B68, B69 and B70 respectively. The velocity measured for these sediments (2.67 km s^{-1}) by Browitt (1971) was used to determine the appropriate delay time beneath each shot for a ray travelling along each of the three refractors. This delay time was removed and a corresponding delay time added, assuming 5 km s^{-1} sedimentary material as the infill, to obtain the correction term.

The two Pg velocities determined (5.90 and 5.91 km s^{-1}) are very similar to the mean Pg velocity measured along line D (5.92 km s^{-1}) and are interpreted as representing arrivals from the same basement. The two P* velocities observed at station UKAEA (6.64 and 6.52 km s^{-1}) can also be interpreted as from the same lower crustal refractor as was found beneath lines D and C. However the value of 7.45 km s^{-1} observed at station DU1 from shots B65-B70 is high for P*, but a minus time analysis (Hagedoorn, 1959) for these shots and the pair of stations DU1/DU2 gave a refractor velocity estimate of 6.40 km s^{-1}, which is consistent with a P* velocity. Apart from the low value of 7.2 km s^{-1} observed at station DU2, the remaining apparent Pn velocities (7.83-8.36 km s^{-1}) are reasonably similar to the Pn velocity range found for line D. There were no reversed velocity measurements along line B and, because of this and the large variation found in the apparent velocities and their dependence on the sedimentary corrections applied, the travel time graphs have not been interpreted in terms of layer thicknesses. Time term analysis is a more suitable method of interpreting this data and the graphs are used to indicate which arrivals are from the particular refractors.

In addition to the Pg and P* segments two other segments

representing crustal arrivals were observed at station DU1. The arrivals from shots B52-B56 define a segment of reciprocal gradient 4.19 km s^{-1} and a negative intercept. This velocity is interpreted as probably representing the 4.7 km s^{-1} Palaeozoic sediment refractor identified by Browitt (1971, 1972) in basin E. The low apparent velocity could be caused by the sediments thickening towards the north-west, and the negative intercept is explained by most of the travel time path being in a higher velocity material (6 or 6.4 km s^{-1}) than the refractor beneath the shots.

The remaining crustal segment observed at this station had an apparent velocity of 3.16 km s^{-1} and was defined by the arrivals from shots B47-B51. This velocity is within the range to be expected for Permo-Triassic sediments (Browitt, 1971) and is interpreted as representing the head wave travelling along the surface of these sediments. The travel times of these arrivals can be explained by a model in which the wave travels for the first short part of its path through the Permo-Triassic sediments and then for a much longer distance through outcropping basement material. To explain the travel times by such a model the boundary between the Permo-Triassic and basement material must occur approximately at the position of shot B51, and the distance of the boundary from the shots gradually increase to a maximum of 6.9 km from shot B47. A Permo-Triassic sediment velocity of 3.16 km s^{-1} (as observed) and a basement velocity of 6.1 km s^{-1} (as determined by time term analysis in section 4.4.) were used in the model. The dimensions of the model were:

Shot	Distance in P-T seds (km)	Travel time(s)	Distance in basement (km)	Travel time(s)	Total Travel time(s)	Observed travel time(s)	Residuals
B51	0.0	0.0	105.6	17.30	17.30	17.10	-0.20
B50	1.0	0.32	106.0	17.38	17.70	17.65	-0.05
B49	2.6	0.82	106.0	17.38	18.20	18.21	0.01
B48	4.5	1.42	106.5	17.46	18.88	18.87	-0.01
B47	6.9	2.18	107.0	17.54	19.72	19.78	0.06

Although the model explains the observed travel times it does not explain why such arrivals are the first to be received. It would be expected that the first arrivals would travel all their path length along the P* refractor. However it is possible that the wave travelling along the P* refractor in basin E may suffer a large loss of energy at the fault separating this basin from the outcropping basement, and so not be recognizable as an arrival at station DU1.

The only reliable Moho velocity determined from the line B time-distance graphs was for shots B65-B70 at station IGS1. The velocity defined by the uncorrected travel times was 7.48 ± 0.13 km s^{-1}, but after correcting the travel times of shots B68-B70 for the underlying Mesozoic sediments a Pn velocity estimate of 8.10 ± 0.17 km s^{-1} was obtained. No Moho depth estimate was determined from this velocity and corresponding intercept time as obviously the structure beneath the shot points is very different to that beneath the receiving station.

4.3.4 Line E

A total of eleven time-distance graphs were constructed for line E. Initially the graphs were plotted using travel times corrected only for variation in shot depth, bathymetry and station elevation, and the intercept times and velocities obtained for these graphs are given in Table 4.1 . However previous work in the region (Chesher et al, 1972; Sunderland,

1972) has shown that there is a Mesozoic sedimentary basin beneath the Moray Firth and, as the sediment thickness is variable across the region, a correction for this sediment variation has to be applied to the travel times. The basin topography determined from gravity modelling (Sunderland, 1972) was used to obtain the sediment correction values, assuming a mean sedimentary velocity of 3 km s^{-1}. The correction term added to each travel time was:

$$\frac{\text{Sediment depth (km)}}{5 \text{ km s}^{-1}} - \frac{\text{Sediment depth (km)}}{3 \text{ km s}^{-1}}$$

assuming a velocity of 5 km s^{-1} for the material (probably Old Red Sandstone) beneath the Mesozoic sediments. Reduced time-distance graphs were plotted using these corrected travel times and are shown in Figures 4.10-4.12 . The velocities and intercepts of each segment obtained by least squares fitting are given in Table 4.4. The scatter on the graphs, shown by the large standard errors, was large before applying the sedimentary corrections, and was increased by these corrections. This is probably due to a highly variable sediment cover and, as in addition there is no reversed velocity coverage, makes it almost impossible to interpret most of the graphs by means of the layer thickness formula.

All the observed velocities can be interpreted in terms of the P* or Moho refractor. The range and mean value found for the P* refractor were 6.32-7.03 km s^{-1} and $6.58 \pm .07$ km s^{-1}, and for the Moho 7.53-8.91 km s^{-1} and $8.00 \pm .12$ km s^{-1}. The observations at stations DU1, DU2, UKAEA, ULA and the Lownet stations define velocities sufficiently accurately to interpret the graphs in terms of layer thicknesses. However as the structure obviously changes considerably from beneath the shots to beneath the receiving stations the layer

TABLE 4.4

LINE E APPARENT VELOCITIES AND INTERCEPTS AFTER CORRECTING FOR THE MESOZOIC SEDIMENTS

Station	Shots	Phase	Velocity (km s^{-1})	Intercept(s)	S.E.
IGS1	E6, 8, 9	Pn	7.68±0.07	3.78±0.18s	0.03
IGS2	E6-E16	Pn	8.91±0.42	8.15±1.10s	0.20
DU1	E3-E17	Pn	8.00±0.26	4.78±1.11s	0.27
DU2	E1-E17	P*	6.40±0.08	1.50±0.23s	0.25
UKAEA	E2-E16	Pn	8.20±0.29	5.83±1.06s	0.31
UAB	E1-E15	P*	7.03±0.17	2.94±0.47s	0.21
ULA	E2-E8	P*	6.32±0.12	1.10±0.38s	0.05
UBL	E1-E14	Pn	8.08±0.57	5.79±1.31s	0.17
LN4	E1-E15	Pn	7.72±0.19	4.62±0.82s	0.22
LN5	E1-E17	Pn	7.60±0.13	4.45±0.51s	0.19
LN6	E1-E16	Pn	7.53-0.16	3.91-0.70s	0.24

Figure 4.10 : The reduced time-distance graphs for line E at (a) station IGS1, (b) station IGS2, (c) station UBL, (d) station ULA.

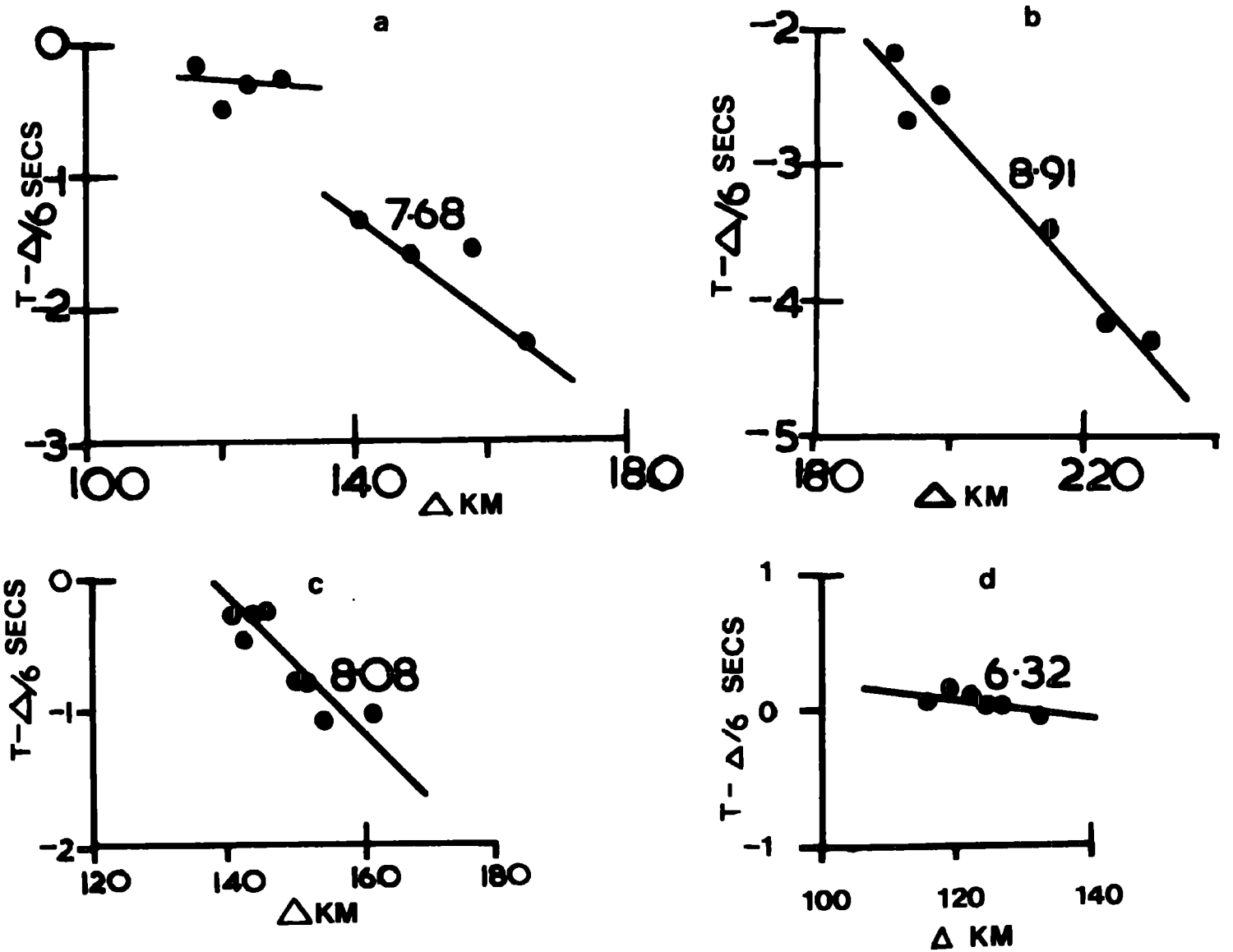
a
7·68
T-Δ/6 SECS
0
-1
-2
-3
100
140
180
Δ KM
b
8·91
T-Δ/6 SECS
-2
-3
-4
-5
180
220
Δ KM
c
8·08
T-Δ/6 SECS
0
-1
-2
120
140
160
180
Δ KM
d
6·32
T- Δ/6 SECS
1
0
-1
100
120
140
Δ KM

Figure 4.11 : The reduced time-distance graphs for line E at (a) station DU2, (b) station UAB, (c) station UKAEA, (d) station DU1.

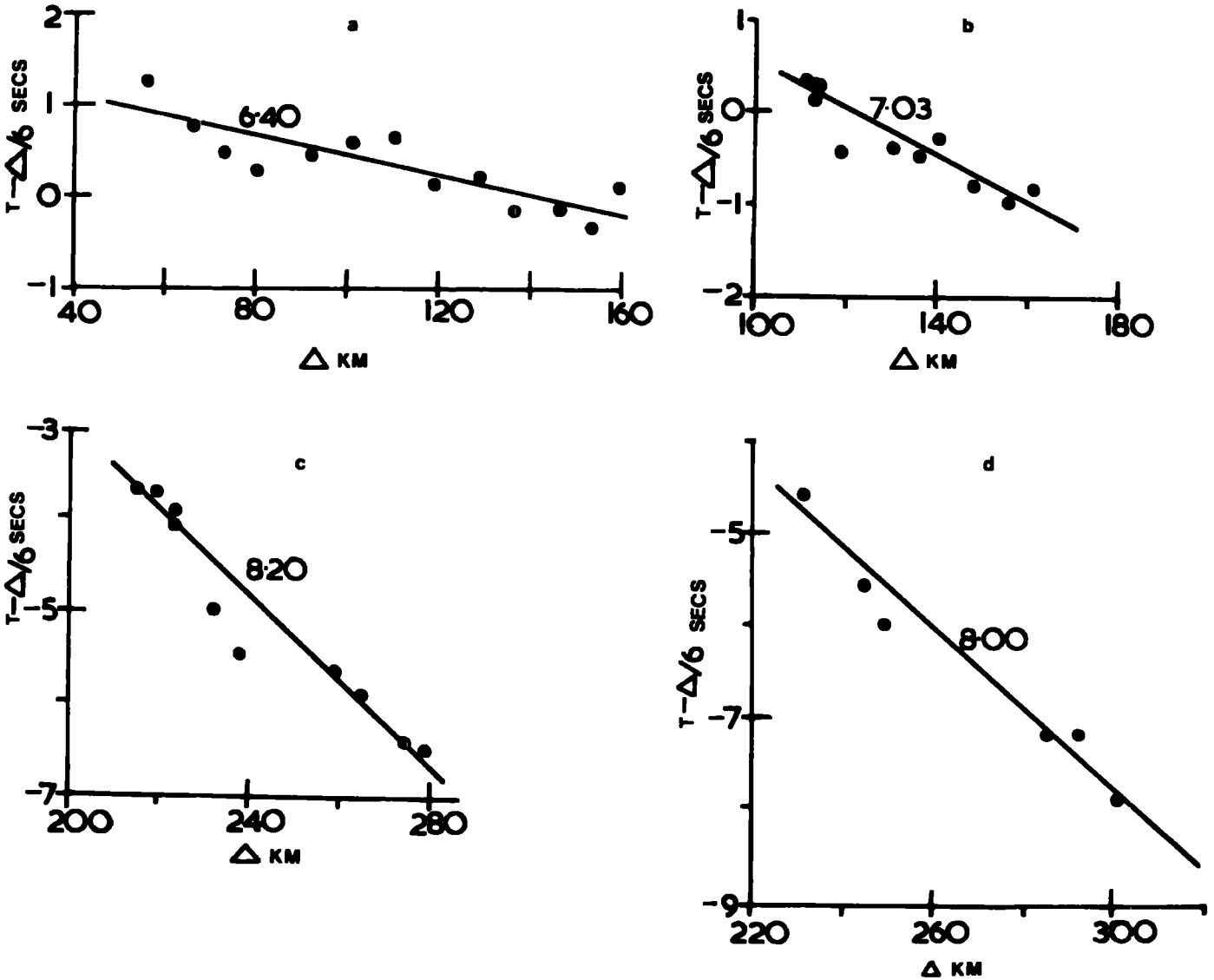
a
6·40
T−Δ/6 SECS
Δ KM
b
7·03
T−Δ/6 SECS
Δ KM
c
8·20
T−Δ/6 SECS
Δ KM
d
8·00
T−Δ/6 SECS
Δ KM

Figure 4.12 : The reduced time-distance graphs for line E at (a) station LN4, (b) station LN5, (c) station LN6.

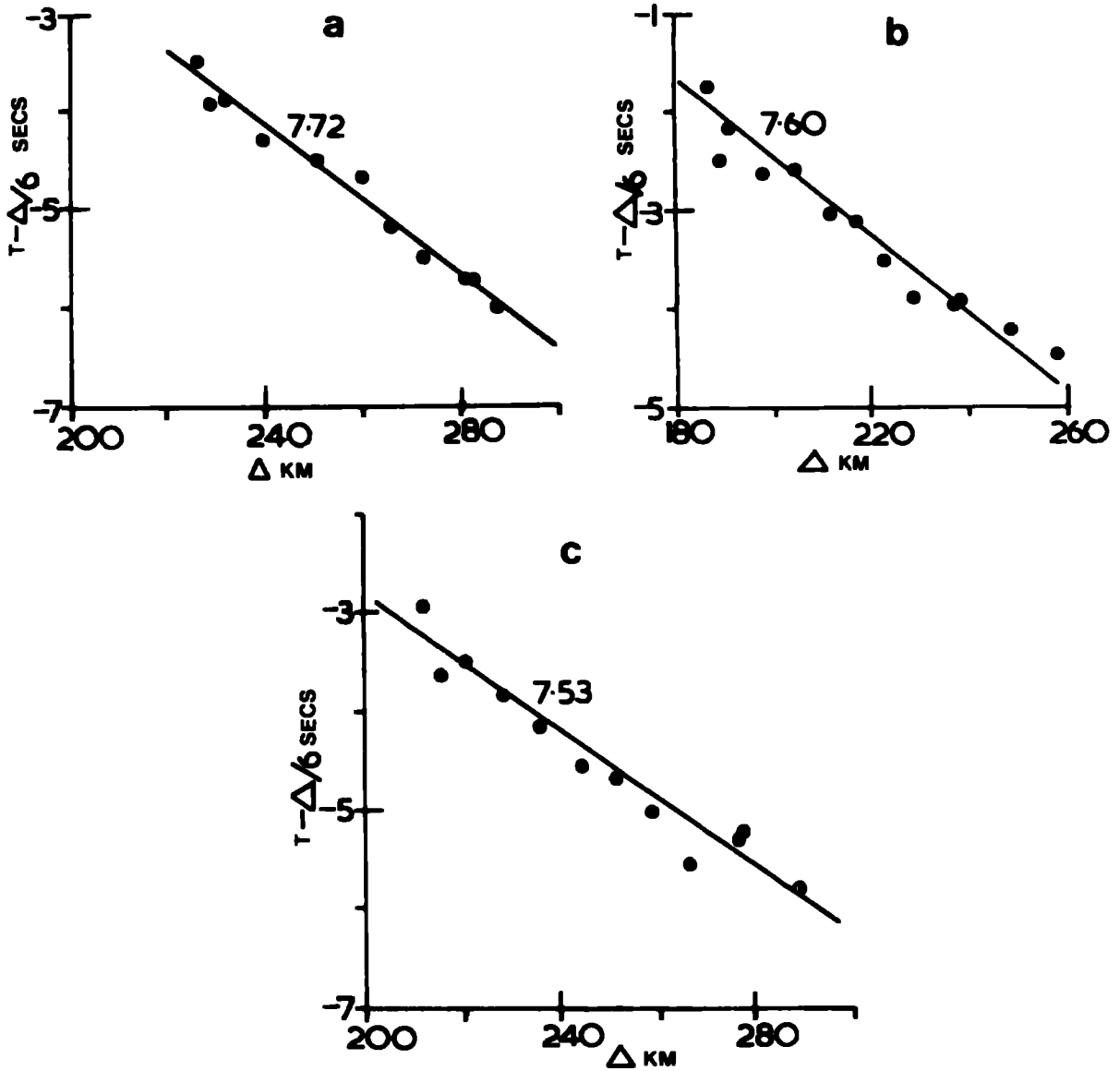
a
7·72
T−Δ/6 SECS
-3
-5
-7
200
240
280
Δ KM
b
7·60
T−Δ/6 SECS
-1
-3
-5
180
220
260
Δ KM
c
7·53
T−Δ/6 SECS
-3
-5
-7
200
240
280
Δ KM

Figure 4.13 : The stacked records of the line 5 shots at station IGS1.

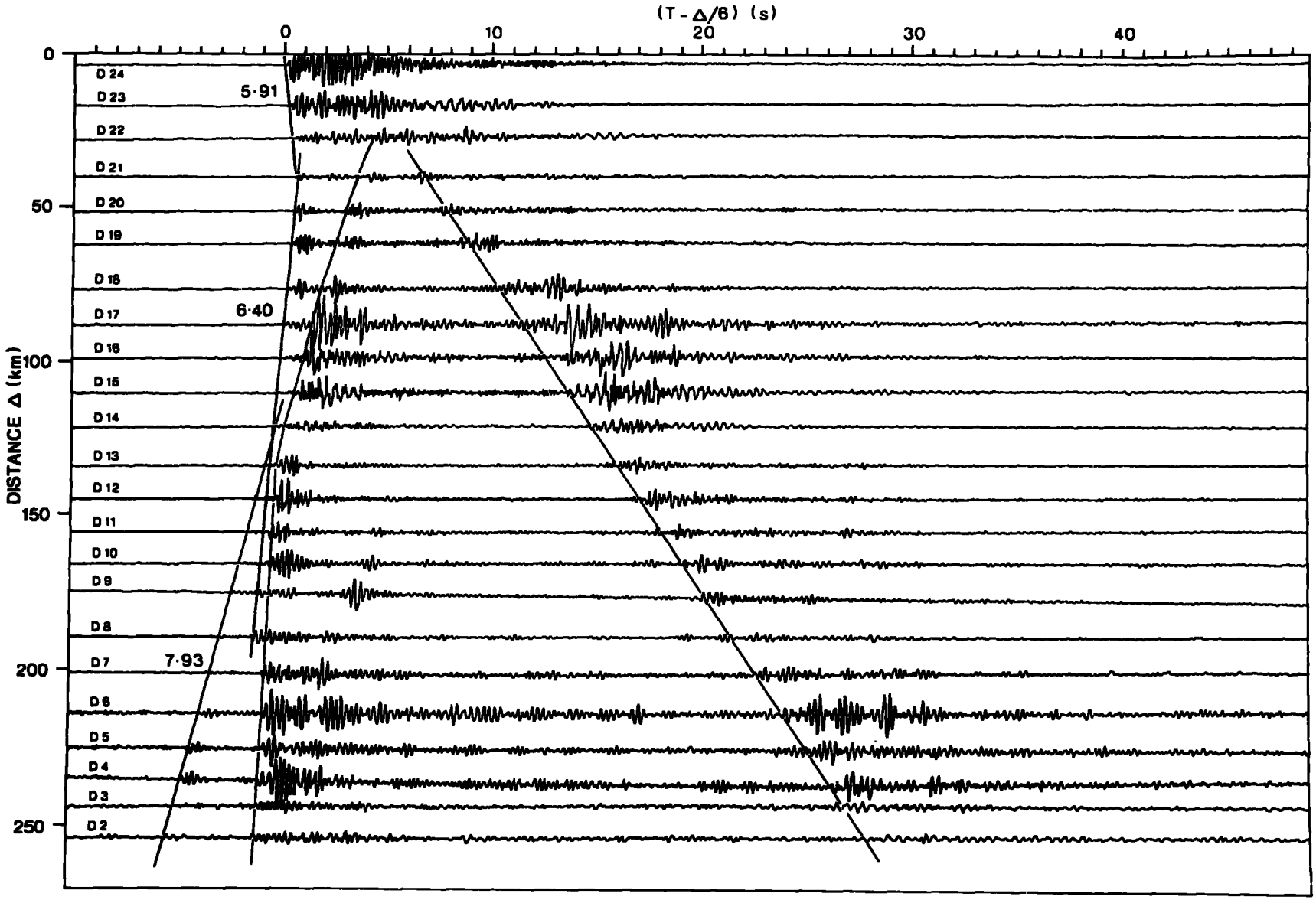
(T - Δ/6) (s)
0
10
20
30
40
DISTANCE Δ (km)
0
50
100
150
200
250
D 24
D 23
D 22
D 21
D 20
D 19
D 18
D 17
D 16
D 15
D 14
D 13
D 12
D 11
D 10
D 9
D 8
D 7
D 6
D 5
D 4
D 3
D 2
5·91
6·40
7·93

Figure 4.14 : The stacked records of the line D shots at station DU1.

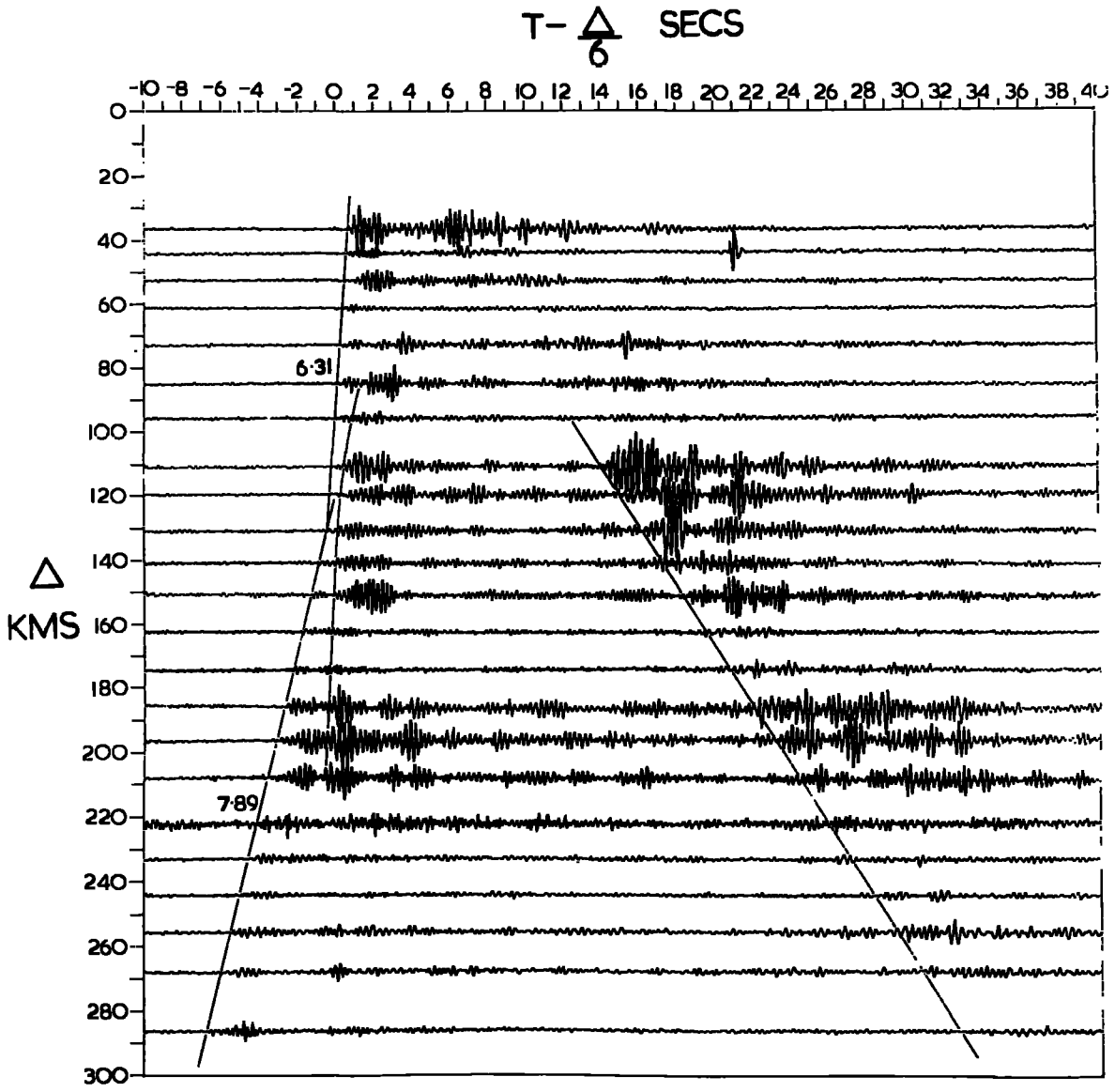
T- Δ/6 SECS
-10 -8 -6 -4 -2 0 2 4 6 8 10 12 14 16 18 20 22 24 26 28 30 32 34 36 38 40
0
20
40
60
80
100
120
140
160
180
200
220
240
260
280
300
Δ KMS
6·31
7·89

Figure 4.15 : The stacked records of the line D shots at station DU2.

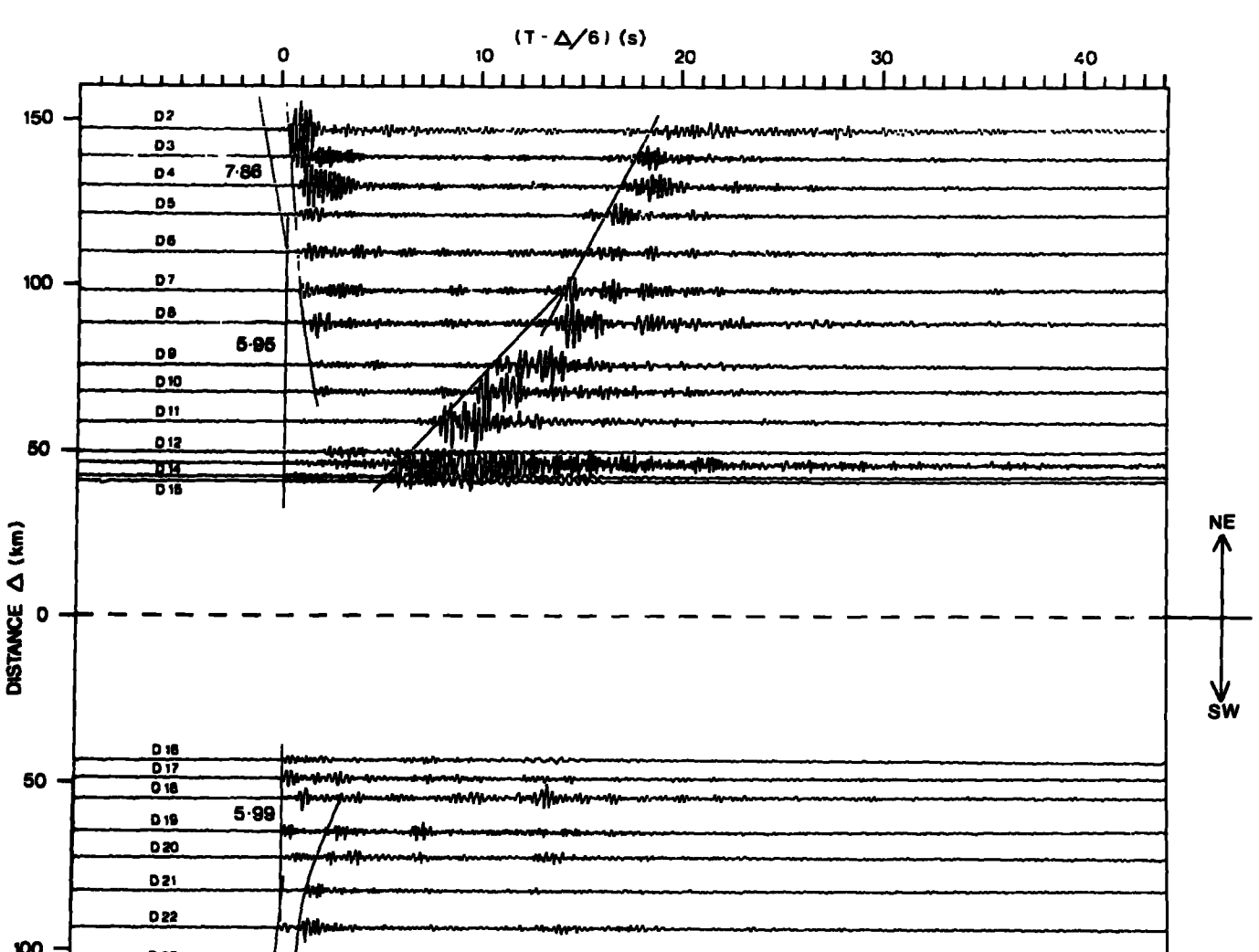
(T - Δ/6) (s)
0
10
20
30
40
150
100
50
0
50
100
DISTANCE Δ (km)
D2
D3
D4
D5
D6
D7
D8
D9
D10
D11
D12
D13
D14
D15
D16
D17
D18
D19
D20
D21
D22
D23
D24
7·86
5·95
5·99
6·49
NE
SW

thickness equation was not used. The graphs have only been used to give an indication of what refractors are present, and which arrivals can be used in the P* and ln time term analyses discussed in the following sections.

4.4 Time Term analysis

The classical method provides the first step in refraction interpretation but it is limited by its assumptions of plane layering and continuity of structures from shot points to station. At best an average structure can only be obtained beneath the line of shots and recording station. In general an average upper structure determined at one station has to be assumed for other stations in order to interpret the arrivals from deeper layers received at these stations. Time term analysis removes some of these inconsistencies. Refractor depths are determined beneath each shot point and, similarly, the lower structure beneath a shot point is interpreted in terms of the upper structure established for the same shot point. This interpretation technique can be used successfully where the shot-station configuration is suitable and the assumptions of the method not violated.

The previous discussion of the time-distance graphs indicated that in general three refractors, Pg, P* and Pn, were present beneath the Scottish Shelf. Time term analysis has been performed on the observed uncorrected first arrival travel times from each of these refractors, and the time terms found and estimated refractor velocities are listed in Table 4.5., and shown in Figures 4.16-4.19. The shot-station configuration of the experiment was best for the Pn time

TABLE 4.5.

TIME TERMS FOR THE SCOTTISH CONTINENTAL SHELF

Site	Pg time term(s)	SE		P* time term(s)	SE		Pn time term(s)	SE	
D2	0.15		(1)						
D3	0.29		(1)	0.42		(1)	2.43	0.16	(6)
D4	0.35		(1)	0.52		(1)	2.30	0.09	(7)
D5	0.36		(1)	0.48		(1)	2.35	0.10	(7)
D6	0.41		(1)	0.32		(1)	2.47	0.10	(4)
D7	0.49		(1)	0.42		(1)	2.75	0.17	(6)
D8	0.30		(1)	0.71		(1)	2.58	0.08	(8)
D9	0.28		(1)	0.76	0.05	(2)	2.58	0.06	(6)
D10	0.39		(1)	0.84	0.07	(2)	2.62	0.11	(7)
D11	0.15		(1)	0.88		(1)	2.58	0.07	(7)
D12	0.31		(1)	0.77		(1)	2.79	0.12	(6)
D13	0.24		(1)				2.52	0.05	(8)
D14	0.14		(1)	0.86		(1)	2.48	0.04	(11)
D15	0.16		(1)	1.26		(1)	2.48	0.06	(12)
D16	0.33		(1)	1.14		(1)	2.56	0.10	(10)
D17	0.30		(1)	0.91		(1)	2.59	0.08	(9)
D18	0.40		(1)	0.78		(1)	2.75	0.05	(10)
D19	0.34	0.04	(3)	0.77		(1)	2.69	0.05	(9)
D20	0.41	0.01	(2)	0.74		(1)	2.72	0.07	(7)
D21	0.36	0.07	(3)	0.54	0.01	(2)	2.82	0.11	(7)
D22	0.37	0.04	(3)	0.52		(1)	2.67	0.06	(9)
D23	0.30		(1)	0.67		(1)	2.70	0.05	(9)
D24									
C1	0.26	0.02	(2)	0.41	0.13	(2)	2.22	0.50	(2)
C2	0.18	0.12	(2)	0.40		(1)	2.31	0.34	(3)
C4	0.42	0.01	(2)	0.29		(1)	2.45	0.11	(4)
C5	0.19	0.19	(2)	0.22	0.04	(2)	2.38	0.16	(4)
C7	0.27	0.03	(2)	0.39	0.09	(2)	2.18	0.04	(2)
C8	0.32	0.06	(2)	0.42		(1)	2.31	0.21	(2)
C9	0.20	0.04	(2)	0.47		(1)	2.50	0.28	(3)
C10	0.34	0.10	(2)	0.60	0.12	(2)	2.31	0.08	(4)
C11	0.38		(1)	0.29	0.10	(2)			
C13	0.44		(1)	0.47	0.09	(2)	2.45		(1)
C14				0.71	0.09	(3)	2.51		(1)

TABLE 4.5. contd.

Site	Pg time term(s)	SE		P* time term(s)	SE		Pn time term(s)	SE	
C15				1.11	0.03	(3)	2.46	0.14	(5)
C16				0.94	0.03	(3)	2.72	0.11	(2)
C17				0.75	0.13	(2)	2.50	0.23	(4)
C19				0.95		(1)			
C20				0.89	0.04	(2)	2.80	0.11	(2)
C21				0.97	0.04	(2)	2.73		(1)
C22				1.20	0.02	(2)	2.29	0.26	(4)
C23				1.17	0.10	(2)	2.42	0.15	(5)
C24							2.27	0.15	(4)
B44							2.83	0.13	(11)
B45							2.85	0.13	(5)
B47							3.05	0.05	(3)
B48							2.66	0.21	(3)
B49							2.63	0.15	(4)
B50							2.78	0.05	(3)
B51				1.13		(1)	3.02	0.01	(2)
B52				1.06		(1)	3.06	0.03	(2)
B53						(1)	3.07	0.04	(2)
B54				1.12		(1)	3.09	0.06	(2)
B55				1.03		(1)	3.01	0.15	(2)
B56				1.11		(1)	3.09		(1)
B57				0.08		(1)	2.42	0.16	(3)
B59				0.11		(1)	2.38	0.12	(3)
B60				0.14		(1)	2.42	0.16	(4)
B61				0.08		(1)	2.32	0.12	(4)
B62							2.81	0.07	(2)
B63							2.88	0.33	(3)
B65	0.48		(1)	0.71	0.01	(2)	2.85		(1)
B66	0.48		(1)	0.64	0.05	(2)	2.56	0.21	(2)
B67	0.52		(1)	0.63	0.19	(2)	2.80	0.19	(2)
B68	0.70		(1)	1.16	0.04	(2)	2.89	0.23	(2)
B69	0.68		(1)	1.25	0.03	(2)	2.95	0.17	(2)
B70	0.67		(1)	1.26		(1)	2.90	0.16	(2)
E1				1.30	0.03	(2)	2.61	0.08	(6)
E2				1.30	0.04	(2)	2.75	0.12	(7)
E3				1.26	0.04	(2)	2.78	0.06	(7)

TABLE 4.5. contd.

Site	Pg time term(s)	SE	P* time term(s)	SE	Pn time term(s)	SE
E4			1.10	0.05 (2)	2.82	0.09 (5)
E5			1.38	(1)	2.87	0.08 (7)
E6			1.32	0.02 (3)	2.86	0.11 (7)
E7			1.56	0.13 (3)	3.15	0.12 (7)
E8			1.59	0.18 (2)	2.98	0.15 (8)
E9			1.23	0.14 (3)	2.92	0.08 (7)
E13			1.31	0.25 (3)	3.07	0.14 (4)
E14			1.45	0.03 (2)	3.05	0.13 (8)
E15			1.02	0.16 (4)	3.13	0.13 (5)
E16			0.70	0.10 (2)	3.05	0.14 (5)
E17			1.03	0.07 (3)	3.30	0.48 (2)
IGS1	0.06	0.02 (13)	0.37	0.02 (20)	2.45	0.03 (47)
IGS2	-0.14	0.02 (14)	0.77	0.04 (5)	2.43	0.06 (30)
IGS3					3.16	0.08 (26)
DU1			0.71	0.02 (15)	2.56	0.05 (17)
DU2	0.17	0.00 (15)	0.82	0.03 (30)	2.78	0.04 (27)
DU3					2.86	0.04 (20)
UKAEA	0.34	0.00 (11)	0.55	0.01 (14)	2.47	0.03 (29)
UAB	-0.02	0.02 (5)	0.48	0.04 (15)	2.99	0.04 (31)
ULA			0.79	0.04 (11)	2.79	0.05 (8)
UBL					3.09	0.05 (32)
MHD					3.63	0.07 (9)
LN1					2.21	0.14 (5)
LN4					3.30	0.07 (14)
LN5					3.48	0.04 (44)
LN6					3.18	0.05 (37)
LN8					3.72	0.09 (10)
LN9					3.12	0.06 (10)
MIR(A)			0.56	0.02 (7)		

Pg 6.10 ± 0.15 km s^{-1}; P* 6.48 ± 0.06 km s^{-1}; Pn 7.99 ± 0.02 km s^{-1}

Figure 4.16 : The time terms and Bouguer anomaly profile observed alone line D.

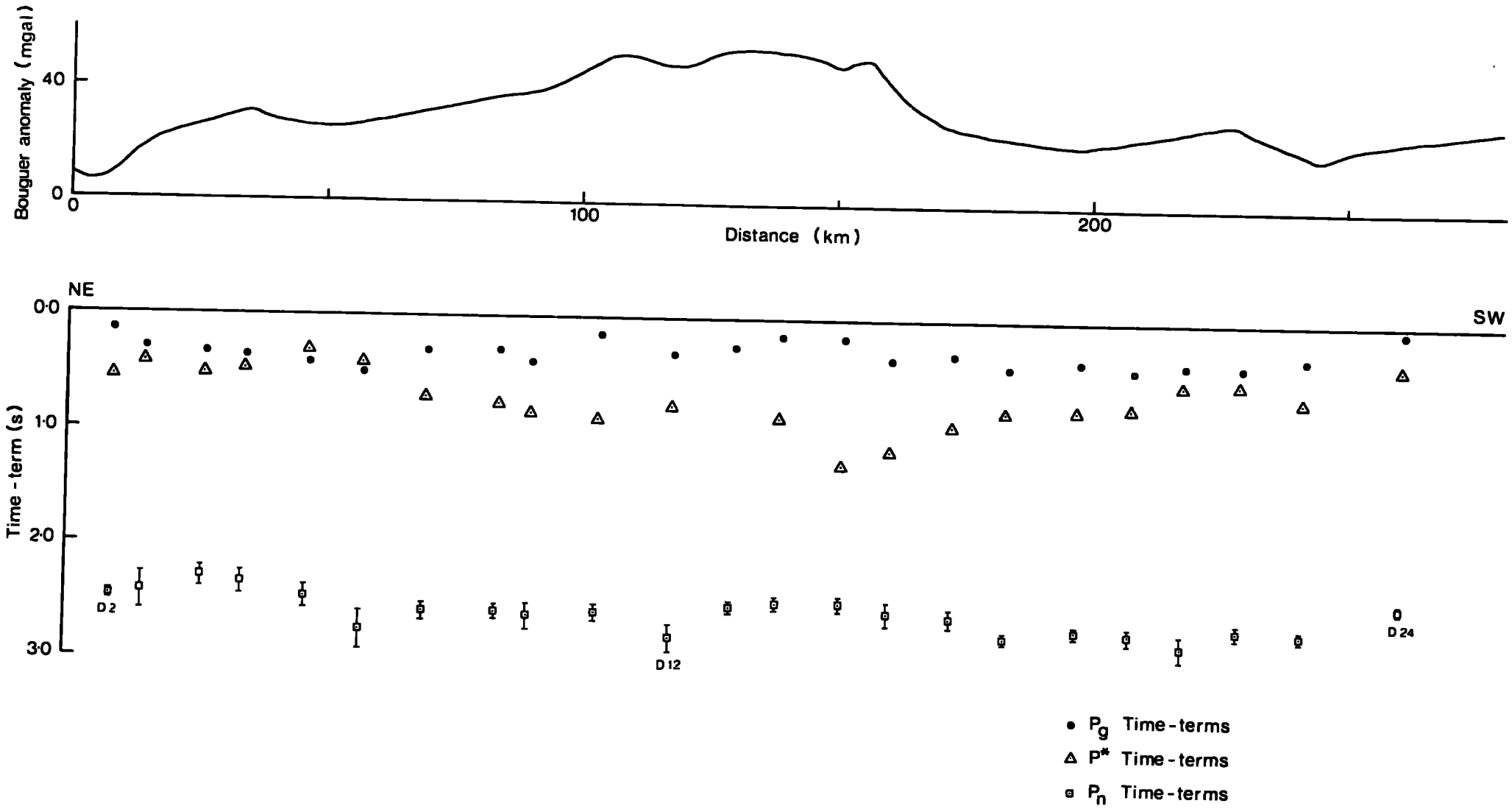
Bouguer anomaly (mgal)
40
0
0
100
200
Distance (km)
NE
SW
0·0
1·0
2·0
3·0
Time - term (s)
D2
D12
D24
• P_g Time-terms
△ P^* Time-terms
▫ P_n Time-terms

Figure 4.17 : The time terms and Bouguer anomaly profile observed along line C.

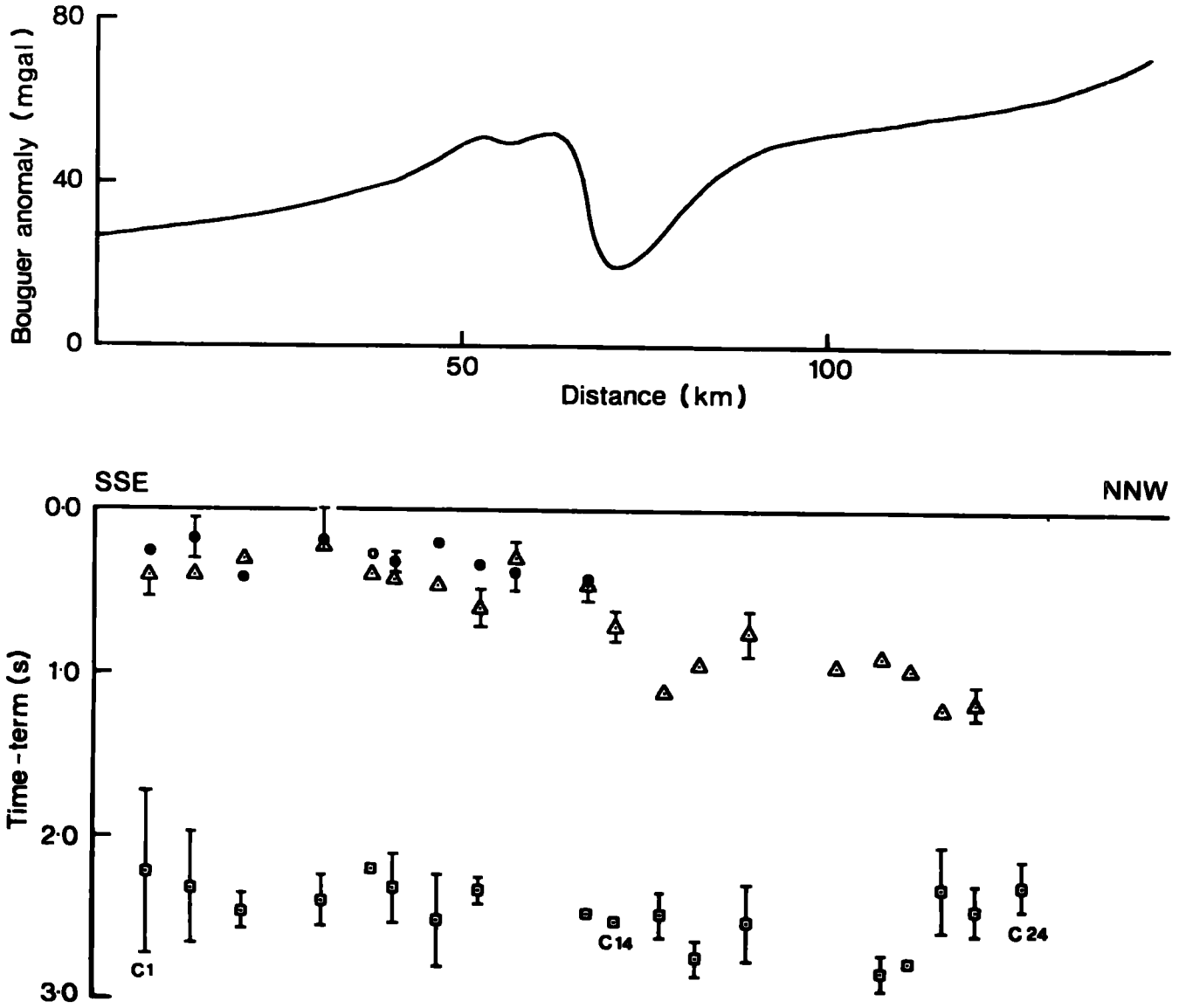
80
40
0
Bouguer anomaly (mgal)
50
100
Distance (km)
SSE
NNW
0·0
1·0
2·0
3·0
Time-term (s)
C1
C14
C24

Figure 4.18 : The time terms and Bouguer anomaly profile observed along line B.

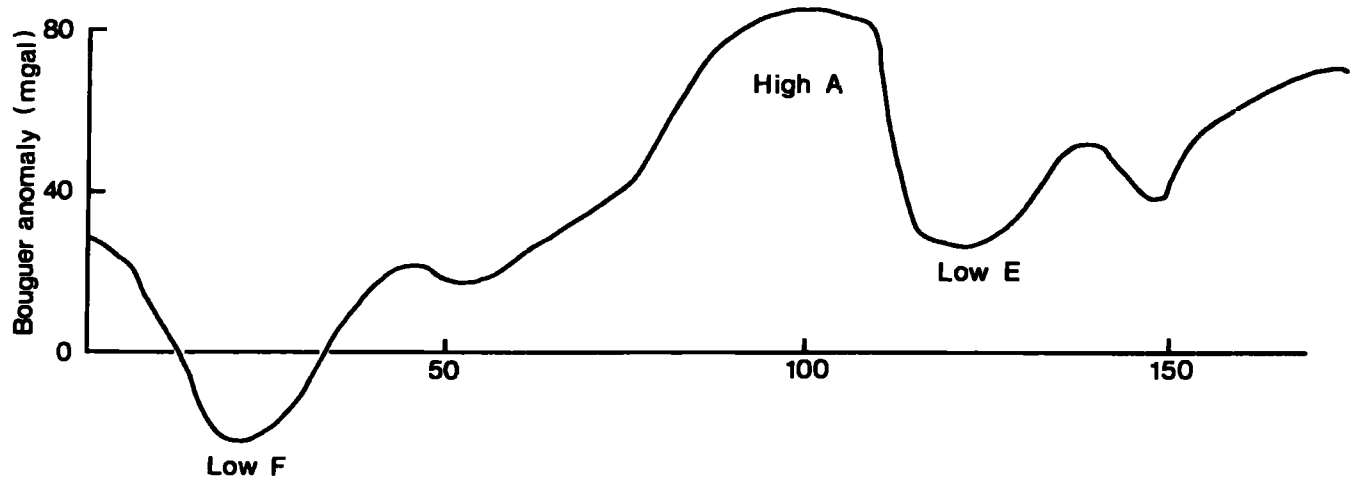
Bouguer anomaly (mgal)
80
40
0
50
100
150
High A
Low E
Low F

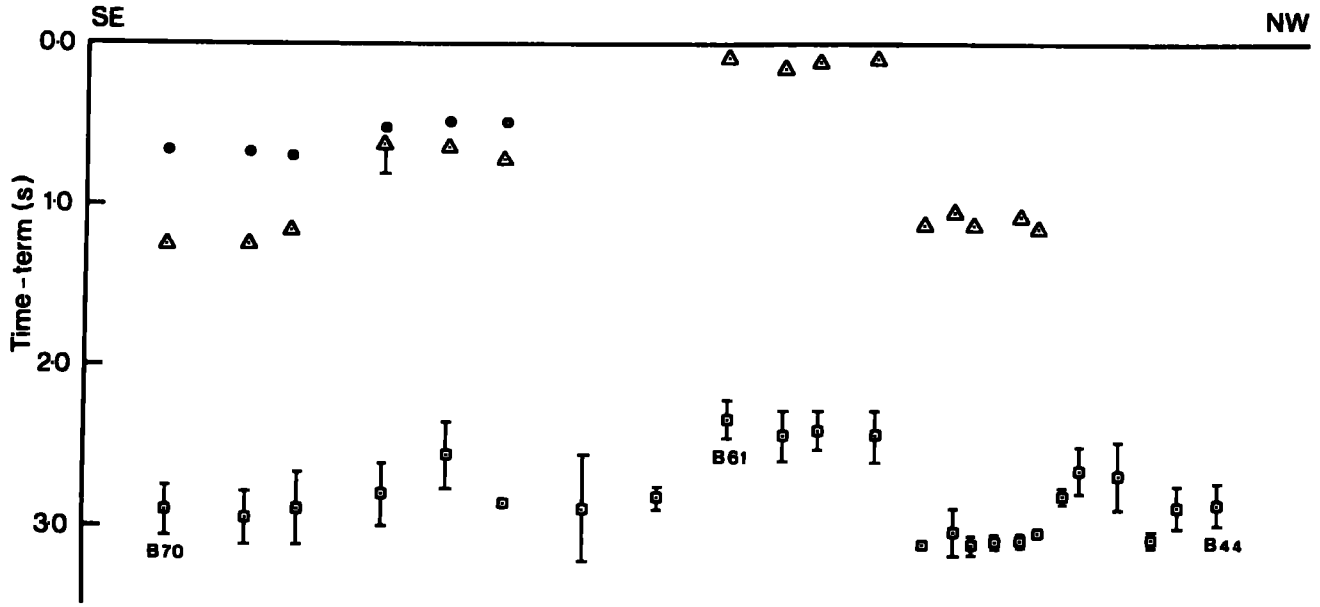
SE
NW
0·0
1·0
2·0
3·0
Time - term (s)
B70
B61
B44

Figure 4.19 : The time terms and Bouguer anomaly profile observed along line E.

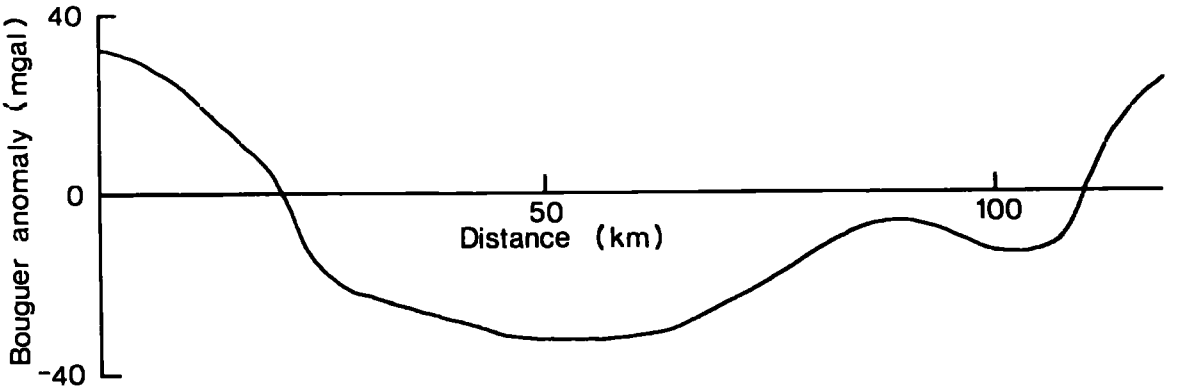
Bouguer anomaly (mgal)
40
0
-40
50
100
Distance (km)

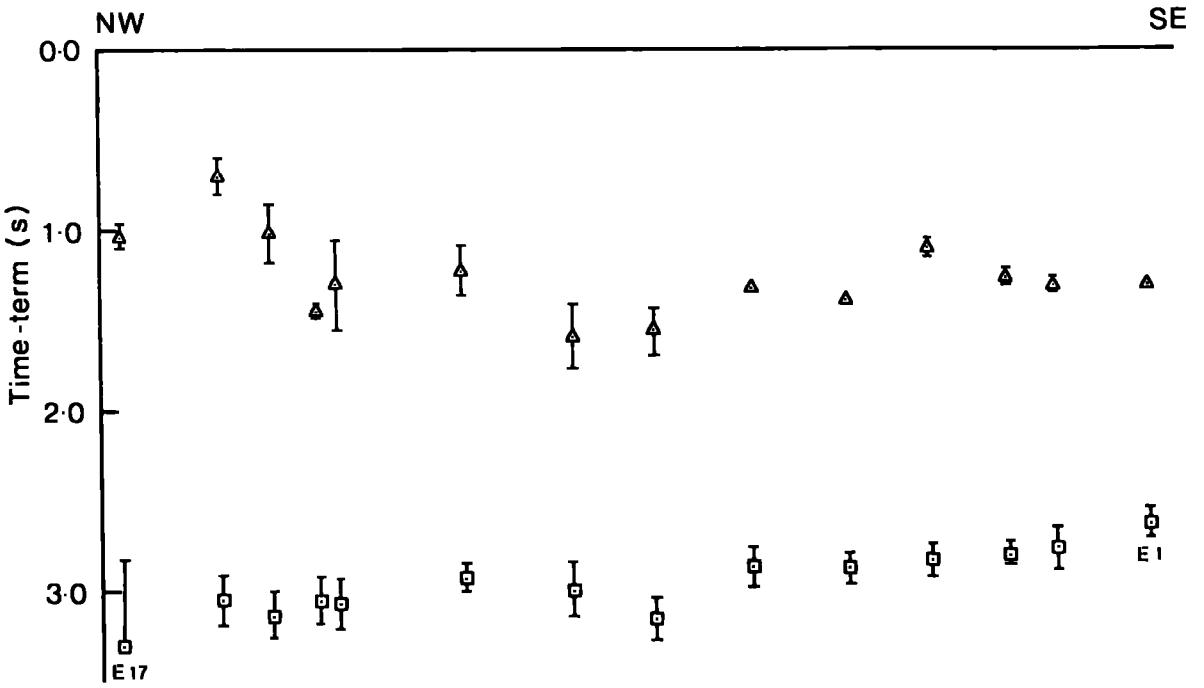
NW
SE
0·0
1·0
2·0
3·0
Time-term (s)
E17
E1

term analysis as there was more reversed coverage and a wider azimuthal range of observation provided by the offset stations. This is reflected in the plots of the experimental error variance of the solutions against the constrained velocity used for the solution (Fig. 4.20). These graphs indicate that a much sharper minimum variance is defined by the correct Pn velocity value than for the correct Pg and P* velocity values, which means that the Pn velocity is better determined. However the overall fit of the solution is good for each refractor as the experimental error variance is small. The internal consistencies are also good for each solution as is shown by the close agreement between the time terms of recording stations and nearby shots:

Pg solution	station	UKAEA	0.34s	D3	0.29s
P* solution	station	IGS1	0.37s	C1	0.41s
Pn solution	station	IGS1	2.45s	C1	2.22s
Pn solution	station	UKAEA	2.47s	D3	2.43s

The residual travel times calculated for each shot-station link were in general quite small (of the order of 0.2s) and showed no correlation with distance or azimuth. This indicates that the residuals were probably caused by measurement errors and not by violation of the assumptions of the time term method. Any travel time that had a residual greater than three standard deviations away from the median residual for the shot or station was removed from the input data and the analysis re-run.

There were sufficient observations of the P* and Pn refractors to compute time term solutions using different data sets. The initial Pn data set consisted only of observations of line D shots, and then observations of lines C, B and E shots were successively added to the data set and a time term analysis performed each time. The initial P* data

Figure 4.20 : The constrained time term velocity versus the fit of the solution for (a) the Pg refractor (b) the P* refractor, (c) the Pn refractor.

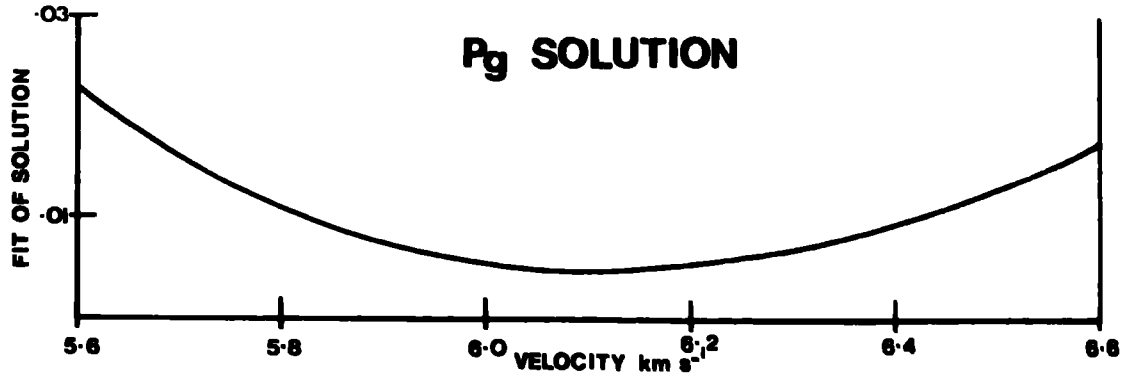
P_g SOLUTION
FIT OF SOLUTION
·03
·01
5·6
5·8
6·0
6·2
6·4
6·6
VELOCITY km s⁻¹

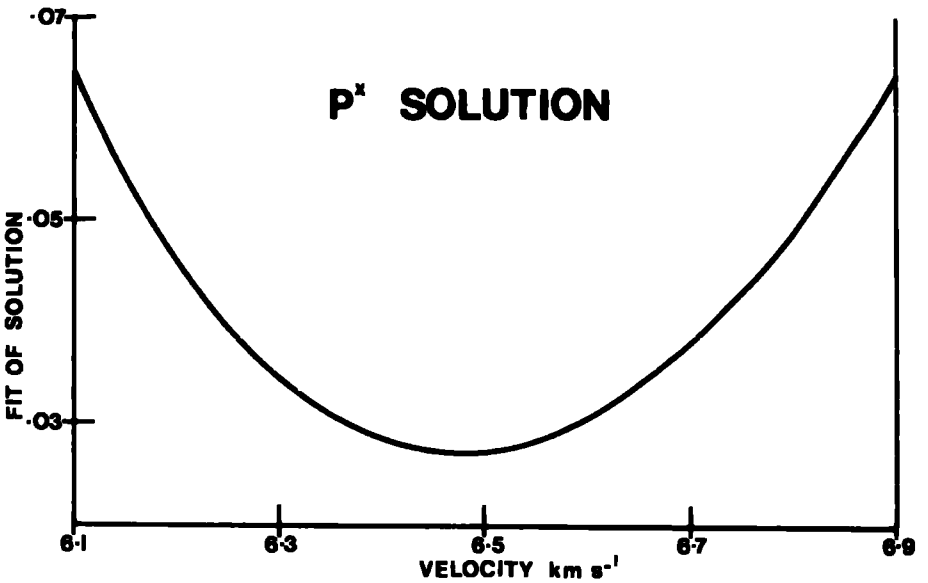
P^x SOLUTION
FIT OF SOLUTION
·07
·05
·03
6·1
6·3
6·5
6·7
6·9
VELOCITY km s⁻¹

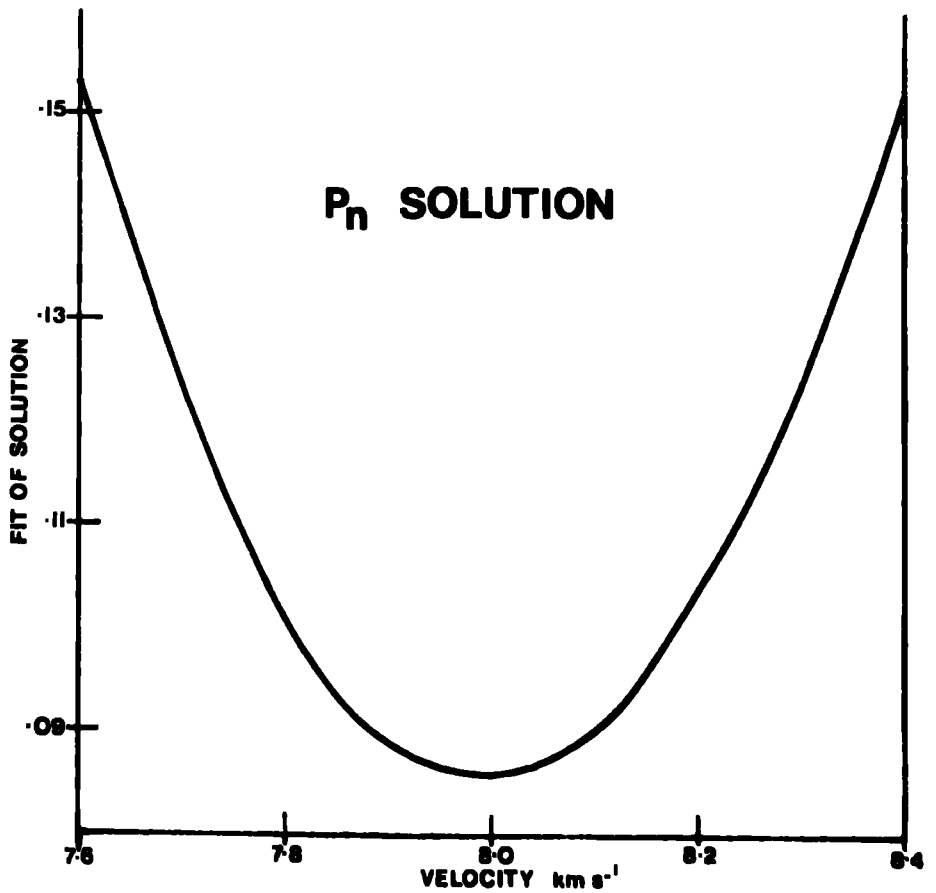
P_n SOLUTION
FIT OF SOLUTION
·15
·13
·11
·09
7·6
7·8
8·0
8·2
8·4
VELOCITY km s⁻¹

set consisted of observations from lines D, C and B shots, and the second and final set also included the observations of the line E shots. In both cases no significant change was found in the original time terms between the first and final data set.

		Station UKAEA	Shot D13
Pn solution	data set 1	2.54	2.47
	data set 2	2.47	2.52
P* solution	data set 1	0.53	0.45
	data set 2	0.55	0.47

This is taken to indicate that the solutions are stable and that no significant discrepancies exist between the data of the different shot lines.

The Pg velocity estimate of 6.1 ± 0.15 km s^{-1} is in close agreement with the basement velocity measured by Browitt (1971), and the Pn velocity of 7.99 ± 0.02 km s^{-1} is a normal Moho velocity value within the range to be expected for Britain (Agger and Carpenter, 1965; Bamford, 1971; Blundell and Parks, 1969; Holder and Bott, 1971). The P* velocity of 6.48 ± 0.06 km s^{-1} has not been observed previously near the British Isles. It is significantly different to the 7.3 km s^{-1} refractor observed beneath Cardigan Bay (Blundell and Parks, 1969), and the P* time terms indicate that it is at a considerably shallower depth.

4.4.1 Line D time terms

The Pg time terms have small positive values along line D with a mean of 0.31s. The interchange position for this analysis was station IGS1 and shot D24, and an almost zero time term (0.09s) was found for this location, probably due to the proximity to the surface of the Lewisian metamorphic basement beneath station IGS1. A mean sedimentary velocity of

5 km s^{-1} was assumed to interpret the Pg time terms in terms of basement depths, and the average time term value was found to represent a sediment cover of 2.7 km. Old Red Sandstone probably accounts for the majority of the sediment cover beneath the line (Watts, 1971), but Mesozoic and Torridonian deposits may occur in the south-west region. Browitt (1971) measured a velocity of 5.25 km s^{-1} for the Old Red Sandstone to the south of the Shetland Islands, and a velocity of 4.7 km s^{-1} for the Palaeozoic (Old Red Sandstone) deposits in basin E to the west of the Shetland Islands. A mean sediment velocity of 5 km s^{-1} is therefore probable, but for a lower velocity the sediment cover is correspondingly reduced. The Pg time terms of shots D11-D15 (mean 0.2s) are significantly smaller than the average for this line. This is to be expected as they occur in a region of relatively shallow basement (Watts, 1971) and correspond to high Bouguer anomaly values (Fig. 4.16).

The P* time terms determined along line D are significantly larger over the central area and, on average, have the smallest values in the north-east. The mean value for the line was 0.69s and was interpreted in terms of a mean P* refractor depth of 9 km, allowing for the overlying 2.7 km thick sedimentary layer and 0.1 km of sea water. As significant differences in time term values were found for various parts of the line, mean time term values were determined for four separate sections. These were each interpreted in terms of refractor depths assuming the mean overlying sediment thickness determined from the Pg time terms of the corresponding section. The results are given in Table 4.6.

The Pn time terms were found to increase towards the

south-west along line D, in agreement with the reversed straight line Pn interpretation. The average Pn value of 2.59s was interpreted in terms of a three layered crust with an assumed sedimentary velocity of 5 km s^{-1} and underlying crustal velocities as determined by the time term analyses. An average crustal thickness of 25.0 km was found. To allow for the variations along the line mean time term values were obtained for the same four sections as previously and interpreted in terms of the overlying thicknesses of material established for these sections. The crustal thicknesses found are given in Table 4.6.

Table 4.6

	Section 1 (D2-D6)	Section 2 (D7-D12)	Section 3 (D13-D17)	Section 4 (D18-D23)	Mean (D2-D23)
Base of sediments	2.7 km	2.8 km	2.0 km	3.1 km	2.7 km
Base of uppercrust	4.9 "	9.7 "	16.3 "	8.2 "	9.0 "
Depth to Moho	23.6 "	25.5 "	23.4 "	26.3 "	25.0 "

The only large variations along the line are in the depth to the P* refractor (the base of the upper crust). It appears that this refractor deepens away from both ends of the line to a maximum depth of approximately 16 km beneath shots D13-D17. However this increase in these time term values could also result from the velocity determined by the analysis (6.48 km s^{-1}) being an overestimate of the true local refractor velocity along line D. As, in general, the P* arrivals from shots D13-D17 are at maximum ranges, for P* arrivals, from all the receiving stations, an overestimate of P* velocity would increase the time terms of these shots relative to those of the nearer shots. This effect is seen to occur by comparison with the results of P* data set 1 (line E data excluded) where the determined P* velocity was 6.41 km s^{-1}.

The maximum variation in P* refractor depth along the line using this time term solution was 8.1 km, compared to 11.4 km using the results of P* data set 2.

The Moho results indicate a general dip to the south-west of approximately 0.67°, although the depths determined beneath shots D7-D12 and D13-D17 indicate a dip in the opposite direction. As these results confirm the reversed straight line interpretation this dip to the south-west is probably a true dip, but the variations in Pn time terms and depths are scarcely significant. A crustal cross section along line D, constructed from the time terms, is presented in Figure 4.21.

4.4.2 Line C time terms

Pg arrivals were only observed from shots C1-C13 and these produced a range in Pg time terms of 0.18-0.44s, with a mean value of 0.30s. These values were interpreted assuming similar overlying sediment material to that beneath line D (5 km s^{-1}), and a range in basement depth of 1.6-3.8 km found, with a mean depth of 2.6 km.

The P* time terms were found to increase abruptly between shots C13 and C14, the mean value for shots C1-C13 being 0.40s and for shots C14-C23, 0.97s. Assuming that the Pg basement is present beneath the two sets of shots, and underlies a uniform 2.6 km sediment cover, then this time term variation represents a variation in depth to the P* refractor of 3.9-14.2 km. However if, as was suggested in section 4.3.2., the Pg basement terminates beneath shots C14-C23, then the P* refractor is at a mean depth of only 7.6 km beneath these shots.

The Pn time terms are reasonably constant along this line with a range of 2.18-2.80s and a mean of 2.43s. The mean

Figure 4.21 : The crustal structure beneath line D determined from the time terms.

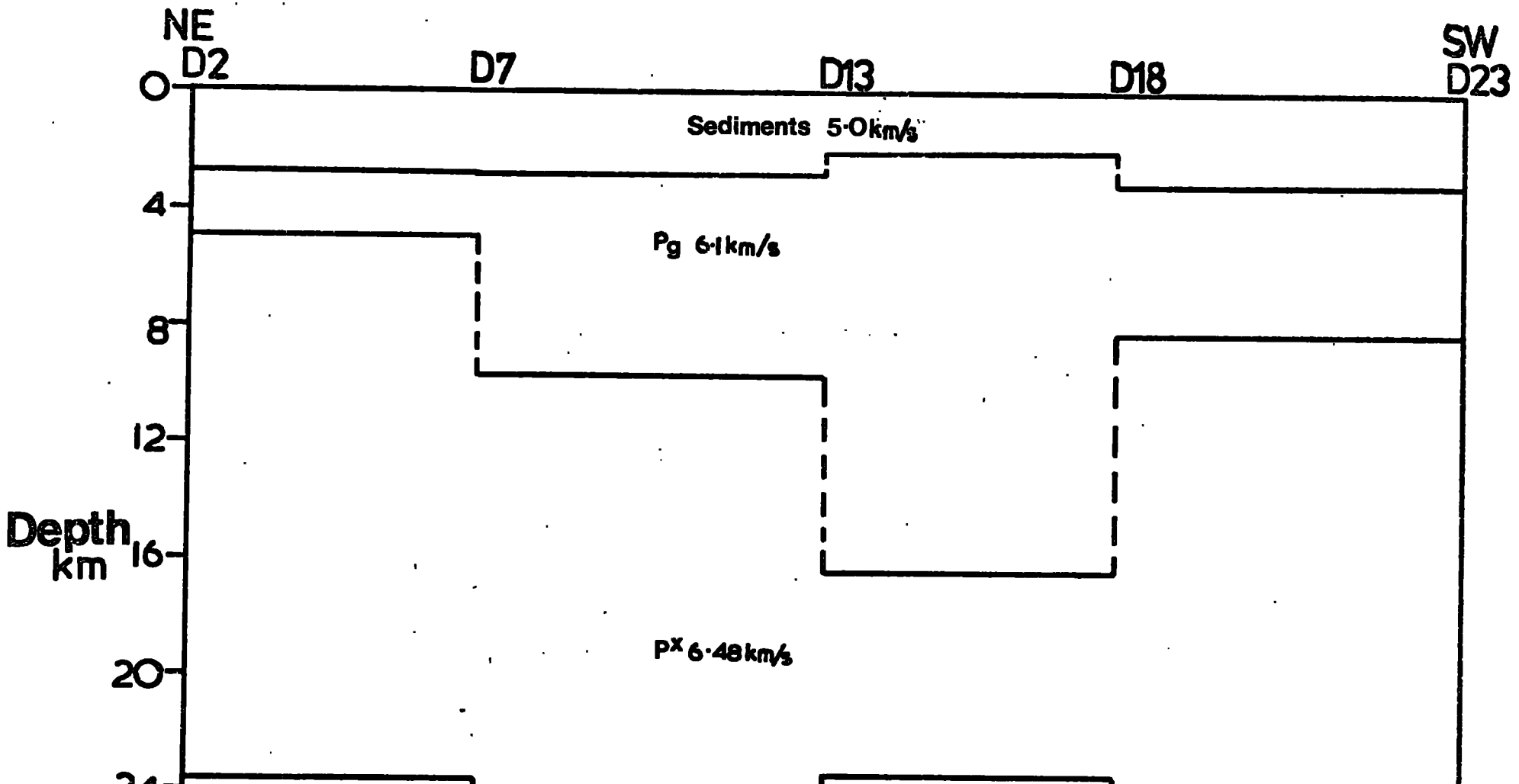
NE
D2
D7
D13
D18
SW
D23
0
4
8
12
16
20
24
28
Depth km
Sediments 5·0km/s
Pg 6·1km/s
Px 6·48km/s
Pn 7·99km/s

value was interpreted in terms of 2.6 km of sediments (5 km s^{-1}) overlying 6.5 km of upper crustal material (6.1 km s^{-1}) and the Moho was found to be at a depth of 23.9 km. However as a variation was found in upper crustal structure the mean Pn time terms for the two regions (shots C1-C13 and shots C14-C23) were also interpreted in terms of crustal thicknesses. A P* refractor depth of 3.9 km beneath the overlying 2.6 km sediment cover was assumed for the first group, and the sediments were assumed to directly overlie the P* refractor at a depth of 7.6 km beneath the second group. Crustal thickness estimates of 23.9 km and 22.4 km respectively were found for the two areas. These two values are probably not significantly different but the results suggest that if anything the crust is thinner beneath shots C14-C23 i.e. sedimentary basin D. The proposed crustal cross section beneath line C, based on the time terms, is given in Figure 4.22.

4.4.3 Line B time terms

The time terms for this line show large lateral variations related to the large local gravity anomalies established on the shelf. It is therefore convenient to present the results of the analyses in terms of a number of separate structural units based on the gravity anomalies and these are listed for the corresponding shot points:

1. Shots B68-B70

These shots were over gravity low F interpreted by Bott and Browitt (in preparation) as a Mesozoic sedimentary basin. The mean Pg, P* and Pn time terms found were 0.68s, 1.22s and 2.91s respectively, and were interpreted in terms of the following crustal structure: 1.4 km of Mesozoic sediments

Figure 4.22 : The crustal structure beneath line C determined from the time terms.

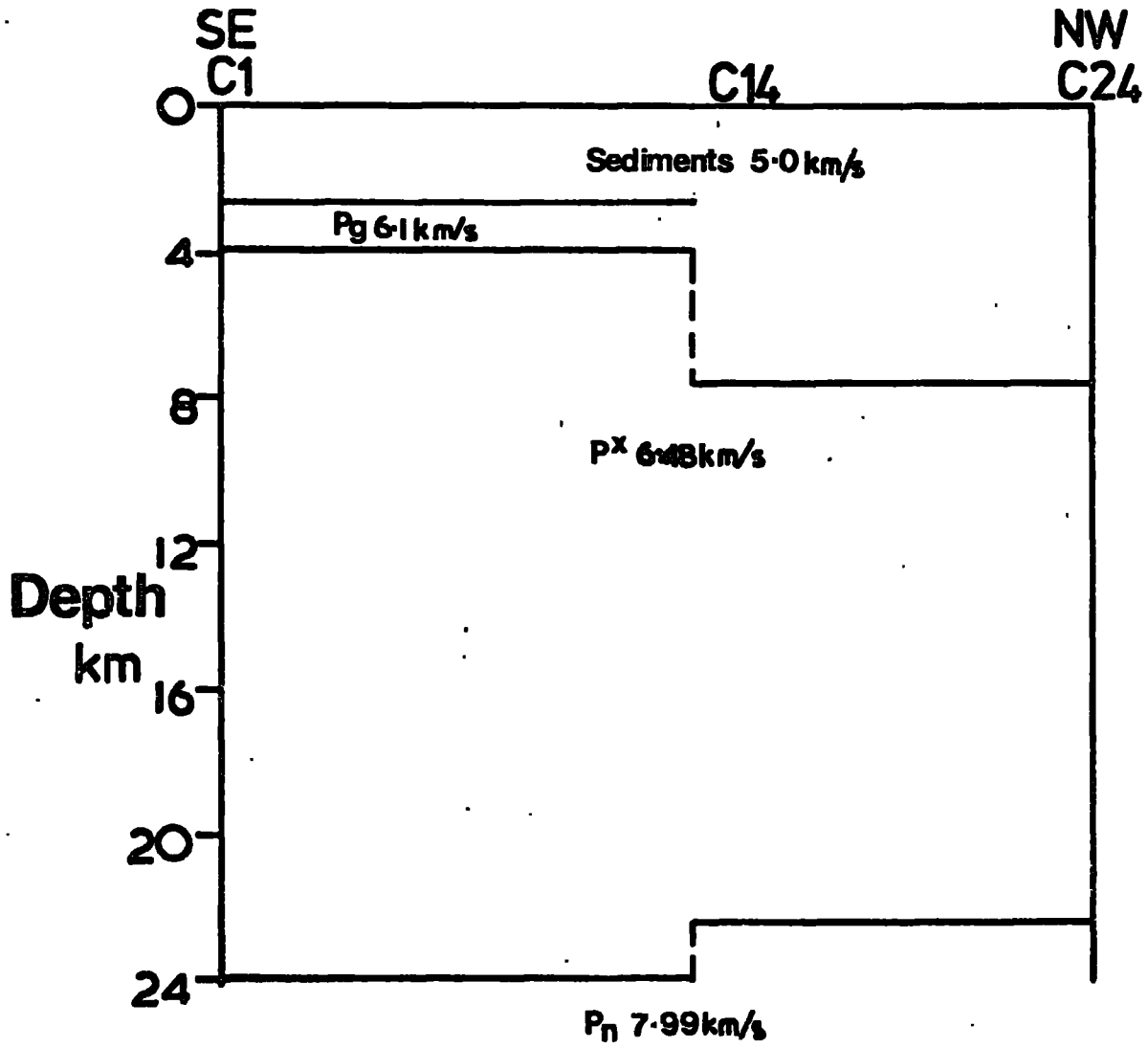
SE
C1
C14
NW
C24
0
4
8
12
16
20
24
Depth
km
Sediments 5·0 km/s
Pg 6·1 km/s
P^x 6·48 km/s
Pn 7·99 km/s

(2.7 km s^{-1}), 1.9 km of Upper Palaeozoic sediments (5.0 km s^{-1}), 9.2 km of upper crustal material (6.1 km s^{-1}) and 12.7 km of lower crustal material (6.48 km s^{-1}), the depth to the Moho being estimated as 25.2 km. The upper crustal structure derived from the Pg time terms is in excellent agreement with that derived from the shallow geophysical investigations of Bott and Browitt.

2. Shots B65-B67

Shots B65-B67 lie over outcropping Upper Palaeozoic sediments (Watts, 1971) to the immediate west of the Mesozoic basin, and have mean Pg, P* and Pn time terms of 0.49s, 0.66s and 2.74s respectively. These values were interpreted in terms of 4.3 km of Upper Palaeozoic sediments (5 km s^{-1}), 2.0 km of upper crustal material and 20.6 km of lower crustal material, the Moho being at a depth of 26.9 km. It is possible that the Pg time terms are too large and that there is not as much as 4.3 km of sediments. If this is so the depth to the P* refractor would be greater than the estimated 6.3 km.

Only Pn time terms could be determined for shots B62 and B63, and their mean value of 2.84s does not differ significantly from that of shots B65-B70.

3. Shots B57-B61

These shots were over gravity 'high A' (Bott and Watts, 1970), which has been interpreted as a region of shallow and/or outcropping high density basement material. All four shots have P* time terms close to zero (mean 0.1s) implying that the P* refractor comes very close to the surface. The mean time term was interpreted to represent a cover of 1.8 km of upper crustal material. This basement material was identified on an unreversed shallow refraction line of 20 km length along the

strike of 'high A' (Browitt, 1971). A velocity of 5.9 km s^{-1} was measured just below the sea bed. Similarly a Pg velocity was observed from the arrivals of these shots at station DU1, so the P* refractor must definitely not outcrop at the surface. However the refractor approaches the surface beneath gravity 'high A' and is probably the cause of the high gravity anomaly. The mean Pn time term of 2.38s was interpreted in terms of 1.8 km of upper crustal material (6.1 km s^{-1}) overlying the lower crustal (P*) layer, the Moho being at a depth of 26.1 km.

4. Shots B51-B56

Shots B51-B56 lie over gravity 'low E' (Bott and Watts, 1970) which has been interpreted as caused by a deep sedimentary basin separated by a fault from gravity 'high A'. Gravity and shallow seismic refraction investigations (Browitt, 1971) indicate that the basin contains about 2.5-3.0 km of Tertiary and Mesozoic sediments overlying up to 4 km of higher velocity and higher density sediments of possible Upper Palaeozoic or Torridonian age. No Pg arrivals were detected from these shots. The mean P* time term of 1.09s was interpreted in terms of 2km of sediment of mean velocity 3 km s^{-1}, and 3.9 km of sediment of mean velocity 5 km s^{-1} directly overlying the P* (6.48 km s^{-1}) basement. If the true local P* velocity is greater than the time term value then the P* time terms will have been underestimated and a greater sediment thickness or a thin Pg layer could be present. The mean Pn time term of 3.06s was interpreted in terms of the previous sedimentary structure underlain by 20.3 km of lower crustal material, the Moho being at a depth of 26.2 km.

5. Shots B47-B50

These shots cross a region of basement uplift within gravity 'low E', which has been detailed by gravity and magnetic anomalies. (Watts, 1971). Pn time terms only could be determined for these shots, and they show more variation (2.63-3.05s) than do those of any of the previous regions. This variation is interpreted as caused by the shallow sedimentary structure associated with this uplifted block, and as the structure is unknown the time terms were not interpreted in terms of Moho depths. The crustal cross section obtained from the line B time terms is presented in Figure 4.23.

4.4.4 Line E time terms

Problems were encountered in interpreting the time-distance graphs of this line (section 4.3.4), but all the arrivals tentatively identified as P* or Pn were included in the appropriate time term analysis. These values had little effect on the previously obtained time term solutions, and no residual travel time for these shots was greater than three standard deviations away from the median residual for the particular shot or station. It is therefore most probable that the travel times of these shots used in the analyses do represent either P* or Pn arrivals.

The P* time term values found for this line can be divided into three main groups:

1. Shots E1-E6 over the south of the Moray Firth with a range in values of 1.10-1.38s and a mean of 1.28s.

2. Shots E7-E14 over the central to northern part of the Firth with a range in values of 1.23-1.59s and a mean of 1.43s.

3. Shots E15-E17 in the northernmost area of the Firth adjacent to the Wick coastline, and having a range in values

Figure 4.23 : The crustal structure beneath line B determined from the time terms.

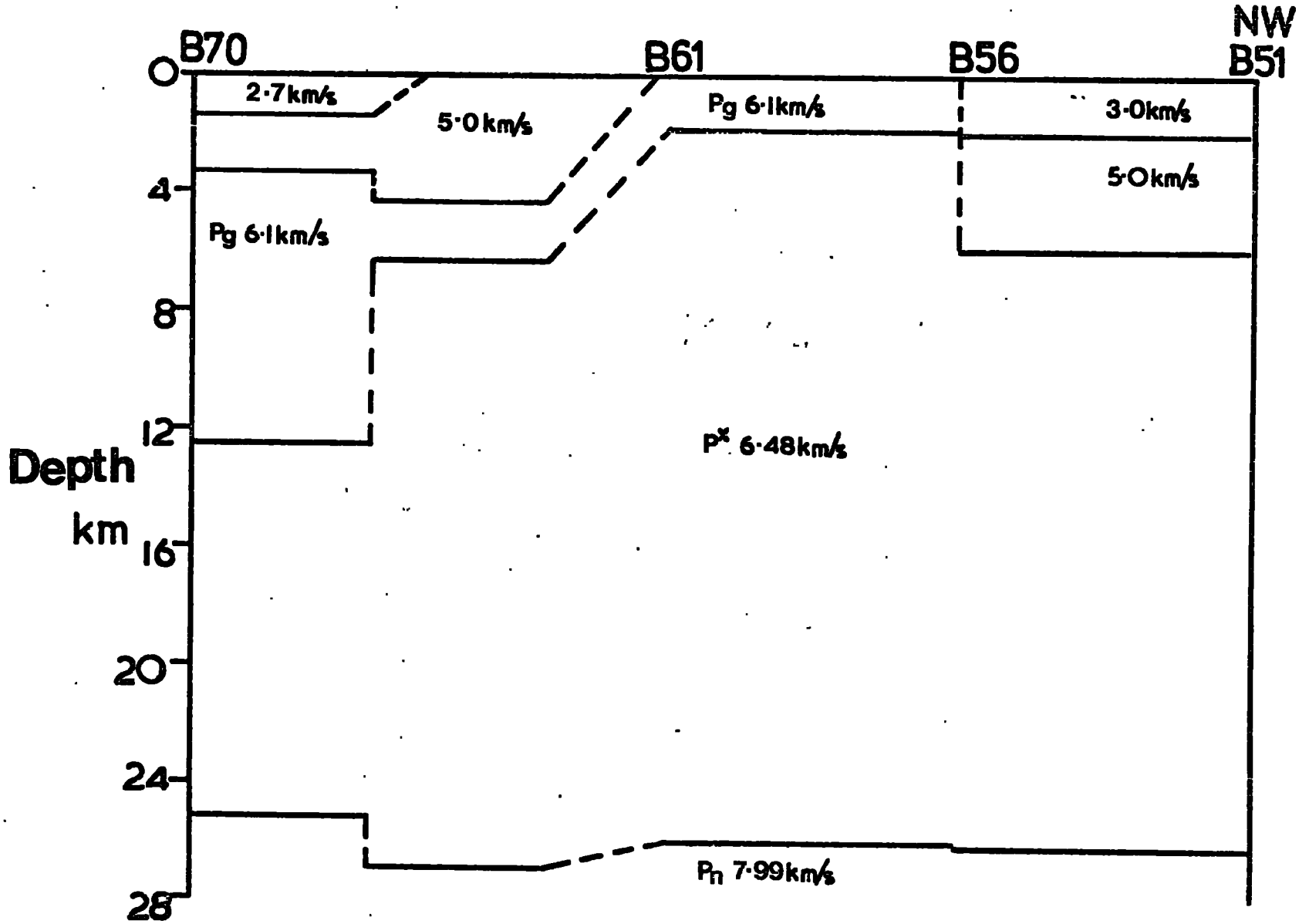
B70
B61
B56
NW
B51
2·7km/s
5·0km/s
Pg 6·1km/s
3·0km/s
5·0km/s
Pg 6·1km/s
Px 6·48km/s
Pn 7·99km/s
Depth
km
0
4
8
12
16
20
24
28

of 0.70-1.03s and a mean of 0.92s.

The variation in these time term values can, in general, be explained in terms of the underlying Mesozoic sedimentary basin. A gravity model of this basin (Sunderland, 1972) indicates that it has fault bounded northern and southern margins, and is assymetric with thicker sediments in the northern region. However there is some discrepancy between these P* time terms and the basin model for the southern region. Shot E1 would be expected to be off the end of the basin and so have a reduced time term, and shots E2 and E3 would be expected to lie over the fairly deep (about 3 km) sediment trough interpreted from the gravity observations to be adjacent to the southern boundary. Accepting these unexplained anomalies the three groups of shots were interpreted to overlie 2 km, 3.5 km and 0.5 km respectively of Mesozoic sediments (mean velocity 3 km s^{-1}), above the Upper Palaeozoic (ORS) deposits directly overlying the P* refractor. The mean P* time terms indicated depths to this refractor for the 3 groups of 7.4 km, 6.6 km and 6.6 km respectively. These results suggest that the P* refractor is at a reasonably constant depth of about 7 km beneath the variable Mesozoic sediments.

The Pn time terms of this line increase across the Moray Firth from south-east to north-west, with a range of 2.61-3.30s and a mean value of 2.95s. Interpreting this mean value in terms of an average Mesozoic sediment thickness of 2 km, and the P* refractor at a depth of 7 km, a mean Moho depth of 24.2 km was found. However the individual shot Pn time terms can be divided into groups corresponding to those obtained for the P* time terms, and have ranges and mean

values of 2.61-2.87s and 2.78s, 2.92-3.15s and 3.03s, and 3.05-3.30s and 3.16s respectively. These three mean values were interpreted in terms of the corresponding upper crustal structure, assuming a lower crustal velocity of 6.48 km s^{-1}, and Moho depths of 22.0 km, 22.8 km and 29.4 km respectively. determined. It would appear from these results that the crust beneath the Moray Firth basin is quite thin (22-24 km), but there is some evidence that just off the basin to the north (shots E15-E17) the crust is substantially thicker (29,4 km).

The crustal cross section across the Moray Firth determined by time term analysis is presented in Figure 4.24.

4.4.5 Receiving station Pn time terms

The receiving stations used in the Pn time term analysis can be divided into three main groups:

1. Those stations located over the Caledonian Foreland i.e. DU1, DU2, DU3, IGS1, IGS2, UKAEA.

2. Those stations over the Caledonian Orogenic Belt i.e. UAB, ULA, UBL, IGS3, MHD.

3. The Lownet array stations located over the Midland valley of Scotland i.e. LN1, LN4, LN5, LN6, LN8, LN9.

The corresponding ranges and mean Pn time term values for these three groups were:

1.	2.43-2.86s	2.59s
2.	2.79-3.63s	3.13s
3.	2.21-3.72s	3.17s

The mean time term of the first group is similar to the mean values for shot lines C and D, and, interpreted in terms of the mean crustal structure established along line D, represents a Moho depth of 25.6 km.

The stations comprising groups 2 and 3 were not

Figure 4.24 : The crustal structure beneath line E determined from the time terms.

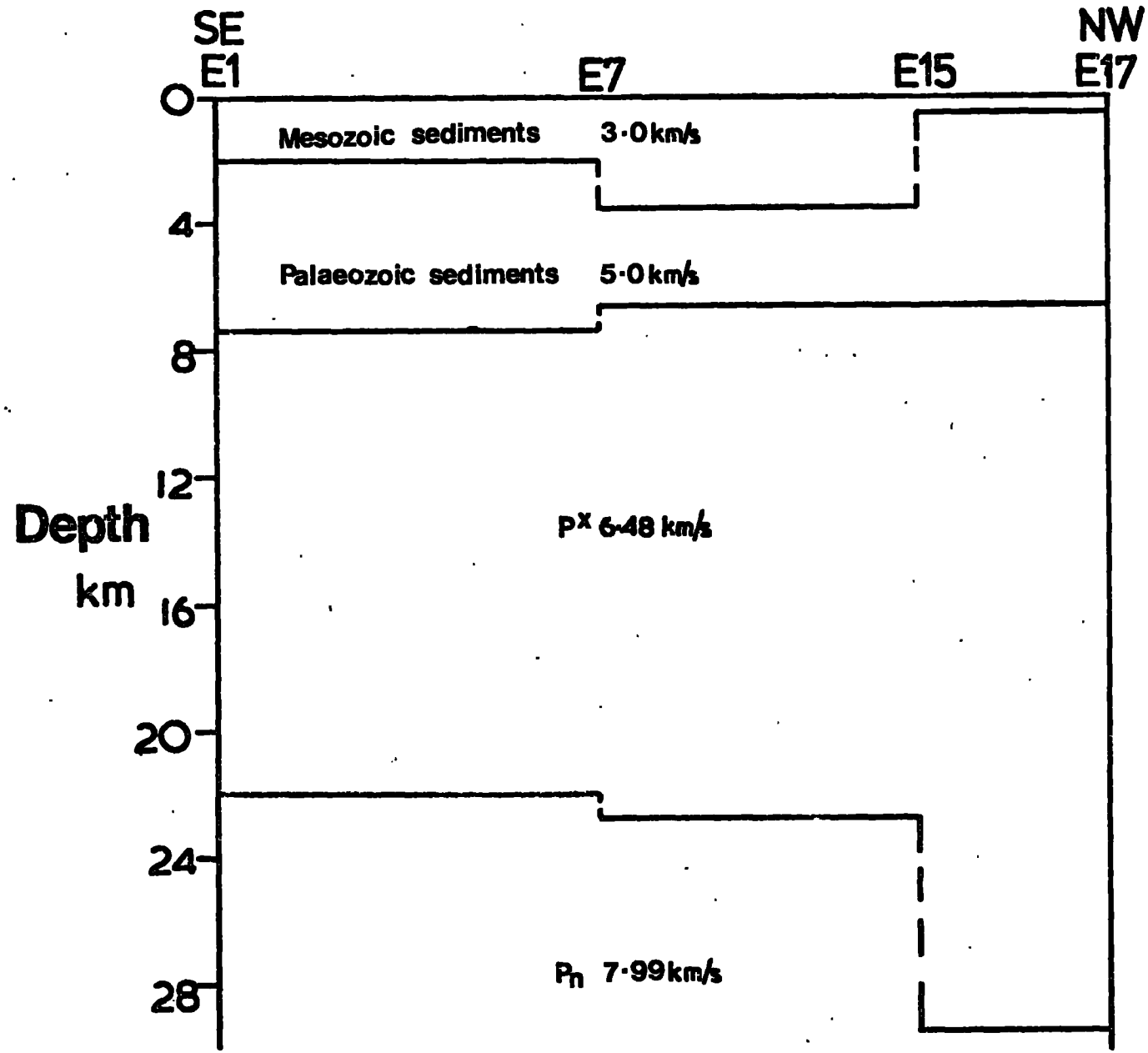
SE
E1
E7
E15
NW
E17
0
4
8
12
16
20
24
28
Depth
km
Mesozoic sediments 3·0 km/s
Palaeozoic sediments 5·0 km/s
P^x 6·48 km/s
P_n 7·99 km/s

sufficiently close to the shots to provide information on the crustal layering but their mean Pn time terms suggest a substantially thicker crust in both cases. All the stations situated over the Orogenic belt were located on basement rocks and so no part of the time term is due to a sedimentary delay. Assuming a mean crustal velocity of 6.1 km s^{-1} (Pg) the crustal thickness is estimated to be 29.5 km beneath the Orogenic belt, and would be greater for a higher mean crustal velocity.

Pn time terms of the order of 3.4s have been established for the lownet array stations from quarry blasts and some large explosions at sea carried out by IGS (Jacob, private communication). Therefore, most probably, the very low value of 2.21s for station LN1 (established by only five observations) is erroneous. This reduces the range of values to 3.12-3.72s with a mean of 3.37s. Crustal velocities of 6.1 and 6.4 km s^{-1} have been observed near the Lownet stations (Crampin, 1970), and so this mean time term valuc was interpreted assuming both these valyes for the mean crustal velocity. Moho depths of 31.8 km and 36.0 km respectively were obtained.

This concludes the first arrival data for the Scottish Continental Shelf. Later arrivals are now dealt with and a geological interpretation presented.

4.5 Later arrivals

4.5.1 PmP phase

The PmP phase is best developed for the arrivals from line D shots and has only been interpreted for this line. The phase is scarcely recognizable for lines C and E shots, and cannot be seen at all on the records of line B shots. This

is probably due to line D only being fired along the strike of the gravity anomalies and structure on the shelf.

The line D shots recorded at station IGS1 show large amplitude secondary arrivals starting at about 50 km and correlatable from shot to shot out to about 240 km (Figure 4.13). A similar group of arrivals was observed for this shot line on the records of station DU1 from about 70-150 km (Figure 4.14). These arrivals are very similar to groups of arrivals observed in south-west England (Holder and Bott, 1971) and are similarly interpreted, out to a certain distance, as the phase reflected from the Moho, PmP. The reasons for interpreting these arrivals as the PmP phase were:

1. The travel time could be fitted by a curved line appropriate to a Moho reflection.

2. The amplitude-distance characteristics of this phase in relation to the Pg, P* and Pn phases were similar to those predicted theoretically by Berry and West (1966).

It can be seen by inspection of the stacked record sections (Figs.4.13 & 4.14) that these secondary arrivals are fitted by a curved line the travel time-distance characteristics of which can be explained by Moho reflections. In order to arrive at the second reason for the interpretation amplitude-distance curves had to be constructed for all the phases. The main causes of amplitude variation at the shot points were reduced by all the shots being of the same size and all but four of the shots being fired on the sea bed. The remaining four shots, D14-D17, were fired within 100 m of the sea bed. The geological structure beneath line D appears to be reasonably uniform, a thin but variable sediment cover over the metamorphic basement, and should cause little amplitude

Figure 4.25 : The amplitude-distance graph for various phases recorded at station IGS1.

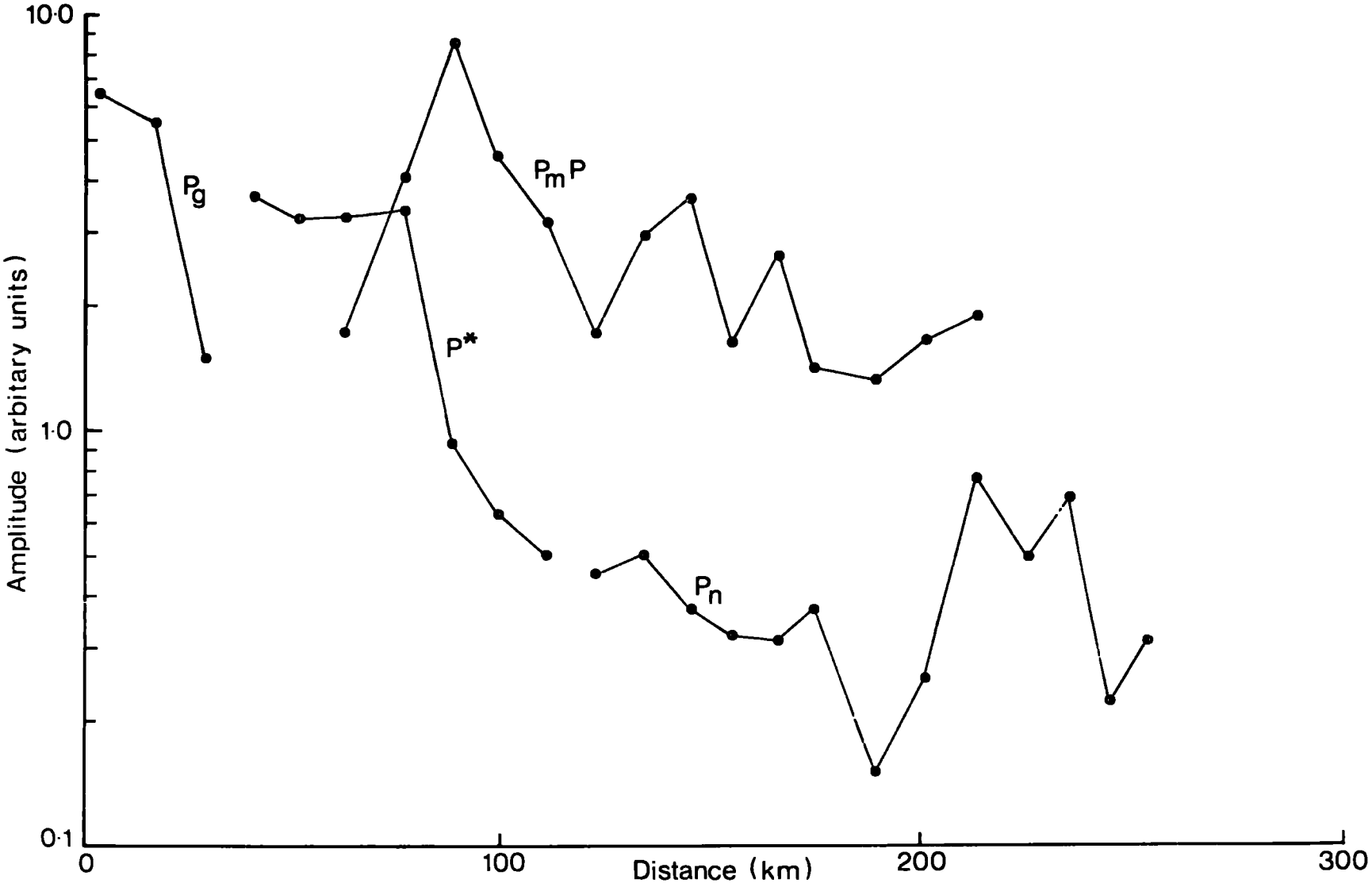
10·0
1·0
0·1
Amplitude (arbitary units)
0
100
200
300
Distance (km)
Pg
PmP
P*
Pn

Figure 4.26 : The amplitude-distance graph for various phases recorded at station DU1.

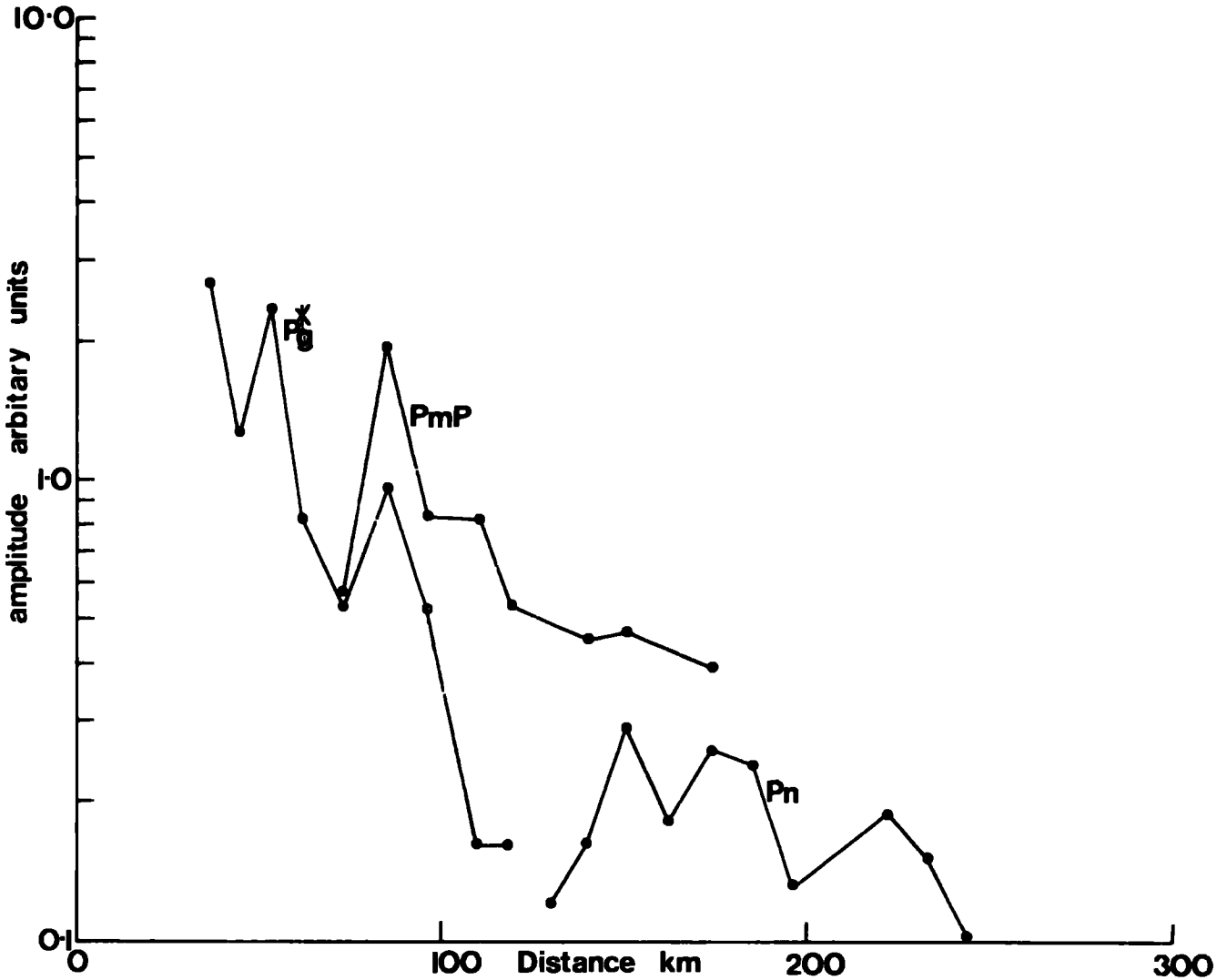
10·0
1·0
0·1
amplitude arbitary units
PmP
Pn
0
100
Distance km
200
300

variations. Frequency response curves were available for both the recording systems at the two stations (IGS1 and DU1), and for the playback equipment in the Durham laboratory. Composite response curves of both the recording and playback equipment were produced for the records of both these stations so that the amplitude variation with frequency could be allowed for. The maximum peak to peak amplitudes of the first four cycles of each phase were measured, corrected for frequency response and any changes in recording system gain, and plotted against distance, as shown in Figures 4.25 & 4.26. It can be seen on these diagrams that the amplitude-distance characteristics of the PmP phases are similar to those theoretically predicted by Berry and West (1966).

The PmP phase has been used to supplement the crustal structure information obtained from the first arrivals. According to geometrical ray theory the maximum amplitude of the PmP phase should occur at the critical distance. Therefore, the distance at which these arrivals were observed to attain maximum amplitude was taken as an estimate of the critical distance. This distance was 90 km for station IGS1 and 85 km for station DU1. However it has been shown by Cerveny (1966) that the amplitude of PmP in fact reaches its maximum at some distance beyond the critical distance. The critical distances were therefore re-estimated to be approximately 75 km and 70 km respectively for the two stations. The method of Holder and Bott (1971), described in section 3.5.1 , was used with these values of critical distance, and the appropriate intercept times and Pn velocities to estimate an average crustal velocity, and therefore a true

crustal thickness, without assuming uniform velocity layers. The values obtained for station IGS1 were a mean crustal velocity of 6.45 km s^{-1} and a crustal thickness of 26.7 km, and for station DU1 6.35 km s^{-1} and 25.8 km. Combining these results an average crustal velocity of 6.4 km s^{-1} and a crustal thickness of 26.2 km were determined. Both of these values are marginally higher than those obtained by assuming a crustal structure consisting of layers of uniform velocity. Assuming that the increase in velocity with depth necessary to explain the mean crustal velocity is limited to the lower crustal layer and is linear throughout that layer, then a velocity of 7 km s^{-1} would be reached at the base of the crust.

Similar large amplitude arrivals were also observed as the stacked records of station DU2 (Fig4.15) but have not been used in any interpretation.

4.5.2 S arrivals

Good consistent S wave arrivals were rarely observed over the Scottish shelf. The onset times of such arrivals were only picked for station IGS1 and line D shots. A least squares fit of the travel times of the S wave arrivals from shots D4-D15 at this station defined a segment with a reciprocal gradient of 3.76 ± 0.05 km s^{-1} and an intercept of $3.35 \pm .66$s. This S wave velocity is approximately equivalent to a P wave velocity of 6.5 km s^{-1} (assuming a normal continental crust value of Poisson's ratio), and the arrivals are therefore interpreted as S*, the headwaves from the lower crustal layer. The layer thickness formula was used to interpret the intercept time in terms of 2.7 km of sediments (S wave velocity 2.81 km s^{-1}) overlying the metamorphic basement (3.43 km s^{-1}), and a depth was found to the S* refractor of 11.6 km. This is similar to the mean value of 9 km calculated for the lower crustal layer from the P* time

Figure 4.27 : The final crustal structure model beneath line D determined from both first and secondary arrivals.

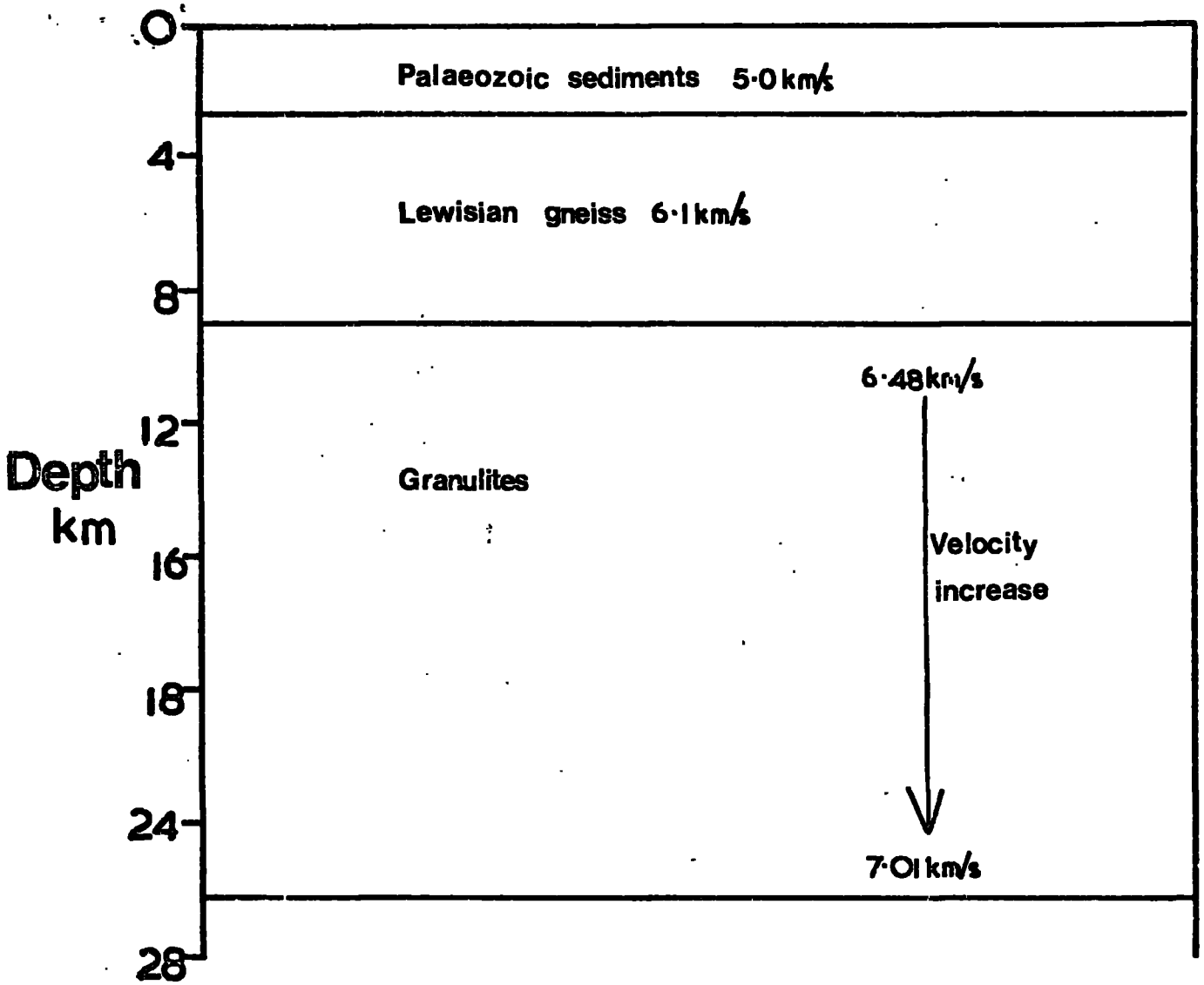
0
4
8
12
16
18
24
28
Depth km
Palaeozoic sediments 5·0 km/s
Lewisian gneiss 6·1 km/s
Granulites
6·48 km/s
Velocity increase
7·01 km/s

terms. The S arrivals can be seen to fall on a curved line near the Moho arrivals crossover distance (Fig. 4.13 shots D13-D18) and reach a maximum amplitude at a similar range to the Pml' arrivals. These arrivals may possibly be interpreted as SmS.

The final crustal structure model along the Scottish shelf computed from both first and later arrivals is presented in Figure 4.27.

4.6 Model travel times

The technique described in section 3.6. was used to calculate the travel times of the Pn and PmP phases travelling through the following line D crustal structure models:

1. The mean crustal structure derived from the time terms and consisting of 2.7 km of sediments (5 km s^{-1}) overlying 6.3 km of basement material (6.1 km s^{-1}) and 16 km of lower crustal material (6.48 km s^{-1}), with a Moho depth of 25 km (Fig. 4.21).

2. The final crustal structure obtained using the PmP phase as well as the first arrivals. This structure is similar to that of model 1 down to the P* refractor, but then the velocity increases linearly with depth till a value of 7.01 km s^{-1} is reached at the base of the crust (26.2 km) (Fig. 4.27).

These models could not be expected to give rise to exact travel times as a uniform structure was assumed extending from beneath the line of shots to the particular receiving station. However it was shown in section 4.4.1. that both the sediment thickness and depth to the P* refractor vary along the shot line, and the Moho may dip at about 1^{o} to the south-west.

PmP arrivals were only identified at stations IGS1 and DU1 from the line D shots, but Pn arrivals were obtained at stations IGS1, IGS2, IGS3, DU1, DU2, DU3, UKAEA, UAB, ULA, MHD, LN5, LN6 and LN8. Theoretical travel times were calculated for all these arrivals for both models, but reasonable agreement between the observed and calculated times was found for only stations IGS1, IGS2, DU1, DU2 and UKAEA. This is explained by these stations only (excluding station DU3 on Skye) being situated over the Caledonian foreland crust, and so the assumption of a uniform structure beneath shot points and receiving stations is only valid for these results. The travel times calculated for the remainder of the stations were found to underestimate the observed times by approximately 0.5-1.5s. The foreland crust has been established as several kilometres thinner than that of the adjacent orogenic belt, and probably also that of the Midland Valley (section 4.4.5.), and so this extra crustal material beneath the receiving stations would be expected to increase the travel times.

The agreement between the observed and calculated travel times found for each phase at stations IGS1 and DU1 is shown in Table 4.7., together with the sums of the squares of the residuals divided by the total number of travel times. These results indicate that both models sufficiently approximate the true crustal structure to produce travel times in quite close agreement, in general, with those observed. However the slight differences in the two models are masked by the departures of the real situation from the assumptions of uniformity involved, and both give rise to equally acceptable travel times. A large discrepancy was found between the

TABLE 4.7.

TRAVEL TIMES CALCULATED FOR CRUSTAL MODELS

Station IGS1

	HOMOGENEOUS LAYERS			VELOCITY INCREASE IN LOWEST LAYER		
	Pn Phase			Pn Phase		
Shot	Observed	Calculated	Residual	Observed	Calculated	Residual
D14	20.08	20.40	-0.32	20.08	20.23	-0.15
D13	21.56	21.89	-0.33	21.56	21.72	-0.16
D12	23.20	23.26	-0.06	23.20	23.08	0.18
D11	24.33	24.52	-0.19	24.33	24.35	-0.02
D10	26.01	25.87	+0.14	26.01	25.69	0.32
D9	26.87	26.92	-0.05	26.87	26.76	0.11
D8	28.57	28.78	-0.21	28.57	28.62	-0.05
D7	30.01	30.22	-0.21	30.01	30.07	-0.06
D6	31.77	31.79	-0.02	31.77	31.64	0.13
D5	33.27	33.33	-0.06	33.27	33.17	0.10
D4	34.37	34.49	-0.12	34.37	34.34	0.03
D3	35.86	35.68	0.18	35.86	35.53	0.33
D2	36.66	36.82	-0.16	36.66	36.66	0.00
	$R^2/n = 0.035$			$R^2/n = 0.026$		
	PmP Phase			PmP Phase		
Shot	Observed	Calculated	Residual	Observed	Calculated	Residual
D18	14.77	14.73	0.04	14.77	14.59	0.18
D17	16.17	16.26	-0.09	16.17	15.94	0.23
D16	17.74	17.82	-0.08	17.74	17.40	0.34
D15	18.97	19.45	-0.48	18.97	18.97	0.00
D14	20.88	21.16	-0.28	20.88	20.68	0.20
D13	22.31	22.89	-0.58	22.31	22.30	0.01
D12	24.14	24.50	-0.36	24.14	23.86	0.28
D11	25.66	26.01	-0.35	25.66	25.20	0.46
D10	27.41	27.61	-0.20	27.41	26.81	0.60
	$R^2/n = 0.106$			$R^2/n = 0.099$		

Station DU1

	HOMOGENEOUS LAYERS			VELOCITY INCREASE IN LOWEST LAYER		
	Pn Phase			Pn Phase		
Shot	Observed	Calculated	Residual	Cbserved	Calculated	Residual
D11	21.29	21.04	0.25	21.29	21.32	-0.03
D12	22.65	22.34	0.31	22.65	22.53	0.12
D13	23.93	23.61	0.32	23.93	23.80	0.13
D14	25.35	25.42	-0.07	25.35	25.26	0.09
D15	26.79	26.87	-0.08	26.79	26.72	0.07
D16	28.30	28.30	0.00	28.30	28.14	0.16
D17	29.81	29.68	0.13	29.81	29.53	0.28
D18	31.43	31.09	0.34	31.43	30.93	0.50

Station DU1 Pn Phase contd.

Shot	Observed	Calculated	Residual	Observed	Calculated	Residual
D19	33.11	32.87	0.24	33.11	32.72	0.39
D20	34.49	34.25	0.24	34.49	34.09	0.40
D21	35.83	35.65	0.18	35.83	35.50	0.33
D22	37.14	37.10	0.04	37.14	36.94	0.20
D23	38.70	38.59	0.11	38.70	38.43	0.27
D24	40.95	40.88	0.07	40.95	40.72	0.23

$R^2/n = 0.041$ $R^2/n = 0.070$

PmP Phase PmP Phase

Shot	Observed	Calculated	Residual	Observed	Calculated	Residual
D6	15.07	14.23	0.84	15.07	14.10	0.97
D7	15.79	15.86	-0.07	15.79	15.60	0.19
D8	17.28	17.40	-0.12	17.28	17.04	0.24
D9	20.48	19.48	1.00	20.48	19.06	1.42
D10	22.60	20.73	1.87	22.60	20.22	2.38
D11	24.15	22.32	1.83	24.15	21.75	2.40

$R^2/n = 1.43$ $R^2/n = 2.41$

observed and calculated travel times for the PmP phase observed at station DU1 for both models, except for shots D7 and D8. As the models satisfactorily explain the Pn and PmP travel times observed at station IGS1 and the Pn travel times at station DU1, this discrepancy probably results in the main from inaccurate picking of the PmP onset at station DU1. Both shots D7 and D8, which are very close to the maximum amplitude range, have small residuals suggesting that the picked onsets are reliable only for these two shots. The limiting range of PmP arrivals for model 2 was calculated to be 183 km, and so the arrivals identified on the records of station IGS1 beyond this range cannot be the PmP phase.

The residuals and sum of the squares of the residuals divided by the total number of the travel times observed at each station are given in Table 4.8., for the remaining close-in receiving stations (IGS2, DU2, UKAEA). No PmP arrivals were picked at these stations but the Pn travel times are equally well explained by either of the two models.

It is obviously more difficult to model the Pn travel times for the lines B and C shots as significant structural variations were found beneath both lines (sections 4.4.2., and 4.4.3.). However as a first step both the line D crustal models were used to calculate Pn travel times for the line C shots, but the times found for the great majority of these shots were at least 0.5s too small. The two different crustal models obtained for line C (section 4.4.2.), a 23.9 km thick crust beneath shots C1-C13, and a 22.4 km thick crust beneath shots C14-C24, were then used to determine theoretical travel times but these gave rise to even smaller values. This failure of either of the two deduced models to

TABLE 4.8.

RESIDUAL TRAVEL TIMES FOR THE CRUSTAL MODELS

	HOMOGENEOUS	VELOCITY INCREASE
IGS2	RESIDUALS	RESIDUALS
D19	-0.02	0.17
D18	0.03	0.12
D17	0.48	-0.32
D16	-0.24	0.39
D15	0.44	-0.28
D14	0.37	0.19
D13	0.13	-0.02
D12	-0.27	0.13
D11	0.32	-0.16
D10	0.10	0.05
D9	0.22	-0.06
D8	0.30	-0.14
D7	-0.79	-0.95
D6	0.45	0.29
D5	0.58	-0.22
D4	0.54	-0.39
D2	0.31	-0.15
	$R^2/n = 0.148$	$R^2/n = 0.099$
UKAEA	RESIDUALS	RESIDUALS
D14	0.13	0.03
D15	0.06	0.09
D16	0.03	0.13
D17	-0.04	0.19
D18	-0.17	0.33
D19	0.03	0.13
D20	-0.07	0.23
D21	0.20	-0.04
D22	-0.13	0.28
D23	-0.13	0.28
D24	-0.04	0.20
	$R^2/n = 0.012$	$R^2/n = 0.055$

TABLE 4.8. contd.

DU2	RESIDUALS	RESIDUALS
D2	-0.18	0.34
D3	-0.05	0.20
D4	-0.04	0.20
D5	-0.24	0.40
	$R^2/n = 0.023$	$R^2/n = 0.089$

generate a close approximation to the observed travel times suggests that there must be some discrepancy between the upper crustal structure determined from the Pg and P* arrivals, and the upper crustal structure underlying the shots that produce Moho arrivals. No attempt was made to calculate Pn travel times for the line B crustal structures as in order to do this satisfactorily the modelling technique (section 3.6) would have to be adapted to allow for variation of structure along the profile.

4.7 Discussion and geological interpretation

The NASP results on the Scottish Shelf have been interpreted in terms of the following crustal structure:

1. A sedimentary layer of variable velocity and thickness occurring over much of the area but not present everywhere. This layer consists mainly of Upper Palaeozoic or earlier sediments and some local Mesozoic basins.

2. A thin upper crustal basement layer of average velocity 6.1 km s^{-1}. The layer varies in thickness up to about 10 km and was not observed everywhere in the region.

3. A lower crustal layer varying in depth from almost zero km up to about 16 km. The velocity at the top of this layer is about 6.5 km s^{-1} but there is evidence from the later arrivals that the velocity increases with depth in this layer to about 7 km s^{-1} at the base of the crust.

4. The Moho at an almost constant depth of 25-26 km with a Pn velocity of 7.99 km s^{-1}.

The final crustal cross-section models are shown in Figures 4.21-4.24 &4.27, and the line D crustal structure was shown to satisfy both the observed Pn and PmP travel times for

the close in stations.

The most distinctive feature of the crustal model is the shallow 6.5 km s^{-1} layer which was found both beneath the foreland crust and also beneath the Moray Firth basin on the orogenic belt. Such a layer has not been detected further south in Britain, but Scrutton (1970) found a 6.3 km s^{-1} layer at fairly shallow depth beneath Rockall Plateau. Part of this plateau belongs to the Caledonian foreland and could be expected to have a similar crustal structure. The time terms (P*) found for this layer show a close correlation with the Bouguer anomalies (Figs. 4.16-4.19), particularly for line B which crosses large local gravity anomalies. This close correlation suggests that the gravity anomalies are partly caused by variation in the depth to the relatively dense P* layer, but this effect is also accentuated by variation in the overlying sedimentary structure. Gravity 'high A' of Bott and Watts (1971) is seen to be caused by the P* layer coming close to the surface (Fig. 4.18), and the decreasing Bouguer anomaly values eastwards are partly caused by the increasing depth to this layer. 'High A', on the basis of gravity and magnetic anomalies, has been interpreted as a region where Lewisian granulites of possible Scourian type occur at or near the surface (Bott and Watts, 1970; Watts, 1971). Therefore the 6.5 km s^{-1} layer is tentatively interpreted as granulite facies Lewisian basement rocks beneath the foreland crust and, although the eastern limit of the surface outcrop of the Lewisian is marked by the Moine thrust, it is possible that this deeper Lewisian refractor extends eastwards beneath the Moray Firth. Gravity investigations on land in north-west Scotland (Bott et al, 1972) indicated that the Laxfordian

rocks are about 0.09 g cm^3 less dense than the Scourian. Such a density increase is of the order of magnitude that would be expected to cause the gravity anomalies associated with the variation in depth to the P* interface, in particular beneath gravity 'high A'. It follows therefore that the overlying 6.1 km s^{-1} basement layer is probably Laxfordian gneisses on the foreland, and Caledonian belt metamorphic rocks in the eastern areas.

A similar correlation between P* time terms and Bouguer anomaly values was observed along line C (Fig.4.17). Shots C13-C17 are over gravity 'low D' of Bott and Watts (1971), and their P* time terms are correspondingly larger. This again suggests that the anomaly may be caused by an increase in depth to the P* layer, but in this case no Pg arrivals were observed so the low gravity values may be the result of thick low density sediments directly overlying the P* refractor at a normal depth.

The foreland crust on the continental shelf has been interpreted to be of an almost constant thickness (25-26 km) despite the quite large variations in the upper crustal structure. The shots on line B cross from gravity 'high A' to 'low E' over a very short distance, and the P* and Pn time terms also indicate an abrupt transition in structure between the two gravity features. However on interpreting these time terms the Moho in both cases is found to be at a depth of about 26 km although, relative to the mean crustal structure established beneath line D, there is a thinning of the sub-sedimentary crust of about 6 km beneath basin E. Similarly a crustal thickness of 25.2 km was found beneath gravity low F (Bott and Watts, 1971) which was interpreted as a Mesozoic

sedimentary basin (Bott and Browitt, in preparation). The Moray Firth basin was interpreted to be underlain by a 22-24 km thick crust which represents both a sub sedimentary layer and total crustal thinning of about 6 km relative to the crustal thickness (29.5 km) established beneath the orogenic belt. This crustal thickness estimate beneath the Caledonian fold belt is about 10-15% greater than the thickness determined for the foreland crust, suggesting that there is still a small residual root present beneath the Scottish Caledonides.

The significance of the crustal structures established beneath the shelf basins, and the nature of and variation in the P* layer will be discussed in more detail in Chapter 6.

CHAPTER 5

The Faeroe Plateau and Faeroe/Shetland Channel and Channel Slopes

5. 1. The Faeroe Plateau

5. 1.1 Introduction

The Faeroe Plateau comprises the Faeroe Islands and surrounding shallow sea areas bounded to the north and west by the 100 fathom bathymetric contour. To the east this contour approaches close to the islands and the plateau is considered to extend out to almost the 500 fathom contour. The following shots on three different lines were fired in this area:-

A1-A6
B1-B16
C39-C52 to the south-east of the islands
C54-C59 to the north-west of the islands

In addition, a short line consisting of 25 lb. shots (Lomonosov line) was fired close to the Soviet recording ship Lomonosov on the south-east edge of the plateau (Fig. 5 .1.)

The Faeroe Islands consist almost entirely of Tertiary basalt lava, but whether the crust beneath this lava is continental or oceanic had not been conclusively determined prior to the project. A continental crust was suggested by Bott and Watts (1971) to improve the fit of the continents around the North Atlantic, and also by Bott et al (1971) in order to explain the Bouguer anomaly gradient from the Iceland-Faeroe Ridge onto the Faeroe Plateau. However Talwani and Eldholm (1972) have interpreted the western boundary of the Faeroe/Shetland Channel as an escarpment marking the Tertiary split of Greenland from Europe, and the crust to the west of this escarpment (beneath the Faeroe Plateau) as oceanic in nature. The Tertiary lava also forms the basement

Figure 5.1 : The shot-receiving station configuration over the Faeroe Plateau.

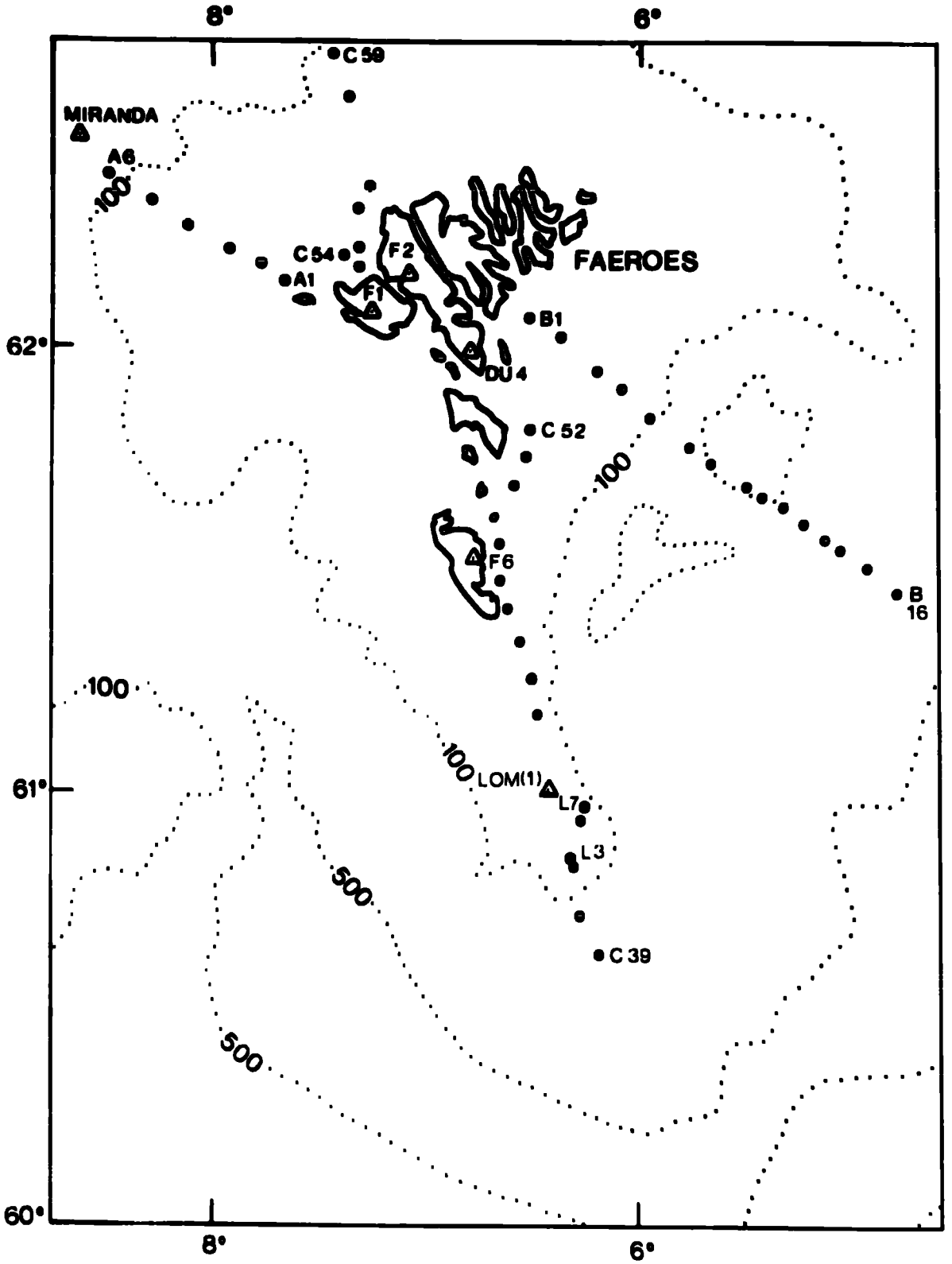
8°
6°
C 59
MIRANDA
A6
100
C 54
F2
FAEROES
A1
F1
B1
62°
DU 4
C 52
100
F6
B
16
100
61°
100
LOM(1)
L7
L3
500
C 39
500
60°
8°
6°

surrounding the islands and is seen on seismic reflection records (Watts, 1970; Lewis, private communication) to dip seawards away from the islands.

There have been two previous shallow seismic refraction investigations on the Faeroe Plateau (Palmason, 1965; Casten, 1973), and these experiments produced contrasting results. Palmason (1965) shot two profiles, one reversed profile on Streymoy and one unreversed profile on Suderoy, and identified three seismic layers. The velocities of, and depths to, the layers identified on Streymoy are summarised below:

Layer 1 3.9km s^{-1} outcrops from Torshavn to Kollafjordur

Layer 2 4.9 km s^{-1} about 0.4 km depth

Layer 3 6.4 km s^{-1} 2.5-4.5 km

These layers were correlated with the upper basalt series, the middle and lower basalt series, and the sub-basalt lava basement respectively, and are similar to the upper layer velocity structure established beneath Iceland (Palmason, 1970). However, an unreversed profile shot at sea (Casten, 1973) found a basement velocity of 5.9 km s^{-1} which would be expected for normal continental crust.

These opposing results did not, therefore, resolve the nature of the crust beneath the Faeroe Plateau and deep seismic refraction observations were needed.

A preliminary interpretation of the NASP results for the Faeroe plateau has already been presented (Bott et al, 1974)

5.1.2 First arrivals time-distance graphs

The observed travel times of all the first arrivals were reduced to a sea level datum to remove the effect of variation in both shot depth and recording station elevation. The correction term added to each travel time was

$$\frac{\text{Water depth}}{5.5} - \frac{(\text{Water depth} - \text{Shot depth})}{1.5} - \frac{\text{Station elevation above S.L.}}{5.5}$$

assuming a mean basement velocity of 5.5 km s^{-1}.

The Free Air Anomaly map compiled by Watts (1970) of the Scotland to Iceland region indicates a gravity low of about 20 mgal amplitude on the south-east Faeroe Shelf. However, more recent gravity measurements (Lewis, private communication) suggest that the 'low' is not a local feature but instead the region of low gravity values extends to the south-east into the Faeroe/Shetland Channel. The low values are probably mainly related to the gradual increase in water depth and sediment thickness as the Channel is approached. However, as little was known of the sediment thicknesses and velocities, both in this region and over the rest of the plateau, no sedimentary corrections were applied.

The method of least squares was used to fit straight line segments to the first arrival time-distance graphs for each station and line, and the velocities and intercepts obtained are given in Table 5.1. In order to effectively expand the time scale, reduced time-distance graphs were also plotted using a reducing velocity of 6 km s^{-1}. These graphs are shown in Figures 5.2.-5.5.

The crustal arrivals from the shots over the Faeroe Plateau were found in general to fall into the following two distinct groups:

1. Arrivals from shots to the north and west of the Faeroe Islands. These defined segments with reciprocal gradients of about 6 km s^{-1}.

2. Arrivals from shots to the south and east of the Faeroe Islands. These defined segments with reciprocal gradients of about 5.2-5.6 km s^{-1}.

Both these groups of arrivals were interpreted as the

TABLE 5.1

APPARENT VELOCITIES AND INTERCEPTS FROM LEAST SQUARES

Station	Shots	Phase	Velocity(km s^{-1})	Intercept(s)	S.E.
DU4	A1-A5	Pg_1	5.91 ± 0.12	0.85 ± 0.23	0.10
	C54-C59	Pg_1	5.92 ± 0.08	0.89 ± 0.12	0.10
	C45-C52	Pg_2	5.51 ± 0.07	0.46 ± 0.14	0.12
	B1-B13	Pg_2	5.25 ± 0.03	0.12 ± 0.06	0.09
	B14, B16	Pn^2	7.67	6.24	
F1	A1-A6	Pg_1	5.83 ± 0.10	0.64 ± 0.14	0.13
F2	A2-A5	Pg_1	6.10 ± 0.41	1.04 ± 0.57	0.25
	C54-C59	Pg_1	6.03 ± 0.10	0.75 ± 0.08	0.11
	C45-C52		4.96 ± 0.04	-0.66 ± 0.12	0.07
	B1, B2	Pg_1	6.00	0.90	
	B3-B11	Pg_2	5.21 ± 0.02	-0.45 ± 0.07	0.05
	B12-B16	Pn^2	8.52 ± 0.25	7.51 ± 0.44	0.07
F6	C49-C52	Pg_2	5.66 ± 0.31	0.31 ± 0.22	0.19
	C39-C48	Pg_2	5.42 ± 0.05	0.48 ± 0.11	0.17
MIR(D)	A3-A6	Pg_1	6.01 ± 0.28	1.30 ± 0.24	0.19
LOM FS(A)	C44D-C46	Pg_2	5.24 ± 0.35	0.23 ± 0.25	0.30
	C43-L7		3.41 ± 0.53	-1.08 ± 0.45	0.23
	C41-L4	Pg_2	5.34 ± 0.29	0.40 ± 0.29	0.12
LOM FS(D)	B10-B16		6.78 ± 0.40	2.66 ± 0.84	0.29
UKAEA	A2-A6	Pn	8.63 ± 0.49	8.45 ± 2.77	0.22
	C54-C59	Pn	8.15 ± 0.39	5.39 ± 2.29	0.18
	B1-B9	Pn	8.37 ± 0.17	6.98 ± 0.72	0.13

Figure 5.2: The reduced time-distance graphs for line A over the Faeroe Plateau at (a) station F2, (b) station F1, (c) station DU4, (d) station UKAEA, (e) station MIR(D).

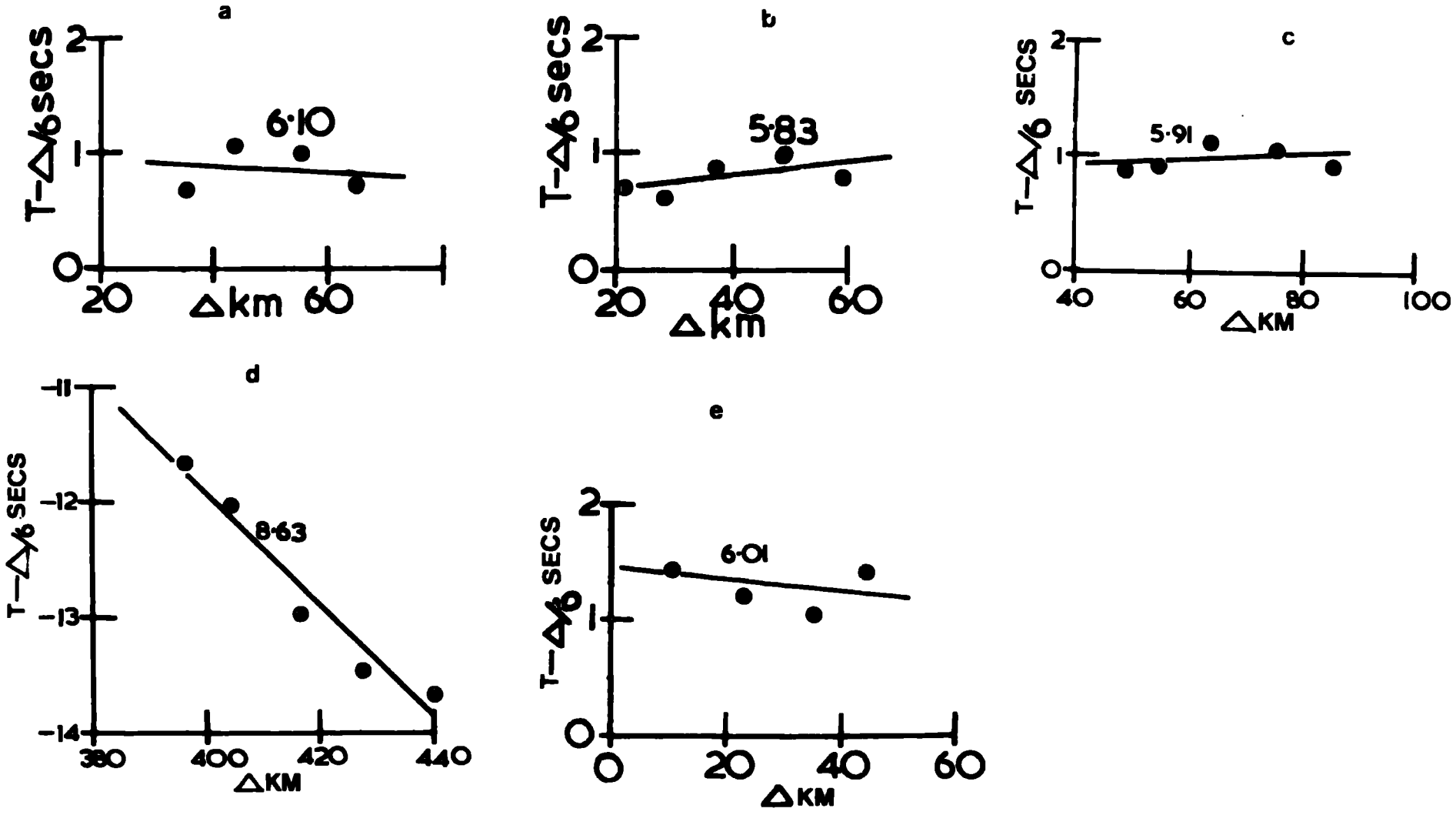
a
T−Δ/6 secs
2
1
0
6·10
20
Δkm
60
b
T−Δ/6 secs
2
1
0
5·83
20
40
60
Δkm
c
T−Δ/6 SECS
2
1
0
5·91
40
60
80
100
ΔKM
d
T−Δ/6 SECS
-11
-12
-13
-14
8·63
380
400
420
440
ΔKM
e
T−Δ/6 SECS
2
1
0
6·01
0
20
40
60
ΔKM

Figure 5.3 : The reduced time-distance graphs for (a) line C to the north at station F2, (b) line C to the north at station UKAEA, (c) line C to the north and to the south at station DU4.

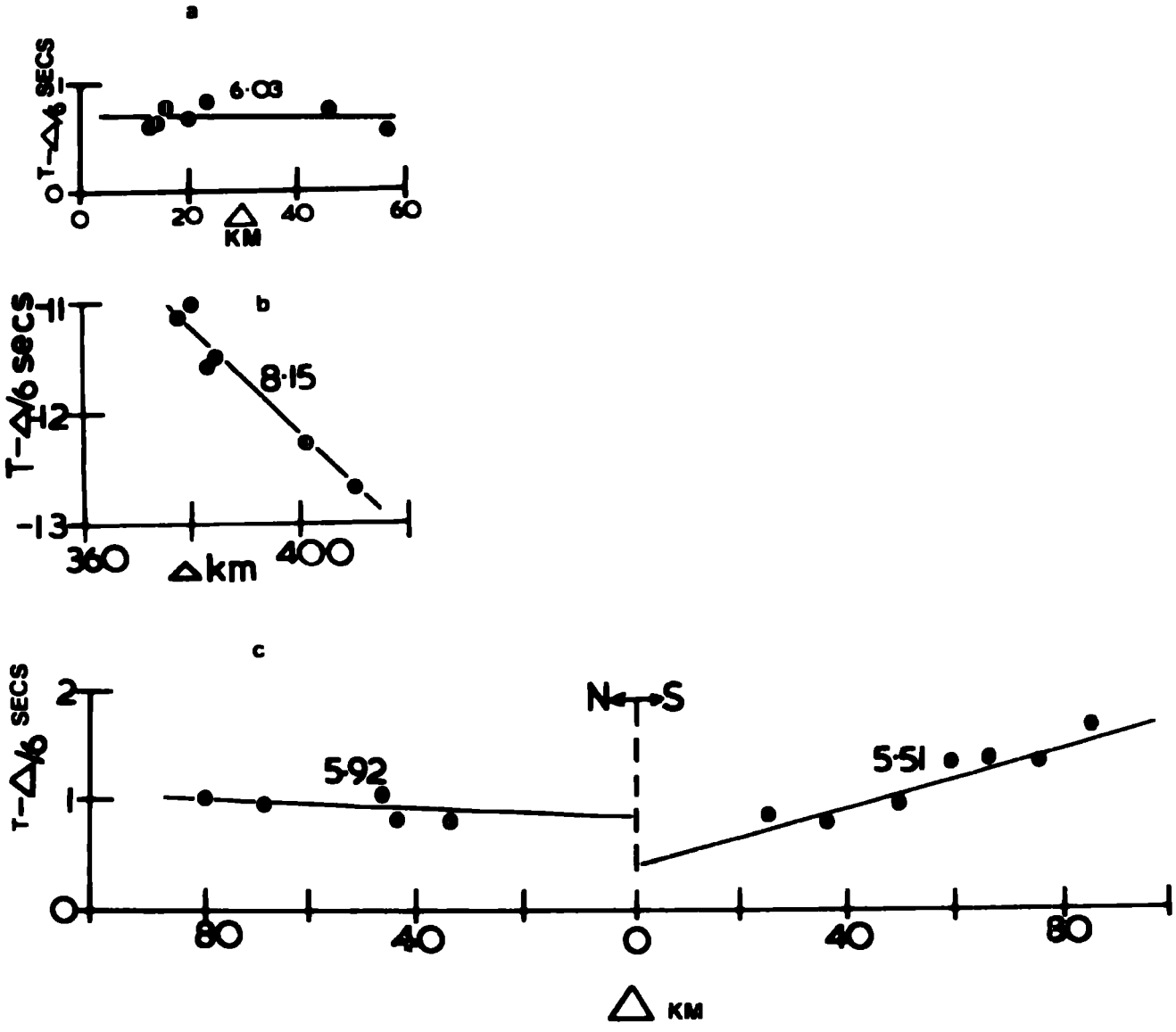
a
T-Δ/6 SECS
1
0
6·03
0
20
40
60
Δ
KM
b
T-Δ/6 secs
-11
-12
-13
8·15
360
Δkm
400
c
T-Δ/6 SECS
2
1
0
N
S
5·92
5·51
80
40
0
40
80
Δ KM

Figure 5.4 : The reduced time-distance graphs for line B over the Faeroe Plateau at (a) station DU4, (b) station UKAEA, (c) station F2, (d) station LOM FS(D)

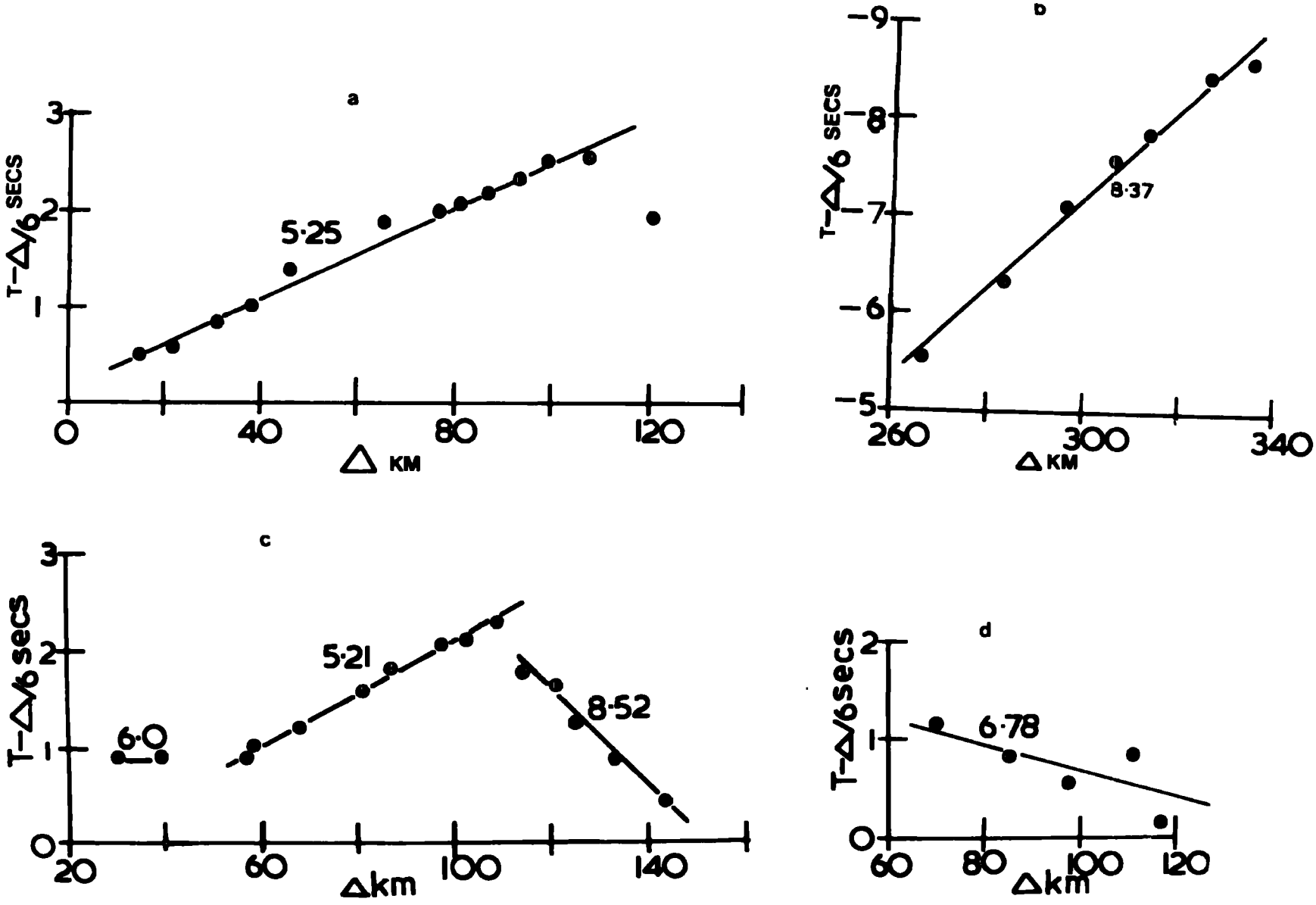
a
T-Δ/6 SECS
3
2
1
5·25
0
40
80
120
Δ KM
b
T-Δ/6 SECS
-9
-8
-7
-6
-5
8·37
260
300
340
Δ KM
c
T-Δ/6 secs
3
2
1
0
6·0
5·21
8·52
20
60
100
140
Δkm
d
T-Δ/6secs
2
1
0
6·78
60
80
100
120
Δkm

Figure 5.5 : The reduced time-distance graphs for line C to the south over the Faeroe Plateau at (a) station F2, (b) station LOM FS(A), (c) station F6.

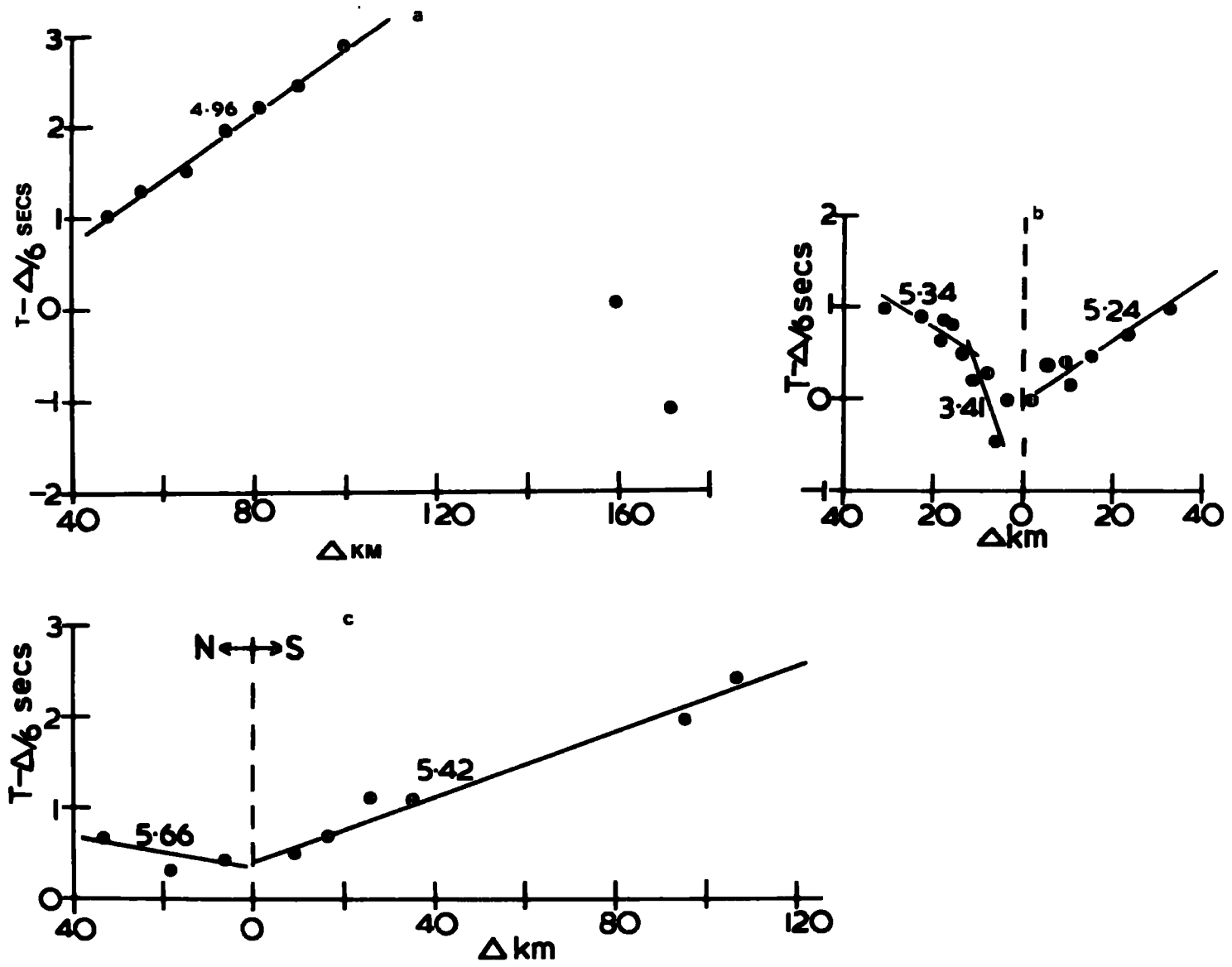
a
4·96
T−Δ/6 SECS
3
2
1
0
−1
−2
40
80
120
160
Δ KM
b
5·34
5·24
3·41
T−Δ/6 secs
2
1
0
−1
40
20
0
20
40
Δ km
c
N←→S
5·42
5·66
T−Δ/6 secs
3
2
1
0
40
0
40
80
120
Δ km

head waves from two distinct basement layers (Pg_1 and Pg_2 respectively) beneath the basaltic lava. Arrivals from one station only, LOM FS(A), provided evidence of a crustal layer beneath the basement. Beyond ranges of about 110 km the arrivals defined segments with reciprocal gradients of about 7.7-8.5 km s^{-1}. These arrivals were interpreted as the Moho head wave Pn.

It was mentioned in Chapter 2 that in addition to the Durham University station (DU4) on the Faeroe Islands, there were six stations (F1-F6) provided by Aarhus University. However, as yet, very few results have been obtained for these stations, but the available data was used in the following sections.

5.1.3 Interpretation of the time-distance graphs

The ranges at which arrivals were observed at stations on the Faeroe Islands were much more limited than for stations on the Scottish mainland and islands. This is explained by noisy sites on the Faeroe Islands as it is impossible to find a suitable location more than 2 or 3 km away from the sea. Shots on line B were received at the maximum ranges (191 km for station DU4), and the stacked records for this line at station DU4 are shown in Figure 5.6 . The only later arrivals that can be identified at this station are S arrivals from shots B5, B8, B11, B12 and B13, and these will be mentioned later.

The time-distance graphs constructed for arrivals from the north and west of the Faeroe Islands (lines A and C to the north-west) define segments with reciprocal gradients of 5.83-6.10 km s^{-1} with a mean value of 5.97 ± 0.09 km s^{-1}. The

Figure 5.6 : The stacked records of the line B shots at station DU4 on the Faeroe Islands.

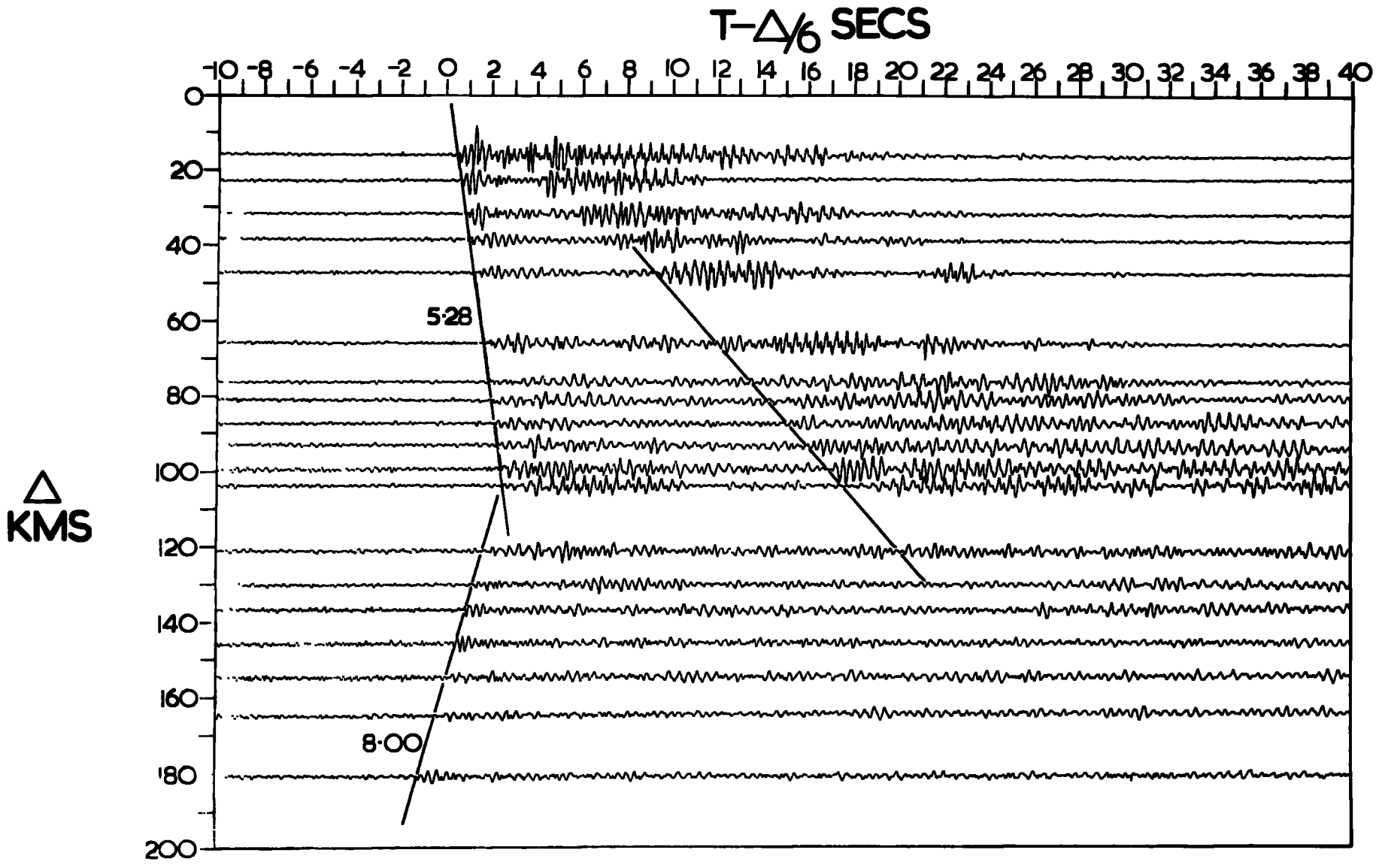
T−Δ/6 SECS
-10 -8 -6 -4 -2 0 2 4 6 8 10 12 14 16 18 20 22 24 26 28 30 32 34 36 38 40
0
20
40
60
80
100
120
140
160
180
200
Δ
KMS
5·28
8·00

observations at station F1 on the Faeroe Islands and at the ship station MIR(D), positioned north-west of the islands along line A, approximately reverse the Pg_1 velocity along line A. The two apparent velocities of 5.83 ± 0.1 km s^{-1} and 6.01 ± 0.28 km s^{-1}, although equal within their standard errors, were interpreted in terms of a basement dipping to the north west at 1.8° with a true velocity of 5.95 km s^{-1}. This reversed velocity is very similar to the mean velocity found in this region. Only stations DU4 and F2 on the Faeroe Islands recorded arrivals from both lines A and C to the north-west, and the results at each station were very similar for the two lines. The arrivals from shots C54B and C55 are approximately 0.15 seconds earlier than expected and those from shot C56 approximately 0.10 seconds later than expected at both of the stations. This variation is explained in terms of variable cover, either the overlying lava or post-Tertiary sediments, above the basement. Basement depths have been determined using the individual values of Pg_1 velocity and intercept time observed at each of the stations for both of the lines. A mean velocity of 4.9 km s^{-1} was assumed for the overlying material as this was the velocity observed by Palmason (1965) for the middle and lower series lavas on the Faeroe Islands, and, from the pattern of outcrop, the upper series would not be expected to the north and west of the islands. The range in the depths determined was 2.9-5.5 km and this scatter may be due to variation in the lava cover at each station. A mean depth of 3.9 km was found. The two results for station DU4 show good agreement (3.7 km and 3.9 km), but there is a significant difference between the results of station F2 (4.3 km and 3.1 km). The largest

depth value found was for station MIR(D) and may result from a changing structure from the Faeroe Plateau to the Iceland-Faeroe Ridge beneath this station.

The time-distance graphs constructed for arrivals from the south and east of the Faeroe Islands (lines B and C to the south-east) define Pg_2 segments with reciprocal gradients of 5.21-5.66 km s^{-1} with a mean value of 5.38 ± 0.08 km s^{-1}. However, the arrivals from shots B1 and B2 at station F2 defined a Pg_1 velocity. Velocities which can be correlated with both the upper lava series and the lower and middle lava series (Palmason, 1965) were also observed beneath these lines. In addition the observations at station LOM FS(D) indicate a lower crustal refractor beneath the line B shots on the plateau.

Two split profile observations of the line C shots were provided by stations F6 and LOM FS(A) and these can be taken to approximately reverse the Pg_2 velocity. The velocities measured along both sides of the split profiles are equal within their standard errors for both stations and could be interpreted to represent a flat basement of velocity 5.54 km s^{-1} or 5.29 km s^{-1} respectively. However, assuming the observed apparent velocities are different then, the results of station F6 indicate a basement of true velocity 5.53 km s^{-1} dipping to the south-east at 2.3°, and the results of station LOM FS(A) indicate a basement of true velocity 5.29 km s^{-1} dipping to the north at 1.3°. These opposing results suggest that a flat basement is probably the most valid interpretation. The individual values of Pg_2 velocity and intercept time observed at each of the stations for both the lines were interpreted in an identical manner to those obtained to the north and west. A range in basement depth of 0.8-2.7 km was found with a mean

value of 1.9 km.

The observations of the line B shots at station F2 are particularly significant as they define both Pg_1 and Pg_2 velocity segments. A Pg_1 velocity is defined by the arrivals from shots B1 and B2 and a Pg_2 velocity from the more distant shots out to a range of about 110 km. These results can be interpreted to indicate that between shots B2 and B3 the higher velocity basement must either deepen considerably or alternatively terminate and be replaced by the lower velocity material. The 6 km s^{-1} basement layer is not observed by the arrivals from shots B1 and B2 at station DU4 as the range to this station is considerably less than to station F2. Assuming that this difference in range is the only factor causing the first arrivals from these two shots to travel along the lower velocity basement to station DU4 and along the higher velocity basement to station F2, then limiting thicknesses of the overlying low velocity basement can be determined. It was found for an assumed 0.8 km lava cover that the higher velocity basement must only be deeper than about 2.2 km below the lava in order not to cause first arrivals at station DU4, but must be deeper than 4.5 km below the lava if no first arrivals are to be received from it at station F2. This suggests that there is between 2.2-4.5 km of lower velocity basement above the higher velocity basement beneath shots B1 and B2. A negative intercept (-0.28 secs.) was observed for the Pg_2 segment at station F2, and a small positive intercept (0.10 secs.) for the corresponding segment at station DU4. Such a difference is to be expected as most of the travel time path to station F2 will have been in the higher velocity material which will cause the negative

intercept. The exact boundary between the two basements is not defined and so it is not known if the intercept observed at station DU4 is due only to lava cover above the basement, or if the value has been reduced by the arrivals travelling in the higher velocity material.

As well as the two basement velocities observed velocities of 4.96 ± 0.04 km s^{-1} and 3.41 ± 0.53 km s^{-1} were determined at stations F2 and LOM FS(A) respectively. These velocities are interpreted as representing arrivals from the lower and middle basalt series, and the upper basalt series respectively, as they are equal to, within their standard errors, the velocities determined for these series on the Faeroe Islands (Palmason, 1965).

A velocity of 6.78 km s^{-1} was defined by the arrivals from line B shots at station LOM FS(D) and is the only evidence of a crustal refractor beneath the two basements established on the Faeroe Plateau. The intercept time of this segment was interpreted in terms of 0.8 km of lava (4.9 km s^{-1}) overlying 5.38 km s^{-1} basement material and, alternatively, 5.97 km s^{-1} basement, and refractor depths of 10.8 km and 15.3 km respectively were found. A refractor of velocity 6.4-6.6 km s^{-1} was identified beneath the North Scottish Shelf (sections 4.3, 4.4) and found at depths of up to 16 km. Also Scrutton (1972) established a refractor of velocity 6.36 km s^{-1} at a depth of about 6 km below the Rockall Plateau and so it seems probable that these three refractors could be similar.

No accurate Pn velocity was defined either by the few Moho arrivals at stations on the Faeroe Islands or by the arrivals at station UKAEA. However, the same crossover

distance of 110 km was observed for the Pg_2 and Pn arrivals from the line B shots at both stations DU4 and F2. This crossover distance was used, assuming a Pn velocity of 8 km s^{-1} to determine a Pn intercept time which was then interpreted in terms of Moho depths. 0.8 km of lava was assumed to overlie firstly the 5.38 km s^{-1} basement and secondly, the 5.97 km s^{-1} basement and, with the assumed Pn velocity of 8 km s^{-1}, Moho depths of 25.1 km and 31.2 km respectively were determined.

A least squares fit of the travel times of the S wave arrivals identified on the stacked records of the line B shots for station DU4 (Fig. 5.6) defined a segment of reciprocal gradient 3.12 km s^{-1}. Assuming a normal continental crustal value of Poisson's ratio, this S wave velocity is equivalent to a P wave velocity of 5.5 km s^{-1}, which is within the range of Pg values observed to the south and east of the Faeroe Islands.

5.1.4 Time term analysis

Time term analysis has been performed for the first arrivals from each of the three refractors, the two distinct sub-lava basements and the Moho, identified on the Faeroe Plateau. The time terms found and the estimated refractor velocities are listed in Table 5.2 . The observed uncorrected travel times were used in each time term analysis, and so the time terms of a particular refractor represent the delay time of every overlying layer, including the sea water.

The shot-station configuration around the Faeroe Plateau is not ideal for time term analysis as there are few reversed velocity estimates. However, statistically the solutions

TABLE 5.2.

TIME TERMS FOR THE FAEROE PLATEAU

Site	Pg_1 time term(s)	SE	Pg_2 time term(s)	SE	Pn time term(s)	SE
A1	0.38	0.01 (2)			2.83	(1)
A2	0.39	0.03 (3)			3.72	(1)
A3	0.68	0.06 (4)			3.76	(1)
A4	0.57	0.07 (4)			3.34	(1)
A5	0.47	0.04 (4)			3.33	(1)
C54A					3.41	(1)
C54B	0.31	0.01 (2)			3.64	(1)
C54C	0.47	0.01 (2)			3.25	(1)
C55	0.37	0.01 (2)			3.34	(1)
C56	0.55	0.02 (2)			3.38	(1)
C58	0.44	0.01 (2)			3.34	(1)
C59	0.37	0.13 (2)				
C39			1.25	(1)		
C41			0.76	0.04 (2)		
C42			0.61	(1)		
C43G			0.45	(1)		
L4			0.62	(1)		
C43F			0.62	(1)		
C44D			0.33	(1)		
C44C			0.32	(1)		
C44			0.28	(1)		
C45			0.52	0.03 (3)		
C46			0.56	0.12 (3)		
C47			0.38	0.04 (2)		
C48			0.36	0.11 (2)		
C52			0.25	0.08 (2)		
B2					3.70	(1)
B3			0.13	0.02 (2)	3.72	(1)
B4			0.22	0.02 (2)	3.69	(1)
B5			0.43	0.10 (2)	3.78	(1)
B7			0.54	(1)	3.93	(1)
B8			0.80	0.05 (2)	3.33	(1)
B9			0.84	0.04 (2)	3.95	(1)
B10			0.84	0.01 (2)	3.59	(1)

TABLE 5.2. contd.

Site	Pg_1 time term(s)	SE	Pg_2 time term(s)	SE	Pn time term(s)	SE
B11			0.94	0.06 (2)	3.96	0.15 (2)
B12			1.02	(1)	3.91	0.08 (2)
B13			1.10	(1)	4.00	0.02 (2)
B14			1.05	(1)	4.00	0.18 (2)
B15					3.78	(1)
B16					3.58	0.10 (3)
DU4	0.51	0.11 (19)	0.37	0.02 (16)	3.89	0.06 (2)
F1	0.31	0.03 (5)				
F2	0.28	0.01 (31)	0.20	0.02 (8)	3.15	0.05 (6)
LOM FS (A)			0.06	0.01 (10)		
MIR (D)	0.63	0.08 (3)				
UKAEA					2.58	0.01 (26)

are satisfactory. The experimental error variance is small for each solution indicating that the overall fit is good, and the magnitude and trend of the travel time residuals do not indicate any violation of the assumptions of the time term method.

5.1.4.1 Pg_1 basement to the north and west

In addition to the travel times for shots on line A and line C to the north-west, this analysis included the travel time data of Palmason (1965), obtained on Streymoy, and also that of Casten (1973) again obtained on Streymoy. These data sets were linked to the NASP data by assuming that shot points 1a and 1b of Palmason were equivalent to stations DU4 and F2 respectively, and that station 2 of Casten was equivalent to station F2.

The basement velocity found by the time term analysis was 5.98 km s^{-1} which is in excellent agreement with the mean velocity obtained along lines A and C (5.97 km s^{-1}), and with the reversed velocity estimate for line A (5.95 km s^{-1}). However, in order to test the effect of velocity variation on the fit of the calculated time terms to the observed travel times, a set of constrained velocities was used to obtain different time term solutions. The estimate of the fit of the solutions obtained (the experimental error variance) was plotted against the constrained velocity used (Figure 5.7.), and it can be seen that a variation of a few tenths of a kilometre per second has very little effect on the fit of the solution. The time terms found for lines A and C were in general between 0.30-0.60 seconds. The range for line C was 0.31-0.55 seconds with a mean of 0.42 seconds and these values

Figure 5.7 : The constrained time term velocity versus the fit of the solution for (a) the Pg_1 refractor, (b) the Pg_2 refractor, (c) the Pn refractor.

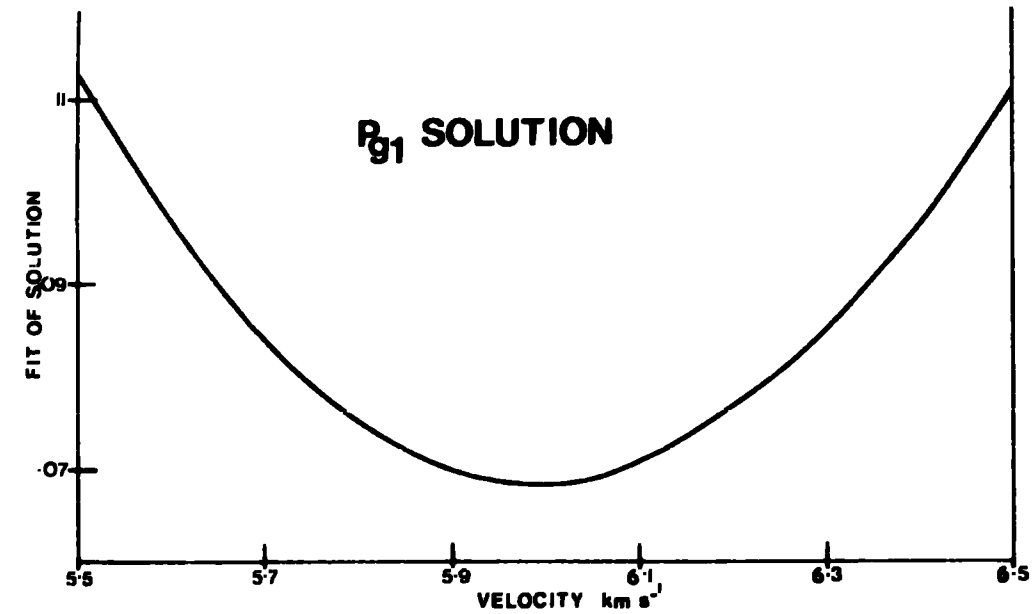
P_{g1} SOLUTION
FIT OF SOLUTION
·11
·09
·07
5·5
5·7
5·9
6·1
6·3
6·5
VELOCITY km s⁻¹

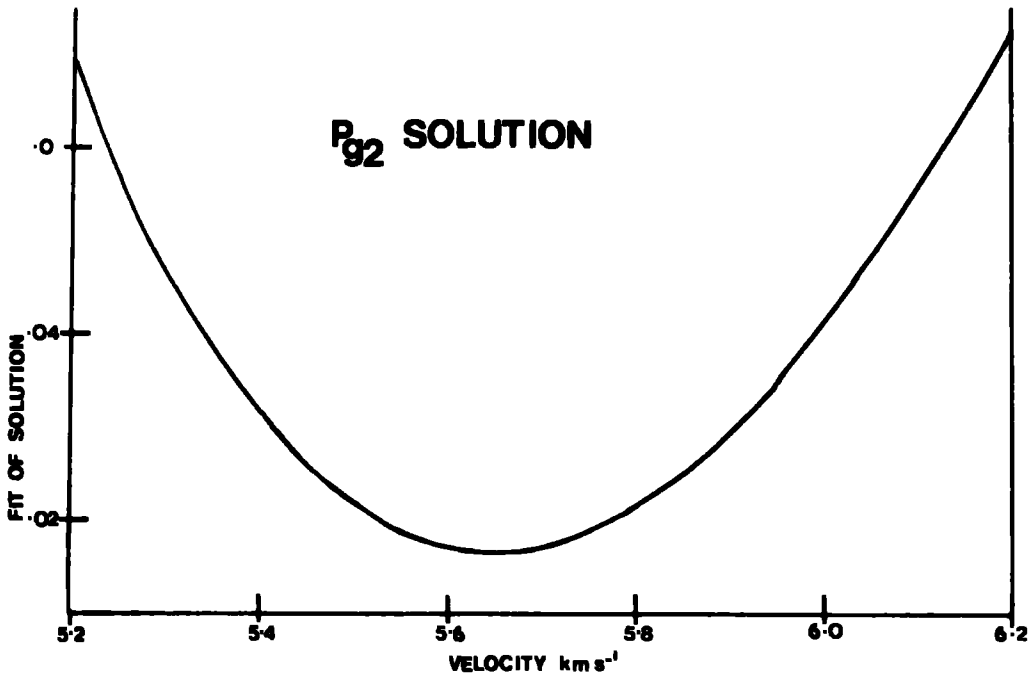
P_{g2} SOLUTION
FIT OF SOLUTION
·0
·04
·02
5·2
5·4
5·6
5·8
6·0
6·2
VELOCITY km s⁻¹

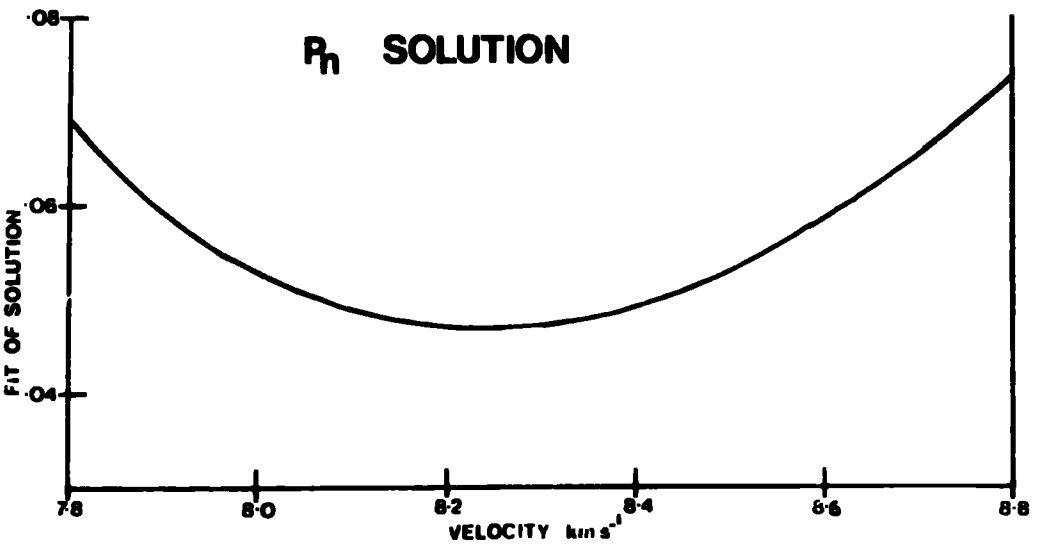
P_h SOLUTION
FIT OF SOLUTION
·08
·06
·04
7·8
8·0
8·2
8·4
8·6
8·8
VELOCITY km s⁻¹

were interpreted in terms of basaltic lava (4.9 km s^{-1}) overlying the basement (5.98 km s^{-1}). A range in depths of 2.4-4.5 km was determined with a mean cover of 3.4 km. Apart from an abnormally large value for shot A3 (0.68s) the range for line A was 0.38-0.57 seconds with a mean of 0.44 seconds. These values were interpreted in a similar manner and represent a depth range of 3.0-4.7 km with a mean value of 3.6 km. A similar variation was found in the recording station time terms (0.26-0.63s) and the depth determined for each station were:

	DU4	4.4 km
	F1	2.6 "
	F2	2.4 "
	F3	4.3 "
	MIR(D)	1.4 "
(Casten, 1971)	S3	2.2 "

These results indicate that the basement is shallowest to the west of the Faeroe Islands (station MIR(D)) and also in the west of the islands (stations F1 and F2) and deepens to the west (station DU4). Similar variation in basement depth is also indicated by the time terms for the stations of Falmason (1965) across Streymoy. These time terms vary from 0.21 seconds in the west to 0.52 seconds in the east near Torshavn and, interpreted in a similar manner, represent a change in depth from 1.8 km to 4.4 km.

5.1.4.2 Pg_2 basement to the south and east

The Pg velocity determined by the analysis was 5.65 km s^{-1} which is significantly greater than the mean value of 5.38 km s^{-1} found from the travel time graphs. This high value may result from the limited number of observations at each site that were used in the time term analysis. Constrained velocities were again used to determine the dependence of the

fit of the solution on the velocity (Figure 5.7.). A sharper minimum was found for the correct velocity suggesting that, in fact, this high value is better determined. The time terms also appear to be quite well determined. Along line B the values increase reasonably uniformly away from the islands as would be expected as both the water depth and sediment cover increase in the same direction. The range in time terms found for this line was 0.13-1.10 seconds with a mean of 0.71 seconds. These values were interpreted assuming only lava (4.9 km s^{-1}) as well as sea water above the basement, and the depth variation determined was 0.74 km to 9.2 km with a mean value of 5.7 km.

The time terms also increase away from the islands along line C from shot C52 to shot C46 (0.25-0.56 s). However, there is then a sharp decrease between shots C45 and C44 (0.52-0.28 s), and then again the values increase reasonably uniformly out to shot C39. The probable explanation is that the time terms of shots C44-C42 were determined only by observations at station LOM FS(A) and these observations may be relatively inaccurate. The range in time terms (0.25-1.25 s) and the mean value (0.52 s) were interpreted making the same assumptions of structure as for line B and a depth range of 2.1 km to 10.4 km found with a mean depth of 4.2 km.

The time terms of the recording stations have been interpreted in the same way. However, it is quite probable that this basement does not extend as far west as stations F1 and F2 in which case depths determined for these stations would be meaningless. The depths found were:

DU4	3.6 km
F6	1.8 "
LOM FS(A)	outcrops

The results indicate a variable lava cover above the basement with a mean thickness of about 5 km. This is slightly greater than found for the higher velocity basement to the north and west. The depth estimates to both basements beneath station DU4 are compatible with the thickness of lower velocity material required beneath shots B1 and B2 in order that these shots give rise to 6 km s^{-1} arrivals at station F2 but not at station DU4.

5.1.4.3 Pn time term analysis

As very few observations of Moho arrivals were available on the Faeroe Islands this analysis relied heavily on the observations at station UKAEA on the Shetland Islands. A Pn velocity of 8.24 ± 0.35 km s^{-1} was determined, the large standard error on the velocity reflecting the limited number of observations at each site. The dependence of the fit on this Pn velocity value was also tested by calculating a set of time term solutions using constrained velocities (Figure 5.7.). A lessening of the goodness of fit of only 0.006 was found by the solution taking a velocity of 8 km s^{-1}. Excepting an anomalously low value for shot A1, the time terms determined are reasonably consistent. The ranges and mean values found for the three lines were:

Line A	3.33-3.76s	3.54s
Line B	3.33-4.00s	3.78s
Line C	3.25-3.64s	3.39s
Combined	3.25-4.00s	3.64s

These ranges were interpreted in terms of 0.1-0.2 km of sea water overlying 4 km of basalt lava (4.9 km s^{-1}) above the 5.98 km s^{-1} basement which is assumed to extend to the Moho. The mean time terms were interpreted in the same manner only assuming a mean water depth of 0.15 km. The crustal thicknesses

found were:

Line A	26.6-30.5 km	28.5 km
Line B	26.3-31.9 km	30.2 km
Line C	26.0-29.4 km	27.2 km
Combined	26.0-31.9 km	29.1 km

Obviously if there is a higher velocity lower crustal refractor or an increase of velocity with depth in the crust these depths will underestimate the true crustal thickness. Alternatively if the 5.65 km s^{-1} basement extended to the Moho, which is improbable for any known type of crust, then the mean crustal thickness determined from the time terms would be 24.6 km.

The Pn time terms of the three recording stations show considerable scatter, but the value for station UKAEA (2.58s) is similar to that determined for this station by the North Scottish Shelf data (2.43s). The mean value of 3.52 seconds for stations DU4 and F2 was interpreted in terms of the previous crustal structure and a Moho depth estimate of 28.8 km determined beneath these stations.

Although the Pn time terms appear to be quite well determined the velocity of 8.24 km s^{-1} may be an overestimate of the true Pn velocity. In order to test the effect of this being an incorrect velocity value a time term solution was obtained using a constrained Pn velocity of 8.0 km s^{-1}. The time terms were correspondingly reduced due to this lower velocity and the mean values for the three lines were:

	Mean Pn time term	Mean Moho depth
Line A	2.91 s	23.0 km
Line B	3.67 s	29.2 "
Line C	2.85 s	22.5 "
Combined	3.34 s	26.5 "

The previous crustal structure was used to interpret these mean time term values and the crustal thickness estimates found are given above. The mean value for stations DU4 and F2

was altered to 3.10 s which, when interpreted in a similar manner, indicated a crustal thickness of 25.2 km. These reduced crustal thickness estimates are still too large to suggest anything but a continental crust beneath the Faeroe Plateau.

5.1.5 Summary and discussion

The travel time graphs show that the first arrivals from the Faeroe Plateau fall into three main groups:

1. Pg_1 arrivals from shots to the north and west of the Faeroe Islands
2. Pg_2 arrivals from shots to the south and east of the Faeroe Islands
3. Pn arrivals recorded from both areas of the Plateau beyond ranges of about 110 km.

The time term analyses velocity estimates for these three groups were 5.98 km s^{-1}, 5.65 km s^{-1} and 8.24 km s^{-1} respectively. Some arrivals at station LOM FS(D) indicated a higher velocity (6.78 km s^{-1}) lower crustal layer at a depth of approximately 10-15 km.

Both the two basement velocities identified are interpreted as respresenting continental metamorphic rocks and the transition between the two, located beneath shots B2-B3 to the east of the islands, is tentatively interpreted as a change in metamorphic grade. The Pg_1 velocity (5.98 km s^{-1}) is very similar to the velocities observed at shallow depths on the Scottish Shelf and interpreted as Lewisian gneisses (section 4.3.), and the Pg_2 velocity (5.65 km s^{-1}) is representative of lower grade metamorphics such as slates.

The Pn velocity is not particularly well determined

beneath the Faeroe Plateau but the Pn time terms appear to be reliable. Various time term estimates have been interpreted in terms of Moho depths for different upper crustal structures, and it appears that the true crustal thickness must be at least 26 km and more probably 30 km. A mean crustal cross section beneath the Faeroe Plateau is presented in Figure 5.8.

The results from the Faeroe Plateau, both basement velocities and crustal thickness estimates, have been interpreted to strongly indicate a continental crust beneath the outcropping Tertiary lava. Palmason (1965) correlated the upper crustal structure of the Faeroe Islands with that of Iceland, mainly on the basis of the 6.4 km s^{-1} basement that he identified beneath the Faeroe Islands. However, the structure beneath Iceland (Palmason, 1970) and the adjacent Iceland-Faeroe Ridge (Bott et al, 1971) is anomalous oceanic and differs in four important respects from the structure established by these NASP results beneath the Faeroe Plateau. (Bott et al, 1974)

1. Continental basement type Pg velocities of 5.2-5.6 km s^{-1} and 5.8-6.2 km s^{-1} are characteristic of the Faeroes, but such velocities have not been observed beneath Iceland.

2. No 6.4-6.8 km s^{-1} layer, tentatively interpreted as oceanic layer 3 (Bott et al, 1971), such as is present beneath Iceland and the Ridge has been firmly established at shallow depth beneath the Faeroes.

3. The high sub-Moho Pn velocity observed beneath the Faeroes is substantially different to the anomalously low value of 7.2 km s^{-1} beneath Iceland.

4. The crustal thickness of about 30 km beneath the Faeroe Plateau is within the range to be expected for continental

Figure 5.8 : The mean crustal structure determined across the Faeroe Plateau.

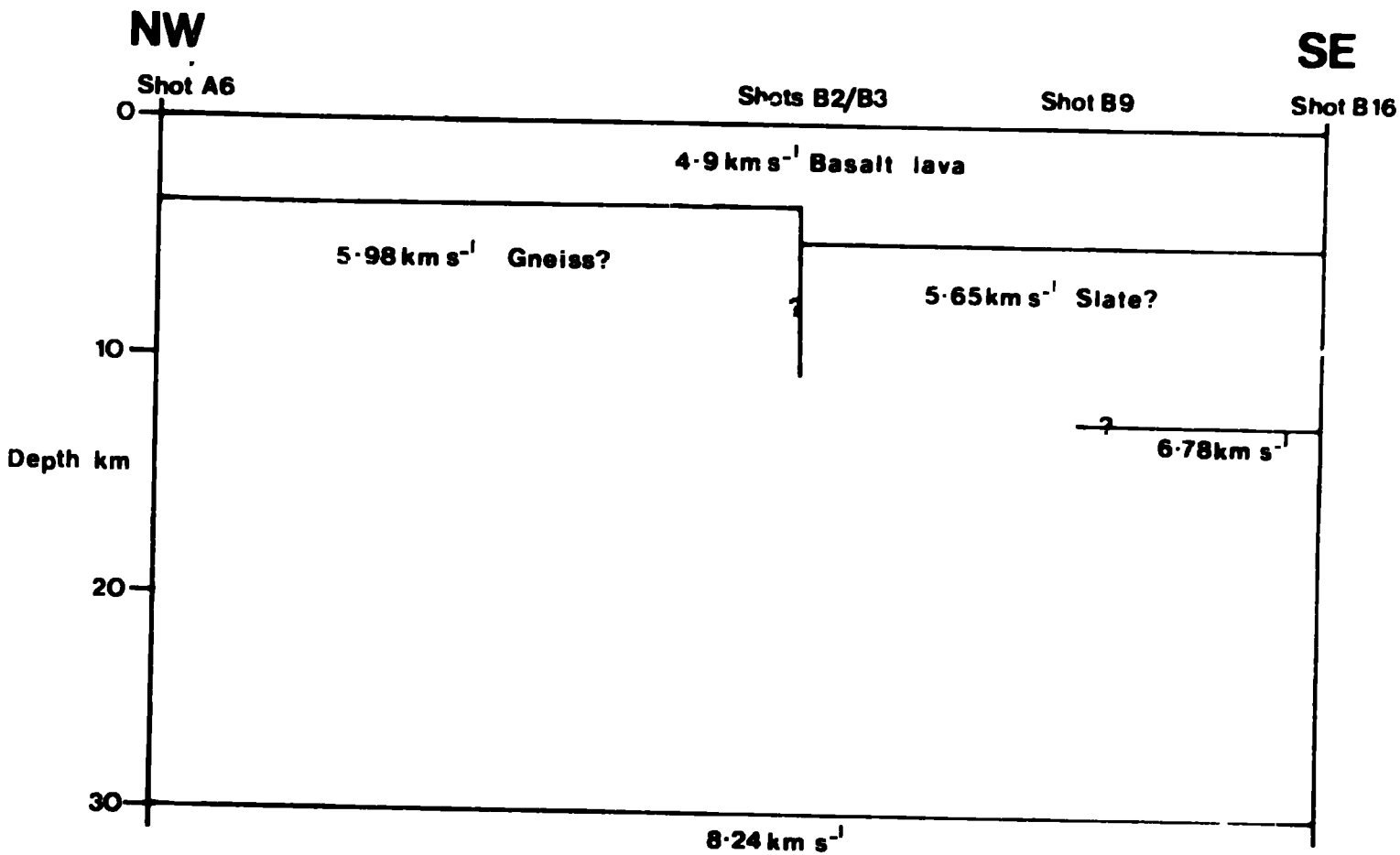
NW
SE
Shot A6
Shots B2/B3
Shot B9
Shot B16
0
10
20
30
Depth km
4·9 km s⁻¹ Basalt lava
5·98 km s⁻¹ Gneiss?
5·65 km s⁻¹ Slate?
?
?
6·78 km s⁻¹
8·24 km s⁻¹

crust around the British Isles (Agger and Carpenter, 1965; Blundell and Parks, 1969; Holder and Bott, 1971) and significantly greater than that determined beneath Iceland (10-18 km) (Palmason, 1970).

The results from the Faeroe Plateau show that the crust beneath the Tertiary lavas is continental in nature and significantly different to that beneath Iceland and the Iceland-Faeroe Ridge. A continental crust has already been established beneath Rockall Plateau (Scrutton, 1972) and is suggested by gravity interpretation over some of the intervening Banks (Himsworth, 1973; Lewis, private communication). These latest results suggest that the Rockall-Faeroe Plateau may form a single microcontinental fragment. This possibility and its implications will be discussed in the following chapter.

5.2. The Faeroe/Shetland Channel and Channel Slopes

5.2.1 Introduction

The Faeroe/Shetland Channel is the trough of relatively deep water separating the Faeroe Plateau from the Scottish Continental Shelf, and is bounded at its south-western end by the Wyville-Thomson Rise and at its north- eastern end passes into the Norwegian Sea. The channel slopes are considered as part of the channel as there is no sharp bathymetric break between then, but rather the gentle gradient of the channel slopes merges into the channel floor.

Little was known of the structure of this region prior to NASP although Moho depths and sediment thicknesses had been estimated by gravity and magnetic methods (Watts, 1970; Himsworth, 1973). Power spectrum analysis was performed on a

magnetic profile along the centre of the Faeroe/Shetland Channel (Himsworth, 1973) and the sediment thickness above basement estimated to be about 2.3 km at about 61°20'N, 4°W. The gravity interpretations indicated crustal thicknesses of 21 km and 18 km. Although these values are intermediate between oceanic and continental crustal thicknesses they do not support the suggestion of Talwani and Eldholm (1972) that the Faeroe/Shetland Channel is a region of subsided continental crust. They are also significantly different to the crustal thickness estimate of 12 km determined by gravity interpretation (Scrutton, 1972) beneath the Rockall Trough which was suggested to be oceanic in origin. The nature of the crust beneath the channel is of considerable importance in determining the history of the evolution of the NE North Atlantic and it was hoped that the results of NASP would resolve the problem.

A reversed seismic refraction line (CB to the north-east and BC to the south-west) was fired along the length of the Faeroe/Shetland Channel with ship receiving stations (MIR and LOM) positioned at each end of the line. Lines B and C shots cross from the Scottish Continental Shelf over the channel and channel slopes onto the Faeroe Plateau (Fig. 2.1.). Shots B19-37 and C31-33 were fired over the channel floor and shots B17 and B18, B38-B45, C25-C30 and C36-C38 were fired over the channel slopes.

5.2.2 The time-distance graphs

The observed travel times of all the arrivals from shots over the channel floor and slopes were first reduced to the sea floor to remove the effect of shot depth variation and to exclude a sea water layer from any crustal structure models. A correction was also applied to each travel time to reduce

every receiving station to a sea level datum. The correction applied was:

$$-\left(\frac{\text{Shot depth (km)} - \text{water depth (km)}}{1.5} + \frac{\text{station elevation (km)}}{6.0}\right)$$

assuming a velocity of 6 km s^{-1} as typical of continental metamorphic basement rocks beneath the receiving stations. No correction was applied for variation in the topography of the sea floor for shots fired over the channel floor, as this variation was reasonably small. The maximum variation along the length of line CB was about 200 m but arrivals were recorded at most of the stations from only short sections of line CB. The maximum topographic variations over these sections was nearer to 50 m. However, the topography over the channel slopes varies from about 100-200 m on the Faeroe Plateau and Scottish Shelf to about 1,000-1,100 m in the channel. This variation was allowed for by reducing the travel times of all the first arrivals from shots over the slopes to a level sea floor datum (1,100 m below sea level), by applying the correction:

$$-(1.100 - \text{Sea floor depression (km)})/2.5$$

A reducing velocity of 2.5 km s^{-1} was used as this is a probable value for the mean sedimentary velocity (Peacock, private communication).

The method of least squares was used to fit straight line segments to the corrected first arrival time-distance graphs for each station and line, and to the later arrival travel times plotted for station LOM BS(A). The velocities and intercepts obtained are given in Table 5.3. The travel times were also plotted as reduced 'time minus distance/6.0' graphs and these are shown in Figures 5.9-5.12.

TABLE 5.3

APPARENT VELOCITIES AND INTERCEPTS FROM LEAST SQUARES

Station	Shots	Phase	Velocity(km s^{-1})	Intercept(s)	S.E.
MIR(B)	CB2-CB4	B	6.57 ± 0.45	1.87 ± 0.15	0.02
	CB5-CB10		3.33 ± 0.08	0.07 ± 0.05	0.04
	+CB16-CB19, CB27-CB31	A	4.40 ± 0.04	0.79 ± 0.04	0.05
	CB22-CB25	B	5.11 ± 0.37	1.08 ± 0.23	0.05
MIR(C)	BC1-BC9	A	4.96 ± 0.26	2.26 ± 0.16	0.11
MIR(A)	C28-C41	B	6.13 ± 0.23	1.93 ± 0.27	0.22
	C31-C33	A	4.83 ± 0.10	0.41 ± 0.01	0.01
LOM FS(B)	CB43-CB46	B	6.59 ± 0.06	3.38 ± 0.05	0.03
	CB37-CB42	Pn	8.04 ± 0.27	5.04 ± 0.33	0.11
LOM FS(C)	BC19-BC29	B	5.93 ± 0.19	3.51 ± 0.12	0.06
LOM FS(D)	B19-B28	A	4.73 ± 0.20	0.31 ± 0.25	0.35
LOM FS(E)	B34-B37	A	4.46 ± 0.31	0.41 ± 0.28	0.11
	B38-B45	B	6.36 ± 0.21	2.36 ± 0.24	0.22
LOM FS(A)	C36-C39	B	6.48 ± 0.10	0.91 ± 0.13	0.05
LOM BS(A)	CB44-CB46	B	5.81 ± 0.06	3.07 ± 0.05	0.03
	+CB43-CB45	B	6.22 ± 0.30	5.00 ± 0.29	0.11
	+CB37-CB42	Pn	7.94 ± 0.12	6.92 ± 0.12	0.05
	BC34-BC39	Pn	8.17 ± 0.29	5.60 ± 0.25	0.07
	+BC34-BC42	Pn	8.37 ± 0.19	7.37 ± 0.17	0.08
LOM BS(B)	B21-B30	A	4.52 ± 0.11	0.86 ± 0.12	0.18
LOM BS(C)	B34-B37		3.78 ± 0.08	0.51 ± 0.08	0.04
	B39-B45	B	6.26 ± 0.28	3.17 ± 0.31	0.25
UKAEA	CB1-CB48	Pn	7.76 ± 0.08	4.40 ± 0.29	0.19
	BC1-BC48	Pn	7.90 ± 0.06	4.69 ± 0.18	0.11

+ denotes that these arrivals are secondary arrivals.

Figure 5.9 : The reduced time-distance graphs for (a) line CB at station MIR(B), (b) line C at station MIR(A), (c) line BC at station MIR(C), (d) line BC at station LOM BS(A), (e) line CB at station LOM BS(A), (f) line BC at station LOM FS(C) (g) line CB at station LOM FS(B).

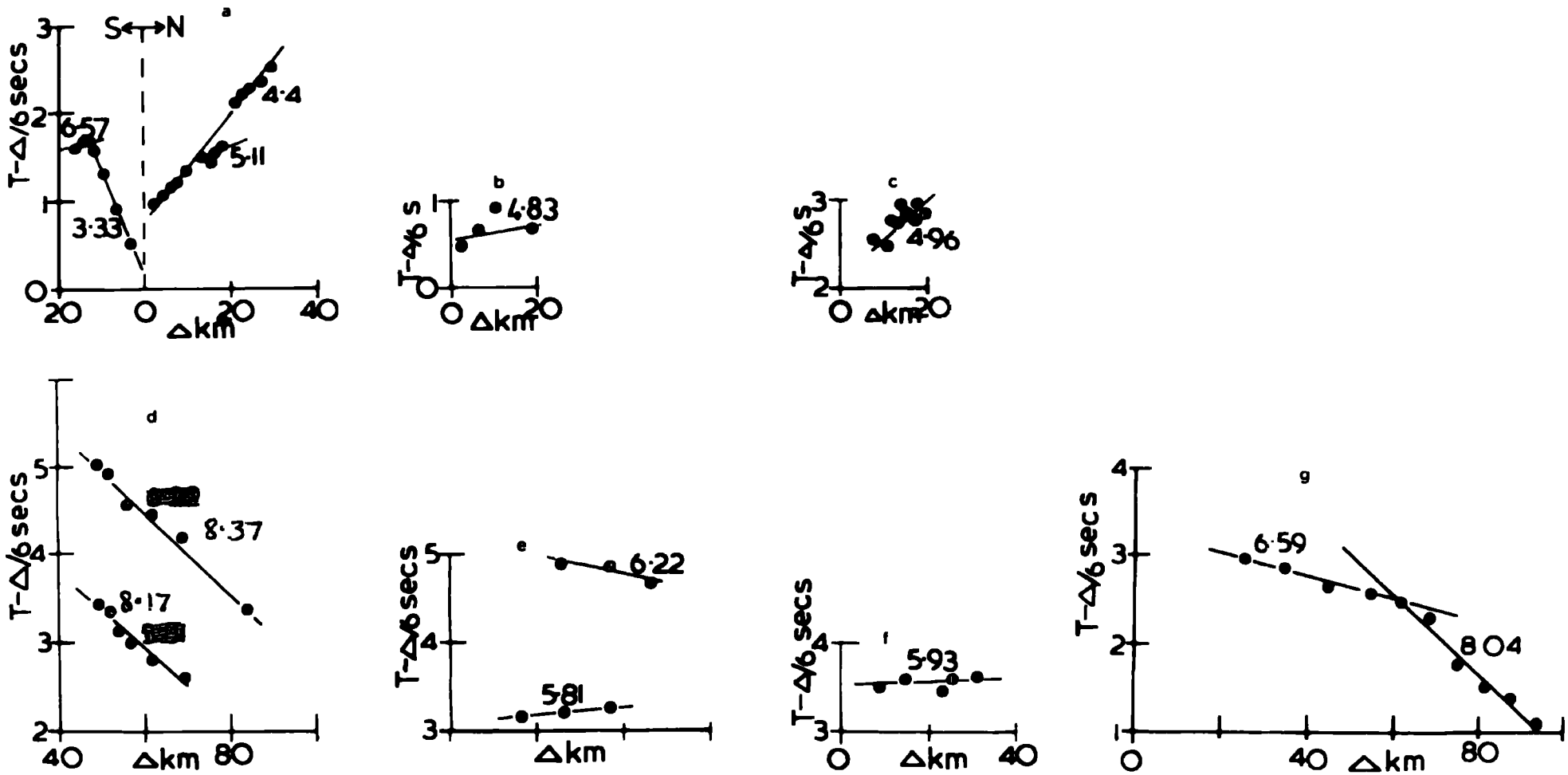
a
S
N
T-Δ/6 secs
6·57
4·4
5·11
3·33
Δkm
b
4·83
T-Δ/6 s
Δkm
c
4·96
T-Δ/6 s
Δkm
d
8·37
8·17
T-Δ/6 secs
Δkm
e
6·22
5·81
T-Δ/6 secs
Δkm
f
5·93
T-Δ/6 secs
Δkm
g
6·59
8·04
T-Δ/6 secs
Δkm

Figure 5.10 : The reduced time-distance graphs for (a) shots B21-B30 at station LOM BS(B), (b) shots B34-B37 at station LOM BS(C), (c) shots B19-B28 at station LOM FS(D), (d) shots B34-B37 at station LOM FS(E).

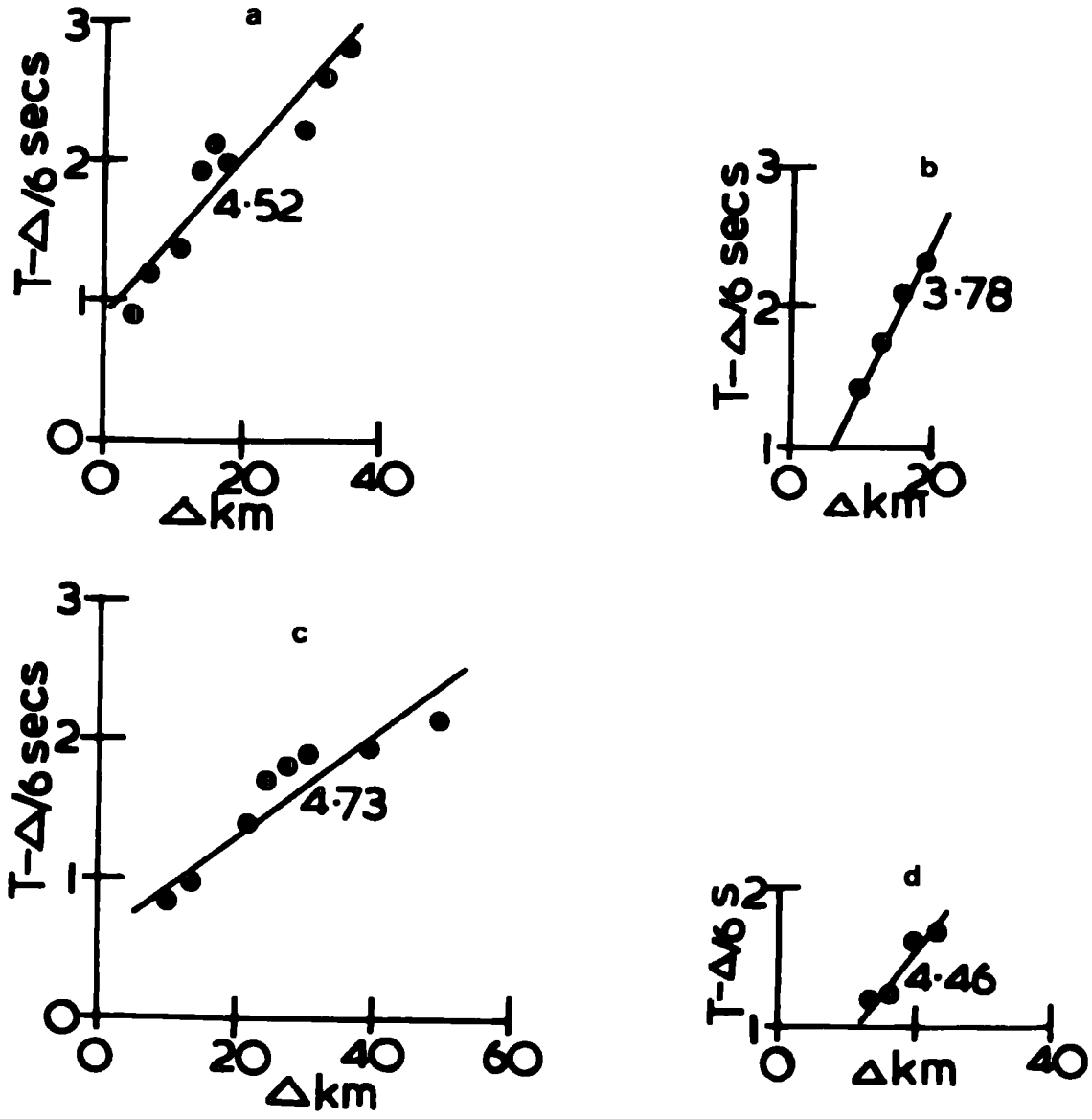
a
T-Δ/6 secs
4·52
Δkm
b
T-Δ/6 secs
3·78
Δkm
c
T-Δ/6 secs
4·73
Δkm
d
T-Δ/6 s
4·46
Δkm

Figure 5.11 : The reduced time-distance graphs of station UKAEA for (a) line CB, (b) line BC.

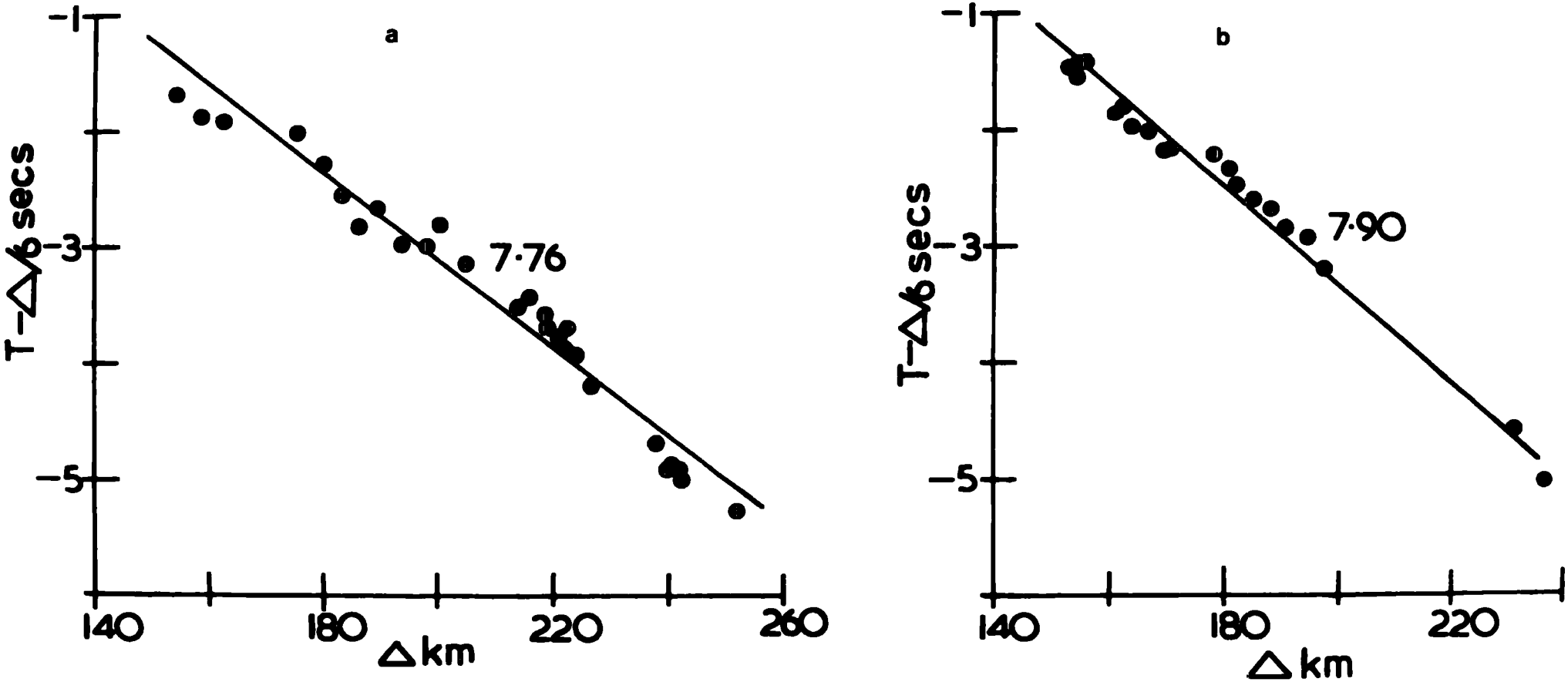
a
b
T-Δ/6 secs
-1
-3
-5
7·76
7·90
140
180
220
260
Δ km

Figure 5.12 : The reduced time-distance graphs for (a) shots C36-C39 at station LOM FS(A), (b) shots B39-B45 at station LOM BS(C), (c) shots B38-B45 at station LOM FS(E), (d) shots C28-C41 at station MIR(A).

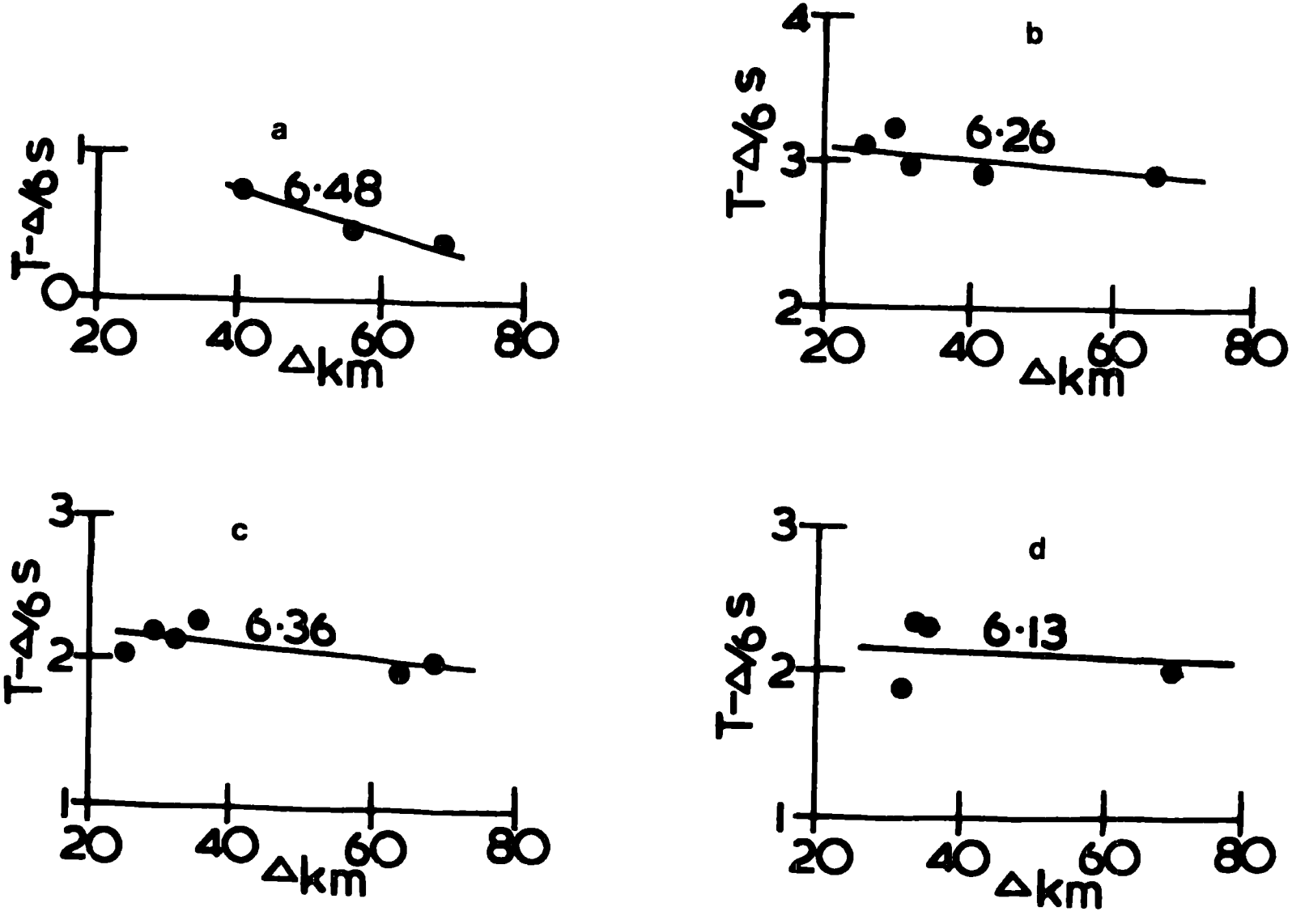
a
6·48
T-Δ/6 s
0
20
40
60
80
Δkm
b
6·26
T-Δ/6 s
4
3
2
20
40
60
80
Δkm
c
6·36
T-Δ/6 s
3
2
1
20
40
60
80
Δkm
d
6·13
T-Δ/6 s
3
2
1
20
40
60
80
Δkm

The arrivals provide evidence of three different refractors beneath the channel and slopes. At ranges up to about 20 km some first arrivals lie on segments with reciprocal gradients of 4.4-5.0 km s^{-1} and with small positive intercepts. These arrivals are interpreted as travelling in the sub-sediment basement layer which will be referred to as layer A. At ranges generally greater than 20 km (but in some cases as small as 5 km) and up to ranges of 50-60 km the first arrivals lie on segments with reciprocal gradients of 5.8-6.6 kms^{-1}. All these arrivals are interpreted as the head waves of a main crustal layer (layer B). Beyond ranges of 50-60 km the first arrivals lie on segments with reciprocal gradients of about 8 km s^{-1} and are interpreted as the Moho head wave Pn.

5.2.3 Interpretation of the time-distance graphs

The ranges of P wave velocity and the mean velocities observed for each refractor beneath the Faeroe/Shetland Channel were:

Layer A	4.40-4.96 km s^{-1}	4.65 ± 0.08 km s^{-1}
Layer B	5.68-6.61 "	6.01 ± 0.15 "
Moho	7.76-8.17 "	7.97 ± 0.10 "

and beneath the channel slopes:

Layer B	6.13-6.48 km s^{-1}	6.31 ± 0.11 km s^{-1}

5.2.3.1 Line CB

Station MIR(B) was positioned at the south-west end of this line and stations LOM FS(B) and LOM BS(A) both at the north-east end of the line. There was only one observation of layer A in the south-west and the observed values of intercept time and velocity were interpreted in terms of a 1.2 km sedimentary cover (2.5 km s^{-1}). Station MIR(B) formed a split

profile with the shot line and assuming that the two higher velocities (5.11 and 6.57 km s^{-1}) measured in opposite directions both represent layer B, the refractor was interpreted to have a true velocity of 5.68 km s^{-1} and dip to the north at 8.7^{o}. The intercept times of these two segments (1.87 ± 0.15s and 1.08 ± 0.23s) may not be significantly different. Their mean value was interpreted assuming a 1.2 km sediment cover (2.5 km s^{-1}) above layer A and a depth of 3.3 km was found for layer B.

Stations LCM FS(B) and LOM BS(A) were positioned approximately only 14 km apart on this line but the velocities observed from the same shots at these two stations were 6.61 ± 0.03 km s^{-1} and 5.81 ± 0.06 km s^{-1} respectively. The ranges of observation at the stations were 25-55 km and 15-40 km respectively, so it is most improbable that the arrivals are from two separate crustal layers. It was assumed that both sets of arrivals were from layer B and the mean velocity (6.21 km s^{-1}) and intercept time (3.23s) were interpreted in the same manner as for station MIR(B) in the south-west. A depth of 9.7 km was found for layer B.

The only other crustal velocity observed along this line (3.3 km s^{-1}) was interpreted as a semi-consolidated sediment refractor. Assuming the mean sedimentary velocity above this layer to be 2 km s^{-1}, a depth of 0.1 km was determined.

The Pn velocity and intercept time observed at station LOM FS(B) were also interpreted assuming the upper crustal structure established beneath the north-east part of the line. The crustal thickness was estimated to be 14.1 km.

5.2.3.2. Line BC

All the stations provided by the ships Lomonosov and Miranda were positioned at the north-east end of this line. However, the only arrivals observed at station MIR(C) were from shots BC1-BC12 travelling to the south-west whereas the Lomonosov stations received arrivals only from shots beyond BC12 travelling to the north-east. The positions of the ship stations in relation to the shot lines are shown in Figure 5.13.

Only one layer A segment was defined by arrivals from this line (4.96 km s^{-1} at station MIR(C)) and, assuming the same overlying sedimentary material as for line CB, the observed velocity and intercept were interpreted in terms of 3.3 km of sediments above the layer A basement. The layer B velocity of 5.93 km s^{-1} observed at station LOM FS(C) is very similar to the velocity observed along line CB at station LOM BS(A) (5.81 km s^{-1}). This observed velocity and intercept were interpreted assuming the upper structure established on this line at station MIR(C), and a depth of 9.7 km was found for layer B. This is the same depth as was found beneath line CB where a different upper crustal structure was used. A Moho depth estimate was obtained along line BC using the Pn observations of station LOM BS(A). Assuming the crustal velocity -depth structure established beneath this line (3.3 km of sediments overlying 6.4 km of layer A) the Moho depth was determined to be 14.2 km, which is in very good agreement with the crustal thickness estimate found for line CB.

5.2.3.3 Lines B and C

The travel time graphs for lines B and C shots over the channel floor defined only layer A segments. Each observed

Figure 5.13 : The relative positions of the shots and the ship receiving stations in the northern part of the Faeroe /Shetland Channel

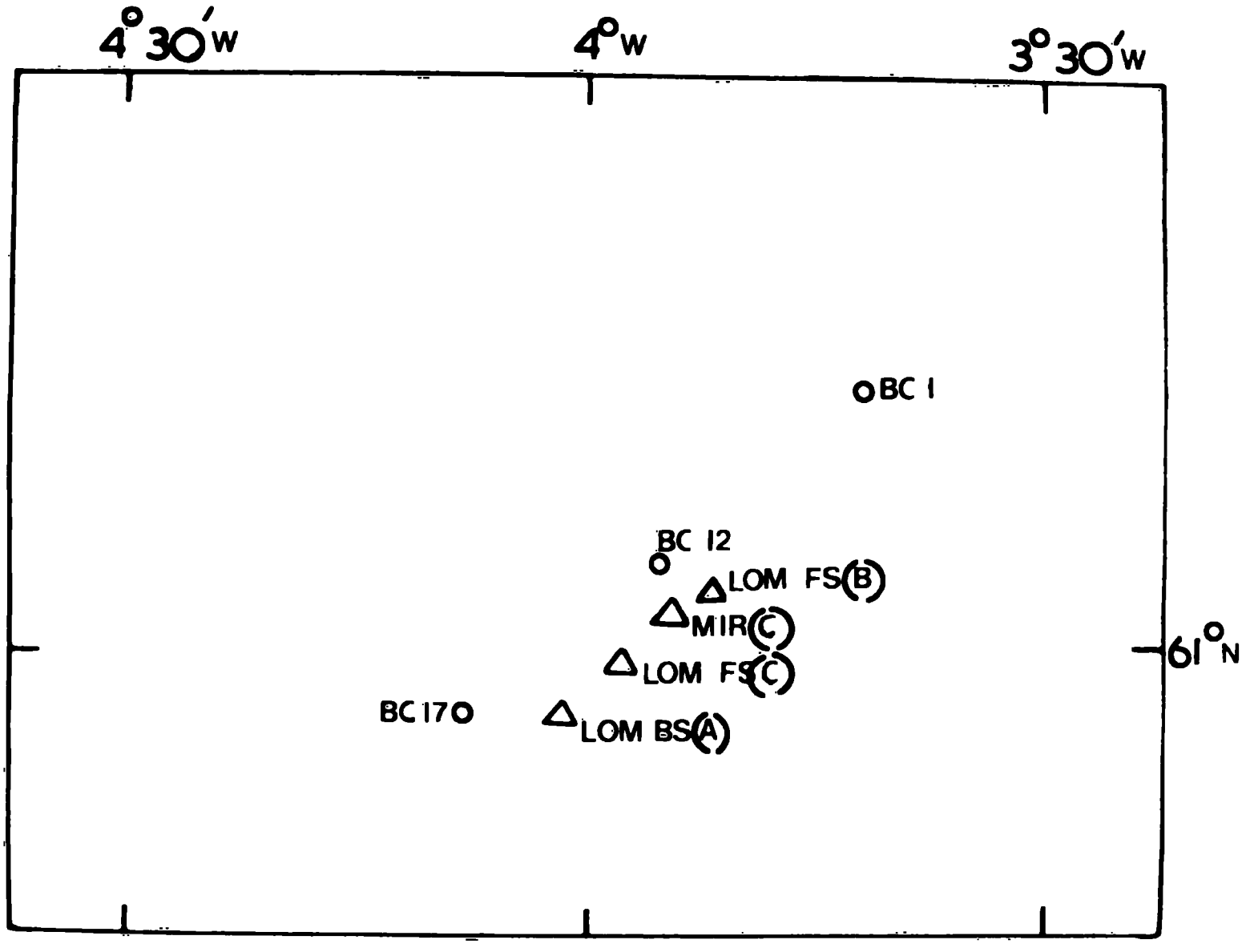
4°30'W
4°W
3°30'W
61°N
BC 1
BC 12
LOM FS(B)
MIR(C)
LOM FS(C)
BC 17
LOM BS(A)

velocity and intercept was interpreted in terms of basement depth assuming overlying sediment of mean velocity 2.5 km s^{-1}. The depths found were:

LOM FS(D)	0.46 km
LOM FS(E)	0.62 "
LOM BS(B)	1.29 "
MIR (B)	0.60 "

Apart from the large value for station LOM BS(B) the depths are reasonably similar with a mean value of 0.56 km.

Layer B velocities only were defined by the arrivals from shots over the channel slopes. The individual velocity and intercept values determined for each station were interpreted in terms of layer B depths. The sediment cover found at the station from the channel floor data was used in the interpretation if available, or otherwise the mean layer A depth of 0.56 km. The depths to layer B were determined as:

LOM FS(D)	6.6 km
LOM FS(E)	2.2 "
LOM BS(C)	10.0 "
MIR (B)	6.4 "

The low value of 2.2 km for station LOM FS(E), positioned on the Faeroe Shelf, is probably erroneous. The remaining depths are approximately of the same order as those observed for this refractor beneath the channel floor (9.7 km).

The Pn segment graphs of the land receiving stations have not been interpreted by means of the layer thickness formula, as this would involve the assumption of plane homogeneous layers extending from the channel to beneath both the Scottish Shelf and the Faeroe Plateau. The intercept values of these graphs have been dealt with in conjunction with the Pn time terms in section 5.2.6.1.

5.2.4 The secondary arrivals

Large amplitude secondary arrivals which can be correlated from shot to shot were seen on the records of the horizontal instruments of station LOM BS(A) for the shots of lines CB and BC (Figs. 5.14, 5.15). Secondary arrivals from both layer B and the Moho defined segments on the time-distance graph of this station for the line CB shots (Fig. 5.9.). In addition a layer B segment was defined by first arrivals. The reciprocal gradients of the two layer B segments are not significantly different and the time offset between the two segments has an almost constant value of about 1.5 seconds. Shots on line BC gave rise to secondary arrivals which defined a time-distance segment of reciprocal gradient 8.37 ± 0.19 km s^{-1} (Fig. 5.9.). First arrivals were also identified for some of these shots and defined a Pn segment of reciprocal gradient 8.17 ± 0.29 km s^{-1}. Again these two velocities are not significantly different and the two segments have a constant time offset of approximately 1.5 seconds. There are two likely possible causes of these large amplitude secondary arrivals:

1. A phase conversion, P to S, somewhere along the travel path, with the S phase arriving after the P phase.

2. The second arrivals represent a phase that has undergone one or multiple reflections between the sea floor and the sea surface, and/or the sea floor and the top of layer A, and/or the top of layer A and the top of layer B.

These possibilities are shown in Figure 5.16.

A phase conversion is improbable as the time difference between the first and second arrival phases is the same for both the layer B and the Moho arrivals. The phase change would have to occur at the same boundary for both sets of arrivals which

Figure 5.14 : The stacked records of the line CB shots at station LOM BS(A).

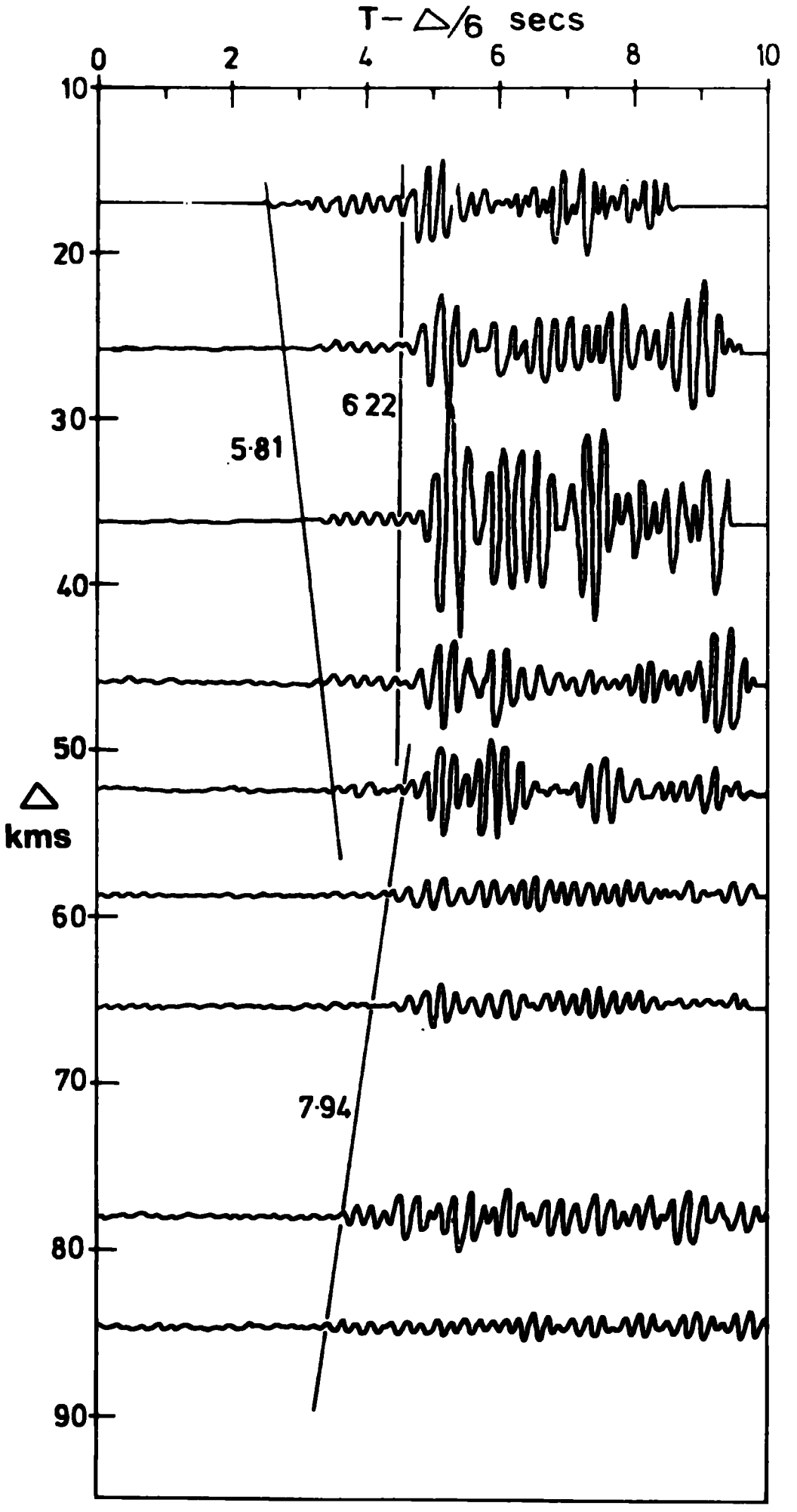
T− Δ/6 secs
0
2
4
6
8
10
10
20
30
40
50
60
70
80
90
Δ
kms
6·22
5·81
7·94

Figure 5.15 : The stacked records of the line BC shots at station LOM BS(A).

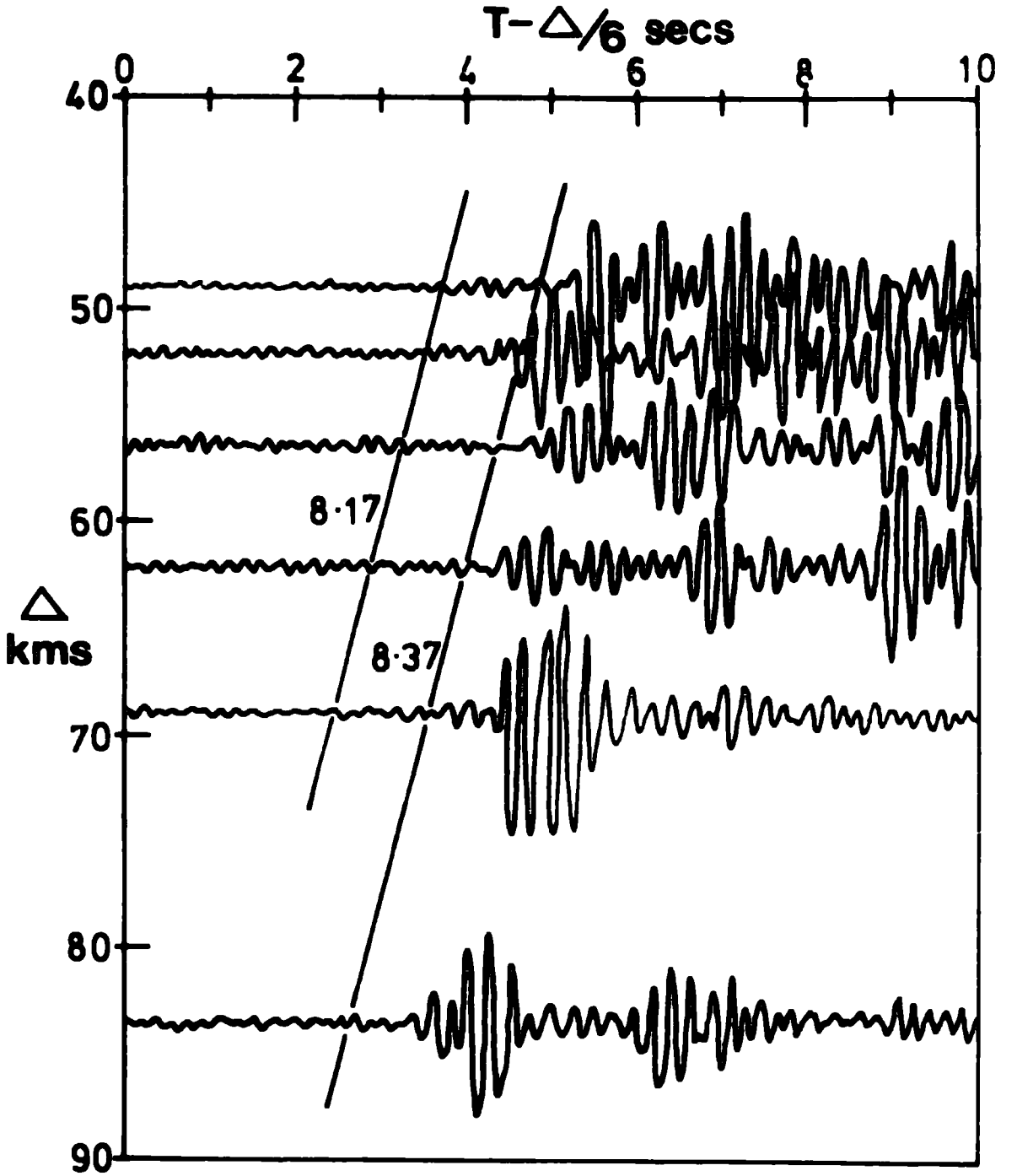
T-Δ/6 secs
0
2
4
6
8
10
40
50
60
70
80
90
Δ
kms
8·17
8·37

Figure 5.16 : The possible causes of the large amplitude secondary arrivals at station LOM BS(A).

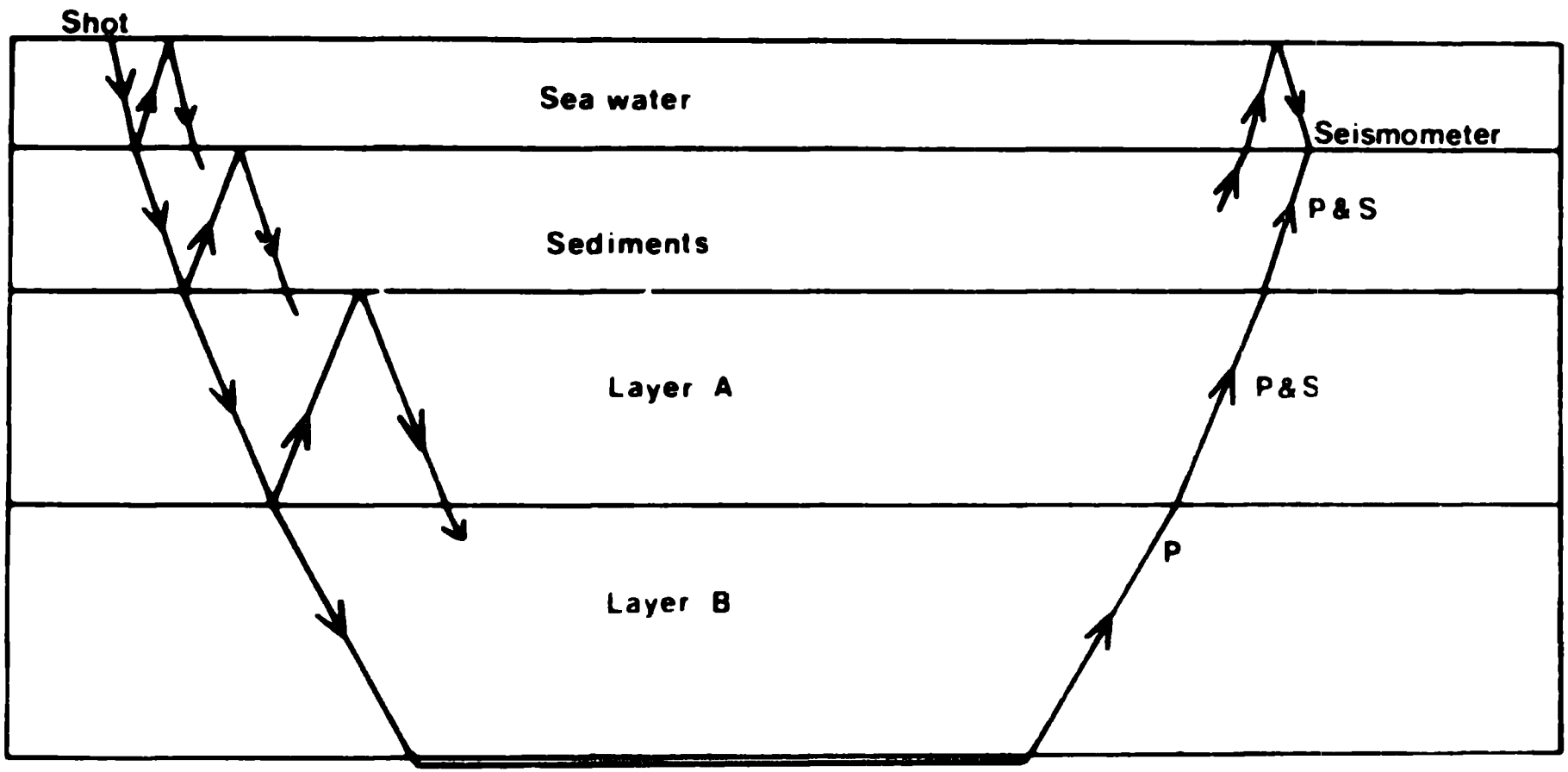
Shot
Sea water
Seismometer
Sediments
P & S
Layer A
P&S
P
Layer B

limits the travel time path of the S phase to between the layer A or layer B refractor, and the sea floor. It is most improbable that the downgoing P wave is converted to an S wave, as the velocities defined by the later arrivals are reasonably normal P head wave velocities. The time differences for a Pn head wave travelling as a P and as an S phase between layer A and the sea floor, and between layer B and layer A were calculated for layer A and layer B depths of:

1. 1.2 km and 3.3 km
2. 3.3 km and 9.7 km

these being the depths of the refractors determined beneath, (1), the south-west and, (2), the north-east parts of the channel. A P to S velocity ratio of 1.78 to 1 was assumed and the time delays found for the two regions were 0.39 s and 0.44s, and 1.08 s and 1.28 s respectively. None of these delays are of the same order of magnitude as the observed delay.

The second possibility of multiple reflections was also tested by calculating the delay introduced by:

1. A reflection between the layer A and layer B interfaces, and between both the layer A and layer B interfaces and the sea floor.

2. A reflection between the sea floor and the sea surface.

The time delays were calculated for a Moho head wave for the same crustal structures as used previously. The delays between the sea floor and layer A in the two regions were determined as 0.9s and 2.5s respectively, and between layer A and layer B refractors as 0.8s and 2.0s respectively. No single reflection can explain the observed time delay but a double reflection between layers A and B of the south-west region would give the correct order of magnitude of delay.

The reflection between the sea floor and the sea surface

for a water depth of 1.1 km was calculated to cause delays to the layer B and Moho head wave arrivals of 1.43 and 1.44s respectively. This is equivalent to the observed delay. The large amplitude of the arrivals may be explained by such a reflection at both the shot and station locations, causing delayed arrivals which interfere constructively to reinforce the amplitude of the onset. Similar large amplitude secondary arrivals have been observed from median valley earthquakes and interpreted in a similar manner (Francis and Porter, 1973).

5.2.5 Summary of the interpretation

The time-distance graphs have been interpreted in terms of three main refractors, layer A, layer B and the Moho, with mean velocities of 4.65 km s^{-1}, 6.16 km s^{-1} and 7.97 km s^{-1} respectively. The overall mean depths of these refractors were determined as 1.24 km, 6.9 km and 14.1 km respectively. There is some evidence of variations in the crustal structure along the line with both layers A and B found at greater depths in the north-east region. However, many of the time-distance segments are defined by only a few points, and inconsistencies were found in the observed data at both ends of the lines along the channel.

The large amplitude secondary arrivals identified on the records of station LOM BS(A) were interpreted as multiples of the first arrivals caused by reflection between the sea surface and the sea floor. The large amplitude may be caused by constructive interference between two such multiples, but no explanation is offered as to why they are mainly apparent on the horizontal instruments.

5.2.6 Time term analysis

Time term analysis could ony be performed on the Pn arrivals from the shots over the Faeroe/Shetland Channel and

Channel slopes. Although there were a reasonable number of observations of layer A and layer B arrivals most shots only gave rise to such arrivals at one station. The coverage of these two layers was therefore found not to provide a sufficient redundancy of data to determine adequate time term solutions.

In all cases the observed uncorrected travel times were used in the time term analyses. Three different first arrival Pn travel time data sets were used to test the consistency of the time term solutions obtained. The first data set (DS1) contained the travel times of the Pn arrivals from shots on lines BC and CB only. Data set 2(DS2) contained all the previous data plus the travel times of the Pn arrivals from shots on lines B and C over the channel floor. The final data set (DS3), the results of which are used in the interpretations, contained all the previous data plus the travel times of the Pn arrivals from shots over the channel slopes. A comparison of the time terms of the same sites for different data sets, shows that the solutions are consistent.

	CB1	CB30	CB47	BC23	LOM BS(A)
DS1	3.87	3.98	2.93	3.23	2.97
DS2	3.81	3.94	2.93	3.22	2.96
DS3	3.79	3.93	2.93	3.22	2.96

The same statistical considerations that were applied to the time term solutions of the Faeroe Plateau data were also applied to these Pn solutions and the results found to be reliable.

The two lines along the channel (CB and BC) were fired in almost the same locations so that some of the shots on line CB were nearly coincident with shots on line BC. This was the

case for the shots listed in Table 5.4 together with their time terms and differences.

Large differences in time term values were observed for the shot pairs CB45/BC31 and CB44/BC33 (0.45 and 1.18 seconds respectively), but the remainder of the coincident shot time terms are reasonably consistent. It is probable that the time term of shot CB44 is incorrect as it is considerably larger than the time terms of the nearby shots, and also the time term of shot BC33 is similar to those of shots BC32 and BC34 and so therefore probably correct.

This comparison of the time terms, as well as the agreement of the results of the three different data sets, shows good internal consistency and suggests that the assumptions of the time term method are valid. All the time terms found for the shots over the Channel floor and slopes are listed in Table 5.5.

The mean t_n time term for line CB was 3.65 seconds, and for line BC 3.22 seconds. However, this is not a valid comparison as there were only three shots on line CB compared to twelve on line BC over the northern area of the channel. Similarly, in the southern area of the channel there were sixteen shots on line CB but only two on line BC, and in the central area eight on line CB and thirteen on line BC. Therefore any variation along the channel will bias the average time term values for the two lines. Mean time terms for each of the three areas of the channel were determined for both lines separately, and then for the combined data of the two lines. The values found were:

TABLE 5.4 COINCIDENT SHOT TIME TERMS FOR LINES CB AND BC

SHOT PAIR	TIME TERMS	DIFFERENCE
CB47	2.93	0.13
BC19	3.06	
CB46	3.02	0.05
BC24	3.07	
CB45	3.64	0.45
BC31	3.19	
CB44	4.36	1.18
BC33	3.18	
CB43	3.66	0.24
BC34	3.42	
CB42	3.55	0.19
BC35	3.36	
CB41	3.35	0.04
BC37	3.31	
CB40	3.19	0.11
BC38	3.30	
CB39	3.46	0.13
BC40	3.33	
CB38	3.34	0.04
BC41	3.38	
CB36	3.50	0.22
BC42	3.28	
CB35	3.58	0.30
BC42	3.28	

TABLE 5.5

Pn Time Terms for the Faeroe/Shetland Channel

Site	Pn time term	S.E.	
CB1	3.81		(1)
CB8	3.64		(1)
CB9	3.68		(1)
CB11	3.54		(1)
CB12	3.74		(1)
CB22	3.77		(1)
CB24	3.91		(1)
CB25	4.09		(1)
CB26	3.82		(1)
CB27	3.85		(1)
CB28	3.88		(1)
CB29	3.94		(1)
CB30	3.94		(1)
CB31	3.94		(1)
CB34	3.74		(1)
CB35	3.59		(1)
CB36	3.50		(1)
CB38	3.35		(1)
CB39	3.46		(1)
CB40	3.20		(1)
CB41	3.36		(1)
CB42	3.29	0.17	(2)
CB43	3.40	0.22	(2)
CB44	3.84		(1)
CB45	3.11		(1)
CB46	3.03		(1)
CB47	2.93		(1)
BC1	3.09		(1)
BC4	3.09		(1)
BC6	3.14		(1)
BC7	3.03		(1)
BC8	3.14		(1)
BC9	3.04		(1)
BC10	3.10		(1)
BC11	3.25		(1)
BC19	3.06		(1)
BC21	3.17		(1)
BC23	3.22		(1)
BC24	3.07		(1)
BC29	3.12		(1)
BC31	3.19		(1)
BC32	3.11		(1)
BC33	3.18		(1)
BC34	3.42	0.02	(2)
BC35	3.67		(1)
BC36	3.45	0.01	(2)
BC37	3.32	0.02	(2)
BC38	3.31	0.00	(2)
BC39	3.41	0.02	(2)
BC40	3.34		(1)

TABLE 5.5 contd.

Site	Pn time term	S.E.
BC41	3.39	(1)
BC42	3.29	(1)
BC47	3.51	(1)
BC48	3.32	(1)
B19	3.29	0.25 (3)
B20	3.59	0.07 (3)
B21	3.76	0.11 (4)
B22	3.41	0.05 (2)
B23	3.67	0.32 (2)
B24	3.11	0.07 (2)
B26	2.86	0.11 (6)
B28	2.38	(1)
B29	2.94	0.14 (6)
B30	2.62	(1)
B31	2.35	(1)
B32	3.16	(1)
B34	3.68	(1)
B35	3.81	0.06 (2)
B36	3.44	0.00 (2)
B37	3.02	0.05 (2)
C31	3.37	0.07 (4)
C32	3.62	0.12 (5)
C33	3.27	(1)
LOM BS(A)	2.96	0.01 (7)
UKAEA	3.17	0.01 (67)
IGS1	4.40	0.07 (8)
IGS2	4.16	0.08 (4)
DU1	3.69	0.06 (12)
DU2	3.81	0.13 (2)
UBL	3.81	(1)
DU4	4.31	0.15 (5)
F2	3.78	0.07 (6)

	South	Central	North
Line CB	3.78	3.45	2.97
Line BC	3.40	3.29	3.12
Combined CB & BC	3.74	3.36	3.09

The northern area was defined as including all shots north of latitude 60° 50'N, the central area all shots between this limit and latitude 60° 25'N, and the southern area all shots to the south of latitude 60° 25'N. The average time terms of the two lines show reasonably close agreement except in the southern area. The discrepancy in this area may be explained by there being only two shots on line BC compared to sixteen on line CB. The average time terms found using the combined data of the two lines increase from north to south along the channel. This is shown in Figure 5.17.

The range in time terms found and the mean values for the shots on lines B and C over both the channel floor and slopes were:

	Channel Floor			Channel Slopes	
	Range	Mean		Range	Mean
B part 1 (19-30)	2.34-3.65	3.15	B pt 1 (17,18)	2.86-2.95	2.90
B part 2 (31-37)	2.35-3.78	3.22	B pt 2 (38-45)	2.38-2.98	2.70
B combined	2.34-3.78	3.18		2.38-2.98	2.74
C part 1 (C25-C29)	-			2.33-3.01	2.56
C part 2 (C36-C41)	-			2.25-2.75	2.48
C combined	2.93-3.58	3.33		2.25-3.01	2.52

All the shots on line B part 1 lie in the northern region, on B part 2 in the central region, and on line C in the southern region. The time term values found for these shots over the channel also appear to have larger values in the south (3.33s) than in the north (3.15s), if the significance of the results is not masked by the scatter on the observations. These time term values have been combined with those of lines CB and BC

Figure 5.17 : The Pn time term profile along the Faeroe/ Shetland Channel.

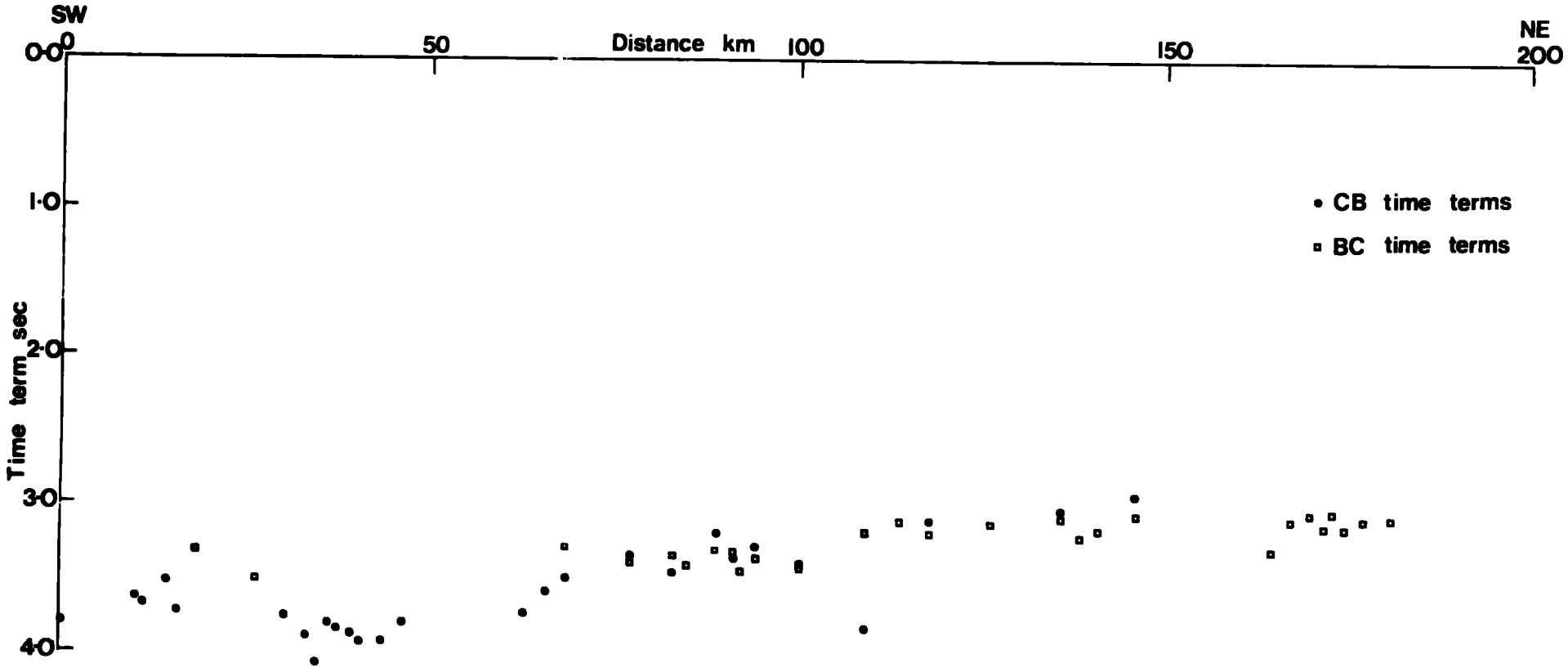
SW
0
50
Distance km
100
150
NE
200
0·0
1·0
2·0
3·0
4·0
Time term sec
• CB time terms
▫ BC time terms

to produce overall mean time term values for the northern, central and southern regions of the Faeroe/Shetland Channel of 3.11, 3.33 and 3.68 seconds respectively.

The mean time terms found for the channel slopes are not as significant as mean values for the channel as the large variations in sea floor topography beneath each shot must be allowed for in interpreting each individual time term.

5. 2.6.1 Interpretation of the time terms

The Pn time terms appear to be known quite accurately for the Faeroe/Shetland Channel but their conversion into Moho depths is dependent on less accurately known upper crustal information. In an attempt to overcome this limitation crustal thickness estimates have been determined for a variety of upper crustal structures.

The mean upper crustal structure determined from all the first arrival travel time data for the channel was 1.24 km of sediments (mean velocity 2.5 km s^{-1}) overlying layer A of mean velocity 4.65 km s^{-1}, and layer B (mean velocity 6.16 km s^{-1}) at a depth of 6.9 km. This structure was used in the evaluation of the mean Moho time terms for the three regions of the channel together with the Pn time term velocity estimate of 8.27 km s^{-1}, and crustal thickness of 15.1, 17.6 and 21.1 km below sea level were found for the north, central and southern regions respectively.

Two different upper crustal structures were determined beneath the north-east region of the line and each of these were used to determine Moho depths beneath the central and northern regions of the channel. The results of line BC at station LOM FS(C) were interpreted in terms of 3.3 km of sediments (2.5 km s^{-1}) above layer A (4.96 km s^{-1}) with layer B

at a depth of 9.7 km. The Pn time terms for the central and northern regions were interpreted to indicate Moho depths beneath this crustal structure of 12.6 km and 10.7 km respectively. Similarly the structure of 3.3 km of sediments (2.5 km s^{-1}) above layer A (4.96 km s^{-1}) with layer B (6.21 km s^{-1}) at a depth of 6.6 km which was determined for line CB results at stations LOM FS(B) and LOM BS(A), was used in the interpretation of the two mean Pn time terms and crustal thickness of 14.4 km and 12.3 km respectively found.

The mean Pn time term of the southern region was also interpreted assuming the crustal structure established in this region by station MIR(B). A lower crustal thickness of 16.4 km was found beneath the 2.1 km of layer A (4.4 km s^{-1}) underlying the 1.2 km of sediments (2.5 km s^{-1}). This resulted in a total crustal thickness beneath the southern region of 19.7 km.

The Pn velocities and intercept times observed at station UKAEA for shots on lines CB and BC were 7.76 km s^{-1} and 4.4 seconds, and 7.90 km s^{-1} and 4.69 seconds respectively. The intercept times were converted into mean shot time terms by subtracting the Pn time term of station UKAEA (2.43 seconds) established by the Scottish Continental Shelf results. These two mean Pn shot time terms were then interpreted in terms of crustal thickness, assuming the average upper crustal structure determined for the channel, but no sea water layer, and the observed Pn velocities to be the true Moho velocity. Moho depths of 11.8 km and 14.4 km respectively were found. The Pn intercept time and velocity observed for the combined plot of all lines B and C data over the channel received at the land stations were interpreted in a similar manner. A mean land receiving station time term of 2.5 seconds was assumed, and the

Moho depth determined to be 24.8 km.

The final crustal cross-sections beneath the Faeroe/ Shetland Channel are presented in Figures 5.18 and 5.19

Each individual time term for the shots fired over the channel slopes was interpreted in terms of crustal thicknesses. The mean sediment and layer A thicknesses and velocities (0.74 km and 5.56 km, and 2.5 km s^{-1} and 4.51 km s^{-1}) determined from shots on lines B and C over the channel and channel slopes, together with the mean layer B velocity (6.31 km s^{-1}) and the time term value of the Pn velocity (8.27 km s^{-1}) were used in the interpretation. The Moho depths found vary from a minimum of 10.3 km to a maximum of 17.2 km, with the largest values found for the central area and the smallest for the southern area. This contrasts with the results found for the channel where the Moho was determined to be deeper beneath the southern area. The mean depth beneath the channel slopes determined from the time terms was 13.7 km, compared to mean depths beneath the channel floor of 11.6 km, 13.3 km, 17.9 km or 19.7 km depending on the upper crustal structure assumed.

The Pn intercept times and velocities observed on the plots of the lines B and C travel times for each of the channel slopes were also interpreted in terms of crustal thickness, assuming the same upper crustal structure as was used in the interpretation of the time terms. Crustal thickness estimates of 21.0 km beneath the Scottish slope and 18.8 km beneath the Faeroes slope were obtained.

5.2.7 Summary and Discussion

The following three refractors were identified beneath the Faeroe/Shetland Channel:

Figure 5.18 : The mean crustal structures determined along the Faeroe/Shetland Channel.

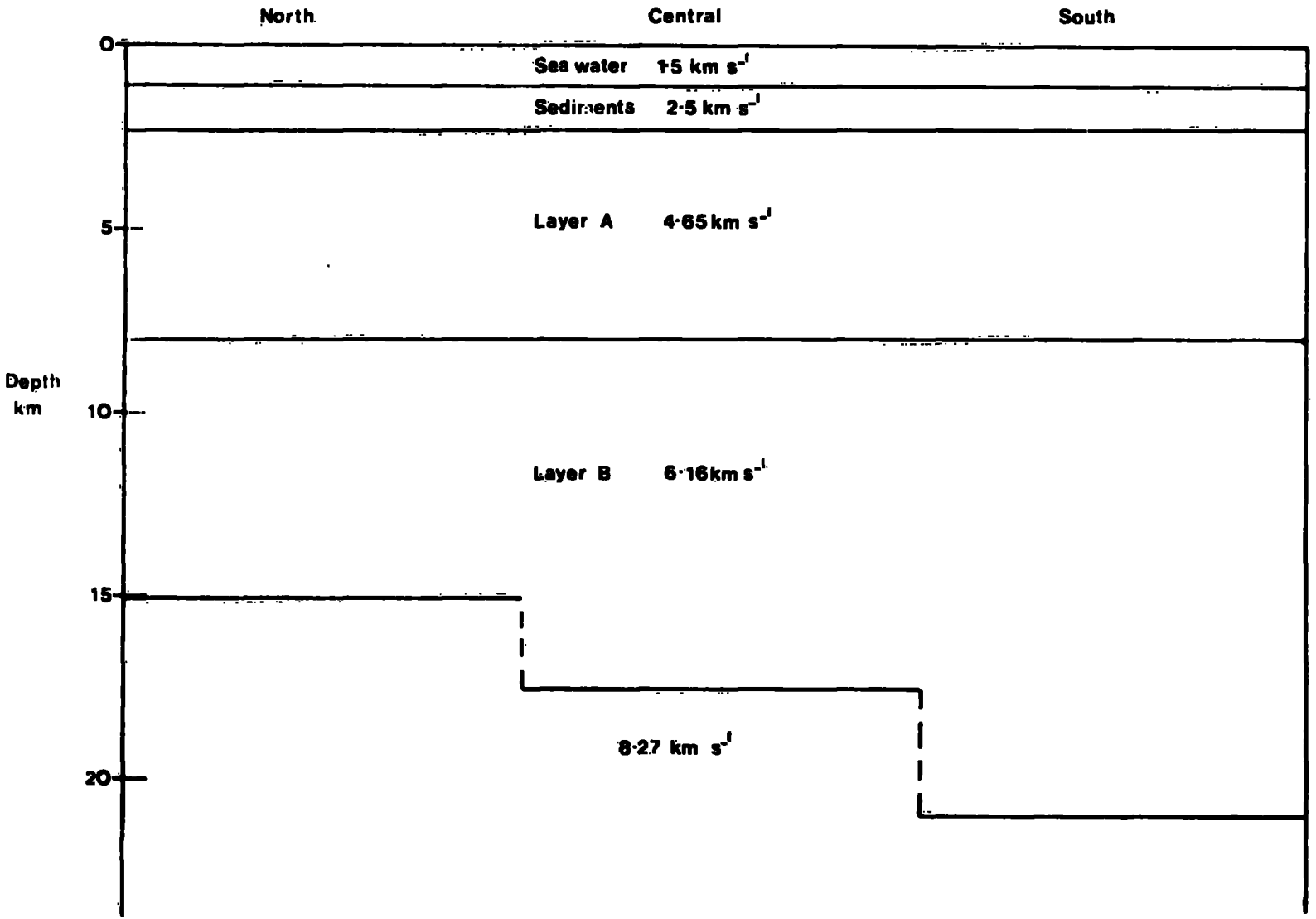
North
Central
South
0
Sea water 1·5 km s⁻¹
Sediments 2·5 km s⁻¹
5
Layer A 4·65 km s⁻¹
Depth km
10
Layer B 6·16 km s⁻¹
15
8·27 km s⁻¹
20

Figure 5.19 : The mean crustal structures determined beneath the Faeroe/Shetland Channel.

A : beneath the northern and central regions assuming the upper crustal structure deduced from the results of line BC

B : beneath the northern and central regions assuming the upper crustal structure deduced from the results of line CB

C : beneath the southern region assuming the upper crustal structure deduced from the results of station MIR(B)

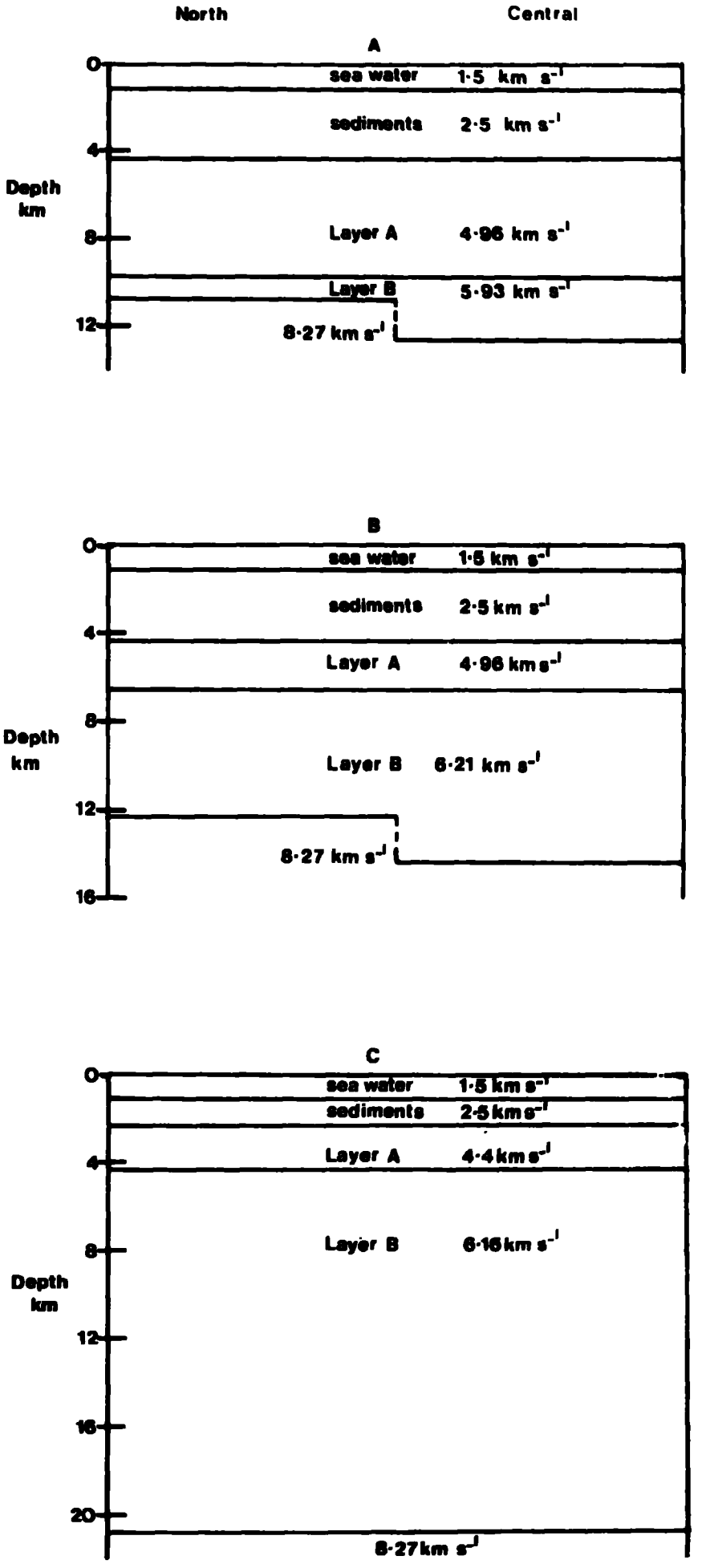
North
Central
A
0
sea water 1·5 km s⁻¹
sediments 2·5 km s⁻¹
4
Depth km
8
Layer A 4·96 km s⁻¹
Layer B 5·93 km s⁻¹
12
8·27 km s⁻¹
B
0
sea water 1·5 km s⁻¹
sediments 2·5 km s⁻¹
4
Layer A 4·96 km s⁻¹
8
Depth km
Layer B 6·21 km s⁻¹
12
8·27 km s⁻¹
16
C
0
sea water 1·5 km s⁻¹
sediments 2·5 km s⁻¹
Layer A 4·4 km s⁻¹
4
8
Layer B 6·16 km s⁻¹
Depth km
12
16
20
8·27 km s⁻¹

1. Layer A interpreted as the sub-sediment basement. This layer has a mean velocity of 4.65 km s^{-1} and is at a mean depth of 1.24 km below the sea floor.

2. Layer B interpreted as the main crustal layer. The mean velocity of this refractor was 6.16 km s^{-1} and it was found to be at a mean depth of 6.9 km.

3. Pn interpreted as the Moho. The mean Pn velocity determined from the travel time graphs was 7.97 km s^{-1}, and the time term analysis value 8.27 km s^{-1}. The mean crustal thickness estimated from the travel time graphs was 14.1 km, and from the time term solutions 15.6 km.

The layer B and Moho refractors were also identified beneath the channel slopes. A mean layer B velocity of 6.31 km s^{-1} and refractor depth of 6.3 km were determined from the travel-time graphs. The mean Moho depth determined from the time terms was 13.7 km.

The layer A basement refractor is correlated with the 4.91 km s^{-1} basement of Ewing and Ewing (1959) in the south of the Faeroe/Shetland Channel, and the 4.72 km s^{-1} basement of Scrutton (1972) in the Rockall Trough. These basement refractors were interpreted to be at depths of 1.81 km and 5.0 km respectively beneath the sea floor. Both the previous two authors agreed that such a basement velocity could represent either consolidated sedimentary rocks or basaltic material of oceanic layer 2. The same reasoning applies to the NASP layer A results from the channel, and so this basement refractor provides no information on the type of crust beneath the area.

The layer B observations are equally ambiguous. The refractor was found to have a mean velocity of 6.16 km s^{-1},

but the scatter on the observations permit the true velocity to have any value between 5.7 km s^{-1} to 6.6 km s^{-1}. A velocity of 5.7-6.2 km s^{-1} could be interpreted in terms of continental metamorphic rocks, but a velocity of 6.6 km s^{-1} could be equally well interpreted as representing either oceanic layer 3 or a lower continental crust refractor such as was identified beneath the Scottish Continental Shelf.

The Moho depth determinations are the most illuminating results as regards the nature of the crust beneath the region. Although the time term interpretations are dependent on the upper crustal velocity distribution, none of the various assumptions of this distribution resulted in a crustal thickness of greater than 21 km, and the most probable thickness estimates lie between 11-18 km. These results are therefore interpreted to rule out the likelihood of subsided continental material beneath the Faeroe/Shetland Channel, as was postulated by Talwani and Eldholm (1972). A continental crustal thickness of 25-26 km has been established beneath the adjacent North Scottish Shelf (sections 4.4,4.5)and a thickness of about 30 km beneath the Faeroe Plateau (Bott et al, 1974).

Subsided continental material between these two areas would be expected to give a crustal thickness estimate of at least 25-30 km.

The crustal thickness estimates are too large to be interpreted as normal oceanic crust, such as was observed in the Norwegian Sea (Ewing and Ewing, 1959). The crustal thicknesses most closely correlate with those found beneath Iceland (Palmason, 1970) and the Iceland-Faeroe Ridge (Bott et al, 1971), where thickness estimates of 8-15 km and 16-18 km respectively were determined. Three main crustal layers were

identified beneath these regions and are summarized as:

	P wave velocity	Layer thickness	
Layer 1	3.2-4.6 km s^{-1}	variable up to 3 km	Tertiary igneous material
Layer 2	5.1-5.8 km s^{-1}	variable up to 6-7 km	Tertiary igneous material
Layer 3	6.5-6.8 km s^{-1}	about 10 km	Oceanic layer 3

The mean layer A velocity of 4.65 km s^{-1} observed beneath the Faeroe/Shetland Channel can be correlated with the higher velocities of layer 1, and interpreted as basaltic material of oceanic layer 2. The mean layer B velocity of 6.16 km s^{-1} cannot be correlated with either layers 2 or 3. However, a wide scatter of layer B velocities was observed (5.68-6.6 km s^{-1}), and it is possible that these velocities arise from a variable composite layer 2/layer 3 structure beneath the channel. The layer B refractor is therefore interpreted in terms of a composite basalt/gabbro layer (oceanic layer 2-layer 3). Normal ln velocities were observed beneath the channel and slopes, similar to beneath the Iceland/Faeroe Ridge (7.84 km s^{-1}) and in contrast to the anomalous value of 7.2 km s^{-1} determined beneath Iceland.

The Faeroe/Shetland Channel and Slopes region is tentatively interpreted as underlain by anomalous oceanic crustal material in some ways similar to the crust beneath the Iceland/Faeroe Ridge. The implications of this crustal structure will be discussed in the following chapter.

CHAPTER 6

The Regional Structure of the North Atlantic between Scotland and the Faeroe Isles

6.1. Introduction

The current knowledge of the structural units of the North Atlantic between Scotland and the Faeroe Isles was outlined in Chapter 1. It was stated that NASP was designed to determine the large scale crustal and upper mantle structures in the region and therefore substantiate or discredit the various theories of the evolution of these areas of the NE North Atlantic. The results for each area are summarized in conjunction with the previously available information, and a discussion is presented of both their individual relevance to hypotheses concerning their nature and evolution, and their overall relevance to the splitting of the North Atlantic.

6.2 The North Scottish Continental Shelf

The NASP results for this region confirm the structures determined from previous geophysical results, and also provide deeper crustal structure information not previously available. A generally thin but variable sedimentary cover above Lewisian metamorphic basement was found on the shelf. The results from line B confirmed the Mesozoic sedimentary basin determined south of the Shetland Islands (Bott and Browitt, in preparation ; Browitt, 1971) and also the outcropping metamorphic basement ridge (Bott and Watts, 1971; Watts, 1970) and adjacent deep Mesozoic/Palaeozoic sedimentary basin (Bott and Watts, 1971; Browitt, 1972). A significant change in structure was determined along line C, at approximately the position of shot C13, in agreement with the transition from shallow metamorphic basement to a Mesozoic sedimentary basin as

interpreted by Watts (1970) from gravity observations.

As well as the metamorphic basement refractor (Pg) a lower crustal refractor (P*) was also established, varying in depth from almost zero km to 16 km depth. This refractor was found both beneath the Caledonian foreland and the orogenic belt regions. It was tentatively interpreted as granulite facies Lewisian metamorphic rocks (Section 4.7.). Although such a refractor has not been previously identified Archaen granulites have been postulated to underlie the Lewisian of north-west Scotland and the continental shelf (Watson, 1973). Gravity interpretations across the Ben Stack line (Bott et al, 1972) indicate that pyroxene granulites similar to those of the outcropping Scourie assemblage to the south also occur beneath the laxfordian to the north. Similarly, it has been suggested by McQuillin and Watson (1973) that the high gravity values observed in east south Uist and southern south Harris are not fully explained by the outcropping partially retrogressed granulites and upper amphibolite facies rocks, and are taken to indicate that granulites underlie the amphibolite facies gneisses. A close correlation was found between the depth to the P* refractor and the Bouguer anomalies over the continental shelf (section 4.7.). Although part of this correlation is caused by the overlying variable sediment thickness a downward density increase of about 0.05-0.10g cm^{-3} at the Pg interface is necessary to explain the observed anomalies. This is of the same order as the density variation deduced, from gravity observations, for the laxfordian and Scourian rocks (0.09 g cm^{-3}) adjacent to the Ben Stack line (Bott et al, 1972), and was taken to suggest that the P* refractor was a layer composed of granulite facies Lewisian basement rocks.

Watson (1973) suggested that the original Archaen granulites were regenerated to a slight extent in Scourian times to give rise to the Scourian gneisses, and then to a much larger extent in Laxfordian times to produce the characteristic biotite-gneiss assemblages. Both these reworkings of the granulites were considered to be metasomatic processes (Watson, 1973) with the lower limit of alteration controlled by the depth to which adequate pore fluid remained. The observed outcrop pattern of the remnant Scourian massifs indicates an inhomogeneous style of reworking, perhaps structurally controlled, and suggests that the buried interface between the laxfordian rocks and the granulites (the P* interface) is probably sharp and disharmonic (Watson, 1973). These deduced characteristics are similar to those observed for the P* refractor beneath the shelf.

Holland and Lambert (1972) do not consider the Scourie and Laxford assemblages to be co-genetic but on the basis of chemical differences suggest that the Laxford assemblage is a much later and lower grade set of metasediments. However, their hypothesis of the laxfordian biotite gneisses representing a supracrustal assemblage on top of the pyroxene granulites does not disagree with the interpretation of the P* refractor as the variable depth interface between the overlying lower grade, and lower density, biotite gneisses, and the deeper granulites.

The depth to the Moho was found to be remarkably consistent beneath the foreland crust on the Scottish Shelf, showing a variation of only a few kilometres. This is quite significant as there are large variations in the upper crustal structure. Beneath both the outcropping basement ridge

(gravity high A) and the adjacent deep sedimentary basin (gravity low E) a Moho depth of 26 km was found, and a depth of 25 km beneath the Mesozoic sedimentary basin south of the Shetland Islands. These crustal thicknesses beneath the sedimentary basins indicate that downfaulting along faults extending throughout the total thickness of the crust was not the mechanism of formation of the basins, as a thicker crust would then be found. Similarly the mean crustal thickness estimate beneath the Moray Firth basin (22-24 km) indicates that crustal thinning has occured in this region relative to the mean thickness determined for the Caledonian orogenic belt crust (29.5 km). Collette (1968) demonstrated by gravity and seismic results that the crust thins beneath the North Sea Basin and that the Basin is probably in isostatic equilibrium. Assuming that the crust was also in isostatic equilibrium before sedimentation then a crustal thinning of 5-7 km is necessary and Collette (1968) attributes this thinning to a phase transition from lower crustal basalt or gabbro material to the denser eclogite phase. The transition is brought about by increased temperature due to the surface sediment loading. Although this mechanism of basin formation could give rise to the crustal thicknesses observed beneath the basins on the Scottish Shelf it is improbable. The continental Moho is most likely not a phase transition boundary but rather a compositional boundary between the granulites of the lower crust and the ultrabasic rocks of the upper mantle. Similarly this mechanism cannot explain such small basins as occur on the Scottish Shelf without also having to involve partial fusion and lateral migration of magma.

A more satisfactory basin formation mechanism related to

continental shelf subsidence has been put forward by Bott (1971) to explain the Scottish Shelf basins. The basin formation is thought to result from the juxtaposition of continental and oceanic crust causing a differential vertical pressure between the two regions, which puts the continental crust into a state of horizontal tension. The result of this tension is to produce normal faulting in the brittle layer (0-10 km) of the continental crust and steady state creep in the lower ductile part of the crust. Bott and Dean (1972) showed by finite element analysis that the physical constants of the rocks underlying the oceanic-continental crust transition zone would produce a stress system that would give rise to the necessary tension to cause the subsidence. The subsidence causes a loss of gravitational energy and will continue until the differential vertical pressure is nulled. The local basins established on the shelf would result from the brittle upper crust subsiding in response to the normal faulting and represent spasmodic subsidence superimposed on the overall gentle sinking of the continental shelf. This would result in a thinned crust beneath the basins, as was observed for the Moray Firth, but these local variations could then be levelled out by similar creep processes after the Basin had been formed. The large sedimentary basin on the Scottish shelf beneath the line B shots was interpreted to have been formed in this manner as a sub-sedimentary crustal layer thinning of about 6 km was observed but with the Moho at the same depth of 26 km as beneath the rest of the shelf.

The mean crustal thickness of 25-26 km established for the Caledonian foreland is relatively small for a continental region. A thin crust is also characteristic of the British

Isles south of the main Caledonian belt (Agger and Carpenter, 1965; Blundell and Parks, 1969; Holder and Bott, 1971), but it appears to be thinner beneath the foreland. The crustal thicknesses determined beneath the Faeroe Plateau (Bott et al, 1974) and Rockall Plateau (Scrutton, 1970) are significantly greater. Similarly a thicker crustal estimate (29.5 km) was determined for the Caledonian Fold belt which was interpreted to indicate that there is still a small residual root beneath the Scottish Caledonides.

The thin crust of the foreland region has associated with it a normal level of Bouguer anomaly values compared to other areas of the British Isles and the Rockall-Faeroe Plateau. This indicates that either the crust or underlying upper mantle must have an anomalously low density. A low density crust is improbable as the crustal velocity-depth structure suggests that normal densities prevail. The underlying upper mantle forming the lower part of the lithosphere or below must therefore be the low density region. This foreland region was affected by the Tertiary igneous activity and uplift which most probably involved a high lithospheric temperature causing the low density values. As the thermal time constant of cooling for the lithosphere is about 60 m yr residual high temperatures, and therefore low densities, could still exist beneath the foreland crust.

6.3. The Faeroe Plateau

A continental crust beneath the Faeroe Plateau is strongly indicated by the NASP results. Two distinct basement velocities were observed but both were too high to be interpreted as either sedimentary or oceanic layer 2 velocities.

The velocities were interpreted as representing continental metamorphic rocks and the transition between the two as a change in metamorphic grade. The higher velocity (about 6 km s^{-1}) is typical of the Laxfordian metamorphic basement present on the Scottish Continental Shelf, but no velocity comparable to the lower velocity (5.2-5.6 km s^{-1}) was observed on the shelf. This latter velocity is fairly typical of slates and, although such material is not found adjacent to Lewisian gneisses in north-west Scotland or on the shelf, the basement to the south and east of the island was interpreted as composed of slates. A 6.4 km s^{-1} layer as observed beneath Iceland was not found and there was no evidence for the presence of oceanic layer 3. The mean crustal thickness of 30 km indicates that continental material must lie beneath the Faeroe Plateau.

The continental nature of the Faeroe Plateau in conjunction with the continental crust established beneath Rockall Plateau, and suggested by various authors beneath the intervening banks, suggests that all the Rockall-Faeroe Plateau is most probably a subsided microcontinental fragment. This confirms the opinion of Bott and Watts (1971) that this region must be included in any continental reconstruction of the North Atlantic, and refutes the hypothesis of Talwani and Eldholm (1972) that the area to the west of the western slope of the Faeroe/Shetland Channel, including the Faeroe Plateau, is underlain by oceanic crust.

The origin of this microcontinental fragment is dependent on the nature and origin of the intervening Rockall Trough and Faeroe/Shetland Channel which will be discussed in the next section.

6.4 The Faeroe/Shetland Channel

The most diagnostic result obtained for the Faeroe/Shetland Channel is the crustal thickness estimate of 11-20 km. This range in thickness, compared to those values determined beneath the Scottish Shelf (section 4.4) and beneath the Faeroe Plateau (Bott et al, 1974), rules out the possibility of subsided continental material beneath the channel, and suggests an anomalous oceanic crust similar to that beneath Iceland and the Iceland-Faeroe Ridge. The two crustal velocities observed beneath the channel could be attributed to either continental or oceanic material, but it was also noted (section 5.2.7) that both velocities are similar to those measured beneath Iceland (Palmason, 1970) and the Iceland-Faeroe Ridge (Bott et al, 1971).

As the results indicate anomalous oceanic material beneath the channel and a continental crust beneath the Faeroe Plateau then, assuming the normal ocean floor spreading hypothesis (Dietz, 1961; Vine and Matthews, 1963), it is most probable that the channel represents a rift between the European and Greenland plates in the opening of the North Atlantic. An oceanic crust has also been indicated by gravity, magnetic and seismic reflection evidence beneath Rockall Trough (Scrutton, 1972; Himsworth, 1973). Vine (1966) suggested that this relatively deep water area was formed as a spreading centre as the Bullard et al (1965) reconstruction of the North Atlantic indicated that Rockall Plateau was continental in nature. Similarly Le Pichon et al (1971) and Laughton (1971) both suggested that Rockall Trough opened near the time of the initial split of the North Atlantic, but the latter author regarded Rockall Trough opening as part of a transform fault

rather than as a spreading centre.

6.5 Discussion of the Faeroe Plateau and Faeroe/Shetland Channel region

Since the Rockall-Faeroe Plateau has been established as a microcontinental fragment and oceanic material found to underlie the Faeroe/Shetland Channel and, probably, Rockall Trough, a remaining problem in interpreting these two deep water areas as zones of opening is the absence of normal ocean floor magnetic lineations. However, magnetic quiet zones of about 400 km width are found along both sides of the North Atlantic (Heirtzler and Hayes, 1967) and have been explained in a number of ways (Pitman and Talwani, 1971), including ocean crust formed in the normal manner but during a period of constant polarity of the earth's magnetic field. Magnetic anomaly evidence has been used with the results of the Joides drilling (site 105) (Pitman and Talwani, 1971) to indicate a time of initial split of the North Atlantic of about 180 myr ago. This date agrees with a Triassic quiet period suggested by Burek (1970). Himsworth (1973) suggested that the Wyville-Thomson Rise separating Rockall Trough from the Faeroe/Shetland Channel was formed during the Tertiary igneous period by extrusion of lava through vents in the ocean floor. No definite age could be established for the Wyville-Thomson Rise but if this hypothesis is correct, then it appears probable that Rockall Trough and the Faeroe/Shetland Channel were formed simultaneously as one oceanic area. The continental margins around this oceanic area were also indicated by Himsworth (1973) on the basis of seismic reflection and bathymetry evidence. No reconstruction of the European plate was attempted by closing Rockall Trough and the Faeroe/Shetland Channel but an

approximate direction of opening was indicated. This evidence suggests that the Faeroe/Shetland Channel opened at the same time and together with Rockall Trough, and therefore probably about 180 myr ago at the initiation of splitting of the North Atlantic. The formation of Rockall Trough can be dated from anomaly 32 as at least prior to 80 myr ago.

A further constraint on the time of formation of the Faeroe/Shetland Channel may be provided by the shelf subsidence and basin formation mechanism put forward by Bott (1971) and discussed in section 6.2. According to this hypothesis basin formation begins after the initiation of splitting and so the age of the sedimentary basins on the Scottish Shelf should provide the age of splitting along the Faeroe/Shetland Channel. However, the time of basin subsidence on the shelf can only be deduced from the age of the sediments in the basins, and it is probable that the oldest sediments found, Torridonian sandstone (Browitt, 1972; McQuillin and Binns, 1973), were downfaulted into the basins. Hallam (1972) presumes that sedimentation was discontinuous in the major basins and that the latest phase of subsidence correlates with the initiation of spreading at the Rekjanes Ridge about 60 myr ago. However, Hall and Smythe (1973) note that the Tertiary structure of the basins was probably controlled by previous structural features and cannot be directly related to the initiation of spreading at the Rekjanes Ridge. It was also suggested by these authors that a detailed stratigraphy of the shelf basins must be established by drilling before a correlation can be obtained with the initiation of rifting. However, it appears that Permo Triassic sediments are the oldest basin deposits (McQuillin and Binns, 1973) which would indicate that

subsidence began about 250-200 myr ago.

6.6 Summary of the formation of the NE North Atlantic

The formation of the NE North Atlantic appears to have begun with an initial split of the Rockall-Faeroe Plateau from the European plate along the Rockall Trough and Faeroe/Shetland Channel. This split most probably occurred at the same time as the separation of the North American continent from Africa, about 180 m yrs ago. Following the initiation of spreading subsidence and basin formation probably began on the margin of the European plate to produce the continental shelf and sedimentary basins observed in this region. Similarly, subsidence must have occurred to the west of the split as presumably the Rockall-Faeroe Plateau was then an upstanding microcontinental fragment. The subsidence of the Hatton-Rockall Basin has been documented by data from the Deep Sea Drilling Project (D.S.D.P. Scientific Staff, 1970) and occurred in various stages between 55-10 m yr ago. This subsidence was therefore not related to the initial split along the Rockall Trough and Faeroe/Shetland Channel, but may have been caused by fracturing due to the initial doming probably formed on the initiation of spreading along the Rekjanes Ridge (Bott, 1973; Brooks, 1973). The initiation of spreading along the Rekjanes Ridge has been dated from anomaly 24 to have commenced about 60 m yr ago (Heirtzler et al, 1968) which correlates with the development of the Thulean igneous province (65-50 m yr ago). Bott (1973) has explained this correlation of igneous activity and the initiation of spreading as caused by a single convective overturn of the asthenosphere of relatively short duration. This would produce a hot magma saturated upper asthenosphere

and cause doming of the lithosphere above. Dyke intrusion in the stretched lithosphere then drives the plates apart. Since the termination of the igneous activity about 50 m yr ago, the European plate has continued to move away from the Greenland plate by spreading at the Rekjanes Ridge. Intense igneous activity is still present beneath Iceland.

6.7 Criticism of NASP and suggested further work

The North Atlantic Seismic Project was in general very successful. Continental crustal structures were established beneath both the Scottish Shelf and the Faeroe Plateau, and anomalous oceanic material was indicated beneath the Faeroe/ Shetland Channel. The exact nature of the material beneath the Channel was not determined, and the project may have been improved on in this respect. The great majority of the shots fired along the channel on lines CB and BC consisted of small charges (25-100 lb), and were only observed at short ranges at the receiving ship stations over the channel. A further refraction experiment using larger charges (600 lb), perhaps more widely spaced, is needed to resolve the nature of the main crustal layer beneath the Channel. However, if this layer consists of variable anomalous oceanic material which may be affected by creep of lower continental crust from beneath the Scottish Shelf then it may be very difficult to resolve the exact structure by seismic refraction.

Air gun profile results and wide angle reflections obtained over the Channel and now being processed at Durham should provide control on the sediments and sub-sedimentary layer. This information could then be used in conjunction with the limiting velocity and layer thickness values obtained by NASP to produce a gravity fit model across the channel. As the

Faeroe/Shetland Channel is separated from Rockall Trough by the Wyville Thomson Rise a reversed seismic refraction line fired along this feature could determine if the two deep water areas are in fact separated by only basaltic material extruded over the oceanic crust.

Very good results were obtained from the North Scottish continental shelf. Some of the receiving stations on the Scottish mainland and surrounding islands did not function well for various shot lines, but due to the large number of stations no vital information was lost. There was little reversed coverage of the upper crustal structure over the shelf and this could have been provided by more use of the receiving ships or sonobuoys. The receiving station time terms in this region were very well determined and should prove useful to other crustal refraction experiments around the British Isles.

Both the Rockall Plateau and the Faeroe Plateau have now been established to be continental in nature and preliminary gravity results indicate that this is also true for the intervening banks. Further gravity interpretations, and perhaps some seismic refraction investigations, over the banks and adjacent regions are required to firmly establish that the Rockall-Faeroe Plateau is one continuous submerged continental region.

APPENDIX A

NASP shot data

Line C parts 1 and 2

Shot no.	Size lbs.	Shot Depth m	Water Depth m	Lat.	Long.	Shot Instant (GMT)
1	300	69	69	58° 41'.31	05° 1.85'W	08 43 40.72
2	300	84	84	58° 44'.36	05° 3.23'W	09 14 21.35
3	300	99	99	58° 48'.02	05° 5.69'W	Not yet available
4	300	91	91	58° 47'.70	05° 7.00'*	15 57 16.43
5	300	89	89	58° 52'.23	05° 13.24'	10 39 48.55
6	1200	Misfire	-	58° 54'.26	05° 7.68'	-
7	300	84	84	58° 57'.31	05° 11.36'	12 21 58.98
8	300	84	84	58° 58'.37	05° 11.24'	13 08 19.26
9	300	74	74	59° 1'.36	05° 12.87'	13 35 26.90
10	300	79	79	59° 4'.56	05° 14.39'	13 53 35.16
11	300	100	109	59° 7'.45	05° 16.08'	14 27 30.47
12	1200	123	123	59° 10'.33	05° 17.77'	14 51 52.40
13	300	99	99	59° 11'.72	05° 18.81'	15 12 46.79
14	300	91	91	59° 13'.57	05° 19.29'	15 46 58.13
15	300	99	99	59° 16'.85	05° 20.58'	16 26 58.74
16	300	100	101	59° 19'.27	05° 22.77'	17 07 32.67
17	300	100	102	59° 22'.14	05° 29.31'	17 47 11.70
18	1200	Misfire	-	59° 26'.55	05° 27.16'	-
19	300	99	99	59° 29'.06	05° 29.05'	18 52 10.73
20	300	100	102	59° 32'.52	05° 31.52'	19 22 14.97
21	300	90	103	59° 34'.33	05° 32.50'	19 42 13.35
22	300	100	105	59° 34'.85	05° 36.82'	20 22 20.11
23	300	100	113	59° 37'.50	05° 39.01'	20 42 28.03
24	1200	139	139	59° 42'.50	05° 36.95'	21 16 37.26
25	1200	320	383	59° 45'.68	05° 39.47'	10 05 56.00
26	600	115	452	59° 47'.05	05° 39.31'	10 36 53.96
27	600	170	573	59° 48'.84	05° 41.87'	11 07 54.58
28	600	170	627	59° 50'.62	05° 41.91'	11 38 35.62
29	600	160	843	59° 56'.20	05° 45.94'	12 12 53.03
30	600	180	984	60° 01'.22	05° 50.30'	12 48 36.96
31	600	150	1107	60° 06'.41	05° 56.53'	13 22 50.62
32	600	155	1167	60° 12'.17	05° 58.34'	13 58 03.15
33	600	155	1938	60° 18'.01	06° 00.66'	14 33 57.04

NASP

Line C pt. 3

Shot no.	Size lbs.	Shot Depth	Water Depth	Lat.	Long.	Shot Instant (G.M.T.)
59	600	162	162	62° 38'.6	7° 26'.15	00 12 46.45
58	300	103	103	62° 33'.1	7° 22'. 6	23 36 52.57
57	300	93	93	-	-	Misfire
56	1200	101	101	62° 21'.3	7° 16'.0	19 56 35.45
55	300	88	88	62° 18'.17	7° 19'.7	20 17 47.74
54A	300	72	72	62° 13'.2	7° 19'.25	20 47 30.56
54B	1200	58	58	62° 10'.7	7° 19'.63	21 13 04.50
54C	300	93	93	62° 12'.25	7° 23'.3	21 32 23.06
53	300	-	-	-	-	Misfire
52	300	57	57	61° 49'.50N	6° 31'.2W	09 19 53.82
51	1200	60	60	61° 45'.78N	6° 33'.0W	Not yet availa
50	600	55	55	61° 41'.78N	6° 36'.35W	10 24 00.49
49	600	65	65	61° 34'.05N	6° 39'.42W	11 08 35.06
48	300	55	55	61° 29'.00N	6° 40'.17W	11 42 30.19
47	300	61	61	61° 25'.05N	6° 37'.93W	12 07 24.87
46	300	95	95	61° 20'.34N	6° 34.81W	13 37 08.97
45	600	138	138	61° 15'.50N	6° 31.30W	14 12 31.54
44	600	138	138	61° 10'.59N	6° 29'.12W	14 47 28.79
A	25	85	154	61° 08'.99N	6° 27'.40W	14 56 17.46
B	25	85	142	61° 07'.49N	6° 27.00W	14 06 14.72
C	25	85	138	61° 05'.76N	6° 25'.81	15 16 10.74
D	25	85	137	61° 03'.08	6° 23'.08	15 44 34.68
43	600	130	140	60° 55.79	6° 17'.31	17 07 57.28
E	25	80	140±10	60° 54.79	6° 18'.35	17 17 47.12
F	25	80	150±10	60° 52.79	6° 19'.96	17 31 10.27
G	25	80	160±10	60° 51.31	6° 19'.59	17 41 10.64
42	600	165	171	60° 49.86	6° 18.86	Not available
41	600	155	195	60° 43.69	6° 18.03	18 37 26.81
40	600	-	-	-	-	Misfire
39	600	160	303	60° 38'.15	6° 12'.47	19 24 31.99
38	600	160	346	60° 33'.76	6° 08'.45	19 34 53.07
37	600	160	338	60° 30'.24	6° 07'.82	20 26 35.96
36	600	170	440	60° 23'.90	6° 02'.00	21 12 55.83

Line B

Shot no.	Size lbs.	Shot Position Lat.	Long.	Shot Instant (GMT)	Water Depth m	Shot Depth m
B1	600	62° 4'.02N	6° 31'.94W	11.38 37.44	50	50
B2	300	62° 1'.42N	6° 22'.87W	12.07 55.68	87	87
B3	600	61° 56'.89N	6° 12'.26W	12.43 18.44	86	86
B4	300	61° 54'.67N	6° 5'.59W	13.07 21.04	127	120
B5	600	61° 50'.93N	5° 57'.80W	13.37 26.55	184	140
B6	300	61° 47'.61N	5° 48'.93W	Misfire	Misfire	
B7	300	61° 46'.71N	5° 46'.14W	14.17 27.76	240	120
B8	300	61° 44'.64N	5° 40'.21W	14.37 24.86	209	120
B9	300	61° 41'.68N	5° 30'.28W	15.12 25.96	182	120
B10	600	61° 40'.28N	5° 25'.81W	15.27 25.32	182	140
B11	600	61° 38'.41N	5° 20'.00W	15.47 32.01	253	140
B12	600	61° 36'.60N	5° 14'.34W	16.07 19.15	287	140
B13	600	61° 34'.76N	5° 8'.50W	16.27 52.05	258	140
B14	600	61° 33'.42N	5° 4'.15W	16.42 08.02	210	140
B15	600	61° 30'.99N	4° 56'.69W	17.07 28.80	223	140
B16	600	61° 27'.60N	4° 48'.73W	17.36 56.21	322	140
B17	600	61° 24'.15N	4° 40'.90W	18.07 09.44	651	140
B18	600	61° 21'.44N	4° 36'.35W	18.27 07.36	850	140
B19	600	61° 18'.18N	4° 28'.40W	18.56 56.09	1023	140
B20	600	61° 15'.27N	4° 20'.07W	19.27 06.88	1093	140
B21	600	61° 12'.45N	4° 11'.83W	19.56 55.87	1057	140
B22	50	61° 11'.42N	4° 9'.07W	20.06 31.39	1040	30
B23	50	61° 10'.41N	4° 6'.43W	20.16 13.42	1057	30
B24	50	61° 9'.43N	4° 3'.74W	20.26 20.10	1089	30
B25	600	61° 8'.19N	4° 0'.83W	Misfire	Misfire	
B26	600	61° 6'.74N	3° 57'.28W	20.52 21.74	1135	140
B27	25	61° 5'.15N	3° 53'.48W	21.06 17.01	1126	80
B28	25	61° 4'.13N	3° 50'.88W	21.16 22.47	1145	80
B29	600	61° 3'.04N	3° 48'.35W	21.27 17.14	1125	140
B30	25	61° 2'.05N	3° 45'.93W	21.36 22.16	1100	80
B31	25	60° 40'.29N	4° 36'.35W	07.41 33.97	108	80
B32	25	60° 38'.43N	4° 36'.56W	08.01 31.80	1077	80
B33	25	60° 37'.39N	4° 33'.73W	Misfire	Misfire	
B34	25	60° 36'.89N	4° 32'.20W	08.16 29.21	1061	80
B35	25	60° 35'.90N	4° 29'.23W	08.26 10.78	1050	80

Line B (contd.)

Shot no.	Size lbs.	Shot Position Lat.	Long.	Shot Instant (GMT)	Water Depth m	Shot Depth m
B36	25	60° 34'.90N	4° 26'.13W	08.36 10.89	1038	80
B37	50	60° 33'.96N	4° 23'.03W	08.46 44.15	1033	30
B38	600	60° 32'.97N	4° 20'.06W	08.57 22.72	981	140
B39	50	60° 31'.96N	4° 17'.07W	09.06 38.52	853	30
B40	100	60° 30'.99N	4° 14'.00W	09.17 16.93	765	85
B41	600	60° 30'.12N	4° 11'.11W	09.27 32.13	677	140
B42	600	60° 27'.59N	4° 1'.86W	09.57 17.60	492	140
B43	600	60° 25'.19N	3° 52'.49W	10.27 21.79	416	140
B44	600	60° 22'.58N	3° 43'.42W	10.57 27.20	309	140
B45	600	60° 21'.27N	3° 38'.87W	11.12 25.49	227	140
B46	300	60° 19'.65N	3° 37'.57W	Misfire	Misfire	120
B47	300	60° 19'.12	3° 36'.28W	12.57 18.08	144	120
B48	300	60° 17'.48N	3° 32'.46W	13.12 25.44	126	120
B49	300	60° 15'.79N	3° 28'.86W	13.27 30.33	120	120
B50	300	60° 14'.68N	3° 26'.54W	13.37 35.73	117	117
B51	300	60° 13'.61N	3° 24'.24W	13.47 36.17	125	120
B52	300	60° 12' 63N	3° 21'.79W	13.57 10.46	126	120
B53	300	60° 11'.76N	3° 19'.04W	14.07 36.32	122	120
B54	300	60° 10'.86N	3° 16'.29W	14.17 28.54	130	120
B55	300	60° 9'.90N	3° 13'.50W	14.27 37.79	138	120
B56	300	60° 8'.43N	3° 9'.73W	14.37 16.34	156	120
B57	300	60° 6'.92N	3° 5'.34W	14.57 16.11	163	120
B58	300	60° 5'.10N	3° 0'.14W	Misfire	Misfire	
B59	200	60° 4'.23N	2° 57'.55W	15.27 28.19	103	104
B60	300	60° 2'.86N	2° 52'.05W	08.37 39.50	85	85
B61	300	60° 1'.51N	2° 44'.13W	09.07 06.31	84	84
B62	300	59° 58'.33N	2° 36'.59W	09.36 42.94	83	83
B63	300	59° 54'.93N	2° 29'.35W	10.06 57.61	91	91
B64				Misfire	Misfire	
B65	300	59° 50'.53N	2° 19'.04W	10.46 49.22	89	89
B66	300	59° 50'.60N	2° 12'.12W	11.06 43.96	92	92
B67	300	59° 51'.62N	2° 2'.11W	11.36 43.07	97	97
B68	300	59° 52'.22N	1° 47'.21W	12.16 51.21	103	103
B69	300	59° 52'.00N	1° 40'.55W	12.36 47.34	105	105
B70	600	59° 51'.25N	1° 30'.05W	13.07 19.35	97	97

Line D

Shot no.	Size lbs.	Shot Position Lat.	Long.	Shot Instant (GMT)	Shot Depth m	Water Depth m
D1	600	-	-	Misfire	-	-
D2	300	60° 10'.57N	1° 43'.61W	15.47 09.70	80	80
D3	300	60° 7' .33N	1° 50'.93W	16.17 02.61	60	60
D4	300	60° 3'.98N	1° 58'.66W	16.47 09.37	88	88
D5	300	60° 0'.82N	2° 06'.44W	17.16 46.18	84	84
D6	300	59° 56'.56N	2° 16'.56W	17.56 50.53	100	100
D7	300	59° 52'.13N	2° 26'.73W	18.37 14.09	86	86
D8	300	59° 48'.26N	2° 36'.46W	19.16 57.62	82	82
D9	300	59° 42'.78N	2° 47'.97W	20.06 52.23	80	80
D10	300	59° 39'.13N	2° 53'.72W	20.37 05.46	84	84
D11	300	59° 34'.45N	3° 0'.73W	21.16 46.89	74	74
D12	300	59° 29'.88N	3° 7'.07W	21.57 10.58	72	72
D13	300	59° 27'.45N	3° 18'.31W	07.07 30.03	72	72
D14	300	59° 23'.28N	3° 27'.82W	07.47 16.33	90	189
D15	300	59° 19'.02N	3° 37'.00W	08.27 03.06	90	160
D16	300	59° 14'.92N	3° 46'.05W	09.07 11.33	80	123
D17	300	59° 10'.90N	3° 54'.75W	09.46 51.35	90	113
D18	300	59° 6'.73N	4° 3'.34W	10.26 57.63	84	84
D19	300	59° 1'.14N	4° 13'.60W	12.27 04.37	50	50
D20	300	58° 56'.67N	4° 21'.17W	13.06 58.19	64	64
D21	300	58° 52'.69N	4° 30'.08W	13.47 07.42	72	72
D22	300	58° 48'.89N	4° 39'.90W	14.27 29.40	76	76
D23	300	58° 45'.32N	4° 50'.76W	15.07 01.02	84	84
D24	300	58° 37'.95N	5° 3'.35W	17.12 07.64	48	48

NASP

Shot Details for Line E

Shot no.	Size lbs	Shot Depth m	Water Depth m	Lat.	Long.	Shot Instant G.M.T.
1	300	43	43	57° 43.6'	02°03.5'	14 53 46.20
2	300	46	46	57° 46.2'	02°08.4'	15 22 25.74
3	600	97	97	57° 49.1'	02°14.5'	15 48 07.59
4	300	70	70	57° 54.1'	02°17.6'	16 22 13.94
5	300	78	78	57° 58.0'	02°20.0'	16 47 16.89
6	600	67	67	58° 02.8'	02°23.4'	17 17 40.78
7	300	58	58	58° 07.0'	02°29.0'	17 47 22.44
8	300	52	52	58° 11.0'	02°35.5'	18 17 23.62
9	600	44	44	58° 15.15'	02°42.0'	18 47 51.24
10	300					Misfire
11	300					"
12	300					"
13	300	58	58	58° 20.8'	02°50.0'	20 37 48.14
14	300	58	58	58° 21.3'	02°50.2'	20 56 44.24
15	300	69	69	58° 24.5'	02°54.4'	21 22 51.87
16	300	66	66	58° 27.5'	02°56.7'	21 42 02.57
17	300	74	74	58° 33.0	02°59.7'	22 21 52.78

NASP

Full shot details for line CB part 1 shot on

July 15th, 1972

Shot no.	Shot lbs.	Shot Depth	Water Depth	Lat.	Long.	Shot GMT	Instant
1	50	50	1053	60° 01'.05	06° 05'.3	13 32	26.56
2	50	50	1059	60° 01'.60	06° 04'.5	13 36	27.90
3	50	55	1065	60° 02'.17	06° 03'.1	13 41	33.70
4	25	80	1072	60° 02'.79	06° 01'.8	13 46	09.75
5	25	85	1081	60° 03'.47	06° 01'.0	13 51	34.65
6	25	85	1083	60° 03'.99	05° 59'.2	13 56	13.61
7	25	Misfire	1077				
8	25	80	1081	60° 05'.25	05° 56'.62	14 06	16.31
9	25	90	1077	60° 05'.80	05° 55'.5	14 11	22.14
10	25	85	1081	60° 06'.35	05° 54'.3	14 16	17.67
11	25	90	1089	60° 06'.93	05° 52'.95	14 21	24.71
12	25	85	1087	60° 07'.43	05° 51'.55	14 26	18.68
13	25	85	1079	60° 07'.74	05° 50'.01	14 31	15.27
14	25	90	1097	60° 08'.60	05° 48'.60	14 37	57.39
15	25	85	1101	60° 09'.16	05° 47'.91	14 41	19.60
16	25	90	1111	60° 09'.63	05° 46'.58	14 46	38.43
17	25	95	1121	60° 10'.33	05° 45'.46	14 51	24.71
18	25	85	1135	60° 11'.00	05° 44'.33	14 56	15.94
19	25	90	1133	60° 11'.60	05° 43'.18	15 01	35 93
20	25	95	1129	60° 12'.26	05° 42'.07	15 06	24.89
21	25	90	1142	60° 12'.85	05° 40'.89	15 11	22.52
22	50	50	1138	60° 13'.47	05° 39'.78	15 16	31.42
23	50	50	1132	60° 14'.06	05° 38'.55	15 21	30.66
24	50	50	1134	60° 14'.66	05° 37'.35	15 26	34.65
25	100	95	1126	60° 15'.22	05° 36'.04	15 31	53.09
26	100	90	1116	60° 15'.82	05° 34'.76	15 36	47.97
27	100	85	1116	60° 16'.41	05° 33'.49	15 41	42.23
28	100	75	1110	60° 17'.01	05° 32'.20	15 46	32.30
29	200	100	1101	60° 17'.73	05° 31'.56	15 51	58.15
30	200	115	1084	60° 18'.79	05° 28'.46	16 02	30.50
31	50	55	1102	60° 19'.93	05° 26'.20	16 11	36.14
32	200		1079	60° 21'.50	05° 21'.31)	Timing system failure	
33	200		1181	60° 22'.64	05° 18'.84)		
34	200	115	1030	60° 23'.60	05° 16'.40	17 17	12.10
35	200	115	1109	60° 24'.67	05° 13'.92	17 27	16.96
36	200	120	1117	60° 25'.72	05° 11'.41	17 37	20.29
37	300	115	969	60° 26'.87	05° 08'.99	17 47	11.54
38	300	115	988	60° 29'.16	05° 03'.82	18 07	27.81
39	300	95	1003	60° 31'.04	04° 58'.13	18 25	51.01
40	300	90	1041	60° 34'.01	04° 54'.25	18 46	48.52
41	300	105	1052	60° 36'.46	04° 49'.50	19 07	09.24
42	300	104	1077	60° 39'.25	04° 44.85	19 27	25.28
43	300	104	1189	60° 41'.29	04° 38.95	19 47	16.64
44	600	100	1204	60° 45'.36	04° 32'.21	20 16	44.30
45	600	120	1069	60° 48'.60	04° 24'.10	20 47	56.14
46	600	125	1093	60° 51'.93	04° 16'.37	21 17	03.18
47	600	125	1107	60° 55'.24	04° 08'.34	21 47	25.10
48	600	100	1112	61° 01'.52	03° 55'.92	22 37	00.00

NASP

Line CB part 2, July 16th, 1972

Shot no.	Shot lbs.	Shot Depth	Water Depth	Lat.	Long.	Shot	Instant GMT
1	50	65	1157	61° 08'.08	03° 42'.31	10 11	55.40
2	50	65	1160	61° 07'.70	03° 43'.20	10 16	53.14
3	50	65	1164	61° 07'.26	03° 44'.24	10 21	54.24
4	25	115	1164	61° 06'.93	03° 45'.05	10 26	46.85
5	25	120	1164	61° 06'.53	03° 45'.91	10 31	45.27
6	25	110	1162	61° 06'.12	03° 46'.88	10 36	40.52
7	25	110	1159	61° 05'.76	03° 47'.68	10 41	37.11
8	25	120	1156	61° 05'.48	03° 48'.55	10 46	46.64
9	25	110	1152	61° 04'.77	03° 50'.39	10 56	39.50
10	25	110	1145	61° 04'.04	03° 52'.22	11 06	50.97
11	25	110	1140	61° 03'.37	03° 53'.94	11 16	39.83
12	25	95	1134	61° 02'.65	03° 55'.71	11 26	31.35
13	25	110	1134	61° 02'.36	03° 59'.49)		
14	25	100	1130	61° 01'.66	04° 00'.88)		
15	50	70	1127	61° 01'.05	04° 02'.33)	Timing system failure	
16	50	85	1128	61° 00'.48	04° 03'.84)		
17	50	70	1126	60° 58'.64	04° 08'.12)		
18	50	75	1122	60° 57'.36	04° 09'.71)		
19	50	70	1116	60° 55'.03	04° 10'.87	15 04	12.75
20	50	65	1115	60° 55'.28	04° 10'.34	15 12	02.32
21	50	60	1116	60° 54'.59	04° 11'.92	15 22	05.89
22	50	60	1112	60° 53'.85	04° 13'.67	15 31	52.05
23	50	65	1114	60° 53'.33	04° 14'.74	15 39	03.02
24	50	60	1114	60° 52'.64	04° 16'.04	15 46	57.73
25	50	70	1113	60° 52'.30	04° 16'.91	15 53	21.07
26	50	65	1112	60° 51'.50	04° 18'.53	16 02	26.30
27	100	110	1113	60° 51'.09	04° 19'.45	16 07	24.75
28	100	105	1112	60° 50'.28	04° 21'.01	16 17	04.44
29	100	110	1110	60° 49'.46	04° 22'.63	16 27	20.18
30	300	105	1108	60° 48'.45	04° 24'.59	Timing failure	
31	200	100	1106	60° 47'.29	04° 26'.62	16 52	08.33
32	200	110	1105	60° 45'.97	04° 29'.09	17 07	08.91
33	200	95	1103	60° 45'.20	04° 30'.86	17 16	47.11
34	200	85	1087	60° 40'.08	04° 41'.82	18 26	40.39
35	200	105	1081	60° 39'.10	04° 43'.74	18 37	00.60
36	200	100	1071	60° 38'.11	04° 45'.70	18 46	56.67
37	300	120	1063	60° 37'.14	04° 47'.62	18 57	11.66
38	300	95	1042	60° 35'.20	04° 51'.54	19 16	51.02
39	300	105	1034	60° 33'.20	04° 55'.42	19 37	09.77
40	300	100	998	60° 31'.25	04° 59'.49	19 57	13.33
41	300	115	968	60° 29'.37	05° 03'.83	20 17	23.63
42	300	110	969	60° 27'.51	05° 08'.19	20 37	18.10
43	300	85	1156	60° 22'.59	05° 17'.26	21 47	01.72
44	300	120	979	60° 20'.58	05° 21'.35	22 08	22.64
45	600	175	1112	60° 16'.03	05° 32'.23	23 12	53.52
46	600	175	1134	60° 13'.80	05° 38'.54	23 42	58.14
47	600	170	1148	60° 11'.50	05° 44'.62	00 12	58.79
48	600	170	1123	60° 09'.33	05° 50'.59	00 42	42.39
49	600	165	1110	60° 07'.16	05° 55'.13	Timing failure	

APPENDIX B

The first arrival travel time data for all the NASP shot points and receiving stations considered in this Thesis.

Station IGS1 — Uncorrected for Shot and Water depths

Shot	Range (km)	Observed travel time(s)
D2	253.69	36.67
D3	244.63	35.87
D4	235.13	34.38
D5	225.84	33.28
D6	213.55	31.77
D7	201.00	30.02
D8	189.44	28.58
D9	174.61	26.88
D10	166.05	26.02
D11	155.32	24.34
D12	145.21	23.21
D13	134.31	21.57
D14	122.45	20.14
D15	110.69	18.72
D16	99.21	16.83
D17	88.07	14.88
D18	76.80	13.01
D19	62.53	10.80
D20	51.55	9.07
D21	40.26	7.13
D22	28.62	5.19
D23	17.01	3.12
D24	3.59	0.75
C1	7.45	1.52
C2	13.27	2.30
C4	20.27	3.80
C5	30.37	5.04
C7	38.54	6.68
C8	40.40	7.06
C9	46.15	7.87
C10	52.28	9.07
C13	66.21	11.35
C14	69.63	11.97
C15	75.84	13.14
C16	80.73	13.82
C17	87.68	14.79
C20	106.65	17.69
C21	110.14	18.31
C22	112.30	18.89
C23	117.63	19.81
C24	125.88	21.11
C25	132.22	21.91
C26	134.60	22.36
C27	138.48	22.37
C28	141.65	22.86
C29	152.66	23.85
C31	173.73	27.08

C32	184.40	28.98
C36	206.19	31.24
C41	245.65	36.10
B26	283.27	41.55
B29	278.44	40.80
B38	217.73	33.29
B39	216.39	31.84
B40	215.19	32.39
B41	214.16	32.31
B42	211.66	32.20
B43	209.87	31.96
B44	208.07	31.41
B45	207.34	31.13
B47	204.58	31.15
B48	203.22	30.66
B49	201.81	30.34
B50	200.90	30.39
B51	200.11	30.52
B52	199.55	30.45
B53	199.36	30.42
B54	199.18	30.40
B59	198.45	29.52
B60	199.53	29.75
B61	202.27	29.92
B62	202.55	30.66
B63	268.78	30.56
B65	204.50	30.89
B66	209.53	31.44
B67	218.02	32.72
B68	229.75	34.32
B69	234.60	34.92
B70	241.97	35.79
E6	165.64	25.87
E7	157.52	25.31
E8	148.89	23.90
E9	140.34	22.71
E14	129.45	21.53
E15	124.11	20.41
E16	120.86	19.62
E17	116.67	19.26
CB42	221.85	34.29
CB43	226.60	34.93
CB44	230.79	36.09
CB45	239.53	36.42

Station IGS2

D2	319.64	44.77
D4	301.20	42.23
D5	291.92	41.03
D6	279.67	39.62
D7	267.20	39.31
D8	255.63	36.77
D9	240.99	35.02
D10	232.74	34.10
D11	222.47	32.60
D12	212.89	31.99
D13	201.49	30.16

D14	189.75	28.53
D15	178.19	26.97
D16	166.89	26.22
D17	155.97	24.12
D18	145.01	23.19
D19	131.43	21.54
D20	121.21	20.06
D21	110.32	18.28
D22	98.82	16.29
D23	86.61	14.43
D24	70.64	11.52
C1	73.94	12.25
C2	74.85	12.42
C4	74.46	12.48
C5	74.20	12.39
C7	81.69	13.49
C8	83.12	13.74
C9	85.95	14.10
C10	89.45	14.75
C11	92.66	15.42
C13	97.67	16.42
C14	100.33	16.99
C15	104.98	18.15
C16	107.97	18.33
C17	110.18	18.40
C20	127.47	20.87
C21	130.38	21.51
C22	130.13	21.76
C23	134.36	22.57
C24	143.83	23.55
C25	149.02	24.55
C26	151.53	24.52
C27	154.28	25.06
C31	184.68	28.01
B26	283.27	41.55
B29	278.44	40.80
B39	256.07	36.99
B43	256.12	37.09
B44	256.67	36.90
B57	256.96	37.07
B60	260.85	37.69
B61	264.79	37.85
B62	266.56	38.06
B63	268.19	38.95
E6	229.45	33.98
E7	222.42	32.95
E8	214.79	32.37
E14	198.13	30.57
E15	193.64	29.63
E16	191.20	29.72

Station IGS3

D4	448.08	61.25
D5	439.15	60.14
D6	427.33	58.50
D7	415.25	57.84
D8	404.29	56.57
D9	389.95	54.84

D10	381.35	54.03
D11	370.50	52.08
D12	360.15	51.52
D14	339.75	48.13
D15	328.65	47.27
D16	317.92	46.20
D17	307.53	44.60
D18	296.98	43.37
D20	272.90	40.40
D21	262.76	39.32
D22	252.71	37.73
D23	242.91	36.26
D24	226.13	33.95
C1	232.52	35.15
C2	237.57	37.65
C4	242.56	35.49
C5	249.28	36.31
C7	258.87	37.65
C8	260.82	37.94
C9	265.89	42.74
C10	271.41	39.47
C11	276.35	40.08
C13	283.65	40.21
C14	286.95	41.54
C15	292.76	42.47
C16	296.86	42.10
C17	301.24	43.24
C21	323.31	45.86
C22	323.85	46.49
C23	328.56	47.16
C24	337.98	48.26
C25	343.65	48.74
C26	346.19	48.98
E1	272.29	39.62
E2	269.83	39.17
E3	266.71	38.97
E5	269.79	39.37
E6	271.56	39.56
E7	271.25	39.63
E8	270.36	39.35
E14	271.30	39.52

Station DU1

D2	36.64	6.79
D3	44.38	7.98
D4	52.90	9.40
D5	61.41	10.67
D6	73.01	12.30
D7	85.09	14.27
D8	96.22	16.28
D9	110.84	18.53
D10	119.50	19.93
D11	130.41	21.29
D12	140.78	22.65
D13	150.90	23.93
D14	162.60	25.40
D15	174.25	26.82

D16	185.62	28.32
D17	196.68	29.82
D18	207.90	31.43
D19	222.17	33.11
D20	233.19	34.49
D21	244.39	35.83
D22	255.93	37.14
D23	267.86	38.70
D24	286.17	40.95
B16	205.84	31.79
B17	196.60	30.26
B18	190.61	29.51
B21	163.39	27.44
B22	160.31	26.50
B23	157.34	26.67
B24	154.36	25.37
B26	146.92	24.12
B28	139.60	22.92
B29	136.67	22.60
B30	133.91	22.47
B34	163.34	27.08
B35	160.53	26.93
B36	157.62	26.16
B37	154.73	25.43
B38	151.96	24.90
B39	149.21	24.48
B40	146.40	24.52
B41	143.76	23.60
B42	135.44	23.04
B43	127.15	21.70
B44	119.37	21.09
B45	115.57	19.96
B47	113.90	19.80
B48	111.08	19.01
B49	108.59	18.18
B50	107.06	18.25
B51	105.60	18.13
B52	104.01	18.13
B53	102.14	17.83
B54	100.34	17.59
B55	98.61	17.04
B56	96.51	16.54
B57	94.10	15.41
B59	90.32	14.88
B60	87.49	14.47
B61	83.17	14.04
B62	82.01	14.08
B63	82.34	15.56
B65	83.82	14.37
B66	80.72	13.87
B67	75.35	13.16
B68	70.70	12.83
B69	70.32	12.79
B70	71.56	13.02
E3	300.71	42.70
E4	291.90	41.85
E5	285.07	40.75
E14	249.07	35.83
E15	244.58	35.30
E17	231.27	34.00

Station DU2

D2	147.76	23.80
D3	139.06	22.51
D4	130.06	21.39
D5	121.41	20.44
D6	110.08	18.61
D7	98.67	16.82
D8	88.71	15.00
D9	75.91	12.88
D10	68.15	11.72
D11	58.61	9.92
D12	49.86	8.64
D13	46.68	8.05
D14	42.65	7.29
D15	41.44	7.11
D16	43.57	7.63
D17	48.17	8.36
D18	54.59	9.49
D19	64.14	11.01
D20	72.34	12.42
D21	82.25	14.07
D22	93.25	15.74
D23	105.25	17.74
D24	121.54	20.09
C1	116.95	19.43
C2	116.41	19.26
C4	119.88	19.62
C5	122.41	20.21
C7	119.41	19.78
C8	119.13	19.67
C9	120.42	19.82
C10	121.85	20.02
C11	123.69	20.38
C13	127.02	21.14
C14	127.95	21.31
C15	130.21	21.79
C16	133.17	22.05
C17	140.46	23.14
C20	148.36	23.99
C21	150.46	23.81
C22	154.60	25.72
C23	158.41	25.17
C24	160.58	25.16
C27	170.20	25.93
C41	259.43	37.28
B16	285.96	40.22
B17	277.59	39.92
B26	236.03	35.28
B29	227.77	34.10
B44	153.23	24.96
B45	149.95	24.74
B47	145.56	24.08
B48	141.93	23.49
B49	138.31	22.99
B50	135.95	22.66
B51	133.71	22.52
B52	131.63	22.34
B53	129.78	22.13

B54	127.92	21.93
B55	125.99	21.40
B56	125.14	21.28
B57	120.32	19.95
B59	115.65	19.52
B60	113.64	19.01
B61	112.36	17.01
B65	100.69	17.07
B66	103.92	17.46
B67	110.53	18.33
B68	119.78	20.44
B69	123.54	21.18
E1	159.78	26.76
E2	153.49	25.78
E3	146.32	24.71
E4	136.55	22.96
E5	128.94	22.11
E6	119.42	20.59
E7	110.23	19.66
E8	101.18	18.21
E9	92.02	16.50
E13	80.02	13.99
E15	72.49	12.64
E16	66.65	11.91
E17	56.14	10.62

Station DU3

D2	412.99	56.86
D4	394.74	54.23
D5	385.67	53.65
D6	373.66	52.07
D7	361.39	50.39
D8	350.22	48.73
D9	335.67	47.34
D10	327.02	46.34
D11	316.12	45.01
D12	305.74	43.79
D13	296.05	42.47
D14	284.65	40.87
D18	240.89	35.36
D19	227.07	33.84
D20	216.34	32.48
D21	205.88	31.24
D22	195.45	30.03
D23	185.21	29.15
D24	168.06	26.52
C8	200.86	32.63
C9	205.86	33.41
C10	211.33	34.19
C11	216.23	34.83
C13	223.47	36.15
C14	226.47	36.84
C15	232.55	37.70
C16	236.63	38.67

Station DU4

C41	144.01	24.73
C45	83.75	15.73
C46	74.37	13.85
C47	65.30	12.36
C48	57.78	11.07
C49	48.58	9.15
C50	35.15	6.73
C52	24.25	4.99
C54A	36.78	7.20
C54B	34.11	6.53
C54C	38.38	7.39
C55	43.75	8.17
C56	46.63	8.87
C58	68.59	12.43
C59	79.11	14.24
B1	15.94	3.18
B2	22.09	4.24
B3	31.70	6.09
B4	38.30	7.35
B5	46.96	9.22
B8	65.82	12.87
B9	76.10	14.65
B10	80.80	15.51
B11	86.96	16.65
B12	92.96	17.85
B13	99.12	19.02
B14	103.70	19.78
B16	120.94	22.08
B17	130.23	23.12
B18	136.33	23.76
B19	145.58	24.76
B20	154.78	26.43
B21	163.81	27.67
A1	48.4	8.97
A2	54.6	10.04
A3	64.4	11.87
A4	75.3	13.46
A5	85.6	15.23
A6	97.9	17.02

Station UKAEA

D2	11.61	2.40
D3	20.66	4.02
D4	30.14	5.61
D5	39.43	7.16
D6	51.73	9.23
D7	64.28	11.30
D8	75.85	13.14
D9	90.67	15.36
D10	99.22	16.78
D11	109.99	18.41
D12	120.19	19.87
D13	130.97	21.57
D14	142.83	22.86
D15	154.59	24.38
D16	166.07	25.84

D17	177.21	27.29
D18	188.49	28.83
D19	202.75	30.41
D20	213.73	31.89
D21	225.02	33.03
D22	236.72	34.82
D23	248.89	36.34
D24	267.12	38.54
C2	258.92	36.57
C5	256.86	36.48
C7	249.67	35.53
C8	248.40	35.25
C16	237.12	33.90
C17	240.28	34.28
C20	234.49	33.47
C21	235.15	33.53
C22	237.63	33.77
C23	237.94	33.82
C31	242.59	35.64
C32	243.44	35.98
C54A	378.20	51.88
C54C	380.20	52.35
C55	383.70	52.39
C56	384.30	52.55
C58	401.80	54.71
C59	410.40	55.72
B1	334.61	47.13
B2	325.36	45.76
B3	312.93	44.27
B4	305.78	43.37
B5	296.20	42.30
B7	283.31	40.89
B8	276.84	39.50
B9	266.52	38.87
B10	261.80	37.94
B11	255.60	37.40
B12	249.57	36.85
B13	243.39	36.13
B14	238.81	35.74
B16	221.39	32.90
B17	211.98	31.33
B18	205.76	31.04
B19	196.46	30.62
B20	187.26	29.42
B21	178.22	28.25
B22	175.09	27.65
B23	172.07	27.28
B24	169.05	26.75
B26	161.43	25.19
B29	150.90	24.69
B31	172.96	26.39
B32	172.31	27.12
B35	164.75	26.80
B36	161.59	26.11
B37	158.47	25.26
B38	155.44	24.75
B39	152.40	24.25
B40	149.31	24.15
B41	146.41	23.52

B42	137.29	22.99
B43	128.15	21.36
B44	119.31	20.20
B45	114.92	19.80
B51	101.08	17.28
B52	98.92	16.88
B54	94.09	16.19
B55	91.71	15.74
B56	88.62	15.34
B57	85.08	13.76
B59	79.18	12.88
B60	75.01	12.27
B61	68.95	11.27
B62	65.13	11.18
B63	62.88	10.90
B65	61.30	10.87
B66	57.09	10.18
B67	50.32	9.11
B68	43.89	8.23
B69	43.09	8.07
B70	44.37	8.28
CB1	251.84	37.37
CB8	242.89	36.12
CB9	241.73	36.02
CB11	239.19	35.57
CB12	237.82	35.61
CB22	226.19	34.23
CB24	223.86	34.09
CB25	222.62	34.12
CB26	221.41	33.71
CB27	220.42	33.62
CB28	219.01	33.48
CB29	218.41	33.47
CB30	215.54	33.12
CB31	213.48	32.74
CB34	204.68	31.61
CB35	202.52	31.20
CB36	200.35	30.85
CB38	194.00	29.93
CB39	189.24	29.47
CB40	186.55	28.88
CB41	183.09	28.62
CB42	180.03	28.35
CB43	175.72	27.99
CB46	162.87	25.85
CB47	158.90	25.27
BC1	152.26	24.63
BC4	152.85	24.70
BC6	153.22	24.80
BC7	153.40	24.71
BC8	153.71	24.86
BC9	154.27	24.82
BC10	154.83	24.95
BC11	155.39	25.17
BC19	160.55	25.60
BC21	162.09	25.90
BC23	163.10	26.07
BC24	163.56	25.98
BC29	166.32	26.36

BC31	168.30	26.67
BC32	169.62	26.75
BC33	170.70	26.95
BC34	177.71	28.05
BC36	180.32	28.36
BC37	181.65	28.43
BC38	184.49	28.74
BC39	187.36	29.17
BC40	190.53	29.50
BC41	194.04	29.97
BC42	197.68	30.31
BC47	230.84	34.54
BC48	236.63	35.04
E2	278.18	40.36
E3	273.58	39.62
E4	264.83	38.65
E5	258.04	37.78
E13	223.78	33.62
E14	222.96	33.53
E15	218.66	32.82
E16	214.21	32.06
A1	389.50	52.67
A2	396.00	54.35
A3	404.80	55.46
A4	416.70	56.48
A5	427.10	57.73

Station UAB

D2	289.63	41.70
D3	280.75	39.99
D4	271.48	39.23
D6	250.59	36.87
D7	238.45	35.31
D8	227.44	34.08
D9	213.08	32.17
D10	204.48	32.04
D11	193.63	29.71
D12	183.28	28.82
D14	163.12	25.87
D15	152.22	24.54
D16	141.78	22.97
D17	131.77	21.85
D18	121.75	20.07
D19	109.00	18.23
D20	99.24	16.71
D21	90.52	15.18
D22	82.74	13.90
D23	76.56	12.78
D24	65.79	10.80
C1	71.32	11.76
C4	78.20	13.58
C5	93.97	15.17
C7	102.41	16.59
C9	110.03	17.93
C10	116.15	19.13
C11	121.75	19.47
C13	130.08	20.94
C14	133.51	21.87

C15	139.71	22.97
C16	144.60	23.61
C17	151.52	24.35
C20	170.53	27.19
C21	174.01	27.47
C24	189.75	29.63
C26	198.48	32.25
B17	371.02	51.79
B18	366.02	51.65
B41	272.26	39.74
B42	268.70	39.82
B43	265.72	39.21
B44	262.65	38.70
B47	257.95	38.23
B49	253.83	37.54
B50	252.47	37.27
B55	247.95	37.19
B57	245.60	36.39
B59	243.94	36.15
B60	243.85	36.22
B61	245.00	36.33
B66	244.07	35.89
B67	251.32	37.05
B68	261.10	38.32
B69	264.94	38.93
B70	270.65	39.60
E1	161.29	26.06
E2	155.39	25.48
E3	148.30	24.35
E5	140.36	23.52
E6	136.39	22.81
E7	130.82	22.06
E9	119.43	20.17
E13	113.91	19.66
E14	113.96	19.56
E15	111.79	19.07
E17	113.23	19.03

Station ULA

D10	228.08	33.76
D11	217.54	32.86
D12	207.45	31.58
D13	199.59	30.33
D15	179.53	27.59
D16	170.14	26.51
D18	152.35	24.70
D19	141.10	23.20
D20	132.54	21.06
D21	125.37	22.09
D22	119.32	20.72
D23	114.85	19.50
D24	105.68	17.95
E2	132.99	22.67
E3	127.04	21.63
E4	124.71	21.20
E6	122.06	21.00
E7	119.04	20.65
E8	115.79	20.08

Station UBL		
D2	372.64	51.55
D6	337.25	47.12
D7	326.38	45.91
D9	303.97	43.08
D10	296.01	42.19
D11	285.96	40.83
D12	276.32	39.94
D13	269.71	39.45
D14	260.52	38.21
D15	251.45	36.90
D16	242.94	35.74
D17	234.86	35.23
D18	226.79	34.28
D19	216.41	32.98
D20	208.42	31.72
D21	201.78	30.94
D22	196.07	30.15
D23	191.57	29.73
D24	181.58	28.28
C4	199.91	30.80
C7	218.20	33.22
C8	220.06	33.11
C9	225.81	34.22
C10	231.93	34.91
C11	237.53	35.79
C13	245.86	37.13
C14	249.29	37.43
C15	255.48	38.10
C16	260.39	37.90
C17	267.32	39.41
C20	286.32	41.83
C21	289.80	42.08
C22	291.95	42.54
C23	297.27	43.12
C24	305.54	43.97
C25	311.88	44.58
C26	314.26	44.88
C28	321.31	45.65
C32	364.06	51.35
C36	385.84	52.72
B41	381.58	53.04
B42	376.93	52.78
B43	372.74	53.15
B44	368.37	51.37
B45	366.26	51.34
B48	359.78	50.35
B49	357.03	49.96
E1	144.70	23.86
E2	142.95	23.91
E3	140.88	23.59
E4	144.01	24.02
E5	146.89	24.63
E6	150.57	24.86
E7	152.50	25.29
E8	154.19	25.34
E14	162.26	26.29

Station MHD

D14	509.55	69.89
D15	498.46	68.33
D16	487.72	67.26
D17	477.29	66.16
D19	453.08	63.21
D20	442.47	61.77
D21	432.17	60.80
D22	421.89	58.81
D23	411.71	57.56
D24	394.49	55.36

Station LN1 (Edinburgh 3 component set)

C2	333.15	46.28
C5	350.24	48.82
C9	365.95	50.15
C10	372.05	51.23
C15	395.50	53.92

Station LN4 (Auchinoon Hill)

E1	226.29	33.99
E2	228.96	34.67
E3	231.93	35.08
E4	239.77	36.00
E5	245.99	36.86
E6	253.64	37.75
E8	265.68	39.47
E9	272.04	40.60
E13	281.18	41.27
E14	282.07	41.62
E15	287.44	42.04

Station LN5 (Blackhill)

D2	449.76	61.41
D3	442.30	61.15
D4	434.61	59.26
D5	427.35	59.23
D6	417.77	56.81
D7	408.02	56.52
D8	399.55	56.26
D9	388.08	54.58
D10	380.76	53.47
D11	371.51	51.60
D12	362.59	50.88
D13	357.54	50.53
D14	349.60	49.91
D15	341.73	48.94
D16	334.41	47.76
D17	327.47	46.89
D18	320.50	46.18
D19	311.41	44.79
D20	304.35	44.04
D21	298.71	43.78
D22	293.95	42.82
D23	290.32	42.73

D24	281.13	41.44
C1	286.53	42.05
C2	292.32	42.92
C4	299.37	43.38
C5	309.32	44.66
C8	319.43	45.98
C9	325.17	47.22
C10	331.28	47.38
C15	354.78	50.74
C16	359.70	51.53
C17	366.77	51.86
C22	391.38	54.71
C23	396.71	55.27
C24	404.84	56.51
C26	413.55	56.69
C27	417.46	58.29
B44	459.86	64.11
E1	186.75	29.43
E2	188.75	29.57
E3	191.00	30.16
E4	198.30	30.85
E5	204.15	31.89
E6	211.37	32.80
E7	217.07	33.75
E8	222.45	34.33
E9	228.41	34.93
E13	237.14	36.10
E14	238.02	36.15
E16	248.38	37.25
E17	258.11	38.59

Station LN6 (Gala Law)

D3	477.50	65.69
D4	470.54	64.75
D5	464.02	63.89
D6	455.42	63.46
D7	446.71	62.50
D8	439.25	60.90
D14	395.14	55.38
D17	376.38	52.84
D18	370.51	52.17
D19	362.78	51.41
D22	348.68	49.52
D23	346.31	49.27
D24	338.71	47.98
C1	343.75	47.92
C2	349.47	48.61
C4	356.61	49.95
C5	366.77	51.12
C7	374.59	52.20
C8	376.35	52.38
C9	382.05	53.29
C10	388.08	53.93
C15	411.35	56.93
C17	423.68	58.05
C22	448.12	60.89
C23	453.47	61.97

C24	461.21	62.94
C26	469.86	63.97
C27	473.85	64.76
B44	506.20	69.80
E1	211.90	32.48
E2	215.72	32.93
E3	220.08	33.66
E4	228.87	34.74
E5	235.79	35.59
E6	244.32	36.77
E7	251.67	37.96
E8	258.76	38.90
E9	266.32	39.56
E13	276.85	41.24
E14	277.78	41.39
E16	289.49	42.53

Station LN8 (Broad Law)

D3	489.48	67.70
D4	482.27	65.73
D5	475.51	65.53
D6	466.58	64.02
D7	457.51	64.00
D8	449.69	62.73
D9	439.01	61.83
D12	414.84	59.48
D13	410.60	57.51
D14	403.35	57.50
D15	396.14	55.76
D16	389.46	54.96
D17	383.13	53.52
D18	376.76	53.78
D19	368.38	52.12
D20	361.83	51.53
D21	356.73	51.87
D22	352.51	50.60
B23	349.41	50.11
D24	340.80	48.54
C4	358.94	51.07
C5	368.97	51.89
C10	390.72	55.93
C15	414.16	58.61
C22	450.84	62.73
C24	464.18	64.93
B44	514.24	70.21

Station LN9 (Craigowl Hill, Dundee)

C4	279.96	40.68
C5	290.20	41.67
C7	297.76	42.60
C10	311.11	44.23
C15	334.23	47.20
C22	371.00	51.92
C23	376.34	52.71
C24	383.92	53.17
C26	392.52	54.50
B44	428.48	59.65

Station F1

A1	22.7	4.50
A2	28.9	5.48
A3	37.7	7.26
A4	49.5	9.26
A5	59.8	10.80
A6	72.1	12.99

Station F2

C39	171.18	27.43
C41	159.83	26.66
C45	100.21	19.57
C46	90.70	17.52
C47	81.56	15.76
C48	74.05	14.29
C49	65.90	12.48
C50	55.24	10.49
C52	48.17	9.07
C54A	13.9	2.95
C54B	12.8	2.72
C54C	16.5	3.52
C55	20.2	4.04
C56	23.5	4.75
C58	46.0	8.41
C59	5.67	10.00
B1	30.8	6.02
B2	39.5	7.47
B3	51.84	9.53
B4	58.94	10.88
B5	68.32	12.62
B7	81.16	15.11
B8	87.63	16.46
B9	97.96	18.42
B10	102.68	19.23
B11	108.88	20.47
B12	114.91	20.92
B13	121.10	21.82
B14	125.68	22.22
B15	133.68	23.15
B16	143.06	24.28
A2	35.5	6.66
A3	43.8	8.45
A4	55.1	10.18
A5	64.9	11.54

Station F6

C39	106.40	20.27
C41	95.12	17.83
C45	35.24	6.99
C46	25.74	5.43
C47	16.62	3.47
C48	9.31	2.07
C49	6.44	1.52
C50	18.48	3.41
C52	33.36	6.26

Station MIR(A)

C2	111.0	20.23
C8	85.7	16.50
C9	79.1	17.03
C10	72.9	14.80
C11	65.1	12.77
C13	55.6	11.21
C15	45.4	8.62
C16	38.9	7.46
C19	25.0	5.32
C20	16.9	4.05
C21	13.2	3.54
C22	12.1	3.59
C23	8.8	2.93

Station MIR(B)

C28	33.82	8.23
C29	20.48	6.23
C31	2.50	1.55
C32	6.89	2.50
C33	18.77	4.87
C36	34.83	8.81
C41	69.25	14.07
CB2	15.50	5.54
CB3	14.00	5.34
CB4	12.48	5.06
CB5	11.30	4.77
CB6	9.50	4.22
CB8	6.47	3.33
CB9	5.17	2.99
CB10	3.80	2.47
CB11	2.35	1.52
CB14	2.26	1.51
CB15	3.35	2.19
CB16	4.74	3.18
CB17	6.27	3.56
CB18	7.78	3.85
CB19	9.23	4.21
CB22	13.57	5.14
CB23	15.06	5.33
CB24	16.55	5.69
CB25	18.08	5.96
CB27	21.03	6.96
CB28	22.62	7.34
CB29	23.88	7.55
CB30	27.04	8.17
CB31	29.87	8.87

Station MIR(C)

BC1	19.80	7.55
BC2	18.51	7.46
BC3	17.16	7.08
BC4	15.86	6.87
BC5	14.64	6.76
BC6	13.30	6.32
BC7	12.10	6.15

BC8	11.02	5.69
BC9	8.58	5.37
BC10	6.12	3.99
BC11	3.72	2.48
BC12	1.13	0.82

Station MIR(D)

A3	44.3	8.85
A4	35.8	6.97
A5	26.6	5.09
A6	10.8	3.17

Station LOM FS(A)

C36	68.0	11.96
C37	55.5	9.95
C39	40.6	7.70
C41	30.6	6.20
C42	23.0	4.75
C43G	18.20	3.74
C43F	16.20	3.55
C43	10.4	2.0
C43E	13.1	2.77
C44D	6.70	1.58
C44C	9.20	2.01
C44B	10.70	2.03
C44A	12.90	3.34
C44	15.48	3.08
C45	23.20	4.63
C46	33.62	6.68
L4	17.30	3.75
L6	8.50	1.68
L7	6.15	0.55

Station LOM FS(B)

CB37	93.50	16.68
CB38	87.00	15.92
CB39	81.20	15.07
CB40	74.40	14.19
CB41	67.60	13.62
CB42	60.07	12.53
CB43	54.30	11.64
CB44	44.40	10.08
CB45	34.30	8.60
CB46	24.90	7.16
CB47	15.40	5.20

Station LOM FS(C)

BC19	14.10	6.65
BC21	16.10	6.86
BC22	18.30	7.29
BC25	22.70	7.95
BC26	24.80	8.70
BC28	28.10	8.97
BC29	30.60	9.38

Station LOM FS(D)

B10	116.34	20.28
B11	110.62	20.04
B12	104.18	18.05
B13	97.81	17.58
B14	93.40	17.52
B15	85.51	15.84
B16	75.61	14.62
B17	65.20	12.87
B18	59.28	12.11
B19	49.26	11.63
B20	39.51	9.84
B21	30.28	8.26
B22	27.20	7.69
B23	24.10	7.08
B24	21.40	6.34
B26	13.77	4.64
B27	10.14	3.93
B28	7.00	3.09

Station LCM FS(E)

B38	25.60	7.54
B39	29.02	8.25
B40	32.23	8.64
B41	35.54	9.24
B42	44.65	10.90
B43	55.30	12.53
B44	63.20	13.25
B45	68.02	14.02

Station LOM BS(A)

CB44	36.2	10.03
CB45	25.9	8.18
CB46	16.8	6.60
BC34	49.0	11.61
BC35	52.0	12.05
BC36	54.6	12.27
BC37	56.7	12.47
BC38	62.0	13.13
BC39	69.0	14.11

Station LOM BS(B)

B21	34.60	9.20
B22	31.20	8.48
B23	28.60	7.66
B24	25.20	7.04
B26	17.85	5.62
B27	13.38	4.85
B28	10.55	3.84
B29	6.11	2.87
B30	4.0	2.26

Station	LOM	BS(C)
B34	9.50	3.67
B35	12.56	4.49
B36	15.80	5.38
B37	19.00	6.18
B38	22.20	6.91
B39	25.25	7.84
B40	29.20	8.54
B41	32.00	8.64
B42	41.15	10.00
B43	51.10	12.15
B45	65.50	13.90

APPENDIX C

Time term analysis program

This is the program of Bamford (1970) modified for use on the IBM 360/67 computer available at the University of Durham. It has also been altered to allow the computation of time term solutions for constrained refractor velocities.

The input data necessary and the output obtained have been described by Bamford (1970), and are also explained by comment cards within the program listing.

```
      C
      C PRELUDE SETS VARIABLE ARRAY DIMENSIONS AND ASSIGNS STORAGE
      C
      C FIRST DATA CARD CONTAINS Q,K AND M
      C
      C       Q = DATA SET IDENTIFIER
      C
      C       K = NUMBER OF SITES
      C
      C       M = NUMBER OF SITES THAT ARE SHOT-POINTS ONLY
      C
            DIMENSION P(100,100),X(100,100),T(100,100),TB(100,1)
            DIMENSION MK(100),NK(100),XB(100,1),PT(100,100)
            DIMENSION E(100,1),B(100,1),SETT(100,1),TT(100,1)
            READ(5,9)Q,K,M
      9      FORMAT(F3.0,2I3)
      C
      C       VA = THE CONSTRAINED VELOCITY
      C       IF A VALUE IS READ IN FOR VA THEN
      C       THIS VALUE IS USED TO COMPUTE THE TIME TERMS
      C
            READ(5,972)VA
      972   FORMAT(F8.3)
      C
      C MAIN PROGRAMME.................
      C
            PRINT 750,Q
      750     FORMAT(1X,2HQ=,F7.3)
      C
      C ASSIGN MATRIX ELEMENTS
      C
            DO 11 I=1,K
            DO 12 J=1,K
            P(I,J)=0.0
            T(I,J)=0.0
            X(I,J)=0.0
         12 CONTINUE
         11 CONTINUE
      C
      C READ COEFFICIENTS P(I,J)
      C
            DO 16 I=1,K
            M1=M+1
            READ(5,17)(P(I,J),J=M1,K)
      17    FORMAT(40F2.0)
      16    CONTINUE
      C
      C READ TIME-DISTANCE DATA
      C
            DO 19 I=1,K
            M1=M+1
            DO 18 J=M1,K
            IF(P(I,J).EQ.0.0)GO TO 6
            READ(5,14)T(I,J),X(I,J)
      14    FORMAT(2F8.5)
          6 CONTINUE
         18 CONTINUE
         19 CONTINUE
      C
```

```
      C NORMALIZE T AND X(SECTION 4.2)
      C
            DO 21 I=1,K
            XB(I,1)=0.0
            TB(I,1)=0.0
            DO 20 J=1,K
            XB(I,1)=XB(I,1)+P(I,J)*X(I,J)+P(J,I)*X(J,I)
            TB(I,1)=TB(I,1)+P(I,J)*T(I,J)+P(J,I)*T(J,I)
         20 CONTINUE
         21 CONTINUE
      C
      C
      C CALCULATE NORMAL COEFFICIENT MATRIX PT(I,J),AIJ IN
      C   SECTION 4.2
      C
            DO 23 I=1,K
            S=0.0
            DO 22 J=1,K
            PT(I,J)=P(I,J)+P(J,I)
            S=S+P(I,J)+P(J,I)
         22 CONTINUE
            PT(I,I)=S
         23 CONTINUE
      871   CONTINUE
      872   CONTINUE
      C
      C MATRIX INVERSION. THE MATRIX INVERSION PROCEDURE CALCULATES
      C THE INVERSE OF THE PT(I,J) MATRIX AND PUTS THE INVERSE IN
      C THE STORAGE LOCATIONS INITIALLY USED FOR PT(I,J) ARRAY.
      C HENCE INVERSE IS CALLED PT(I,J)
      C
            CALL ARRAY(2,K,K,100,100,PT,PT)
            CALL MINV(PT,K,DZZ,MK,NK)
            CONTINUE
            WRITE(6,1935)DZZ
      1935  FORMAT(1X,F10.6)
      C
      C MATRIX MULTIPLICATION TO OBTAIN E(I,1) AND B(I,1);THESE ARE
      C THE MATRICES EI AND FJ DEFINED IN SECTION 4.2
      C
      688   CONTINUE
      689   CONTINUE
            E(I,1)=0.0
            B(I,1)=0.0
            CALL GMPRD(PT,XB,B,K,K,1)
            CALL GMPRD(PT,TB,E,K,K,1)
            CALL ARRAY(1,K,K,100,100,PT,PT)
         24 CONTINUE
         25 CONTINUE
            DO 1866 I=1,K
            DO 1877 J=M1,K
            IF(P(I,J).EQ.0.)GO TO 1877
      1877  CONTINUE
      1866  CONTINUE
      C
      C CALCULATE  C, D AND V; CIJ , DIJ , V   IN SECTION 4.2
      C
            PRINT 26
            IF(VA.GT.0.)GO TO 1740
         26 FORMAT(1HO,37HOBSERVATIONAL AND THEORETICAL RESULTS)
```

```
120      1740  DSQ=0.0
121            CD=0.0
122            DO 30 I=1,K
123            DO 29 J=1,K
124            IF(P(I,J).EQ.0.0)GO TO 28
125            C=T(I,J)-E(I,1)-E(J,1)
126            D=X(I,J)-B(I,1)-B(J,1)
127            CD=CD+(C*D)*P(I,J)
128            DSQ=DSQ+(D*D)*P(I,J)
129            PRINT 27,I,J,T(I,J),X(I,J),C,D
130         27 FORMAT(1X,I3,1X,I3,1X,F8.3,1X,F8.3,1X,F9.4,1X,F9.4)
131         28 CONTINUE
132         29 CONTINUE
133         30 CONTINUE
134            V=DSQ/CD
135      C
136      C PRINTING OF RESULTS
137            IF(VA.GT.0.)GO TO 893
138            PRINT 31,Q,K,M,V,CD,DSQ
139            GO TO 892
140      893   WRITE(6,31)Q,K,M,VA
141      892   CONTINUE
142         31 FORMAT(1X,3HSET,F6.1,12HNO.OF SITES=,I4,9HNO.SHOTS=,I4,
143           16X,2HV=,F7.4,F9.1,F9.1)
144            PRINT 32,DSQ
145         32 FORMAT(1X,30X,7HSUMDSQ=,F11.4)
146            DO 1911 I=1,K
147            DO 1912 J=M1,K
148            IF(P(I,J).EQ.0.)GO TO 1912
149      1912  CONTINUE
150      1911  CONTINUE
151      C
152      C SUMDSQ IS THE SUM OF SQUARED PARTIAL RESIDUALS USED IN THE
153      C DESIGN STUDY FOR CMRE(SECTION 8.4)
154      C
155      C
156      C CALCULATE TIME TERMS FROM E AND B ARRAYS
157      C
158      C      AI = EI - FI/V.................SECTION 4.2
159      C
160            DO 33 I=1,K
161            IF(VA.GT.0.)GO TO 891
162            TT(I,1)=E(I,1)-B(I,1)/V
163            GO TO 33
164      891   TT(I,1)=E(I,1)-B(I,1)/VA
165         33 CONTINUE
166            PRINT 34
167         34 FORMAT(1H1,3X,9HRESIDUALS)
168            N=0
169            SMDLSQ=0.0
170            DO 38 I=1,K
171            DO 37 J=1,K
172            IF(P(I,J).EQ.0.0)GO TO 36
173            IF(VA.GT.0.)GO TO 1121
174            DEL=T(I,J)-TT(I,1)-TT(J,1)-X(I,J)/V
175            SMDLSQ=SMDLSQ+P(I,J)*DEL*DEL
176            PRINT 35,I,J,DEL
177            GO TO 1123
178      1121  DEL=T(I,J)-TT(I,1)-TT(J,1)-X(I,J)/VA
179            SMDLSQ=SMDLSQ+P(I,J)*DEL*DEL
```

```
   35 FORMAT(1X,3X,I3,4X,I3,5X,F10.5)
1123  N=N+1
C
C USE T(I,J) ARRAY AS ARRAY OF RESIDUALS
C
      T(I,J)=DEL
      GO TO 37
   36 CONTINUE
      T(I,J)=0.0
   37 CONTINUE
   38 CONTINUE
      PRINT 39,SMDLSQ
   39 FORMAT(1HO,26HSUM OF SQUARED RESIDUALS =,F15.6)
C
C ERROR COMPUTATION ASSUMING UNIFORM VARIANCE OF ALL DATA
C
      NARM=N-K-1
      PRINT 456,NARM
456   FORMAT(I4)
      VRT=SMDLSQ/(N-K-1)
      VRINV=VRT/DSQ
      PRINT 457,VRT,VRINV
457   FORMAT(2F9.1)
      IF(VA.GT.0.)GO TO 1176
      VRV=VRINV*(V**4)
      GO TO 1193
1176  VRV=VRINV*(VA**4)
1193  SEV=SQRT(ABS(VRV))
      PRINT 457,SEV
      DO 40 I=1,K
1292  SETT(I,1)=SQRT(ABS(PT(I,I)*VRT))
   40 CONTINUE
      PRINT 41
   41 FORMAT(1H1,3X,10HTIME TERMS)
      DO 43 I=1,K
      PRINT 42,I,E(I,1),B(I,1),TT(I,1),SETT(I,1),PT(I,I)
   42 FORMAT(1X,2HA(,I3,2H)=,F9.3,1H-,F9.3,2H/V,4X,F8.4,5X,
     1F8.4,9X,F6.4)
   43 CONTINUE
      PRINT 44,VRT
   44 FORMAT(1HO,29HESTIMATE OF QVERALL FIT. VRT=,F11.5)
      PRINT 45,VRINV
   45 FORMAT(1HO,25HVARIANCE OF RECIP.VEL = ,F11.8)
      PRINT 46,SEV
   46 FORMAT(1HO,29HSTANDARD ERROR OF VELOCITY = ,F9.6)
C
C ERROR COMPUTATION ASSUMING UNIFORM VARIANCE OF
C DATA AT EACH SITE
C
      PRINT 300
  300 FORMAT(1H1,35HBERRY/WEST ERRORS.SQUARED RESIDUALS)
      PRINT 301
  301 FORMAT(1HO,1X,4HSITE,8X,8HTIMETERM,7X,14HSTANDARD ERROR
     1,7X,3HSSQ)
C
C SSQ IS THE SUM OF SQUARED RESIDUALS FOR A SITE
C RESIDUALS ARE STORED IN T(I,J) ARRAY
      DO 307 I=1,K
      SSQ=0.0
      SETT(I,1)=0.0
```

```
240           FNBITS=0.0
241           DO 302 J=1,K
242           SSQ=SSQ+T(I,J)*T(I,J)*P(I,J)+T(J,I)*T(J,I)*P(J,I)
243           FNBITS=FNBITS+P(I,J)+P(J,I)
244         302 CONTINUE
245           IF(FNBITS.LT.1.001)GO TO 304
246           FNB=FNBITS*(FNBITS-1.0)
247           SETT(I,1)=SSQ/FNB
248           SETT(I,1)=SQRT(SETT(I,1))
249           PRINT 303,I,TT(I,1),SETT(I,1),SSQ
250         303 FORMAT(1X,2X,I3,9X,F8.1,10X,F7.3,9X,F11.2)
251           GO TO 306
252         304 PRINT 305,I,TT(I,1)
253         305 FORMAT(1X,2X,I3,9X,F7.3,2X,17HINSUFFICIENT DATA)
254         306 CONTINUE
255         307 CONTINUE
256       C
257       C FINISH OF BERRY/WEST ERROR CALCULATIONS
258       C
259       C NEXT SECTION CALCULATES A HISTOGRAM OF RESIDUALS
260       C
261       C THIS SECTION REQUIRES AS DATA THE UPPER(UPLIM) AND LOWER
262       C (LLIM) LIMITS OF RESIDUALS AND THE WIDTH(WIDTH) OF THE
263       C RESIDUAL WINDOW
264       C
265           READ(5,100)ALLIM,UPLIM,WIDTH
266       100  FORMAT(3F6.2)
267           PRINT 101
268       101 FORMAT(1H1,18HRESIDUAL HISTOGRAM)
269           ANN=0.0
270       C
271       C DEFINE A MOVING 'WINDOW' BY UP AND DN
272       C
273         102 ANN=ANN+1.0
274           UP=ALLIM+ANN*WIDTH
275           DN=ALLIM+(ANN-1.0)*WIDTH
276           NWIDTH=0
277           DO 107 I=1,K
278           DO 106 J=1,K
279           IF(P(I,J).EQ.0.0)GO TO 105
280           IF((T(I,J).GE.DN).AND.(T(I,J).LT.UP))GO TO 103
281           GO TO 104
282         103 NWIDTH=NWIDTH+1
283         104 CONTINUE
284         105 CONTINUE
285         106 CONTINUE
286         107 CONTINUE
287           PRINT 108,DN,UP,NWIDTH
288         108 FORMAT(1HO,8HIN RANGE,F6.1,2HTO,F6.1,4X,I6)
289           IF(UP.LT.UPLIM)GO TO 102
290           PRINT 109,ALLIM
291         109 FORMAT(1HO,14HLOWER LIMIT = ,F6.2)
292           PRINT 110,UPLIM
293         110 FORMAT(1X,14HUPPER LIMIT = ,F6.2)
294           PRINT 111,WIDTH
295       111  FORMAT(1X,8HWIDTH = ,F5.3)
296       C
297       C HISTOGRAM SECTION COMPLETED
298       C
299       C
```

```
300      C NEXT SECTION WRITES OUT RESIDUALS AGAINST DISTANCE IN
301      C ASCENDING ORDER OF DISTANCE
302      C
303      C IF A NUMBER(ONE OF N) IS THE (I+1)TH IN A SERIES THEN
304      C IT HAS I NUMBERS LESS THAN IT IF THAT SERIES IS ONE OF
305      C ASCENDING ORDER. THE NEXT SECTION USES THIS IDEA TO LIST
306      C RESIDUALS AGAINST DISTANCE IN ASCENDING DISTANCE ORDER
307      C
308      C
309           PRINT 200
310         200 FORMAT(1H1,25HRESIDUALS VERSUS DISTANCE)
311           PRINT 201
312         201 FORMAT(1H0)
313           M1=M+1
314      C ANALYSIS OF RESIDUALS AT EACH RECORDING STATION IN TURN
315           DO 207 I=M1,K
316           K2=0.0
317         202 K2=K2+1
318      C USE PT(I,J) ARRAY TO STORE POSITION OF A PARTICULAR
319      C DISTANCE IN ASCENDING ORDER SERIES
320           PT(K2,I)=0.0
321           POS=0.0
322           IF(P(K2,I).EQ.0.0)GO TO 206
323           DO 205 J=1,K
324           IF(P(J,I).EQ.0.0)GO TO 204
325           IF(X(J,I).LE.X(K2,I))GO TO 203
326           GO TO 204
327         203 POS=POS+1.0
328         204 CONTINUE
329         205 CONTINUE
330           PT(K2,I)=POS
331         206 IF(K2.LT.K)GO TO 202
332         207 CONTINUE
333      C
334      C PRINTING OF RESIDUALS AGAINST DISTANCE
335      C
336           DO 218 I=M1,K
337           TOT=0.0
338           DO 209 J=1,K
339           IF(P(J,I).EQ.0.0)GO TO 208
340           TOT=TOT+P(J,I)
341         208 CONTINUE
342         209 CONTINUE
343           PRINT 210,I
344         210 FORMAT(1H0,4HSITE,I3,4X,8HDISTANCE)
345           PRINT 211
346         211 FORMAT(1H0,2X,9HRESIDUALS,3X,8HDISTANCE)
347           SEQ=0.0
348         212 SEQ=SEQ+1.0
349           DO 217 J=1,K
350           IF(P(J,I).EQ.0.0)GO TO 216
351           IF(PT(J,I).EQ.SEQ)GO TO 213
352           GO TO 215
353         213 PRINT 214,T(J,I),X(J,I)
354         214 FORMAT(1X,F10.5,2X,F8.3)
355         215 CONTINUE
356         216 CONTINUE
357         217 CONTINUE
358           IF(SEQ.LT.TOT)GO TO 212
359         218 CONTINUE
```

```
360      C
361      C END OF RESIDUAL VERSUS DISTANCE ANALYSIS
362      C
363      C
364      C THE NEXT SECTIONS DETERMINE MEDIANS AND COMPUTE DEVIATIONS
365      C FROM THEM
366      C THE MEDIAN IS THE MIDDLE NUMBER OF A SEQUENCE ARRANGED IN
367      C ASCENDING ORDER....IF THE SEQUENCE HAS AN EVEN NUMBER OF
368      C ELEMENTS THE MEDIAN IS THE MEAN OF THE MIDDLE TWO.
369      C
370      C IN BOTH THE FOLLOWING SECTIONS 'BAD' EXPRESSES THE DEVIATION
371      C OF A PARTICULAR RESIDUAL FROM THE APPROPRIATE MEDIAN AND
372      C 'HOWBAD' EXPRESSES THIS DEVIATION IN UNITS OF STANDARD
373      C DEVIATION FROM THE MEDIAN.
374      C
375      C
376      C ANALYSIS OF MEDIANS FOR SHOT-POINTS
377      C PT(I,J) IS AGAIN USED TO STORE SEQUENCE NUMBERS
378      C
379           PRINT 400
380        400 FORMAT(1H1,29HANALYSIS OF MEDIANS FOR SHOTS)
381           PRINT 401
382        401 FORMAT(1HO)
383           M1=M+1
384           DO 407 I=1,K
385           K2=0
386        402 K2=K2+1
387           PT(I,K2)=0.0
388           POS=0.0
389           IF(P(I,K2).EQ.0.0)GO TO 406
390           DO 405 J=M1,K
391           IF(P(I,J).EQ.0.0)GO TO 404
392           IF(T(I,J).LE.T(I,K2))GO TO 403
393           GO TO 404
394        403 POS=POS+1.0
395        404 CONTINUE
396        405 CONTINUE
397           PT(I,K2)=POS
398        406 IF(K2.LT.K)GO TO 402
399        407 CONTINUE
400      C DETERMINE MEDIAN
401           DO 430 I=1,K
402           FNBITS=0.0
403           FNO=0.0
404           FNO1=0.0
405           DO 408 J=M1,K
406           FNBITS=FNBITS+P(I,J)
407        408 CONTINUE
408           IF(FNBITS.LT.1.001)GO TO 426
409           A=SIN(FNBITS*2.0*ATAN(1.0))
410           A=ABS(A)
411           IF(A.LT.0.1)GO TO 411
412           FNO=(FNBITS-1.0)/2.0
413           FNO1=FNO+1.0
414           DO 410 J=M1,K
415           DIFF=PT(I,J)-FNO1
416           DIFF=ABS(DIFF)
417           IF(DIFF.GT.0.001)GO TO 409
418           FMED=T(I,J)
419        409 CONTINUE
```

```
      410 CONTINUE
          GO TO 416
      411 FNO=FNBITS/2.0
          FNO1=FNO+1.0
          DO 415 J=M1,K
          DIFF=PT(I,J)-FNO
          DIFF=ABS(DIFF)
          IF(DIFF.GT.0.001)GO TO 412
          FMED1=T(I,J)
          GO TO 414
      412 DIFF=PT(I,J)-FNO1
          DIFF=ABS(DIFF)
          IF(DIFF.GT.0.001)GO TO 413
          FMED2=T(I,J)
      413 CONTINUE
      414 CONTINUE
      415 CONTINUE
          FMED=(FMED1+FMED2)/2.0
      416 CONTINUE
C     FMED IS THE MEDIAN
          DEVMED=0.0
          DO 418 J=M1,K
          IF(P(I,J).EQ.0.0)GO TO 417
          DEVMED=DEVMED+(T(I,J)-FMED)*(T(I,J)-FMED)
      417 CONTINUE
      418 CONTINUE
          FNBIT1=FNBITS-1.0
          DEVMED=SQRT(DEVMED/FNBIT1)
          PRINT 419
  419   FORMAT(1HO,1X,4HSITE,3X,8HTIMETERM,2X,6HMEDIAN,2X,
     18HSTAN.DEV)
          PRINT 420,I,TT(I,1),FMED,DEVMED
      420 FORMAT(1X,1X,I3,3X,F7.3,3X,F7.3,1X,F7.3)
          PRINT 421
      421 FORMAT(1X,22HDEVIATIONS FROM MEDIAN)
          PRINT 422
      422 FORMAT(1X,7HLINK TO,4X,9HDEPARTURE)
          DO 425 J=M1,K
          IF(P(I,J).EQ.0.0)GO TO 424
          BAD=T(I,J)-FMED
          HOWBAD=ABS(BAD)/DEVMED
          PRINT 423,J,HOWBAD,BAD
      423 FORMAT(1X,2X,I3,2X,F6.3,6X,F6.3)
      424 CONTINUE
      425 CONTINUE
          GO TO 429
      426 PRINT 427
  427   FORMAT(1HO,1X,4HSITE,3X,8HTIMETERM,2X,6HMEDIAN,2X,
     18HSTAN.DEV)
          PRINT 428,I,TT(I,1)
      428 FORMAT(1X,1X,I3,3X,F7.3,4X,17HINSUFFICIENT DATA)
      429 CONTINUE
      430 CONTINUE
C
C THE NEXT SECTION IS VIRTUALLY A DUPLICATE OF THE LAST ONE.
C IT ANALYSES MEDIANS AT RECORDING STATIONS
C
          PRINT 500
      500 FORMAT(1H1,29HANALYSIS OF MEDIANS FOR STTNS)
          PRINT 501
```

```
  501 FORMAT(1HO)
      M1=M+1
      DO 507 I=M1,K
      K2=0.0
  502 K2=K2+1
      PT(K2,I)=0.0
      POS=0.0
      IF(P(K2,I).EQ.0.0)GO TO 506
      DO 505 J=1,K
      IF(P(J,I).EQ.0.0)GO TO 504
      IF(T(J,I).LE.T(K2,I))GO TO 503
      GO TO 504
  503 POS=POS+1.0
  504 CONTINUE
  505 CONTINUE
      PT(K2,I)=POS
  506 IF(K2.LT.K)GO TO 502
  507 CONTINUE
      DO 530 I=M1,K
      FNBITS=0.0
      FNO=0.0
      FNO1=0.0
      DO 508 J=1,K
      FNBITS=FNBITS+P(J,I)
  508 CONTINUE
      IF(FNBITS.LT.1.001)GO TO 526
      A=SIN(FNBITS*2.0*ATAN(1.0))
      A=ABS(A)
      IF(A.LT.0.1)GO TO 511
      FNO=(FNBITS-1.0)/2.0
      FNO1=FNO+1.0
      DO 510 J=1,K
      DIFF=PT(J,I)-FNO1
      DIFF=ABS(DIFF)
      IF(DIFF.GT.0.001)GO TO 509
      FMED=T(J,I)
  509 CONTINUE
  510 CONTINUE
      GO TO 516
  511 FNO=FNBITS/2.0
      FNO1=FNO+1.0
      DO 515 J=1,K
      DIFF=PT(J,I)-FNO
      DIFF=ABS(DIFF)
      IF(DIFF.GT.0.001)GO TO 512
      FMED1=T(J,I)
      GO TO 514
  512 DIFF=PT(J,I)-FNO1
      DIFF=ABS(DIFF)
      IF(DIFF.GT.0.001)GO TO 513
      FMED2=T(J,I)
  513 CONTINUE
  514 CONTINUE
  515 CONTINUE
      FMED=(FMED1+FMED2)/2.0
  516 CONTINUE
      DEVMED=0.0
      DO 518 J=1,K
       IF(P(J,I).EQ.0.0)GO TO 517
      DEVMED=DEVMED+(T(J,I)-FMED)*(T(J,I)-FMED)
```

```
  540         517 CONTINUE
  541         518 CONTINUE
  542             FNBIT1=FNBITS-1.0
  543             DEVMED=SQRT(DEVMED/FNBIT1)
  544             PRINT 519
  545       519   FORMAT(1HO,1X,4HSITE,3X,8HTIMETERM,2X,6HMEDIAN,2X,
  546            18HSTAN.DEV)
  547             PRINT 520,I,TT(I,1),FMED,DEVMED
  548         520 FORMAT(1X,1X,I3,3X,F7.3,3X,F7.3,1X,F7.3)
  549             PRINT 521
  550         521 FORMAT(1X,22HDEVIATIONS FROM MEDIAN)
  551             PRINT 522
  552         522 FORMAT(1X,7HLINK TO,4X,9HDEPARTURE)
  553             DO 525 J=1,K
  554              IF(P(J,I).EQ.0.0)GO TO 524
  555             BAD=T(J,I)-FMED
  556             HOWBAD=ABS(BAD)/DEVMED
  557             PRINT 523,J,HOWBAD
  558         523 FORMAT(1X,2X,I3,2X,6X,F6.3)
  559         524 CONTINUE
  560         525 CONTINUE
  561             GO TO 529
  562         526 PRINT 527
  563       527   FORMAT(1HO,1X,4HSITE,3X,8HTIMETERM,2X,6HMEDIAN,2X,
  564            18HSTAN.DEV)
  565             PRINT 528,I,TT(I,1)
  566         528 FORMAT(1X,1X,I3,3X,F7.3,4X,17HINSUFFICIENT DATA)
  567         529 CONTINUE
  568         530 CONTINUE
  569       C
  570       C    END OF MEDIAN ANALYSES
  571       C
  572             STOP
  573              END
ND OF FILE
```

APPENDIX D

Theoretical travel time program

The program calculates the travel time of the head wave and reflected wave from the nth refractor, where n = 1 to 10. All the layers must be horizontal and of constant velocity apart from the layer immediately above the deepest refractor. The velocity may increase linearly with depth in this layer. The minimum and maximum ranges at which reflections can be detected when a velocity increase with depth is present is also determined.

Input

The input data required is explained by comment statements within the program.

The first two data cards each consist of an identifier. The first identifier is used to terminate the program if no more data is to follow, and the second identifier is used to determine whether the travel times are computed for plane homogeneous layers or if a linear velocity increase with depth is allowed for in the lowermost layer.

The number of layers and each layer thickness and velocity are then read in on separate cards. The final data required is the number of shots and the shot-station ranges which are again read in on separate cards.

Output

If the travel times are computed for homogeneous plane layering the output takes the following form:-

HOMOGENEOUS PLANE LAYERING

SHOT	RANGE	REFRACTED T.T.	REFLECTED T.T.
1	120.68	17.21	17.53

and for a velocity increase with depth in the lowest layer:-

LINEAR VELOCITY INCREASE WITH DEPTH IN LOWEST LAYER

LIMITING RANGE OF MOHO REFLECTIONS

MINIMUM RANGE	MAXIMUM RANGE
60.84	171.72

SHOT	RANGE	REFRACTED T.T.	REFLECTED T.T.
1	240.76	32.48	34.22

```
      DIMENSION Z(10),V(10),DIST(300),TR(10),TRF(300),
     1TOT(300),PL(10),TT(10),TRA(300),BTOT(300)
C
C     DT = DATA IDENTIFIER  IF DT < 10
C     THEN PROGRAM TERMINATES
C
2000  READ(5,11)DT
11    FORMAT(F3.0)
      IF(DT.LT.10.)GO TO 200
C
C     AZ = MODEL IDENTIFER  IF AZ < 10 THEN
C     A LINEAR INCREASE OF VELOCITY WITH DEPTH
C     IS ASSUMED IN THE LOWEST LAYER
C
      READ(5,11)AZ
      IF(AZ.LT.10.)GO TO 20
C
C     THE FOLLOWING PART OF THE PROGRAM COMPUTES
C     TRAVEL TIMES FOR PLANE HOMOGENEOUS LAYERS
C
      READ(5,12)N
C
C     N = NO. OF LAYERS
C
12    FORMAT(I3)
      DO 30 I=1,N
      READ(5,13)Z(I)
13    FORMAT(F8.3)
      DEP=DEP+Z(I)
30    CONTINUE
      NN=N+1
      DO 31 I=1,NN
      READ(5,13)V(I)
C
C     V = LAYER VELOCITY
C
31    CONTINUE
      READ(5,12)M
C
C     M = NO. OF SHOTS
C
      DO 32 I=1,M
      READ(5,13)DIST(I)
C
C     DIST = SHOT-STATION RANGE
C
32    CONTINUE
C
C     THIS SECTION COMPUTES HEAD WAVE TRAVEL TIMES
C
      DO 33 I=1,M
      TK=0.
      DO 34 J=1,N
      RB=V(NN)**2-V(J)**2
      TR(J)=2.*Z(J)*SQRT(RB)/(V(NN)*V(J))
      TK=TK+TR(J)
34    CONTINUE
      TS=DIST(I)/V(NN)
      TRF(I)=TS+TK
```

```
      33    CONTINUE
C
C     THIS SECTION SEARCHES FOR
C     CORRECT SHOT-STATION RANGE
C
      DO 35 I=1,M
      NTN=0
      NKN=0
C
C     TINC = INCREMENTAL ANGLE
C
      TINC=0.1
      AI=0.
      TL=0.
      NTN=0
   21 AI=AI+TINC
      TL=0.
      TL=TL+Z(1)*TAN(AI)
      DO 36 J=2,N
      C=1.-(V(J)*SIN(AI)/V(1))**2
      IF(C.LE.0.)GO TO 130
      CD=Z(J)*V(J)*SIN(AI)/(V(1)*SQRT(C))
      TL=TL+CD
   36 CONTINUE
      DIFF=ABS(DIST(I)-2.*TL)
C
C     LIMIT OF TOLFRANCE SET AT 0.05KM
C
      IF(DIFF.LT.0.05)GO TO 100
      NTN=NTN+1
      IF(NTN.GT.200)GO TO 50
      R=2.*TL-DIST(I)
      IF(R.GT.0.)GO TO 130
      GO TO 21
  130 AI=AI-TINC
      TINC=TINC/10.
      GO TO 21
C
C     THIS SECTION STOPS THE PROGRAM
C     IF AN ERROR IN THE INPUT DATA
C
   50 WRITE(6,40)
   40 FORMAT(1X,5X,'MORE  THAN  200  ITERATIONS  REQUIRED')
      GO TO 200
C
C     THIS SECTION COMPUTES REFLFCTED TRAVEL TIMES
C
  100 DO 39 J=2,N
      AT=V(J)*SIN(AI)/V(1)
      D=AT**2
      DD=1.-D
      DC=AT/SQRT(DD)
      AB=ATAN(DC)
      PL(J)=Z(J)/COS(AB)
      TT(J)=PL(J)/V(J)
      TOT(I)=TOT(I)+TT(J)*2.
   39 CONTINUE
      PK=Z(1)/COS(AI)
      TOT(I)=TOT(I)+PK*2./V(1)
   35 CONTINUE
```

```
120     C
121     C       PRINTING OF RESULTS
122     C
123             WRITE(6,666)
124     666     FORMAT(1X,10X,'HOMOGENEOUS   PLANE   LAYERING')
125             WRITE(6,42)
126     42      FORMAT(1HO,/,5X,'SHOT    RANGE    REFRACTED T.T.
127            1    REFLECTED T.T.')
128             DO 51 I=1,M
129             WRITE(6,43)I,DIST(I),TRF(I),TOT(I)
130     43      FORMAT(1X,5X,I3,3X,F8.3,7X,F6.3,12X,F6.3)
131     51      CONTINUE
132             GO TO 2000
133     C
134     C       THE FOLLOWING PART OF THE PROGRAM COMPUTES
135     C       TRAVEL TIMES FOR A VELOCITY INCREASE WITH DEPTH
136     C
137     20      READ(5,12)N
138     C
139     C       N = NO. OF LAYERS
140     C
141             DO 300 I=1,N
142             READ(5,13)Z(I)
143     C
144     C       Z = LAYER THICKNESS
145     C
146     300     CONTINUE
147             LM=N-1
148             DO 301 I=1,LM
149             READ(5,13)V(I)
150     C
151     C       V = LAYER VELOCITY
152     C
153     301     CONTINUE
154             READ(5,89)VA,VB,VC
155     C
156     C       VA = VELOCITY AT TOP OF LOWER LAYER
157     C       VB = VELOCITY AT BASE OF LOWER LAYER
158     C       VC = VELOCITY AT TOP OF HALF-SPACE
159     C
160     89      FORMAT(3F8.0)
161             READ(5,12)M
162             DO 873 I=1,M
163     C
164     C       M = NO. OF SHOTS
165     C
166             READ(5,13)DIST(I)
167     C
168     C       DIST = SHOT-STATION RANGE
169     C
170     C
171     C       THIS SECTION COMPUTES MINIMUM AND
172     C       MAXIMUM RANGES FOR THE REFLECTION
173     C
174     873     CONTINUE
175             ALAM=0.
176             ATP=V(1)/VC
177             ACT=ARSIN(ATP)
178             AHC=Z(1)*TAN(ACT)
179             DO 607 J=2,LM
```

```
180             AAH=Z(J)*ATP
181             AH=V(1)**2-((V(J)**2)*(ATP**2))
182             ALN=SQRT(AH)
183             ALM=AAH/ALN
184             ALAM=ALAM+ALM
185         607 CONTINUE
186             CK=(VB-VA)/Z(N)
187             AKAN=(V(1)**2/ATP**2)-VA**2
188             AKA=SQRT(AKAN)
189             AVAK=(V(1)**2/ATP**2)-VB**2
190             AVK=SQRT(AVAK)
191             AVA=(AKA-AVK)/CK
192             AMIN=2.*(ALAM+AVA+AHC)
193             ACTL=0.
194             TLT=V(1)/VB
195             CTL=ARSIN(TLT)
196             CH=Z(1)*TAN(CTL)
197             DO 574 J=2,LM
198             CHC=Z(J)*TLT
199             CPCT=V(1)**2-((V(J)**2)*(TLT**2))
200             CCT=SQRT(CPCT)
201             CLC=CHC/CCT
202             ACTL=ACTL+CLC
203         574 CONTINUE
204         C
205         C       THIS SECTION PRINTS THE LIMITING RANGES
206         C
207             CK=(VB-VA)/Z(N)
208             CCPC=(V(1)**2/TLT**2)-VA**2
209             CBPC=SQRT(CCPC)
210             CLCP=CBPC/CK
211             RAN=2.*(ACTL+CLCP+CH)
212             WRITE(6,466)
213         466 FORMAT(1X,5X,'LINEAR  VELOCITY  INCREASE  WITH
214            1  DEPTH  IN  LOWEST  LAYER')
215             WRITE(6,771)
216         771 FORMAT(1HO,/,5X,'LIMITING   RANGE   OF   MOHO
217            1   REFLECTIONS')
218             WRITE(6,138)
219         138 FORMAT(1HO,/,5X,'MINIMUM   RANGE
220            1           MAXIMUM   RANGE')
221             WRITE(6,514)AMIN,RAN
222         514 FORMAT(1X,10X,F8.3,18X,F8.3)
223         C
224         C       THIS SECTION COMPUTES HEAD WAVE TRAVEL TIMES
225         C
226             DO 414 I=1,M
227             NTN=0
228             TOPL=0.
229             SPL=0.
230             STL=0.
231             TOKL=0.
232             BTOT(I)=0.
233             DO 330 J=1,LM
234             TKR=V(J)/VC
235             AIT=ARSIN(TKR)
236             PPL=TAN(AIT)*Z(J)
237             TOPL=TOPL+2.*PPL
238             SPL=Z(J)/COS(AIT)
239             STL=SPL/V(J)
```

```
240             TOKL=TOKL+2.*STL
241      330    CONTINUE
242             DS=DIST(I)-TOPL
243             AC=VC/VA
244             CAT=AC+SQRT(AC**2-1)
245             CA=ALOG(CAT)
246             AB=VC/VB
247             ABT=AB+SQRT(AB**2-1)
248             ABB=ALOG(ABT)
249             ARB=2.*(CA-ABB)/((VB-VA)/Z(N))
250             SOB=1.-(VA/VC)**2
251             SIB=SQRT(SOB)
252             SAB=1.-(VB/VC)**2
253             SUB=SQRT(SAB)
254             TUB=2.*(SIB-SUB)/((VB-VA)/Z(N))
255             ATTL=ARB-TUB
256             TRA(I)=TOKL+ATTL+DS/VC
257      C
258      C      THIS SECTION SEARCHES FOR
259      C      CORRECT SHOT-STATION RANGE
260      C
261             AI=0.
262             TINC=0.1
263      221    AI=AI+TINC
264             IF(DIST(I).GE.RAN)GO TO 918
265             TL=0.
266             TL=Z(1)*TAN(AI)
267             DO 830 J=2,LM
268             PR=Z(J)*SIN(AI)*V(J)
269             PT=V(1)**2-((V(J)**2)*(SIN(AI)**2))
270             IF(PT.LE.0.)GO TO 230
271             PLT=SQRT(PT)
272             RP=PR/PLT
273             TL=TL+RP
274      830    CONTINUE
275             RK=(V(1)**2/SIN(AI)**2)-VA**2
276             IF(RK.LE.0.)GO TO 230
277             RKK=SQRT(RK)
278             TK=(V(1)**2/SIN(AI)**2)-VB**2
279             IF(TK.LE.0.)GO TO 230
280             TKK=SQRT(TK)
281             TMP=(RKK-TKK)/((VB-VA)/Z(N))
282             TL=TL+TMP
283             DIFF=ABS(DIST(I)-2.*TL)
284             IF(DIFF.LT.0.5)GO TO 1000
285             NTN=NTN+1
286             IF(NTN.GT.500)GO TO 50
287             R=2.*TL-DIST(I)
288             IF(R.GT.0.)GO TO 230
289             GO TO 221
290      230    AI=AI-TINC
291             TINC=TINC/2.0
292             GO TO 221
293      C
294      C      THIS SECTION COMPUTES REFLECTED TRAVEL TIMES
295      C
296      1000   DO 239 J=2,LM
297             AT=V(J)*SIN(AI)/V(1)
298             D=AT**2
299             DD=1.-D
```

```
 300              DC=AT/SQRT(DD)
 301              AB=ATAN(DC)
 302              BPL=Z(J)/COS(AB)
 303              BTT=BPL/V(J)
 304              BTOT(I)=BTOT(I)+BTT*2.
 305       239    CONTINUE
 306       99     FORMAT(1X,F12.2)
 307              BPK=Z(1)/COS(AI)
 308              CRA=VB*SIN(AI)/V(1)
 309              BRT=VB/(VA*CRA)
 310              BARD=BRT+SQRT(BRT**2-1)
 311              BAR=ALOG(BARD)
 312              BCT=1./CRA
 313              BACD=BCT+SQRT(BCT**2-1)
 314              BAC=ALOG(BACD)
 315              BLB=BAR-BAC
 316              BTB=2.*BLB/((VB-VA)/Z(N))
 317              BTOT(I)=BTOT(I)+BPK*2./V(1)+BTB
 318       414    CONTINUE
 319       C
 320       C      PRINTING OF RESULTS
 321       C
 322              WRITE(6,42)
 323              DO 738 I=1,M
 324              IF(DIST(I).LT.RAN)GO TO 876
 325       918    WRITE(6,614)
 326       614    FORMAT(1HO,/,5X,'NO  REFLECTION  AT  THESE  RANGES')
 327       876    WRITE(6,43)I,DIST(I),TRA(I),BTOT(I)
 328       738    CONTINUE
 329              GO TO 2000
 330       200    STOP
 331              END
END OF FILE
```

References

AGGER, H.E., and CARPENTER, E.W. 1964. A crustal study in the vicinity of the Eskdalemuir seismological array station. Geophys. J., 9, 69-83.

AVERY, D.E., and BURTON, G.D., and HEIRTZLER, J.R., 1968. An aeromagnetic survey of the Norwegian Sea. J. geophys. Res., 73, 4583-4600.

BAMFORD, S.A.D., 1970 An appraisal of the seismic refraction method in crustal studies. Ph.D. Thesis, University of Birmingham.

BAMFORD, S.A.D., 1971 An interpretation of first arrival data from the continental margin refraction experiment. Geophys. J.R. astr. Soc., 24, 213.

BAMFORD, S.A.D., and BLUNDELL, D.J., 1970. The south-west Britain continental margin experiment. Inst. of Geol. Sci. Report. 70-14, 143.

BANCROFT, A.M., 1960 Gravity anomalies over a buried step. J. Geophys. Res., 65, 1793-1807.

BERRY, M.J., and WEST, G.F., 1966 Reflected and head wave amplitudes in a medium of several layers. In The Earth beneath the continents, editors Steinhart, J.S., and Smith, T.J., Geophys. Monogr., No 10, 464-481.

BIDSTON, B.J., 1970 A geophysical investigation of the Faeroe-Shetland Channel. M.Sc. Thesis, University of Durham.

BIRCH, R.W.J., 1973 Data processing and computer techniques for marine seismic interpretation. Ph.D. Thesis, University of Durham.

BIRTHILL, J.W., and WHITEWAY, F.E., 1965 The application of phased arrays to the analysis of seismic body waves. Phil. Trans.R.Soc., 258A, 421-494.

BLUNDELL, D.J., and PARKS, R., 1969 A study of the crustal structure beneath the Irish Sea. Geophys. J.R. astr.Soc., 17, 45-62.

BOMFORD, G., 1962 Geodesy. Clarendon Press, Oxford. 561pp.

BOTT, M.H.P., 1971 Evolution of young continental margins and formation of shelf basins. Tectonophysics, 11, 319-327.

BOTT, M.H.P., 1973 The evolution of the Atlantic north of the Faeroe Islands. In Implications of continental drift to the Earth Sciences, Academic Press. 175-189.

BOTT, M.H.P., BROWITT, C.W.A., and STACEY, A.P., 1971 — The deep structure of the Iceland-Faeroe ridge. Marine geophys. Res., 1, 326-351.

BOTT, M.H.P., and BROWITT, C.W.A., (in preparation) — Interpretation of geophysical observations between the Orkney and Shetland Islands.

BOTT, M.H.P., and DEAN, D.S., 1972 — Stress systems at young continental margins. Nature phys. Sci., 235, 23-25.

BOTT, M.H.P., HOLLAND, J.G., STORRY, P.G., and WATTS, A.B., 1972 — Geophysical evidence concerning the structure of the Lewisian of Sutherland, N.W. Scotland J. geol. Soc. Lond., 128, 599-612.

BOTT, M.H.P., SUNDERLAND, J., SMITH., P.J., CASTEN, U., and SAXON., S., 1974 — Evidence for continental crust beneath the Faeroe Islands. Nature, Lond., 248, 202-204.

BOTT, M.H.P., and WATTS, A.B., 1970 — Deep sedimentary basins proved in the Shetland-Hebridean continental shelf and margin. Nature, Lond., 225, 265-268.

BOTT, M.H.P., and WATTS, A.B., 1971 — Deep structure of the continental margin adjacent to the British Isles. In The Geology of the East Atlantic Continental Margin. Symposium, Cambridge, 1970. Inst. Geol. Sci. Report No. 70/14, 2, 93-109.

BROOKS, C.K., 1973 — Rifting and doming in southern East Greenland. Nature phys. Sci., Lond., 244, 23-25.

BROWITT, C.W.A., 1971 — Seismic refraction experiments between Iceland and Scotland. Ph.D. Thesis, University of Durham.

BROWITT, C.W.A., 1972 — Seismic refraction investigations of deep sedimentary basins in the continental shelf west of Shetlands. Nature, Lond., 236, 161-163.

BULLARD, E.C., EVERETT, J.E., and SMITH, A.G., 1965 — The fit of the continents around the Atlantic. Phil. Trans. R.Soc., 258A, 41-51.

BUREK, P.J., 1970 — Magnetic reversals : Their application to stratigraphic problems. Am. Assoc. Petroleum Geologists Bull., 54, 1120-1139.

CASTEN, U., 1973 — The crust beneath the Faeroe Islands. Nature phys. Sci., Lond., 241, 83-84.

ČERVENÝ, V., 1966 — On dynamic properties of reflected and head waves in the n-layerd Earth's crust. Geophys. J.R. astr. Soc., 11, 139-147.

CHESHER, J.A., DEEGAN, C.E., ARDUS, D.A., BINNS, P.E., and FANNIN, N.G.T., 1972 — IGS Marine drilling with M.V. Whitethorn in Scottish Waters 1970-71. Inst. Geol. Sci. Report No. 72-10.

COLLETTE, B.J., 1960 — Gravity Expeditions 1948-58, 5, Part 2. Delft University Press.

COLLETTE, B.J., 1968 — On the subsidence of the North Sea Area. In Geology of Shelf Seas, editor, Donovan, D.T., Oliver and Boyd, 15-30.

CRAMPIN, S., JACOB, A.W.B., MILLER, A., and NEILSON, G., 1970 — The Lownet radio-linked seismometer network in Scotland. Geophys. J.R. astr. Soc., 21, 207-216.

DAVIES, D., and FRANCIS, T.J.G., 1964 — The crustal structure of the Seychelles Bank. Deep Sea Res., 11, 921-927.

DEARNLEY, R., 1962 — An outline of the Lewisian complex of the Outer Hebrides in relation to the Scottish mainland. Q. JL. geol. Soc., Lond., 112, 15-44.

DIETZ., R.S., 1961 — Continent and ocean basin evolution by spreading of the sea floor. Nature, Lond., 190, 854-857.

DOBRIN, M.B., 1960 — Introduction to geophysical prospecting. McGraw-Hill, 446pp.

D.S.D.P., Scientific Staff, 1970 — Deep Sea Drilling Project : Leg 12. Geotimes, 15, 10-14.

EWING, J., and EWING, M., 1959 — Seismic refraction measurements in the Atlantic Ocean basins, in the Mediterranean Sea, on the Mid-Atlantic Ridge and in the Norwegian Sea. Bull. geol. Soc. Am., 70, 291-318.

FINLAY, T.M., 1930 — The Old Red Sandstone of Shetland. Part 2. North-western area. Trans. R. Soc. Edinburgh, 56, 671-694.

FLINN, D., 1969 — A geological interpretation of the Aeromagnetic maps of the continental shelf around Orkney and Shetland. Geol. J. 6, 279-292.

FLINN, D., 1970 — The Great Glen Fault in the Shetland area. Nature. Lond., 227, 268.

FLINN, D., MILLER, J.A., EVANS, A.L., and PRINGLE, I.R., 1968 — On the age of the sediments and contemporaneous volcanic rocks of western Shetland. Scott. J. Geol. 4, 10-19.

FRANCIS, T.J.G., and PORTER, I.T., 1973 — Median valley seismology: the Mid-Atlantic Ridge near 45°N. Geophys. J.R. astr. Soc., 34, 279-311.

HAGEDOORN, J.G., 1959 — The plus-minus method of interpreting seismic refraction sections. Geophys. Prospect., 7, 158-182.

HALL, J., and SMYTHE, D.K., 1973 — Discussion of the relations of Palaeogene ridge and basin structures of Britain to the North Atlantic. Earth and planet. Sci. Lett. (Neth)., 19, 54-60.

HALLAM, A., 1965 — Jurassic, Cretaceous and Tertiary sediments. In The Geology of Scotland, editor Craig, G.Y., Oliver and Boyd, Edinburgh, 401-416.

HALLAM, A., 1972 — Relation of Palaeogene ridge and basin structures and vulcanicity in the Hebrides and Irish Sea regions of the British Isles to the opening of the North Atlantic. Earth and planet. Sci. Lett. (Neth)., 16, 171-177.

HEILAND, C.A., 1968 — Geophysical exploration. Hafner Publishing Co., 1013pp.

HEIRTZLER, J.R., and HAYES, D.E., 1967 — Magnetic boundaries in the North Atlantic. Science, N.Y., 157, 185-187.

HEIRTZLER, J.R., DICKSON, G.O., HERRON, E.M. PITMAN, W.C., III and Le PICHON, X., 1968 — Marine magnetic anomalies, geomagnetic field reversals, and motions of the ocean floor and continents. J. geophys. Res., 73, 2119-2136.

HIMSWORTH, E.M., 1973 Marine geophysical studies between northwest Scotland and the Faeroe Plateau. Ph.D. Thesis, University of Durham.

HOLDER, A.P., 1969 A seismic refraction study of the earth's crust beneath south-west Britain. Ph.D. Thesis, University of Durham.

HOLDER, A.P., and BOTT, M.H.P., 1971 Crustal structure in the vicinity of south-west England. Geophys. J.R. astr. Soc., 23, 465-489.

HOLLAND, J.G., and LAMBERT, R.ST. J., 1973 Comparative major element geochemistry of the Lewisian of the mainland of Scotland. In The Early Precambrian of Scotland and related rocks of Greenland, editors, Park, R.G., and Tarney, J., University of Keele.

JOHNSON, M.R.W., 1965 Torridonian and Moinian. In The Geology of Scotland, editor Craig, G.Y., Oliver and Boyd, Edinburgh, 79-113.

LAUGHTON, A.S., 1971 South Labrador Sea and the evolution of the North Atlantic : Nature, Lond., 232, 612-616.

Le PICHON, X., HYNDMAN, R.D., and PAUTOT, G., 1971 Geophysical study of the opening of the Labrador Sea. J. geophys. Res., 76, 4724-4743.

LONG, R.E., 1974 A compact portable seismic recorder. Geophys. J.R. astr. Soc., 37, 91-98.

McQUILLIN, R., BACON, M., and BINNS, P.E., 1973 The Blackstones Tertiary igneous centre. J. geol. Soc. Lond., 129, 317.

McQUILLIN, R., and BINNS, P.E., 1973 Geological structure in the Sea of the Hebrides. Nature phys. Sci., Lond., 241, 2-4.

McQUILLIN, R., and BROOKS, M., 1967 Geophysical surveys in The Shetland Islands, Geophys. Paper No. 2, H.M.S.O., 22pp.

McQUILLIN, R., and WATSON, J., 1973 Large scale basement structures of the Outer Hebrides in the light of geophysical evidence. Nature phys. Sci. 245, 1-3.

MATTHEWS, D.J., 1939 Tables of the velocity of sound in pure water and in sea water for use in echo-sounding and sound ranging. Second edition. Hydrographic Department, Admiralty, London. H.D., 282, 52pp.

MILLER, J.A., and FLINN, D., 1966 — A survey of the age relations of Shetland rocks. Geol. J., 5, 95-116.

MOORBATH, S., and WELKE, H., 1969 — Isotopic evidence for the continental affinity of the Rockall Bank, North Atlantic. Earth and planet. Sci. Lett., 5, 211-216.

NOE-NYGAARD, A., 1962 — The Geology of the Faeroes. Quart. J. geol. Soc. Lond., 118, 375-383.

PALMASON, G., 1965 — Seismic refraction measurements of the basalt lavas of the Faeroe Islands. Tectonophysics, 2, 475-482.

PALMASON, G., 1970 — Crustal structure of Iceland from explosion seismology. Societas Scientiarum Islandica, Reykjavik, 187pp.

PITMAN, W.C.III., and TALWANI, M., 1971 — Sea-floor spreading in the North Atlantic Bull. geol. Soc. Am., 83, 619-649.

RASMUSSEN, J., and NOE-NYGAARD, A., 1970 — Geology of the Faeroe Islands, C.A. Reitzels Forlag, Copenhagen, 142pp.

RICHEY, J.E., 1961 — Scotland : The Tertiary volcanic districts. Third edition. H.M.S.O., 120 pp.

ROBERTS, D.G., 1969 — New Tertiary volcanic centre on the Rockall Bank. Nature, Lond., 223, 819.

ROBERTS, D.G., ARDUS, D.A., and DEARNLEY, R., 1973 — Precambrian rocks drilled on the Rockall Bank. Nature phys. Sci., Lond., 244, 21-23.

ROBERTS, D.G., MATTHEWS, D.H., and EDEN, R.A., 1972 — Metamorphic rocks from the southern end of Rockall Bank. J. geol. Soc., Lond., 128, 501-506.

SCRUTTON, R.A., 1970 — Results of a seismic refraction experiment on Rockall Bank. Nature. Lond., 227, 826-827.

SCRUTTON, R.A., 1972 — The crustal structure of Rockall Plateau Microcontinent. Geophys. J.R, astr. Soc. 27, 259-275.

SHIMSHONI, M., and SMITH, S.W., 1964 — Seismic signal enhancement with three component detectors. Geophysics, 29, 664-671.

STRIDE, A.H., CURRY, J.R., MOORE, D.G., and BELDERSON, R.H., 1969 — Marine geology of the Atlantic continental margin of Europe. Phil. Trans. R. Soc., 264A, 31-75.

SUNDERLAND, J., 1972 Deep sedimentary basin in the Moray Firth. Nature phys. Sci., Lond., 236 24-25.

TALWANI, M., and ELDHOLM, O., 1972 Continental margin off Norway : A geophysical study. Bull. geol. Soc. Am., 83, 3575-3606.

TARLING, D.H., and GALE, N.H., 1968 Isotopic dating and palaeomagnetic polarity in the Faeroe Islands. Nature, Lond., 218, 1043-1044.

THORNBURGH, H.R., 1930 Wave front diagrams in seismic interpretation. Bull. Am. Assoc. Petroleum Geologists. 14,2.

VINE, F.J., 1966 Spreading of the ocean floor : new evidence. Science, N.Y., 154, 1405-1415.

VINE, F.J., and MATTHEWS , D.H., 1963 Magnetic anomalies over ocean ridges. Nature, Lond., 199, 947-949.

WALTON, E.K., 1965 Lower Palaeozoic Rocks - Stratigraphy. In The Geology of Scotland, editor Craig, G.Y., Oliver and Boyd, Edinburgh, 161-200.

WATERSTON, C.D., 1965 Old Red Sandstone. In The Geology of Scotland, editor Craig, G.Y., Oliver and Boyd, Edinburgh, 269-308.

WATSON, J., 1963 Some problems concerning the evolution of the Caledonides of the Scottish Highlands. Proc. geol. Ass., 74, 213-258.

WATSON, J., 1965 Lewisian. In The Geology of Scotland, editor Craig, G.Y., Oliver and Boyd, Edinburgh, 49-77.

WATSON, J, 1973 Effects of reworking on high-grade gneiss complexes. Phil. Trans. R. Soc., 273A, 443-455.

WATTS, A.B., 1970 Geophysical investigations in the Faeroes to Scotland region, north-east Atlantic. Ph.D. Thesis, University of Durham.

WATTS, A.B., 1971 Geophysical investigations on the continental shelf and slope north of Scotland. Scott. J. Geol., 7, 189-218.

WILLMORE, P.L., and BANCROFT, A.M., 1960 The time term approach to refraction seismology. Geophys. J.R. astr. Soc., 3, 419-432.

WILSON, G.V., EDWARDS, W., KNOX, J., JONES, R.C.B., and STEPHEN, J.V., 1935 — The geology of the Orkneys. Mem. geol. surv. Scott. 205pp.

WINCHESTER, J.A., 1973 — Pattern of regional metamorphism suggests a sinistral displacement of 160 km along the Great Glen Fault. Nature phys. Sci., Lond., 246, 81-84.